Wound Repair in Sensory Organs of the Avian Inner Ear

by

Jonathan Edward Bird

A thesis submitted in partial fulfillment of the requirements for the degree of Doctor of Philosophy.

Department of Physiology, University College London.

November 2006.

ProQuest LLC
789 East Eisenhower Parkway
P.O. Box 1346
Ann Arbor, MI 48106-1346

To my family

Gdy się człowiek spieszy, to się diabeł cieszy

THESIS CORRECTIONS – JONATHAN E BIRD

Page 14
Replaced "Both types receive afferent and efferent projections from the spiral ganglion cells of the auditory nerve" with "Both types receive afferent and efferent projections from the VIIIth nerve".

Page 14
Replaced "boundaries of the cochlea duct" with "boundaries of the cochlear duct".

Page 16
Replaced "see Section 0" with "see Section 1.3".

Page 17
Replaced "see Section 0" with "see Section 1.3".

Page 22
Replaced "from the spiral ganglion cells" with "from the superior olivary complex in the brainstem".

Page 22
Deleted "outnumbering hair cells by several-fold".

Page 25
Deleted "also known as noise-induced hearing loss,".
Deleted "In extremis".

Page 36
Deleted "cryptic".
Replaced "The regulation of the Rac GTPase activity by Cool-1 (a Rac GEF) is critical for contact inhibition when the opposing wound edges meet" with "The sub-cellular redistribution of Cool-1 (a Rac GEF) from focal adhesions to cell-cell junction is critical for contact inhibition as the opposing wound edges meet".

Page 37
Deleted "where they act to separate the nucleus during anaphase".
Replaced "see section on epithelial migration" with "see Section 1.5.1".
Deleted "in a process called 'zipping' ".
Replaced "Zipping" with "This zippering action".

Page 38
Replaced "repair" with "closure"
Replaced "restitution" with "repair"

Page 40
Deleted "Selden *et al.* (1981) reported a similar increase in proliferation when colchicine was used to disrupt microtubules and cause cells to retract from one another, thereby severing extracellular linkages."

Page 43
Replace entire paragraph with "This introduction has drawn broad parallels between the general events of wound repair and those occurring subsequent to hair cell loss in sensory epithelia. To further our understanding of the avian inner ear and how it is able to regenerate so effectively, the experiments that follow will examine some of these potential equivalencies. In particular, they will focus upon epithelial repair; a process poorly understood within hair cell sensory organs. To that end, experiments will examine both epithelial reorganisation and proliferative induction in response to hair cell trauma, and attempt to identify signalling pathways that coordinate these processes in the avian inner ear."

Page 44, 64, 69, 109, 139
Replaced "phallotoxin" with "phalloidin".

Page 58
Deleted "multiple".

Page 67, 68, 82
Deleted "cryptic".

Page 69
Replaced "into a characteristic ellipse" with "as shown before".
Replaced "AJCs at the epithelial surface did not rearrange into the elliptical formation characteristic of normal wounds" with "AJCs at the epithelial surface did not rearrange, as was characteristic of a normal wound".
Replaced "This data demonstrated that cable formation was absolutely dependant upon *de novo* actin polymerisation" with "This data demonstrated that cable formation was an actin dependant process".

Page 71
Replaced "Intense NM-myosin IIB labelling was associated with AJCs that constituted the apical portion of the actin cable" with "NM-myosin IIB also associated with the actin cable at the epithelial surface".

Page 73
Deleted "and sufficient".

Page 78
Replaced "It follows that laser ablation of the sensory epithelium was multi-cellular in nature, destroying *both* support and hair cells without bias. Laser ablation is thus similar to mechanical injury, and can be considered qualitatively equivalent." with "It follows that laser ablation of the sensory epithelium was similar to a mechanical wound, destroying both support and hair cells".

Page 82
Deleted "Considering that lamellipodia are widely documented as motile structures, this technique was limited to providing a 'snapshot' of their activity".

Page 83
Deleted "An interesting experiment will be to assess the impact of wiskostatin, a N-WASP inhibitor, upon the wound closure process (Peterson et al., 2004)".
Replaced "Taken together, it has been shown" with "It is proposed that".
Replaced "It is now proposed that" with "It is now suggested that".

Page 84
Replaced "according to the inertial resistance" with "adapting to the resistance".
Replaced "This might reflect asymmetries in both the mechanical stiffness and inertia of the surrounding epithelium" with "This might reflect asymmetries in the mechanical stiffness of the surrounding epithelium".

Page 87
Deleted "; the so called spatio-temporal profile".

Page 88
Replaced "It remains to be seen whether the repair mechanisms described here are active during specific pathologies of inner ear sensory epithelia" with "It remains to be seen whether the repair mechanisms described here are also active *in vivo*.

Page 90
Replaced "BrdU was almost exclusively found within support cells" with "BrdU was usually restricted to support cells".

Page 92
Replaced "It must be stressed that although hair cells were absent from the wound environs, support cells were present within this region, having completed the closure process during the experiment (see Chapter 3)" with "Although hair cells were absent from the original wound site, support cells were present within this region (see Chapter 3)".

Page 101
Replaced "This was an important" with "This was important".

Page 103
Replaced "Phosphoinositide 3-kinases (PI3Ks) belong to a family of heterodimeric lipid kinases that catalyse phosphorylation of $PI(4,5)P_2$ at the 3' position to yield $PI(3,4,5)P_3$" with "Class I phosphoinositide 3-kinases (PI3Ks) catalyse phosphorylation of $PI(4,5)P_2$ at the 3' position to yield $PI(3,4,5)P_3$.

Page 104
Replaced "approximately" with "approximate".

Page 106
Deleted "As support cells of the mammalian utricular epithelium are capable of proliferation, this may represent a difference in the upstream signalling."

Page 114
Replaced "In the period 12-24 hours only, the hair cell and inclusion body densities appeared to be inversely proportional with respect to each other. Within this interval, two separate exponential functions were fitted to the phair cell and inclusion body estimates, and half-lives of 7.5 and 6.1 hours calculated respectively."
With
"In the period 12-24 hours only, the population of hair cells and inclusion bodies were inversely proportional with respect to each other. Within this interval, two separate exponential functions were fitted to the hair cell and inclusion body populations, and half-lives of 7.5 and 6.1 hours calculated respectively."

Page 125
Deleted "To address the specific question of inclusion bodies,"

Page 138
Replaced "Clearly, the total loss of hair cells induced by streptomycin treatment would represent an inordinate challenge for the limited numbers of macrophages shown here." with "It is unclear whether the limited number of macrophages present would be sufficient to deal with the total loss of hair cells, such as that induced using streptomycin."

Page 141
Deleted "These requirements were characteristic of either a mechanical or a diffusible factor, as opposed to a biochemical signal presented on the hair cell surface."

Page 152
Deleted "entirely".

END

Abstract

Hair cells are the sensory receptors of the inner ear, converting sound and accelerations into neuronal signals. Unlike mammals, birds are able to regenerate their sensory function after auditory or vestibular trauma. Sensory regeneration requires a composite programme of epithelial repair, hair cell production and functional reinnervation. The purpose of this thesis was to explore the mechanisms of epithelial repair in the avian inner ear, and examine their contribution within the broader process of sensory regeneration.

An epithelial cell culture model of the chick utricle (*Gallus gallus*) was developed to facilitate *in vitro* experimentation. Initial investigations utilised laser ablation to create wounds in the sensory epithelium. Epithelial wounds were found to heal within 4 hours using a contractile acto-myosin cable in combination with lamellipodia driven cell crawling. Nuclear incorporation of BrdU was also used to assess support cell proliferation at the sites of epithelial wounds. Proliferation was significantly increased within 48 hours of laser ablation, and was spatially restricted to the areas of epithelial trauma. The increase was strongly reduced by pharmacological blockade of PI3K, but only partially so using inhibitors of the ERK and JNK MAP kinases. The response of the avian sensory epithelium to aminoglycoside ototoxicity has also been investigated. Streptomycin sulphate was used to induce extensive hair cell death in explant cultures of the chick utricle. During this process, support cells were found to remodel and eliminate the hair cell from the epithelial surface. Time-lapse microscopy of β-actin-EGFP revealed that support cells formed a cable of f-actin around the hair cell neck. The cable subsequently constricted to repair the epithelial defect, and in doing so severed and ejected the hair bundle. Support cells adjacent to a dying hair cell also extended pseudopodia basolaterally to form a distinctive calyx of f-actin around the soma. Simultaneous time-lapse recordings of β-actin-EGFP with TOTO-3 revealed that the support cell calyx was a phagocytic structure, which culminated in the engulfment of the hair cell. These results demonstrated that support cells have a proactive role in both maintenance of epithelial integrity and the removal of corpses during hair cell death.

Table of contents

Table of abbreviations

AJC	Apical junction complex
ATP	Adenosine 5'-triphosphate
BrdU	5-bromo-2'deoxyuridine
cAMP	Cyclic adenosine monophosphate
CKI	Cyclin kinase inhibitor
CI	Contact inhibition
DAPI	4',6-Diamidino-2-phenylindole
DDI	Density dependent inhibition
DIC	Differential interference contrast (Nomarski optics)
DIV	Days *in vitro*
EGFP	Enhanced green fluorescent protein
EMT	Epithelial mesenchymal transition
ERK	Extracellular signal related kinase
FBS	Foetal bovine serum
GAP	GTPase activating protein
GEF	GTP exchange factor
GTP	Guanosine-5'-triphosphate
HEPES	4-(2-hydroxyethyl)-1-piperazineethanesulphonic acid
JNK	c-Jun N-terminal kinase
mAb	Monoclonal antibody
MAPK	Mitogen activated protein kinase
M199E	Medium 199 with Earle's salts
M199H	Medium 199 with Hank's salts
MLCK	Myosin light-chain kinase
PI3K	Phosphoinositide 3-OH kinases
PBS	Phosphate buffered saline
SEM	Standard error of the mean

Table of figures

Acknowledgements

On a professional basis, I must thank my supervisor Dr. Jonathan Gale for his help and guidance throughout this project. I would like to thank Drs. Nicolas Daudet and Julian Lewis at Cancer Research UK for introducing me to the wonders of chick developmental biology. I also extend my gratitude to Dr. Mark Warchol who ensured that my short stay in St. Louis was both enjoyable and scientifically productive.

I owe a special acknowledgement to Zoë, whose support and companionship have steeled me through the trials and tribulations of the past 12 months. To Dad, Mum and Caroline, thank you for welcoming me back home and for supporting me financially during the latter stages of my research and writing. I only wish that my grandparents were here to share in this moment. Finally, I would like to thank the Mann family, Giovanni, Lynn and Sophie for inviting me into their home and making me feel so welcome there.

I would like to thank both the Medical Research Council for funding my studentship, and Deafness Research UK whose financial support made my work in the USA possible.

Declaration

The work presented herein is entirely that of the author.

The RCASBP(B)-β-actin-EGFP plasmid was generated by Dr. Nicolas Daudet, Cancer Research UK.

1 Introduction

The ability to detect mechanical stimuli is a fundamental theme throughout the animal kingdom, allowing the organism to sample and interact with its environment. Undoubtedly, the most intricate array of mechanical sensors is found within the auditory and vestibular organs of the vertebrate inner ear: these endow the organism with the ability to perceive sound and accelerations. At the core of these systems is the sensory hair cell, which transduces mechanical energy into electrical signals to be processed by the central nervous system. Sensory hair cells are vulnerable to a range of pathologies that can interfere with their sensitive function, and ultimately lead to their death. Hair cell death has a profound implication for the sensory modalities that they encode, and manifests as a hearing or balance disorder. As the mammalian inner ear displays a limited potential for hair cell replacement, acquired sensory deficits tend to be permanent in nature. This is not the case in other vertebrates, where complete sensory regeneration can be achieved through an effective program of hair cell replacement. Amongst animals that are known to regenerate their sensory hair cells, Aves are the only class of warm-blooded vertebrates that are known to do so. For this reason, the avian inner ear has proved an intriguing model for studies into vertebrate hair cell regeneration and its ancillary mechanisms.

This introduction will encompass the basic anatomy of the avian and mammalian inner ear, in addition to describing the general physiology of sensory transduction. It will cover the common aetiologies of hair cell pathology, and the documented mechanisms of regeneration. In addition to research that has been performed in the inner ear, this introduction will draw insight from the general field of repair and regeneration as observed in other epithelial systems.

1.1 The mammalian inner ear

The mammalian inner ear is located within the temporal bone, in a hollow cavity known as the bony labyrinth. The bony labyrinth consists of an elaborate network of chambers that together form the otic capsule and the vestibule with its semicircular canals. Within the bony labyrinth resides the membranous labyrinth, a continuous compartment that closely follows the shape of its bony enclosure. Both the bony and membranous labyrinths are fluid filled with perilymph and endolymph respectively, the ionic composition of which is critical for normal function (see below). Perilymph is

similar to normal extracellular fluids, with sodium as the main cation[1] (Na^+: 148 mM, K^+: 4.2 mM, Cl^-: 119 mM, Ca^{2+}: 1.3 mM). Conversely, endolymph is representative of an intracellular fluid, with potassium as the main cation[1] (Na^+: 1.3 mM, K^+: 157 mM, Cl^-: 132 mM, Ca^{2+}: 23 μM). The membranous labyrinth is formed of epithelial tissues that constitute the six sensory organs of the inner ear: the cochlea, utricle, saccule and the three cristae (see Figure 1.1). The cochlea is the auditory organ of the mammalian inner ear, and is responsible for the detection of sound (see Section 1.1.1). The remaining five organs form the vestibular system. In combination with the ampullae of the semicircular canals, the cristae detect rotational accelerations, whilst the utricle and saccule report linear accelerations (see Section 1.1.2). All of the inner ear sensory organs receive afferent and efferent innervations from the VIIIth cranial nerve. The morphology and function of these organs will now be described in more detail.

Figure 1.1 - The mammalian inner ear. The membranous labyrinth of the mammalian inner ear is divided into a *pars superior* and *pars inferior*. The pars superior comprises the semicircular canals and the utricle, whilst the pars inferior contains the saccule and cochlea. The cochlea has been sectioned to reveal its internal structure. Adapted from Tortura & Grabowski: Principles of Anatomy and Physiology, 8th edition.

[1] fluid compositions are quoted from Wangemann (2006).

1.1.1 The auditory system

The cochlea is the sensory organ of the auditory system, deriving the name quite literally from its shell-like appearance when viewed externally. Figure 1.1 is a depiction of a cochlea isolated from the temporal bone, which has been sagitally sectioned to reveal its internal architecture. Within the otic capsule, the cochlear duct coils along its length, spanning radially from the modiolus to the lateral wall. The fluid space within the cochlea duct is known as the scala media and is filled with endolymph. The basal and apical surfaces of the cochlear duct make contact with the scalae tympani and vestibuli respectively. These fluid compartments contain perilymph. Figure 1.2A is a slice through one turn of the cochlea demonstrating the relationship of these different compartments. The scalae tympani and vestibuli are physically separated by the cochlea duct, except at the very apex of the cochlea, where a small aperture called the helicotrema unites them. The boundaries of the cochlea duct are constituted by Reissner's membrane at the scalae media/vestibuli interface and by the basilar membrane at the junction of scalae media/tympani. The lateral wall of the cochlea duct houses the stria vascularis. The stria vascularis is responsible for secreting K^+ ions back into the endolymph, as well as generating the +80 mV endocochlear potential (Wangemann, 2002). Lying upon the basilar membrane within the cochlea duct is the organ of Corti, the sensory epithelium of the auditory system (see Figure 1.2B).

The organ of Corti is an intricate structure comprising two primary types of polarised epithelial cell: hair cells and support cells. Some types of support cells surround and prevent neighbouring hair cells from making contact with one another (Deiter's, Hensen's, pillar and inner phalangeal cells), whilst others form homogenous epithelial sheets at the edges (inner sulcus and Claudius's cells). There are two types of sensory hair cell within the organ of Corti: inner and outer hair cells. In a cross section, inner hair cells are arranged in a single row, whilst outer hair cells form three parallel rows (see Figure 1.2B). Inner hair cells are responsible for sensation of sound energy, whereas outer hair cells participate in an active amplification mechanism (see below). Both types receive afferent and efferent projections from the spiral ganglion cells of the auditory nerve. Inner hair cells receive primarily afferent innervation, whilst that of outer hair cells is mainly efferent. The surface of the organ of Corti is known as the reticular lamina, which is a mosaic of hair cell and support cell membranes. Sensory hair bundles project from the surface of the reticular lamina into the scala media, where

they are bathed in endolymph. The tectorial membrane overlays the organ of Corti, and makes contact with the outer hair cell bundles. For a more detailed treatise on cochlear anatomy, the reader is referred to an excellent review by Raphael *et al.* (2003).

The ability of the cochlea to detect sound derives from the mechanical properties of the organ of Corti and the basilar membrane. Incoming sound pressure changes are communicated from the middle ear to the scala tympani through the oval window. The subsequent pressure differential between the scalae tympani and vestibuli sets up a travelling wave within the basilar membrane. As the basilar membrane and organ of Corti are displaced relative to the tectorial membrane, a shearing force is exerted upon the hair cell bundles. This results in sensory transduction and increased activity at the

Figure 1.2 - The cochlea and organ of Corti. The cochlea contains the auditory sensory epithelium of the mammalian inner ear. **A)** A section through one turn of the cochlea showing the different fluid compartments: SV – scala vestibuli, SM – scala media, ST – scala tympani. The organ of Corti is found within the scala media, and is highlighted within the grey rectangle. **B)** A section through the organ of Corti, reproduced from the original lithograph by Retzius (1881). This cross section depicts how the intricate architecture is constructed from the various support cells and hair cells.

afferent synapse. The exact mechanisms of hair cell transduction will be discussed later (see Section 0). The exquisite frequency selectivity displayed by the cochlea is based upon varying the mechanical properties of the basilar membrane as it extends from base to apex of the cochlea, thus altering the resonant frequency at which oscillations are sustainable. This creates a tonotopic map along the length of the cochlea, with high and low frequencies represented at the base and apex respectively. This also means that any individual hair cell has a characteristic frequency to which it will respond maximally, depending upon its location within the cochlea. Thus, the cochlea can be thought of as an auditory spectral analyser, spatially separating the frequency components of a complex waveform before they are encoded and transmitted to the central nervous system via the hair cells.

Another property of the cochlea is its remarkable sensitivity to low sound pressure levels. The organ of Corti is so sensitive that the inner hair cells can detect basilar membrane (BM) deflections in the order of a few nanometers. At sound pressure levels approaching the auditory threshold, electromechanical feedback in the guise of the cochlear 'amplifier' is used to destabilise the system and allow smaller BM displacements to elicit a response. Outer hair cell somatic motility is a major contributor to the cochlear amplifier, and disruption of this leads to a significant reduction in cochlear sensitivity. The presence of an active amplification mechanism is betrayed by the *emission* of sound from the cochlea, so-called otoacoustic emissions (OAEs). The details of these, plus other potential amplification schemata are beyond the scope of this introduction (reviewed by Fettiplace and Hackney, 2006).

1.1.2 The vestibular system

The vestibular system is comprised of the vestibule and three semicircular canals (see Figure 1.1). The vestibule houses the utricle and saccule, sensory organs that are responsible for the detection of vertical and horizontal linear accelerations respectively. They are referred to as the otolith organs, owing to the calciferous crystalline 'otoliths' that are present upon their surface. As the utricle and saccule share a very similar structure, this section will focus largely upon the utricle. The utricular macula consists of a mosaic of support cells and hair cells that combine to form a sensory epithelium (see Figure 1.3A). Overlying the epithelium is a gelatinous otolithic membrane, which infiltrates around the sensory hair bundles. A layer of calcium carbonate otoliths is

resident at the surface of this membrane. Two types of hair cell have been described within the utricular macula, designated type I or II based upon their morphology and distribution (see Figure 1.3B). Type I hair cells are flask-shaped and are surrounded by a large afferent nerve calyx. Type II hair cells are cylindrical, and receive multiple bouton innervations. Additionally, type I hair cells are located exclusively within the striola of Werner, a band of cells that extends laterally offset around one edge of the utricle (see Figure 1.4C). An interesting property of the utricle is that both type I & II hair cells are orientated toward the striola; conversely, in the saccule, hair cells are orientated away from the striola. For details of how hair cell orientation is determined, see Section 0.

Figure - 1.3 Sensory organs of the vestibular system. The vestibular system consists of five sensory organs, the utricle, saccule and three cristae. **A)** A section through the utricle depicts the organisation of support cells and hair cells within the macula. A gelatinous membrane containing calciferous otoliths couples accelerations to the sensory hair cells. **B)** Hair cell specialisations within the utricular macula. Type I hair cells are innervated by a single afferent calyx, whilst type II cells receive multiple bouton innervations. **C)** Cross-section of the ampulla with its associated crista. A gelatinous cupula couples fluid movement within the semicircular canal to the sensory hair cells. Similar hair cell specialisations are found here. Images are adapted from Tortura & Grabowski: Principles of Anatomy and Physiology, 8th edition.

The ability of the utricle and saccule to sense linear acceleration relies upon the specialised otoconial matrix. The relatively high inertia of an individual otolith is such that as the macula experiences acceleration, it will take slightly longer for its velocity to change. Thus, a shearing force is established upon the hair bundle resulting in sensory transduction. In this manner, head movements can be directly translated into afferent nerve activity. The functional significance of type I hair cells of the striola is yet to be fully understood, although their large calyxeal afferents are known to endow them with fast, high fidelity synaptic transmission. As with the organ of Corti, the epithelial surface of the utricle is bathed in a K^+ rich endolymph that is essential for sensory transduction. However, there is no equivalent to the endocochlear potential within the vestibular system.

The other portion of the vestibular system is the semicircular canals, which measure rotational accelerations. There are three semicircular canals within the labyrinth (designated lateral, anterior, posterior), each with a single ampulla at the junction with the vestibule (see Figure 1.1). Each ampulla contains a single crista, a sensory patch comprised of support cells and hair cells (see Figure 1.3C). The surface of the crista is encased within a gelatinous plug, known as the cupula, which extends to ceiling of the ampulla. As the head experiences a rotational acceleration in a single plane, the inertia of the fluid within the canal exerts a pressure upon the cupula. The resulting displacement exerts a shearing force across the hair bundles, and stimulates sensory transduction. Since the three semicircular canals are orientated orthogonally within the labyrinth, rotational accelerations can be detected in three dimensions.

1.2 Comparative anatomy of the avian inner ear

The avian inner ear shares remarkable homology with the mammal, however there are important differences that will be highlighted here. Ultrastructurally, the biggest disparity is found within the auditory system, where the anatomy differs radically from the mammal. The avian auditory organ is called the basilar papilla, and presents as a slightly curved, tubular structure running along the length of the cochlea duct (see Figure 1.4A). A cross-section of the basilar papilla depicts the sensory epithelium separating the scalae media and tympani from each other (see Figure 1.4B). The basilar papilla has no specialisations equivalent to the organ of Corti. Instead, a graded increase in hair cell height is observed moving from the inferior to superior edges. Hair cells have been classed as tall, intermediate or short depending upon their height (Takasaka and Smith, 1971). Although possessing a distinct anatomy, the general topology of the basilar papilla is similar to the mammalian cochlea. The scalae media, tympani and vestibuli are still present, and there is a tectorial membrane which overlays the sensory hair cells. In some respects, the basilar papilla can be considered as an uncoiled cochlea. Continuous with the distal portion of the basilar papilla is the macula lagena, which is covered in an otolithic membrane, similar to that of the saccule and utricle. The macula lagena is uniquely found within amphibians and birds. The physiological functions of this organ are unclear, although recent studies have suggested that it might be sensitive to electromagnetic fields, and thus act as a navigational compass (Harada et al., 2001).

The avian vestibular system is largely analogous to that of the mammal. Of specific interest to this thesis are the structural differences within the utricular macula. The utricular macula can be divided into a series of zones, based upon the distribution of type I & II hair cells (see Figure 1.4C). The cotillus is located centrally, and is separated from the rampa by the striola (Jorgensen, 1989). In mammals, the cotillus contains type II, whilst the striola constitutes a single band of type I. In contrast, the striola found in the avian utricle forms two bands of type I, separated by a thin band of type II (see Figure 1.4D). The 'reversal zone', where bundle polarity is flipped by 180 degrees, is located within the central band of type II hair cells.

Functionally, sensory transduction occurs in a similar fashion to that of the mammalian inner ear (see Section 1.3). The chick basilar papilla also displays a tonotopic response, with high frequencies represented at the base, and low frequencies

at the apex (Manley et al., 1987). Concentrations of K^+ in the endolymph are also similar to that described in mammals (Runhaar et al., 1991). The endocochlear potential in an adult bird is +15 mV, which is lower than that recorded in mammals (Poje et al., 1995). Avian hair cells have not been shown to display somatic motility, though the basilar papilla is still capable of generating spontaneous OAEs (Chen et al., 2001).

Figure 1.4 - The avian inner ear. The membranous labyrinth of the avian inner ear. **A)** The inner ear of a chicken (*Gallus domesticus*) taken from the original lithograph by Retzius (1881). **B)** Cross section of the auditory epithelium, the basilar papilla, showing its internal structure. Abbreviations are as follows: basilar membrane (BM), ganglion cells (GC), hyaline cells (H), habenula perforata (HP), inferior fibrocartilaginous plate (IFP), scalae media, tympani & vestibuli (ScM, ScT, ScV), short hair cells (SHC), superior fibrocartilaginous plate (SFP), tegmentum vasculosum (TV), tall hair cells (THC), tectorial membrane (TM). **C)** A surface view of the utricular macula depicting the cotillus, rampa and striola regions. **D)** A cross section of the avian striola showing the inner (IZ) and outer zone (OZ) that contain type I hair cells, separated by type II cells of the middle zone (MZ). Figures are adapted from: (B) Tanaka et al. (1978), (C,D) Jorgensen (1989).

1.3 The sensory epithelium and mechano-transduction

A fundamental function of any hair cell epithelium is its ability to convert mechanical energy into electrical signals, a phenomenon termed mechano-transduction. By coupling the hair cell to mass-loaded structures, sensory systems use mechano-transduction to represent accelerations and sound. The preceding sections have described a wide range of physical incarnations, ranging from the relative simplicity of utricular macula to the complex architecture within the organ of Corti. Despite their differences, all share a common physiological and anatomical basis. Hair cell epithelia are constructed from two primary cells types, support cells and hair cells. These cells are organised to form a pseudo-stratified columnar epithelium. In this generalised example, support cells extend from the basal lamina (basement membrane) to the epithelial surface (also known as the reticular lamina). Only support cells make contact with the basal lamina, whereas both hair cells and support cells contribute to the surface of the epithelium. The surface of the epithelium is bathed in endolymph, whilst the base and intercellular spaces contain perilymph.

Hair cells are the mechano-sensitive receptors within the sensory epithelium. In contrast with some sensory systems, hair cells do not possess axons or dendritic arbors. Instead, they are polarised neuroepithelial cells that originate from the ectoderm. The apical pole of the hair cell is equipped with a specialised organelle known as the hair bundle, comprised of between 10 and 300 individual stereocilia. Each stereocilium is a rigid rod-shaped para-crystalline array of actin filaments that insert into the cuticular plate, an actin rich cytoplasmic organelle at the apex of the hair cell (Flock and Cheung, 1977; DeRosier et al., 1980; Tilney et al., 1980). Neighbouring stereocilia are connected to each other by a series of extracellular linkages (Pickles et al., 1984; Furness and Hackney, 1985; Goodyear and Richardson, 1992), such that when displaced they move in concert, flexing around their insertion points in the cuticular plate (Flock et al., 1977). In addition to the stereocilia, most hair cells also possess a single tubulin-based kinocilium that is offset laterally with respect to the hair bundle (Wersall, 1956). The position of the kinocilium relative to the stereocilia denotes the axis of hair bundle sensitivity. Movement of the bundle towards the kinocilium depolarises the hair cell membrane potential, whilst movement away results in a hyperpolarisation (Harris et al., 1970; Hudspeth and Corey, 1977).

The mechanisms that couple bundle displacement to changes in the hair cell receptor potential are now increasingly well understood (reviewed by Fettiplace and Hackney, 2006). Displacement is thought to gate a non-selective cation channel within the hair bundle, altering its open probability and allowing an inward current to pass. As the epithelial surface of the hair cell is bathed in endolymph fluid, the predominant cation present is K^+. The inward flux of K^+ ions depolarises the hair cell membrane, which subsequently activates voltage-gated calcium channels toward the basolateral pole of the hair cell. The calcium influx triggers the release of neurotransmitter into the synaptic cleft, generating an excitatory postsynaptic potential (EPSP) within the afferent nerve fibre (reviewed by Trussell, 2002). Hair cells can also receive direct efferent innervation from the spiral ganglion cells. Transduction is greatly facilitated by the positive endocochlear potential (EP), which creates an electrical gradient to drive K^+ ions into the hair cells.

A fundamental question is how displacement of the hair bundle is able to gate the mechanoelectrical transducer (MET) channel to allow K^+ influx. Hudspeth et al. (1979) showed that the stereocilia were essential for mechano-transduction, and that the kinocilium was not required. The observation of small extracellular 'tip' links between adjacent stereocilia led to the suggestion that these might gate the MET channel directly as the bundle was displaced (Pickles et al., 1984). Consistent with this theory, disruption of extracellular linkages using a Ca^{2+} chelator such as BAPTA results in the cessation of mechano-transduction (Zhao et al., 1996). Several proteins required for mechano-transduction have been associated within the tip link structure, including cadherin-23 and protocadherin-15 (Alagramam et al., 2001; Di Palma et al., 2001; Siemens et al., 2004; Ahmed et al., 2006), as well as myosin-1c (Holt et al., 2002). The TRPA1 potassium channel was recently proposed as the MET (Corey et al., 2004), however it transpires that knockout models are able to hear and balance normally (Kwan et al., 2006).

The other type of cell within the sensory epithelium is the support cell. The support cell (also known as a supporting cell) is the predominant cell type in the sensory epithelium, outnumbering hair cells by several-fold. As the only cell type that contacts the basal lamina, support cells quite literally form the structural foundation of the sensory epithelium. Support cells are columnar and each extends a process to the

surface of the epithelium. Sensory hair cells occupy the paracellular space in between these processes, such that each hair cell is surrounded basolaterally by a number of support cells. Neighbouring hair cells are thus physically isolated from one another. In contrast to the basal lamina, the epithelial surface consists of a mosaic of both hair cell and support cell processes. These apical processes are interlinked with an extensive tight junction network, which has been proposed to maintain the separation of the differing ion compositions present in endolymph and perilymph (Jahnke, 1975; Gulley and Reese, 1976). Adherens junctions are also present in the adluminal space immediately beneath the tight junction network (Gulley and Reese, 1976; Nadol, 1978). The nature of these junctions serves to create a barrier that is impermeable to ions and other molecules, in addition to providing a structural integrity to the epithelium. The importance of this barrier function is highlighted by knockout studies of the tight junction gene *claudin-14*, which results in extensive hair cell death shortly after hearing onset (Wilcox et al., 2001; Ben-Yosef et al., 2003). Toward the base of the epithelium, an extensive network of gap junctions connects neighbouring support cells together, creating a functional syncytium (Gulley and Reese, 1976; Santos-Sacchi and Dallos, 1983). Gap junction plaques are not observed at the interface between hair cells and support cells.

In addition to forming a large portion of the sensory epithelium, support cells are also essential for the recycling of K^+ ions (reviewed by Wangemann, 2006). Potassium is excreted from the hair cell's basolateral membrane, accumulating in the extracellular space during sensory transduction. Given that K^+ ions cannot escape through the tight-junctional barrier at the epithelial surface, a mechanism for K^+ removal is required to maintain homeostasis. Support cells are able to remove K^+ from the hair cell basolateral membrane and transport it back toward the stria vascularis (or equivalent) via neighbouring support cells. The importance of this system is highlighted with mutant knockouts of *Kcc4*, a support cell K^+/Cl^- co-transporter, which results in hair cell death shortly after hearing onset (Boettger et al., 2002). Gap junctions are critical for K^+ recycling, and mutations in the constituent connexin subunits result in deafness (Kelsell et al., 1997).

Although support cells have no *direct* role in mechano-transduction, there is evidence that they can receive both afferent and efferent innervations (Cotanche et al.,

1992; Fechner et al., 2001). The function of this innervation is unclear, though there is suggestion that it modulates contractility and alters the mechanical properties of the sensory epithelium (Cotanche et al., 1992).

1.4 Repair and regeneration of hair cell sensory epithelia

In contrast with amphibians and fish, whose sensory maculae continue to produce hair cells throughout adult life (Corwin, 1981, 1985), hair cell production in the avian and mammalian cochlea ceases during embryogenesis (Ruben, 1967; Sans and Chat, 1982; Tilney and Tilney, 1984; Katayama and Corwin, 1989). This belief was challenged in two seminal papers, where it was reported that adult birds were able to replace hair cells lost as a result of cochlea trauma (Cotanche, 1987; Cruz et al., 1987). These studies used either acoustic trauma or gentamicin administration to destroy hair cells in the basilar papilla. Both groups made the unexpected observation that after an initial period of loss, the hair cell population recovered to within pre-trauma levels. Hair cell replacement was accompanied by an almost complete restoration of auditory function (McFadden and Saunders, 1989). Subsequent studies with tritiated thymidine demonstrated that replacement hair cells were in fact the product of support cell division (Corwin and Cotanche, 1988; Ryals and Rubel, 1988). A similar observation was made in the postnatal avian vestibule, where hair cells are also produced continually through mitosis (Jorgensen and Mathiesen, 1988). These experiments provided the first evidence that support cells of the postnatal avian inner ear were able to re-enter the cell cycle and produce new sensory hair cells. This section considers the panoply of events that occur during sensory hair cell regeneration in a chronological order, including the initial mechanisms of hair cell death, epithelial repair and the ensuing production of replacement hair cells. It will encompass experimental work taken from both the avian and mammalian inner ear.

1.4.1 Sensory hair cell death

By definition, the function of a regenerative program is to replace hair cells that have been lost from the sensory epithelium. It follows that initiation of the regenerative program is inextricably linked to the loss of sensory hair cells. The mechanisms of hair cell loss and their associated cellular signals are therefore of great interest. For regeneration studies, the experimental interventions most frequently used to destroy hair cells are acoustic trauma or the administration of ototoxic agents.

Acoustic trauma, also known as noise-induced hearing loss, induces hair cell loss through two concurrent mechanisms: mechanical overstimulation and metabolic stress. Due to the structural properties of the basilar membrane *in vivo*, the exact location of hair cell loss depends upon the spectral content of the auditory stimulus employed. There is a range of effects that can occur in response to mechanical overstimulation. At moderate sound pressure levels (~100 dB SPL), these can be manifest as damage to individual stereocilia within the hair bundle, whereas at higher sound pressures (~110 dB), the stereocilia can become completely splayed and the tip links severed (Robertson et al., 1980; Liberman and Dodds, 1987; Clark and Pickles, 1996). *In extremis*, when the mammalian cochlea is exposed to sound pressures of up to 160 dB SPL, the organ of Corti can be physically disrupted (Bohne and Rabbitt, 1983; Hamernik et al., 1984; Wang et al., 2002). This type of catastrophic insult literally ruptures cell membranes, in addition to permeabilising the epithelial barrier normally constituted by the reticular lamina. A related effect of acoustic overstimulation / noise trauma is glutamate excitotoxicity within the afferent nerve terminals and spiral ganglion neurons (reviewed by Pujol and Puel, 1999). Whilst this can lead to swelling and disruption of the afferent synapse, it does not necessarily result in hair cell death.

A more subtle mechanism of noise-induced hair cell loss can be attributed to metabolic stress and the accumulation of reactive oxygen species (ROS) within the cochlea (reviewed by Henderson et al., 2006). Noise trauma induces apoptosis within cochlea hair cells, which can be rescued by inhibitors of the c-Jun N-terminal kinase (Pirvola et al., 2000; Wang et al., 2003). Noise trauma also results in the activation of the caspase family of cysteine proteases (Nicotera et al., 2003; Yang et al., 2004), however the ability of caspase inhibitors to rescue hair cells has not been reported. Noise trauma also results in the production of high levels of ROS within the cochlea (Yamane et al., 1995; Ohlemiller et al., 1999). ROS are a normal byproduct of the electron transport chain within mitochondria, and increasing amounts are produced as the metabolic demand of the cell increases. Whilst a definitive mechanism linking ROS to apoptosis has yet to be identified, administration of free radical scavengers can rescue hair cells from noise-induced apoptosis, thus providing a strong causal link between the two (Ohinata et al., 2000; Seidman et al., 2003; Lynch et al., 2004).

As an alternative to acoustic trauma, the administration of ototoxic agents allows the auditory and vestibular organs to be targeted both *in vivo* and *in vitro*. Several compounds that find clinical use, the aminoglycoside antibiotics and platinum-based DNA alkylating agents, also possess an undesired yet potent ototoxic activity. This section will focus upon the aminoglycoside antibiotics, which are used extensively throughout hair cell research. Members of the aminoglycoside family include amikacin, gentamicin, netilmicin, kanamycin, neomycin, streptomycin and tobramycin. Their function as antibiotics derives from the ability to bind the 30S ribosomal subunit, thus interfering with bacterial protein translation. Although aminoglycosides are largely cell-impermeable, they can pass through the MET channel and rapidly enter the hair cell (Marcotti et al., 2005). Exposure of the mammalian cochlea and avian basilar papilla to aminoglycosides both *in vivo* and *in vitro*, results in hair cell loss that progresses in severity from base to apex of the organ (Hawkins, 1950; Theopold, 1977; Cruz et al., 1987; Hashino et al., 1991). A similar graded response is observed in the utricle, where type I hair cells of the striola are more sensitive to aminoglycoside insult than their type II counterparts within the cotillus (Wersall and Hawkins, 1962; Lindeman, 1969; Weisleder and Rubel, 1993; Kotecha and Richardson, 1994; Forge et al., 1998; Matsui et al., 2000). Exposure to aminoglycosides triggers apoptosis in hair cells of both the auditory and vestibular organs, which can be prevented by co-administration of caspase inhibitors (Forge, 1985; Forge and Li, 2000; Cunningham et al., 2002; Matsui et al., 2002; Matsui et al., 2003). Inhibitors of the c-Jun N-terminal kinase have also been shown to rescue hair cells from aminoglycoside-induced apoptosis both *in vivo* and *in vitro* (Pirvola et al., 2000; Ylikoski et al., 2002; Wang et al., 2003). Whilst apoptosis appears to be the predominant mechanism of hair cell death in the sensory epithelium, a recent study has suggested that chronic administration of aminoglycosides can also lead to a necrotic cell death (Jiang et al., 2005). As with noise trauma, aminoglycosides appear to promote the production of ROS within hair cells (Hirose et al., 1997). Aminoglycosides are able to form a complex with iron (Fe^{3+}), which can then react with unsaturated fatty acids to form ROS and lipid peroxides (reviewed by Rybak and Whitworth, 2005). Accordingly, the administration of free radical scavengers can rescue hair cells from aminoglycoside-induced hair cell loss (Garetz et al., 1994; Sha and Schacht, 1999, 2000).

1.4.2 Repair of the sensory epithelium

During periods of acoustic or aminoglycoside induced hair cell death, the sensory epithelium undergoes a number of structural alterations. Amongst these is the removal of the hair cell corpse from within the sensory epithelium. In the mammalian inner ear, hair cell corpses in the cochlea appear to be retained beneath the reticular lamina (Forge, 1985; Raphael and Altschuler, 1991b; Li et al., 1995; Forge and Li, 2000; Abrashkin et al., 2006), whilst those in the utricle undergo a combination of ejection and retention (Li et al., 1995; Lang and Liu, 1997). Of the corpses that are retained beneath the epithelial surface, there is mounting evidence that they are phagocytosed by the surrounding support cell population (Forge, 1985; Li et al., 1995; Forge and Li, 2000; Abrashkin et al., 2006). In contrast, aminoglycoside and acoustic trauma models of the avian auditory and vestibular organs report that corpse removal occurs through ejection (Cotanche, 1987; Cotanche and Dopyera, 1990; Weisleder and Rubel, 1993; Matsui et al., 2000; Mangiardi et al., 2004), although there is some limited evidence of retention (Jorgensen, 1988; Raphael, 1993). Irrespective of how the hair cell corpse is eliminated, neighbouring support cells expand to form a 'phalangeal scar' at the surface of the sensory epithelium (Hawkins, 1976; Forge, 1985; Cotanche and Dopyera, 1990; Raphael and Altschuler, 1991a; Meiteles and Raphael, 1994). In situations where the hair cells are retained within the epithelium, support cell processes sever and separate the hair bundle and cuticular plate from the soma.

Scar formation has been proposed as a mechanism to maintain the integrity of the reticular lamina during periods of hair cell loss, thus preventing the ingress of K^+ rich endolymph into the perilymphatic space (Bohne and Rabbitt, 1983; Forge, 1985; Raphael and Altschuler, 1991a). Functional studies using a lanthanum tracer have shown that the barrier properties of the reticular lamina are maintained during aminoglycoside ototoxicity (McDowell et al., 1989). This is not so clear in the case of acute acoustic trauma, where the transient appearance of hair cell sized 'holes' have been reported in the reticular lamina (Bohne and Rabbitt, 1983). Corresponding functional studies using microscopic carbon particles have confirmed that the reticular lamina may be temporarily permeabilised by acute acoustic trauma (Ahmad et al., 2003). The discrepancy between acute acoustic trauma and aminoglycoside treatment possibly reflects the disruptive nature of the former intervention, compared to the controlled degradation of the latter. The importance of a repair mechanism to maintain

the epithelial barrier has been highlighted in a study where the reticular lamina was damaged using a micropipette. Cody *et al.* (1980) demonstrated that the loss of sensory function was evident in areas distal to the original site of hair cell loss, consistent with hair cell depolarisation due to an influx of K^+ ions into the perilymph. It has also been proposed that K^+ influx is responsible for the delayed degeneration of hair cells and support cells that can occur after an acoustic trauma (Bohne and Harding, 2000). Whilst no experiments have definitively shown that exposure of the hair cell basolateral surface to endolymph is toxic *in vivo*, it is likely given the electrical properties of the cell membrane. Thus, a critical function of the support cell population is to maintain the integrity of the reticular lamina and ensure the continued separation of endolymph from perilymph, even during periods of pathophysiology.

The mechanisms that control phalangeal scar formation are poorly understood. The scar itself is enriched with cytokeratins and filamentous actin, highlighting the importance of the support cell cytoskeleton in its formation (Raphael and Altschuler, 1991b; Meiteles and Raphael, 1994). There is some evidence for increased expression and activation of the Rac1 and Cdc42 GTPases following acoustic and aminoglycoside insult, however how these function in the varying cell types is unknown (Gong et al., 1996; Jiang et al., 2006). Amongst the very earliest physiological signals elicited by hair cell damage, the elevation of cytosolic Ca^{2+} and phosphorylation of c-Jun N-terminal kinase (JNK) in neighbouring support cells has been described (Gale et al., 2004; Matsui et al., 2004; Piazza et al., 2006). It remains to be seen whether these signals are involved in scar formation or not.

In parallel to the repair of the sensory epithelium, mention should be made regarding the contribution of macrophages. Macrophages are recruited to sites of hair cell loss in both the mammalian and avian inner ear (Warchol, 1997; Bhave et al., 1998; O'Halloran and Oesterle, 2004; Hirose et al., 2005), where they have been shown to engage in phagocytic activity (Balak et al., 1990; Jones and Corwin, 1993, 1996; Warchol, 1997). Thus, one function for these cells appears to be the removal of dead hair cell debris. Macrophages are also able to secrete a variety of cytokines, which have been shown to influence other aspects of the regenerative process (see Section 1.4.3).

1.4.3 Regeneration I - support cell proliferation

Since the original demonstrations of avian hair cell regeneration, research has identified and characterised several processes that can contribute to the functional recovery observed after trauma (reviewed by Corwin and Oberholtzer, 1997; Stone and Rubel, 2000b; Bermingham-McDonogh and Rubel, 2003). Potential mechanisms that have been proposed thus far involve support cell proliferation, phenotypic conversion and hair cell repair, the contribution of each being dependent upon the system studied. As introduced earlier, support cell proliferation was the first regenerative mechanism to be described in the avian inner ear. Support cells in the avian basilar papilla undergo terminal mitosis during embryogenesis, corresponding with the cessation of hair cell production (Jorgensen and Mathiesen, 1988; Katayama and Corwin, 1989, 1993). Although there is no further mitotic production of hair cells in the adult organ, there is a small activity at the distal end that accounts for the production of additional support cells (Oesterle and Rubel, 1993). In response to acoustic trauma or aminoglycoside insult, support cells in the basilar papilla are triggered to proliferate and subsequently differentiate into new hair cells and support cells (Corwin and Cotanche, 1988; Ryals and Rubel, 1988; Girod et al., 1989; Raphael, 1992; Hashino and Salvi, 1993; Stone and Cotanche, 1994; Tsue et al., 1994; Bhave et al., 1995). In contrast to the basilar papilla, the avian utricle displays a basal level of support cell proliferation that correlates with an ongoing production of hair cells throughout postnatal life (Jorgensen and Mathiesen, 1988; Roberson et al., 1992). The rate of production is matched by a corresponding rate of loss, maintaining the hair cell population at a constant size (Jorgensen and Mathiesen, 1988). Accordingly, estimates for the lifetime of a single vestibular hair cell are in the order of several weeks (Kil et al., 1997; Goodyear et al., 1999). As with the basilar papilla, the utricle is able to increase rates of support cell proliferation and hair cell production in response to aminoglycoside insult (Oesterle et al., 1993; Weisleder and Rubel, 1993; Weisleder et al., 1995; Bhave et al., 1998; Stone et al., 1999; Matsui et al., 2000).

The regenerative potential of the mammalian inner ear differs appreciably from that of Aves and other vertebrates. Support cells of the mammalian cochlea and vestibular organs exit the cell cycle during embryogenesis, signalling the cessation of mitotic activity in the inner ear sensory epithelia (Ruben, 1967; Sans and Chat, 1982). Neither acoustic trauma nor aminoglycoside insult elicits mitotic activity within the

cochlear sensory epithelium, consistent with its inability to regenerate hair cells after insult (Hawkins, 1973; Roberson and Rubel, 1994; Daudet et al., 1998). In the mammalian utricle, support cell proliferation can be induced by aminoglycoside treatment, however its magnitude and that of the corresponding regeneration are severely restricted (Forge et al., 1993; Warchol et al., 1993). The mammalian utricle is also able to regenerate a limited number of hair cells through phenotypic conversion (see Section 1.4.4). Nonetheless, the inability of support cells to effectively re-enter the cell cycle *en masse* severely curtails the regenerative potential of the mammalian inner ear. An important goal of inner ear research is to understand why mammalian support cells are unable to proliferate in response to hair cell loss, unlike their non-mammalian counterparts. An approach to this conundrum, rather than focusing on why it does not occur in mammals, has been to study support cells and how they are triggered to proliferate in other systems. To that end, some studies have sought to identify factors that regulate proliferation within the avian support cell population. The timeframe within which these factors act is reasonably well defined, with initial S-phase entry occurring within 16-24 hours of acoustic, aminoglycoside or laser insult (Hashino and Salvi, 1993; Stone and Cotanche, 1994; Bhave et al., 1995; Warchol and Corwin, 1996). This latency is broadly consistent with the support cell population being in the G0 or G1 interval of the cell cycle at the time of insult. Although the factors promoting cell-cycle progression have not been conclusively identified, the data accrued thus far has provided important clues to their nature.

Early *in vitro* experiments suggested that all of the factors required for support cell proliferation and hair cell production were intrinsic to the avian sensory epithelium itself (Warchol and Corwin, 1993). Even the associated mesenchyme proved dispensable, as epithelial preparations of the utricle demonstrated (Warchol, 1995). In addition to originating within the epithelium, co-culture of damaged and undamaged basilar papillae suggested that at least one of these proliferative factors was diffusible and acted in a paracrine manner (Tsue et al., 1994). Since these original reports, the effects of various growth factors have been characterised upon the avian and mammalian sensory epithelium, however their role during regeneration is far from clear (reviewed by Oesterle and Hume, 1999). For example, basic fibroblast growth factor (FGF-2) has been shown as a potent mitogen within epithelial cultures of the mammalian utricle (Zheng et al., 1997), however it acts to *reduce* support cell

proliferation and promote hair cell differentiation in the avian utricle (Oesterle et al., 2000; Carnicero et al., 2004). Other mitogens, such as insulin growth factor (IGF-1), and transforming growth factor (TGFα) have been shown to promote support cell proliferation in cultures of both the avian and mammalian inner ear (Lambert, 1994; Yamashita and Oesterle, 1995; Oesterle et al., 1997; Zheng et al., 1997; Warchol, 1999). TGFα is a particularly interesting factor, as it can be secreted by activated macrophages. Macrophages are present extensively throughout the sensory epithelia of the avian inner ear, and are recruited to sites of hair cell loss (see Section 1.4.2). A possible role for macrophages was demonstrated by Warchol (1999), where treatment with dexamethasone elicited a reduction in support cell proliferation induced through aminoglycoside insult.

Some form of lateral inhibition exerted by hair cells upon support cells may also regulate proliferation in the avian inner ear. This is supported by observations that support cell proliferation is confined to within areas of hair cell loss (Stone and Cotanche, 1994; Warchol and Corwin, 1996). Notch signalling is a classic mediator of lateral inhibition in the inner ear (reviewed by Lewis, 1998). During embryonic development, activation of the Notch receptor by its corresponding Delta1 ligand is able to regulate cell fate specification through the expression of the Hairy/Enhancer of Split (Hes) transcription factors. Using this mechanism, a nascent hair cell is able to prevent a neighbouring cell from adopting a similar fate. In the regenerating avian inner ear, upregulation of Delta1 expression has been correlated with increased support cell proliferation (Stone and Rubel, 1999). It remains to be seen whether Notch signalling controls support cell proliferation in response to hair cell loss, or whether it acts to specify the fate of post-mitotic cells. A second proposed mechanism of lateral inhibition utilises cadherins, which are a component of the epithelial adherens junction. N-cadherin interactions regulate support cell proliferation in the avian utricle, and they may form the basis of a density dependent system (Warchol, 2002).

In addition to extracellular factors, research has also focused upon a number of intracellular signalling cascades that regulate support cell proliferation within sensory epithelia. In the chick basilar papilla, there is some evidence that elevation of cytosolic cAMP using 8-bromo-cAMP or forskolin can trigger support cell proliferation

(Navaratnam et al., 1996). In the same study, support cell proliferation induced by aminoglycoside insult was effectively reduced using a protein kinase A inhibitor. Similar effects have been observed in cultures of the mammalian utricle, where brief treatment with forskolin can trigger the normally quiescent sensory epithelium to proliferate (Montcouquiol and Corwin, 2001a). These studies highlight the importance of cAMP and PKA signalling in both avian and mammalian tissues. Other studies have looked at the involvement of phosphoinositide 3-OH kinase (PI3K) and the mitogen activated protein kinases (MAPKs) during support cell proliferation. In the murine utricular epithelium, growth factor induced support cell proliferation is strongly dependent upon PI3K signalling (Montcouquiol and Corwin, 2001b). A similar dependence has been reported during serum-induced proliferation in the avian utricular epithelium (Witte et al., 2001). The aforementioned studies also demonstrated that inhibition of the $p44/42^{ERK1+2}$ MAPK was able to significantly reduce support cell proliferation. Thus, several proliferative signalling pathways appear to be conserved between the avian and mammalian sensory epithelium. Involvement of these intracellular signalling cascades during hair cell regeneration has yet to be shown.

1.4.4 Regeneration II - phenotypic conversion and hair cell repair

The second proposed mechanism of regeneration is the direct phenotypic conversion of support cells into sensory hair cells. Several lines of evidence indicate that this phenomenon occurs within damaged inner ear sensory epithelia. The observation that a significant proportion of regenerated hair cells fail to incorporate a mitotic marker in both the basilar papilla (Roberson et al., 1996; Roberson et al., 2004), and the mammalian utricle (Li and Forge, 1997), provides evidence for their non-mitotic production. These studies described an intermediate cell phenotype within the regenerating tissues, exhibiting both a hair bundle at the apical pole in addition to contacting the basement membrane. This morphology has been proposed as evidence for phenotypic conversion of support cells. However, BrdU positive hair cells that differentiate from a support cell division can also exhibit a similar morphology, and caution must be exercised when identifying phenotypic conversion based upon morphological data alone (Stone and Rubel, 2000a). In further support of non-mitotic production, hair cell regeneration occurs in the presence of mitotic inhibitors such as cytosine arabinoside or aphidicolin in both the avian basilar papilla (Adler and Raphael,

1996; Adler et al., 1997), the mammalian utricle (Zheng et al., 1999), and the bullfrog saccule (Baird et al., 2000; Gale et al., 2002).

A third proposed mechanism of functional regeneration is the intracellular repair of damaged hair cells. There is some evidence in the immature mammalian inner ear that mechanical or drug-damaged hair cells can survive within the epithelium and subsequently develop a replacement hair bundle (Sobkowicz et al., 1996, 1997; Zheng et al., 1999). A similar phenomenon has been reported in the bullfrog saccule (Baird et al., 2000; Gale et al., 2002). It is reasonable to assume that in studies where extensive lesions are created, hair cell repair is unlikely to be a significant factor in the ensuing regeneration.

1.4.5 Strategies to promote mammalian regeneration

One of the goals of inner ear research is to provide insight into how regeneration might be stimulated in mammals. Current efforts to that effect can be broadly categorised into intrinsic and extrinsic strategies. Intrinsic strategies are ones that act upon the endogenous cell population to promote proliferation or phenotypic conversion. Extrinsic strategies advocate the introduction of stem cells precursors into the damaged inner ear, however these will not be considered here.

As described earlier, one of the factors limiting mammalian regeneration is the poor induction of support cell proliferation in response to hair cell loss. Attempts to address these using exogenously applied growth factors have met with limited success (see Section 1.4.3). An alternate approach to drive support cell proliferation has been to interfere directly with the cell cycle machinery. One example is $p27^{kip1}$, a cyclin dependent kinase inhibitor (CKI) that is expressed by postmitotic support cells in the mammalian cochlea (Chen and Segil, 1999; Lee et al., 2006). Homozygous deletion of $p27^{kip1}$ from the inner ear results in increased numbers of hair cells and support cells produced within the sensory epithelium (Lowenheim et al., 1999; Kanzaki et al., 2006). It is also associated with a severe hearing loss, which results from the abnormal organisation of the sensory epithelium in postnatal animals. Another CKI gene that has been experimented with is $p19^{Ink4d}$, whose deletion also results in hair cells re-entering the cell cycle (Chen et al., 2003). In these experiments, proliferating hair cells rapidly undergo apoptosis, resulting in a severe hearing loss. Finally, several groups have

examined the role of the retinoblastoma protein, pRb in cell-cycle regulation of sensory epithelia. Deletion of *Rb* from within the inner ear results in hair cells undergoing mitosis (Sage et al., 2005), although these cells subsequently undergo apoptosis resulting in a profound deafness (Mantela et al., 2005; Sage et al., 2006). A clear theme arising from these knockout experiments is that caution must be exercised when manipulating the mitotic status of support cells and hair cells in the inner ear.

A separate approach has been to try to mimic phenotypic conversion of support cells within the mammalian inner ear. This has become possible through discovery of the bHLH transcription factor Math1, the mouse homolog of the *Drosophila* gene *atonal*. Math1 is essential for hair cell development and its deletion in *Math1* knockout mice results in the complete absence of hair cells throughout the auditory and vestibular organs (Bermingham et al., 1999). Consistent with Math1 being a key inducer of hair cell differentiation, ectopic expression *in vitro* results in the appearance of additional hair cells within the sensory epithelium (Zheng and Gao, 2000; Woods et al., 2004). A similar observation has been reported *in vivo*, where adenoviral delivery of *Math1* generates hair cells within and in areas surrounding the sensory epithelium (Kawamoto et al., 2003). In a promising report, Izumikawa *et al.* (Izumikawa et al., 2005) showed that *in vivo* inoculation with a *Math1* adenovirus was able to drive phenotypic conversion of cochlear support cells into hair cells, in addition to eliciting a recovery of auditory function. This constitutes the first demonstration of functional hair cell regeneration in a mammal, but requires further study and characterisation.

1.5 General mechanisms of epithelial wound repair

Epithelial tissues are found extensively throughout the animal body, where they act as multi-purpose barriers between neighbouring tissue compartments or the external environment. Epithelia can possess a wide range of properties, and may be secretory, absorptive or exhibit selective permeabilities to different ion species. Damage sustained through direct trauma, pathophysiology or cellular turnover within the epithelium all threaten to disrupt its normal function. The prompt repair of a damaged epithelium is thus of utmost importance for the continued homeostasis and normal physiology of an animal. This statement is especially pertinent when applied to sensory epithelia of the inner ear. In addition to their direct role in mechanosensation, these epithelia form an impermeable barrier that separates the endolymph from the perilymph. This separation

is critical for auditory and vestibular function, and is reflected by the formation of epithelial scars at sites of hair cell trauma: indicative of a repair mechanism (see Section 1.4.2). When investigating specific mechanisms of epithelial repair in the inner ear, insight can be gathered from studies that use more established models. To that end, this section presents a review of the general mechanisms that are involved during epithelial repair. For brevity, it focuses upon the repair of simple epithelia/monolayers, and does not cover multi-striated systems such as the epidermis; excellent reviews exist for these more complex systems (reviewed by Martin, 1997).

1.5.1 Epithelial migration

Wound repair relies upon a number of cellular mechanisms that are active in both adults and embryos (reviewed by Woolley and Martin, 2000; Jacinto et al., 2001). One such event is the ability of cells to migrate as an epithelial sheet, a process that is fundamental to both morphogenesis and wound closure (Trinkhaus, 1984). Amongst the first observations of directed migration, Rand (1915) proposed that a wounded epithelium would continue to migrate until cell-cell contact was established at its edges. Abercrombie *et al.* (1954) demonstrated a similar phenomenon *in vitro*, conceiving the term 'contact inhibition' (CI) to describe how motile fibroblasts become stationary upon contact with other cells. CI was also demonstrated within epithelial sheets, where cells in contact with the periphery of an epithelium suppressed its migration *in vitro* (Vaughan and Trinkaus, 1966). In essence, wound repair can be considered as an example of cell migration, where trauma creates a new free edge within the epithelium. The opposing sides of the wound then migrate toward each other, covering the denuded area and repairing the defect. At a microscopic level, the migration of a wounded epithelium is associated with several changes amongst its constituent cells. Migrating epithelial cells at the wound border undergo extensive deformations; in addition to projecting filopodia and lamellipodia, they become flattened and distended as they move into the denuded area (Vasiliev et al., 1969; Folkman and Moscona, 1978; Takeuchi, 1979; Radice, 1980; Takeuchi, 1983). Early studies using cytochalasin B and colcemide showed that epithelial wound migration was dependent upon reorganisation of both the actin and microtubule cytoskeleton (Yarnell and Schnebli, 1974; Selden and Schwartz, 1979). Epithelial cells also reorientate their microtubule organising centre (MTOC) to face the direction of migration, as well as forming actin stress fibres that connect to the basal lamina through focal adhesions (Gotlieb et al., 1981; Gordon et al.,

1982; Gordon, 1983; Hergott et al., 1989; Gordon and Staley, 1990). Myosin associates with actin stress fibres to form an actomyosin contractile apparatus (Hormia et al., 1985; Nusrat et al., 1992; Conrad et al., 1993).

Since these original descriptions of epithelial wound migration, the molecular biology of cell movement, and the central role of the cytoskeleton has been well documented (reviewed by Ridley et al., 2003). In particular, the Rho family of small GTPases has an important role in coordinating the wound closure process. The characteristics of the response, which includes stress fibre, lamellipodia and filopodia formation are controlled by the Rho, Rac and Cdc42 proteins respectively (Nobes and Hall, 1995). Unlike Rho and Cdc42, the Rac GTPase is indispensable for epithelial wound migration, with the introduction of dominant negative constructs preventing both cell crawling and lamellipodia formation at the leading edge (Fenteany et al., 2000). For these arresting effects to be realised, Rac must be inhibited in cells up to several rows behind the wound edge. This is consistent with the projection of 'cryptic' lamellipodia from behind the leading edge, suggesting that a substantial portion of the epithelium actively migrates, rather than being pulled by cells at the margin (Farooqui and Fenteany, 2005). The regulation of the Rac GTPase activity by Cool-1 (a Rac GEF) is critical for contact inhibition when the opposing wound edges meet (Zegers et al., 2003). Disruption of this regulatory pathway results in migration that fails to stop once the wound is closed, resulting in cells building up and protruding out of the epithelium. Whilst not essential for epithelial migration, the Cdc42 GTPase is required for cell polarisation and for the correct fusion as the wound edges meet (Nobes and Hall, 1999; Jacinto et al., 2000). Additional functions of the Rho GTPase will be covered in the following section.

1.5.2 Actin cables

In addition to the migratory behaviour of epithelial cells described above, a parallel mechanism has been shown to drive wound closure in some systems. Martin & Lewis (1992), reported that a cable of filamentous actin formed around incisional wounds in the epidermis of chick embryos. The multicellular cable was continuous around the leading wound edge, and was proposed to act as a contractile 'purse-string', coordinating movement and physically pulling the wound edges together. Bement *et al.* (1993), demonstrated a similar phenomena in the gut epithelium, where an acto-myosin

cable formed around incisional wounds. Preceding these findings, acto-myosin cables had already been described during cytokinesis, where they act to separate the nucleus during anaphase (reviewed by Field et al., 1999). Contractile actin cables have since been shown to underlie the morphogenetic processes of dorsal closure in *Drosophila melanogaster* (reviewed by Harden, 2002), in addition to driving the repair of sub-cellular wounds and extruding dying cells from epithelia (Bement et al., 1999; Rosenblatt et al., 2001). This section will focus upon actin cables engaged in multicellular wound repair and dorsal closure, although many of the mechanisms covered are of relevance to the other examples cited (reviewed by Kiehart, 1999).

Analogous to that described for epithelial migration, cable formation is an active process requiring *de novo* polymerisation of actin filaments (McCluskey and Martin, 1995). The Rho GTPase is intimately involved in the formation of an actin cable around the epithelial wound (Brock et al., 1996; Wood et al., 2002), as is its effector Rho kinase (Russo et al., 2005). Similar observations have been made in *Drosophila*, where disruption of the Rho GTPase leads to defects in actin cable formation and dorsal closure (Magie et al., 1999; Bloor and Kiehart, 2002; Jacinto et al., 2002). The other prototype Rho GTPases, Rac and Cdc42 do not appear to be directly involved in cable formation, although they have other functions during wound closure (see section on epithelial migration). Formation is rapid, with actin filaments accumulating into the cable within minutes of wounding (Brock et al., 1996; Wood et al., 2002). Once assembled, the actin cable is a multicellular structure that connects to neighbouring cells through the adherens junctions, creating a mechanical syncytium (Brock et al., 1996; Danjo and Gipson, 1998; Wood et al., 2002). Adherens junctions are critical for the structural integrity of the actin cable, and disruption of extracellular cadherin interactions result in its disassembly (Danjo and Gipson, 1998). As the actin cable contracts and describes an ever decreasing perimeter, cells detach from the leading edge in a process called 'zipping' (Brock et al., 1996; Jacinto et al., 2000). Zipping allows the actin cable to shorten, whilst allowing cells to maintain a reasonably normal morphology as they are pulled over the denuded area.

It is clear that the actin cable forms the leading edge of the wounded epithelium, however an important question has been whether it actually drives closure by *generating* a contractile force, or whether it serves to coordinate the movement of cells

along the wound border. The motor protein non-muscle myosin II has been shown to associate with the actin cable during wound and dorsal closure, suggesting that it is indeed capable of generating contractile force (Young et al., 1993; Brock et al., 1996; Danjo and Gipson, 1998). In epithelial wounding models, inhibition of the myosin light chain kinase is able to prevent actin cable contraction, consistent with its role regulating NM-myosin II activity (Russo et al., 2005). Null mutations of the NM-myosin II (*zipper*) gene in *Drosophila* embryos results in defective cable formation and irregular dorsal closure; however, this phenotype renders it difficult to assess whether the actin cable is contractile or not (Young et al., 1993; Jacinto et al., 2000). This problem was overcome using laser ablation to destroy regions of the embryo and ultimately determine whether they are involved in force generation. These studies have demonstrated that the majority of force required during dorsal closure is provided by the actin cable itself (Kiehart et al., 2000; Hutson et al., 2003). More recently, Franke et al. (2005) have used ectopically expressed NM-myosin-GFP to rescue the dorsal closure defect in *zipper* embryos. The resulting expression mosaics show that cells expressing the fluorescent rescue construct are able to contract, whilst those expressing at a lower level become stretched and distended. Taken together, these studies provide strong evidence that actin cables are contractile and that they require NM-myosin II to generate forces during wound repair and dorsal closure.

In addition to powering morphogenetic events and repair of multicellular wounds, actin cables have also been described in the restitution of single cell epithelial defects. When a cell is mechanically disrupted in the gallbladder epithelium, the neighbouring cells are able to move together and extrude the dying cell within thirty minutes (Hudspeth, 1975). The rapid epithelial repair of the defect is also accompanied by the restoration of the transepithelial resistance, a measure of how permeable the epithelium is to ionic flux. Similar experiments in MDCK monolayers have shown that the repair of a single cell defect utilises an acto-myosin cable to squeeze the corpse out of the epithelium, in addition to pulling neighbouring cells together (Rosenblatt et al., 2001). In agreement with findings from larger wounds and dorsal closure, this study demonstrated the requirement for Rho GTPase activity in actin cable formation, and for myosin light chain in cable contraction. Similar results have been reported in a gut epithelial cell line (Florian et al., 2002).

Epithelial migration and actin cables are not necessarily mutually exclusive modes of wound closure; there is evidence that they can cooperate in a number of systems. Bement *et al.* (Bement et al., 1993) demonstrated that lamellipodia project into the denuded area of a wound, in advance of the actin cable. Whilst not absolute proof that these cells provided motile force independently of the actin cable, it is highly suggestive that they were crawling. More substantive evidence has come from experiments in *Drosophila*, where in the absence of an actin cable, Rho mutant embryos are able to re-epithelialise wounds using cell crawling (Wood et al., 2002). Whilst contractile actin cables are not present in stripe wounds of the type commonly used in migration assays, acto-myosin bundles are present at the wound border (Farooqui and Fenteany, 2005). Disruption of these bundles using Rho kinase or NM-myosin II inhibitors does not halt wound closure, instead making migration less coordinated and cohesive. Thus, actin cables can be involved in coordinating cell movements, as well as driving them.

1.5.3 Proliferation

Wounding is not just associated with the physical repair of the epithelial defect, but also with proliferation amongst the surviving cell population. Early investigations into wound closure noted that there was an increase in DNA synthesis approximately 12 hours after the onset of migration (Todaro et al., 1965; Vasiliev et al., 1969; Dulbecco and Stoker, 1970). Furthermore, DNA synthesis was generally restricted to cells that were migrating into the denuded area, providing anecdotal evidence that DNA synthesis was the sequel of cell migration. Abolition of cell migration using cytochalasin B has been shown to block DNA synthesis (Selden et al., 1981), however these experiments are difficult to interpret given that mitotic signalling is regulated in part by the cytoskeleton (Huang and Ingber, 2002). Irrespective of this, it is quite clear that cell proliferation is not required for cell migration or successful wound re-epithelialisation (Lipton et al., 1971; Sponsel et al., 1994; Farooqui and Fenteany, 2005).

One of the major mechanisms regulating epithelial proliferation derives from the phenomenon of density dependent inhibition (DDI); a mechanism that acts to reduce proliferation as the density of an epithelium approaches an arbitrary upper limit (Stoker and Rubin, 1967). This phenomena is distinct from the regulation of cell motility through contact inhibition (CI), as first described by Abercrombie *et al.* (Abercrombie

and Heaysman, 1954). How is DDI regulated in an epithelial system? Assuming there is an adequate supply of basic nutrients, cell-cell contact appears to be the predominant regulatory factor. The proteolytic digestion of cell-surface proteins by trypsin has been shown to strongly stimulate proliferation in cell monolayers, due to the severing of lateral extracellular linkages (Sefton and Rubin, 1970). Selden *et al.* (1981) reported a similar increase in proliferation when colchicine was used to disrupt microtubules and cause cells to retract from one another, thereby severing extracellular linkages. Cadherins associated with the adherens junction are one example of an extracellular linkage that connects neighbouring cells together. Interfering with cadherin function has been shown to regulate cell proliferation, highlighting their potential importance in DDI signalling (St Croix et al., 1998; Levenberg et al., 1999; Warchol, 2002).

The framework of DDI can be used to explain the increase of proliferation observed in a wounded epithelium. The physical event of migration is associated with flattening of the soma and a *de facto* reduction in the local cell density. Given that cells at the wound edge migrate significantly more than those in unwounded areas, the local density in the wound falls below a threshold, whilst remaining unperturbed elsewhere (Rosen and Misfeldt, 1980). This concurs with observations of proliferation being restricted to within the original wound area, as this is the only area that experiences a significant reduction in density. Proliferation within the wound will continue to occur until the cell density within the wound is restored to its normal upper value. Thus, proliferation can be triggered by a reduced cell density in the wound that occurs as a direct result of cell migration. Cell morphology may also be a contributing factor to proliferative signalling in wounded epithelia (Folkman and Moscona, 1978). Many cells require both a flattened morphology and a network of actin stress fibres in order to respond to mitotic stimuli (reviewed by Huang and Ingber, 1999); this is the exact morphology displayed by cells migrating into a wounded area.

1.5.4 Wound signalling

A remaining question is how these reparative processes are initiated in response to wounding. This section will cover the growing number of signals that have been shown to communicate epithelial damage and coordinate the ensuing repair. One of the earliest recorded signalling events elicited by mechanical wounding is an intercellular calcium (Ca^{2+}) wave that spreads within cells proximal to the wound site. The increase

in cytosolic Ca^{2+} occurs within seconds of wounding, and can remain elevated for several minutes (Hansen et al., 1993; Sammak et al., 1997). Several mechanisms have been proposed to account for the initial increase in cytosolic Ca^{2+} observed in wound edge cells. One such mechanism relies upon the transient permeabilisation of the plasma membrane by local trauma: a phenomenon known as 'scrape-loading' (McNeil et al., 1984). This can allow a range of molecules, including ions such as Ca^{2+}, to temporarily traverse the plasma membrane and enter the cytoplasm. Another rich source of signalling arises from wound-induced cell lysis, which results in the release of biologically active molecules into the extracellular space. Adenosine 5'-triphosphate (ATP) is one such molecule that is stored in high concentrations (~ mM) within cells and elicits a diversity of purinergic signalling upon its release (reviewed by Burnstock, 2006). As an example, epithelial cells respond to exogenously applied ATP by mobilising Ca^{2+} from their internal stores (Hansen et al., 1993). The requirement for *extracellular* ATP in wound-induced signalling is supported by evidence that Ca^{2+} waves can propagate across acellular regions (Sammak et al., 1997), and that apyrase can inactivate the Ca^{2+} mobilising effects of wound-conditioned media (Klepeis et al., 2001). Once mobilised within the cytoplasm, Ca^{2+} is a potent modulator of cell physiology and has the potential to regulate a wide range of signalling pathways (reviewed by Berridge et al., 2003). Accordingly, wound-induced Ca^{2+} signalling appears to be essential for the initial cell migration observed during repair (Tran et al., 1999).

Downstream of these rapid signalling events, several effector proteins have been implicated during the initial stages of epithelial repair. The activation of transcription factors is an important part of this process. The immediate early gene (IEG) c-fos is expressed within 15 minutes of wounding (Verrier et al., 1986; Martin and Nobes, 1992), and subsequent studies have shown that c-jun, krox-20 and krox-24 (egr-1) can also be induced (Dieckgraefe et al., 1997; Dieckgraefe and Weems, 1999; Tran et al., 1999; Grose et al., 2002). Antisense knockdown of c-fos elicits a reduction in the rate of wound edge migration, highlighting the importance of this IEG in the repair process (Tran et al., 1999). In this particular example, the induction of c-fos could be prevented by blocking wound-induced Ca^{2+} signalling; demonstrating a link between Ca^{2+} and transcriptional activity. Defective wound migration is also evident in cells which are null for c-jun (Li et al., 2003). In contrast to c-fos and c-jun, genetic deletions of krox-

20 or krox-24 do not display any wound healing phenotype (Grose et al., 2002). IEG expression is typically driven through signalling pathways like that of the mitogen activated protein kinases (MAPK). In particular, $p44/42^{ERK1/2}$ (ERK) activity has been shown to induce a number of IEGs during epithelial wounding (Dieckgraefe and Weems, 1999). ERK is activated symmetrically around the wound site, corresponding with a similar induction of c-fos (Martin and Nobes, 1992; Nobes and Hall, 1999). Inhibition of Ras or ERK activation is also able to prevent wound-induced cell migration (Nobes and Hall, 1999; Matsubayashi et al., 2004).

Some mechanisms of wound signalling appear to occur without any transcriptional component. For example, Brock *et al.* (1996) have shown that an actin cable begins to form within two minutes of wounding, which is clearly too rapid for the transcription of new gene products. What are the signals that can trigger cytoskeletal reorganisation within this short timeframe? One suggestion is that wounding releases mechanical tensions that are present within the epithelium and that the redistribution of force is sufficient to induce cytoskeletal reorganisation (Sherratt et al., 1992). This theory is based upon observations that within minutes of being placed under a longitudinal stress, actin filaments within a cell are able to realign along a parallel axis (Kolega, 1986). A molecular explanation has yet to be proposed for this phenomenon, although many studies are reporting how mechanical forces can influence cell biology (reviewed by Ingber, 2006). Another suggestion for the rapid reorganisation is that the initial wound signals are able to influence the cytoskeleton directly. MAPK might play a role here as many of them have cytosolic phosphorylation targets, in addition to nuclear ones. For example, ERK has been shown to phosphorylate myosin light chain kinase (MLCK), whilst JNK has been shown to target paxillin (Huang et al., 2003). An alternative/parallel explanation is that wound-induced Ca^{2+} signalling is able to activate (indirectly or otherwise) a wide range of protein kinases, which can subsequently regulate the Rho GTPases though GEFs such as Tiam1 (reviewed by Rossman et al., 2005). Although a relatively new area of research, there is growing evidence for the requirement of RhoGEFs during wound closure (Zegers et al., 2003).

1.6 Scope of research

This introduction has drawn broad parallels between the general events of wound re-epithelialisation and proliferation to those that occur subsequent to hair cell loss in avian sensory epithelia. To further our understanding of how the avian inner ear responds to insult, the experiments that follow will examine these potential equivalencies. In particular, they will focus upon epithelial repair, which is poorly understood within hair cell sensory organs. Repair is of especial interest; since this process is potentially active during hair cell death, it may contain cues that direct the ensuing regenerative programme. To that end, experiments will examine both cytoskeletal reorganisation and proliferative induction in response to epithelial trauma, and attempt to identify signalling pathways that coordinate these processes.

2 Materials and methods

2.1 Materials

2.1.1 General reagents

Laboratory reagents were purchased from Sigma unless otherwise stated. Alexa Fluor conjugated phallotoxins and IgG secondary antibodies were obtained from Molecular Probes (Invitrogen, UK). Protein kinase and other small molecule inhibitors were obtained from Calbiochem (EMD Biosciences, UK).

2.1.2 Cell culture reagents

Cell culture media and heat inactivated foetal bovine serum (FBS) were purchased from GIBCO (Invitrogen, UK). Abbreviations have been used throughout to denote standard media formulations:

M199H: Medium 199 with Hank's salts, 25 mM HEPES & 50 μM phenol red.
M199E: Medium 199 with Earle's salts, 25 mM HEPES & 50 μM phenol red.
M199: Medium 199 with Earle's salts.
DMEM: Dulbecco's Modified Eagle Medium, 10 mM HEPES.

2.1.3 Plasmids

The cDNA encoding the enhanced GFP human β-actin (β-actin-EGFP) fusion protein was excised from a pcDNA3.1 vector (a kind gift from Professor Steven Moss; Institute of Ophthalmology, UCL, UK) and sub-cloned into the Cla12 adaptor plasmid. The β-actin-EGFP cDNA was then excised using the Cla1 enzyme, and ligated into the Cla1 site of the RCASBP(B) construct (Morgan and Fekete, 1996) to generate the RCASBP(B)-β-actin-EGFP plasmid. The orientation of the insert was controlled by sequencing, and the plasmid DNA solution (1-2 mg/ml) used for electroporation was prepared using the EndoFree purification kit (Qiagen, UK).

2.1.4 Primary antibodies

Primary antibodies used for immunocytochemistry are listed below. The species from which the antigen was derived has been indicated, along with the working dilution

used. Unless specified, all incubations were performed overnight at 4°C in a blocking solution.

1:1000 αp44/42^{ERK1+2} di-phospho (YT), mouse mAb IgG (M8159, Sigma).
1:100 αMyosinIIB (chick), mouse mAb IgG (CMII 23, Iowa Hybridoma Bank, USA).
1:100 αBrdU (human), mouse mAb IgG_1 (555627, BD Biosciences, USA).
1:500 αBrdU-Alexa 488, IgG_1 direct conjugate (A21303, Molecular Probes).
1:500 αKUL01 (chick), mouse mAb IgG_1 (a gift from Prof. Goddeeris).
1:500 αHCS-1 (chick), mouse mAb IgG_{2A} (a gift from Prof. J. Corwin).
1:1000 αHCA (chick), mouse mAb IgG_1 (a gift from Prof. G. Richardson).

2.2 Animals

Chicken embryos were maintained in accordance with UK Home Office and UCL local regulations. Postnatal chickens were housed at the Animal Care Facility, Central Institute for the Deaf, Washington University (St Louis, MO, USA) in accordance with NIH and local guidelines. *In ovo* electroporation of RCASBP(B)-β-actin-EGFP and maintenance of infected embryos until E19 was authorised under a UK Home Office Project License.

2.2.1 Embryonic chickens

Fertile White Leghorn (*Gallus gallus*) chicken eggs were obtained from Henry Stewart and Co. Ltd. (UK). Embryos were maintained at 38°C in a humidified rocking incubator. Embryos were killed on day 21 in accordance with Schedule 1 of the UK Animals in Scientific Procedures Act 1986.

2.2.2 Postnatal chickens

Fertile White Leghorn (*Gallus gallus*) chicken embryos were obtained from Charles River SPAFAS (MA, USA). Embryos were hatched and transferred to a heated brooder where food and water were supplied. P7-14 chickens were anaesthetised using a rising concentration of carbon dioxide, and killed in accordance with NIH guidelines.

2.2.3 In ovo electroporation of chick embryos

Fertile White Leghorn embryos (see Section 2.2.1) were kept at 38°C in a humidified incubator. Eggs were windowed to allow access to the developing embryo, and were staged according to the Hamburger-Hamilton charts (Hamburger and Hamilton, 1992). Electroporation of the inner ear primordium was performed whilst the otic vesicle was forming (stage 12), and before it closed (stage 14). To aid visualisation, concentrated fast green was mixed 1:10 with RCASBP(B)-β-actin-EGFP plasmid DNA (1 μg/μl in Tris-HCl pH 8.0). This solution was loaded into a glass micropipette, and mounted on a micro-pressure injector. Gold plated platinum electrodes were connected to an ECM 830 generator (BTX, PA, USA) that was programmed to deliver the electroporation waveform (10v, 4 x 30 ms pulse-width). Under a dissecting microscope, the vitelline membrane was gently punctured, and sterile PBS added to separate it from the embryo. The vitelline membrane was cut away to allow adequate access using the micromanipulators. The electrodes were lowered into the egg using a micromanipulator, and positioned across the dorsal-ventral axis with the cathode facing the otic vesicle. A second manipulator was used to position the micropipette tip just inside the cup. The otic vesicle was filled with plasmid DNA solution, and the electroporation waveform immediately applied. After electroporation, the manipulators were carefully removed, the egg sealed with clear tape and returned to the incubator. One day later, embryos were examined for EGFP fluorescence using an AxioPlan microscope with a low magnification objective. EGFP negative embryos were destroyed by freezing at minus 20°C. Positive embryos were returned to the incubator and maintained up until E19.

2.3 Dissection

All dissections were performed in a laminar flow hood using aseptic sterile technique. Chick heads were briefly sprayed with 70% ethanol before the overlying skin was removed. Subsequent harvest of the vestibular organs was dependant upon developmental stage.

2.3.1 Embryonic gross dissection (medial approach)

For chicken embryos up to E21, the bone was still relatively soft, allowing the skull to be cut into two halves along the sagittal plane. Once the brain was removed, the two halves of the skull were placed into chilled dissection media (M199H). Coarse

forceps were used to remove **bone from the medial side of the temporal bone,** until the otoliths of the saccule and utricle were visible. Fine forceps were then used to remove the saccule and utricle into a spoon for transfer to fresh dissection media.

2.3.2 Postnatal gross dissection (lateral approach)

Due to calcification of the skull at this age, a lateral approach to the temporal bone was employed. A scalpel blade was used to slice a thin sagittal section from the side of the head, fully exposing the middle ear. Forceps were used to remove the collumella and tympanic membrane revealing the oval and round windows of the basilar papilla. Bone was carefully removed directly posterior to the oval and round windows, exposing the hook region at the base of the basilar papilla. The hook was grasped firmly using forceps and the basilar papilla removed with a sharp tug. The saccule and utricle were contained within the temporal bone just superior to the oval window. Forceps were used to score around this region, such that the temporal bone could be removed intact from the skull and placed in dissection media (M199H). The excised temporal bone was then fully opened by placing fine forceps into the bony suture and prising the two sides apart. The ampullae, saccule and utricle were teased out using forceps.

2.3.3 Micro-dissection of the utricle

Iridectomy scissors were used to dissect away the semicircular canals, as well as the lateral and superior ampullae. The otoconial membrane was removed by gentle aspiration using a 200µl pipette. Utricles were either cultured as whole explants (see Section 2.4.2), or prepared as epithelial cultures (see Section 2.4.1).

2.4 Cell culture

All cultures were maintained in an incubator at 37°C with a humidified 5% CO_2 atmosphere. Procedures involving cell cultures were performed in a laminar flow hood using established aseptic techniques.

2.4.1 Epithelial culture of the utricular sensory epithelium

The epithelial culture technique described here is adapted from Warchol (2002). Dissected utricles were incubated for 30 minutes at 37°C, 5% CO_2 in M199E supplemented with 0.5 mg/ml thermolysin. Utricles were then transferred to chilled M199H 10% FBS for 10 minutes in order to stop the enzymatic reaction. The utricular

macula was trimmed into a square shape using iridectomy scissors, and then cut into quarters using a sapphire knife. The shearing action created by both scissors and knife was sufficient to separate the sensory epithelium from the stroma. The sensory epithelium was then gently teased away using a hypodermic needle. Pieces of epithelial tissue were transferred to glass cover-slipped culture dishes containing M199E 10% FBS (#0 cover-slip, Mattek, MA, USA). Coverslips were coated beforehand for 3 hours using either: a) 100 μg/ml laminin b) 100 μg/ml laminin & 50 μg/ml fibronectin. To make the epithelium adhere flat to the glass coverslip, the culture media was withdrawn for a brief period (< 10 seconds), and then replaced. In the majority of cases this was sufficient to make the epithelium adhere flat to the coverslip. *Embryonic* cultures were maintained in M199E 10% FBS, for 1-2 days before they were used in experiments. *Postnatal* cultures were maintained in DMEM 10% FBS for at least 7 days before use.

2.4.2 Whole organ culture

Whole utricles were maintained as free-floating explants in sterile 36 well culture plates with 0.5 ml of M199E 2.5% FBS. Utricles were orientated such that the stereocilia were facing upwards, away from the base of the culture well.

2.5 Epithelial & whole organ experiments

All epithelial experiments were performed at room temperature (25°C), unless otherwise stated. Where inhibitors were added to culture medium, the final concentration of solvent was kept at or below 0.1%.

2.5.1 Laser wounding setup

Epithelial wounds were created using the Micropoint system (Photonic Instruments Inc., IL, USA). Briefly, the setup consisted of a pulsed nitrogen laser (70kW peak output, 70ns, 337 nm) coupled to coumarin dye cell (337 nm input, 440 nm output). The λ-shifted laser beam was then collated through a lens into the epi-fluorescence port of a Zeiss Axiovert 100TV. The laser beam was focused onto the epithelial sample using a 40x Fluar objective (1.4 NA, oil immersion). Several pulses of the laser were sufficient to disrupt the tissue, and leave a fracture in the glass coverslip. Puncture wounds of the sensory epithelium were achieved by holding the microscope

stage steady whilst discharging the laser. Stripe wounds were created by moving the stage, to create in effect a series of puncture wounds.

In epithelial cultures that were expressing the RCASBP(B)-β-actin-EGFP construct, an additional consideration was to place the laser wound near, or within a patch of expressing cells. To achieve this, the sample was illuminated briefly using a mercury vapour lamp and a FITC filter set. Neutral density filters were used to limit the exposure intensity. A suitable patch of expression was located and placed under the laser target reticule. The laser was then discharged to wound the epithelium.

2.5.2 Wound healing experiments

Culture medium was replaced with M199E two hours before a laser ablation was made. Epithelia were wounded as described above, and returned to the cell-culture incubator. For live imaging experiments, ablated epithelia were removed briefly from the incubator and imaged using the 40x Fluar objective with DIC optics. Epithelia were imaged at the same position at 10, 30, 60, 120, 180 and 240 minutes post ablation to create a discrete time-lapse series. Cultures were returned to the incubator when not being imaged.

For examining the effects of inhibitors upon epithelial structure, cultures were pre-incubated for two hours using M199E supplemented with either: a) 20 μM U0126, b) 30 μM Y-27632, c) 100 μM blebbistatin (±), d) 0.1 μM cytochalasin D, e) 0.1% DMSO vehicle control. Cultures were laser ablated, and returned to the incubator for 1, 2, 3 or 4 hours before they were fixed using 4% paraformaldehyde. Samples were processed for myosin IIB and/or phalloidin immunocytochemistry (see Section 2.7).

2.5.3 BrdU incorporation experiments

For experiments using the embryonic model, culture media was replaced one hours after laser ablation with M199E 10% FBS, supplemented with 3 μg/μl BrdU. Cultures were subsequently fixed in 4% paraformaldehyde 48 hours after original laser ablation was made. Fixed samples were processed for HCS-1 and BrdU immunocytochemistry (see Section 2.7.3).

For experiments using the postnatal model, epithelial cultures were pre-incubated for one hour using DMEM 10% FBS supplemented with either a) 10μM U0126, b) 15μM SP600125, c) 30μM LY294002, d) 0.1% DMSO. Epithelia were then wounded and returned to the incubator. One hour after ablation, culture media was cycled with fresh DMEM 10% FBS containing the inhibitor and 3 μg/μl BrdU. Culture media was cycled again 24 hours after the original wound was made with media containing fresh inhibitor solutions and BrdU. Cultures were fixed in 4% paraformaldehyde 48 hours after the original wound was made. Fixed samples were processed for BrdU immunocytochemistry (see Section 2.7.3).

2.5.4 ERK activation assay

For the standard activation time course, cultures were pre-incubated for 2 hours using M199E. Epithelia were then laser ablated and returned the cell culture incubator. After 5, 30 or 60 minutes, epithelia were removed from the incubator and fixed using 4% paraformaldehyde. Epithelia constituting the one-minute time point were fixed immediately after laser ablation. The test the potency of the MEK inhibitor U0126, epithelia were pre-incubated for 2 hours with either a) 20 μM U0126, b) 0.1% DMSO. Epithelia were laser wounded, and returned to the incubator for 5 minutes prior to fixation. All epithelia were processed for αphospho-ERK immunocytochemistry (see Section 2.7.2), and counterstained with phalloidin.

2.5.5 Streptomycin treatment of whole organs

Whole organs were maintained for at least 24 hours *in vitro* before used for experimentation. Culture media was cycled using fresh M199E 2.5% FBS supplemented with 1 mM streptomycin sulphate. Utricles were incubated for a further 12, 18 or 24 hours, and then fixed. A 48 hours time point was devised by incubating utricles in 1mM streptomycin for 24 hours, and then for a further 24 hours in normal media without streptomycin. Control utricles were sham operated with M199E 2.5% FBS, and fixed 24 hours later. Utricles were subsequently processed for either αHCS-1 or αKUL01 immunocytochemistry (see Section 2.7.2). All utricles were counterstained using phalloidin and DAPI.

2.6 Confocal time-lapse imaging

2.6.1 Imaging apparatus

Imaging of live cell preparations was performed using a Nipkow spinning disk confocal microscope (Ultraview ERS, Perkin Elmer, UK), attached to a Zeiss Axiovert 200 inverted microscope. Long-term focus stability was achieved using an anti-vibration air table, and by incubating the entire microscope stage at 37°C. A small perspex chamber mounted on the microscope stage allowed the sample to be maintained in a balanced air 5% CO_2 atmosphere for the duration of the experiment. This allowed bicarbonate to be used as the primary media pH buffer. Imaging media consisted of M199, without HEPES or phenol red. In particular, HEPES was omitted as it is known to be phototoxic, producing hydrogen peroxide when irradiated by UV or visible light (Zigler et al., 1985). This placed an *absolute* requirement for a 5% CO_2 atmosphere to be present at *all* times; in the absence of a secondary buffer system, the pH would exceed 8 $\log_{10}$ units within minutes. To ensure continuous pH buffering, all solutions were bubbled with sterile-filtered 5% CO_2 before use, Mattek dishes were sealed under a 5% CO_2 atmosphere, and 5% CO_2 was supplied to the incubation chamber at all times.

2.6.2 Imaging EGFP in epithelial cultures

Epithelial cultures of RCAS-β-actin-EGFP positive utricles were prepared in exactly the same manner as wild-type tissues (see Section 2.4.1). Epithelial cultures were maintained in M199E 10% FBS for at least two days before use. Two hours before the experiment commenced, culture media was replaced with M199 imaging media. An area of expression was located, and a laser ablation made as described in Section 2.5.1. Immediately after ablation, the culture was transferred to the Nipkow system. Approximately five minutes elapsed between laser ablation and the commencement of the time-lapse. A 63x NeoFluar objective (1.4NA, oil immersion) was used to locate the epithelial wound using brightfield illumination, and for subsequent epi-fluorescent confocal imaging. A 488 nm laser line was used to excite the EGFP fluorophore, and epi-fluorescence collected through a long pass GFP filter (LP 505nm). The Ultraview imaging suite was set up to capture a single image every 3 minutes. The CCD camera was set to capture at 2 x 2 binning (640 x 512 effective pixels).

2.6.3 Imaging EGFP & TOTO-3 in whole organs

Freshly isolated RCASBP(B)-β-actin-EGFP positive utricles were transferred to a Mattek dish in M199H, and positioned underneath a sterile platinum harp threaded with fine nylon. Utricles were orientated with the epithelial surface and stereocilia facing towards the coverslip. The harp was positioned to hold the utricle at the anterior and posterior edges only. Due to the slight curvature of the organ, the intervening region was typically suspended above the coverslip, but still within the objective's working distance. This arrangement preserved stereocilia morphology *in vitro*, and could be maintained for at least 72 hours. Once correctly restrained, M199H was replaced with pre-gassed M199 media. At this stage, 1 mM streptomycin sulphate was optionally added to the culture medium. For dual-channel recordings, 0.1 μM TOTO-3 was also added to the imaging media. TOTO-3 is large (1355 MW) cell-impermeant cyanine dimer that fluoresces in the far-red spectrum upon binding DNA. TOTO-3 was excited using the 647 nm laser line. The dish was then sealed under a balanced air 5% CO_2 atmosphere, carefully transferred to the microscope stage, and left to settle for one hour. Utricles were imaged using a 63x NeoFluar objective (1.4NA, oil immersion), with the Nipkow system set to capture a 40 μm z-stack (20 x 2 μm) every 5 minutes. The CCD camera was set to 2 x 2 binning (640 x 512 effective pixels).

For single-channel EGFP experiments, a 488 nm dichroic mirror was used in conjunction with a 505 nm long-pass emission filter. This ensured maximum transmission of the EGFP signal. EGFP fluorescence was excited using a 488 nm laser line. For dual-channel EGFP & TOTO-3 experiments, a multi-wavelength 488/568/647nm dichroic was used in conjunction with a band-pass 505 nm and a long-pass 650 nm emission filter. The use of a multi-wavelength dichroic mirror resulted in reduced transmission efficiencies, and lower signal to noise ratios. EGFP and TOTO-3 were excited using a 488 nm and 647 nm laser line respectively.

2.7 Immunocytochemistry

All washes were 3 x 5 minutes in 0.01 M phosphate buffered saline (PBS). All incubations were performed at room temperature unless otherwise stated.

2.7.1 Fixation

Tissues were fixed using 4% paraformaldehyde in 0.01 M PBS for 1 hour (whole organs) or 30 minutes (epithelial cultures). Tissue that was not processed immediately for immunocytochemistry was stored at +4°C in PBS with 0.05% (w/v) NaN_3 added as a preservative.

2.7.2 Primary antibodies + detection

Samples were pre-incubated with horse blocking solution (PBS, 0.2% Triton X-100, 10% horse serum) for one hour to permeabilise cell membranes and reduce non-specific binding protein interactions. Antibodies were diluted to the required concentration in blocking solution (see Section 2.1.4), and incubated overnight at +4°C. Antibody binding was assessed *in situ* using immunofluorescence. After the specified incubation period, primary antibodies were removed and the samples were thoroughly washed. Samples were then incubated in goat blocking solution (PBS, 0.2% Triton X-100, 10% goat serum) for 30 minutes. Alexa Fluor donkey α-goat IgG secondary antibodies were centrifuged briefly, diluted 1:500 into blocking solution and then incubated with the tissue sample for 2 hours. Samples were washed and counterstained (see Section 2.7.4). Incubation with the secondary antibody alone served as a negative control for the primary labelling.

2.7.3 BrdU Immunocytochemistry

Detection of BrdU required a retrieval step in order to expose the antigen from within nuclear DNA. If appropriate, epithelia were first incubated overnight with 1:500 HCS-1 and reacted with IgG_{2A} Alexa 546 as before. Epithelia were then incubated for 30 minutes in 2N HCl, followed by 30 minutes in blocking solution. Epithelia were incubated overnight in 1:500 αBrdU-Alexa 488 conjugate. BrdU labelled epithelia were counterstained using DAPI. Alexa 546 appeared to tolerate the limited exposure to HCl.

2.7.4 Counterstains

Samples were incubated for 30 minutes with 10 μM DAPI and/or 1:100 of an Alexa 633 phalloidin conjugate diluted in PBS 0.2% Triton X-100. Samples were washed, and mounted in a solution of 90% glycerol, 10% PBS. Samples were stored at +4°C until imaged.

2.7.5 Confocal imaging

Fluorescent samples were visualised using a Zeiss LSM 510 system attached to a motorised Axiovert 200 microscope. Samples were imaged using a selection of objectives: 10x Fluar (0.5 NA, air), 20x Plan-Apochromat (0.7 NA, air) or 63x Plan-Apochromat (1.3 NA, oil immersion).

2.8 Visualisation & data analysis

2.8.1 Software

TIFF and LSM images from the Zeiss 510 system were processed and analysed using freely available open-source software. ImageJ, a JAVA based analysis package was used for general morphometric analysis and cell counts (http://rsb.info.nih.gov/ij/, NIH, USA). OsiriX was used for 3-dimensional visualisation of LSM files (http://osirixmac.com). Images captured using the Nipkow system were analysed using proprietary software from Perkin Elmer, or imported into Volocity for 3d visualisation (Improvision, UK). Numerical data was compiled in Excel 2004 (Microsoft, UK). All subsequent analyses and graphs were produced using this software. Figures and illustrations were prepared using Creative Studio (Photoshop & Illustrator, Adobe, UK).

2.8.2 Image calibration

Images captured using the Axiovert 100TV or the Nipkow system required a reference in order to make calibrated measurements. A reticule with 10 μm graduations was imaged using the appropriate objectives for both systems. The resulting calibration set was then calculated as both pixel/μm and μm/pixel. Calibration data for the Zeiss LSM 510 was embedded within the image file, and was accessible through ImageJ & OsiriX.

2.8.3 Wound area analysis

For puncture-wounds, TIFF images captured during the experiment were imported into Photoshop, and the lasso tool used to trace around the actin cable. The calculated wound area (in pixels) was then converted to μm^2 using the appropriate calibration set. The time-course of closure was quantified by calculating the area circumscribed by the actin cable at the following times (10, 30, 60, 120, 180 & 240

minutes post-injury) for each epithelial wound. All measurements were normalised to the original wound area at 10 minutes, and expressed as a percentage. Percentage data from each time-point was then averaged to give an overall measure of the wound closure process.

For stripe-wounds, TIFF images captured immediately after laser ablation were imported in Photoshop. A 600 μm region was selected along the central region of the epithelial wound. The area bounded by the wound was then traced using the lasso tool, and converted into μm^2 using the appropriate calibration. This area was then divided by the length of the selected region (600 μm) to yield the width of a rectangle of equivalent area. This was mathematically identical to integrating individual widths along the length of the wound.

2.8.4 BrdU analysis

For puncture-wounds, TIFF images of the epithelium were imported into Photoshop for analysis. A circle with a calibrated radius of 100 μm was centred upon the laser fracture mark on the culture coverslip. BrdU positive nuclei within the circle were then counted. If a nucleus fell upon the perimeter of the analysis circle, a rule was used to assign whether they were counted or not. Nuclei that intersected the upper semi-circle were discounted, whilst those intersecting the lower semi-circle were included. Control data was obtained by placing the analysis circle in the centre of an unwounded epithelium. To avoid unintentional bias, the control region was selected before the BrdU signal was revealed.

For stripe-wounds, TIFF images of the postnatal model stripe wounds were also imported into Photoshop for analysis. A rectangle with calibrated dimensions of 200 x 600 μm was orientated with its longitudinal axis running along the laser fracture marks. This created an analysis region that incorporated 100 μm either side of the original laser ablation site. BrdU positive nuclei were counted within the rectangle, with rules used to assign nuclei that intersected the edge of the analysis region (see above). Control data was obtained using the identical analysis region to count BrdU positive nuclei in an unwounded region of the same epithelium. Control regions were placed at least 300 μm away from the edge of a wounded analysis region. To avoid bias, the control region was

selected before the BrdU signal was revealed, and counts were made blind with respect to treatment group.

2.8.5 Calyx analysis

For analysis in fixed preparations, confocal z-series of the utricle were loaded into OsiriX. A square 40'000 μm^2 region of interest was selected blindly (200 x 200 μm) from the central cotillus. Two types of object were defined within the region of interest: a hair cell and a calyx. The histological characteristics of each object are summarised below.

	Hair cell	Calyx
HCS-1	Concentrated at the basolateral plasma membrane, and within an annulus at the epithelial surface.	At the basolateral plasma membrane or diffuse within the cytosol. No annulus visible at the epithelial surface.
DAPI	Normal chromatin structure with or without evidence of pyknosis / karyorrhexis.	None present, or with severely fragmented chromatin structure (pyknosis / karyorrhexis).
Phalloidin	Hair bundle continuous with the epithelial surface and soma. Normal basolateral distribution around the soma.	No hair bundle continuous with the epithelial surface or soma. Increased density of f-actin surrounding the soma (a calyx).

These objects were counted within the region of interest. The two definitions were mutually exclusive; an object could only be included in one of the two groups. Objects that intersected the upper or left boundaries of the region of interest were included, whilst those intersecting the bottom and right boundaries were excluded. Two such regions were counted from each utricle (total sample area 80'000 μm^2), and were averaged and normalised to yield object densities for each utricle. Object counts were made blind with respect to treatment group.

To quantify calyx activity within live-cell β-actin-EGFP preparations, individual hair cells were followed during the first 24 hours of time-lapse imaging. Hair cells were selected blindly at the beginning of the time-lapse record, to avoid any potential bias. Hair cells did not necessarily have to be infected; their position could be inferred from support cell morphology. The time-lapse record was advanced on a frame-by-frame basis and activity around individual hair cells noted. A calyx was counted if the surrounding support cells extended pseudopodia around the hair cell soma, and if their apices united to decapitate the hair bundle. The number of hair cells removed via this mechanism during the first 24 hours was expressed as a percentage of the starting population. 110 hair cells were sampled from streptomycin time-lapse experiments (n = 4 utricles), compared with 100 hair cells in sham-imaged controls (n = 3 utricles). Percentages were averaged between experiments to yield a final estimate of calyx activity in both streptomycin and sham-imaged treatment groups.

To quantify the timing of calyx induction relative to TOTO-3 uptake, individual hair cells were again observed on a frame-by-frame basis. To avoid selection bias, time-lapse recordings were advanced using the TOTO-3 signal only. As nuclei fluoresced with TOTO-3, the β-actin-EGFP signal was revealed to establish whether infected support cells were neighbouring the hair cell nucleus. If so, the frame number corresponding to the initial pseudopodial formation was designated f_{CALYX}. To determine the frame where TOTO-3 fluorescence was elevated, a separate sample was taken to establish the mean (x) and standard deviation (σ) of the nuclear signal from earlier in the sequence. The frame where nuclear TOTO-3 fluorescence exceeded an arbitrary threshold ($x + 3\sigma$) was designated f_{TOTO}. The frame difference $\Delta f = f_{TOTO} - f_{CALYX}$ was then plotted as a frequency histogram. Using this technique, 21 hair cells were sampled from 2 streptomycin treated utricles (n = 2 utricles).

2.8.6 Statistical tests

Comparisons between two statistical distributions were performed using the two-tailed Student's *t*-test. Group comparisons were performed using one-way ANOVA. The confidence interval was defined as 5% ($\alpha = 0.05$), and the null hypothesis was rejected if the calculated p-value did not exceed this value. All data are expressed as mean ± standard error of the mean (SEM), unless otherwise stated.

3 Wound repair in laser ablated sensory epithelia

3.1 Introduction

The avian inner ear is unique amongst warm-blooded vertebrates for its ability to regenerate after hair cell loss. In order to restore function to the affected organ, the regenerative process combines multiple programs of epithelial repair and *de novo* hair cell production (see Section 1.4). Whilst the mechanisms of hair cell production have been studied in detail, the ability to repair the epithelium is less well understood. Chronologically, the repair process is of particular interest, as it may provide direct cues that orchestrate the subsequent production of sensory hair cells. This chapter documents a repair process in the avian sensory epithelium, and investigates some of the underlying mechanisms.

To facilitate study of these phenomena, the protocols in this chapter utilise an epithelial preparation of the chick utricular macula (Warchol, 2002). This model provides excellent access for microscopic examination, and allows the sensory epithelium to be maintained for several days *in vitro*. To simulate trauma, laser ablation was used to wound utricular epithelium in a repeatable and well-defined manner. Initially, differential interference microscopy (DIC) was used to assess how the sensory epithelium responded to a wound of this nature. Epithelial wounds were found to close reliably within several hours of laser ablation. Immunocytochemistry identified pronounced cytoskeletal remodelling associated with the wound closure process. The full extent of cytoskeletal activity was revealed using confocal time-lapse of sensory epithelia expressing a β-actin-EGFP fusion protein. The mechanisms underlying wound closure were investigated using a combination of immunocytochemistry and pharmacological inhibitors of non-muscle (NM) myosin II or Rho kinase. The activation of a MAPK stress response pathway was also demonstrated, and its function during wound closure assessed. These results will be discussed in relation to wound closure described in other epithelial systems.

3.2 Results

3.2.1 Culture of the utricular sensory epithelium in vitro

Epithelial cultures of the avian utricle sensory epithelium were prepared as described in Section 2.4.1. Cultures of the sensory epithelium were allowed to adjust to the *in vitro* environment for at least 24 hours following dissection. Figure 3.1A shows a low magnification image of an epithelium fixed after 48 hours in culture. Typically, the centre of the culture adhered flat to the substratum, whilst cells lining the perimeter grew into the surrounding space. The presence of hair cells throughout the sensory epithelium was confirmed using immunocytochemistry for HCA (Bartolami et al., 1991), a stereocilial antigen thought to be PTPRQ (Figure 3.1B; Goodyear et al., 2003). Inspection of the epithelium at a higher magnification revealed that it retained a pseudo-stratified structure, with support cells at the base packed together in tight apposition (Figure 3.1C), and hair bundles clearly visible at the epithelial surface (Figure 3.1D).

3.2.2 Wounding the sensory epithelium using laser ablation

In order to simulate epithelial damage, a pulsed laser micro-beam was used to create puncture wounds in the centre of a culture. A single pulse from the laser was sufficient to instantaneously disrupt the tissue, although several pulses were typically used to create a wound. Figure 3.1E shows a live epithelial culture immediately after laser wounding. A milieu of cell debris persisted in the denuded area, which made the full extent of damage difficult to visualise. The incident laser energy also left a characteristic fracture in the underlying coverslip, which could be used to locate the wound site in subsequent procedures.

3.2.3 Wounded sensory epithelia heal within 4 hours

To examine how the epithelium responded to damage of this nature, laser wounded cultures were returned to the incubator and imaged at specific intervals using DIC optics (n = 7). A typical time-lapse of an epithelial wound is shown in Figure 3.2. Within ten minutes of laser ablation, debris had sufficiently dispersed such that viable cell somas could be distinguished from those that were not (Figure 3.2A). Nuclei lacking a soma or plasma membrane were observed within the wound space, characteristic of cell lysis. Thirty minutes after laser ablation, a distinct border formed around the perimeter of the wound (Figure 3.2B). The border appeared to extend completely around the wound, at some points describing an ellipse. Sixty minutes after

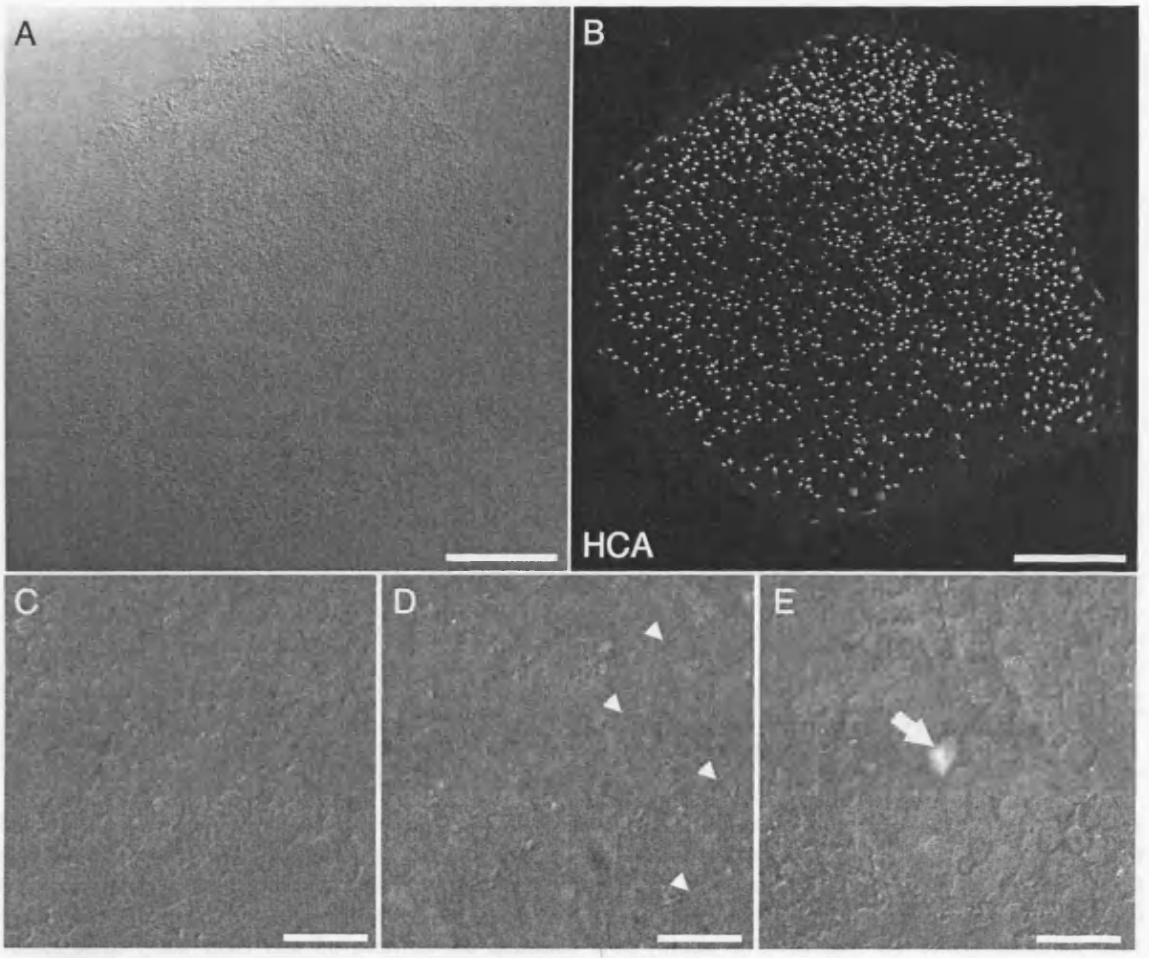

Figure 3.1 - Culture of the utricular sensory epithelium *in vitro*. A) Image of a fixed utricular sensory epithelium cultured on a glass coverslip. The sensory epithelium adhered flat to the substratum. **B)** HCA immunocytochemistry demonstrates the presence of sensory hair cells within the epithelium. **C-E)** Higher magnification images of the live epithelium *in vitro* captured using DIC. **C)** Image focused at the base of the epithelium reveals the support cell somas. **D)** Image at the epithelial surface shows the sensory hair bundles (arrowheads) protruding into the lumen. **E)** Image of the sensory epithelium immediately after laser ablation. The glass coverslip has been fractured by the incident laser radiation (arrow). Scale bars represent 200 μm (A,B) and 20 μm (C,D,E).

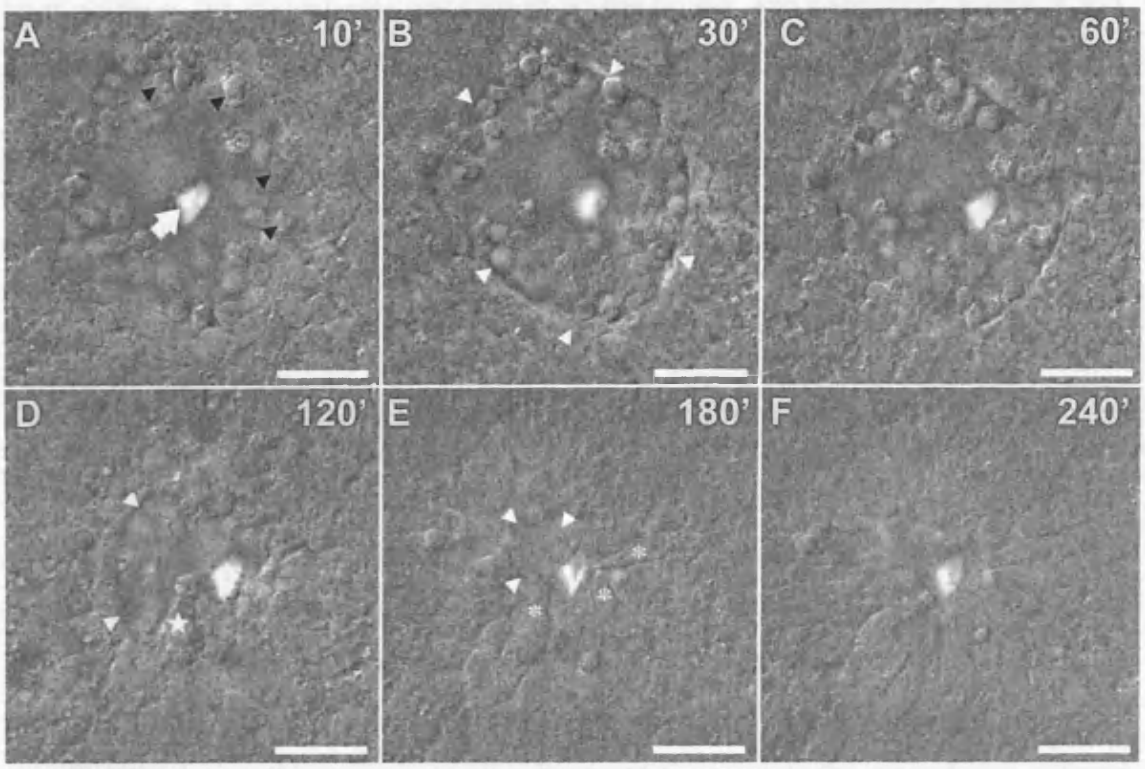

Figure 3.2 - Epithelial wound closure in response to laser ablation. Epithelial cultures of the sensory epithelium were laser ablated and returned to the cell culture incubator. Samples were removed briefly at the times indicated, and epithelial wounds imaged using DIC. **A)** Ten minutes after ablation, the full extent of damage is visible. Cells proximal to the site of incident radiation (white arrow) have been lysed. Cell nuclei from lysed cells can be seen in the denuded area (black arrowheads). **B)** Thirty minutes after ablation, a distinct border has formed around the epithelial wound (white arrowheads). Cell debris was still present within the denuded area. **C)** Sixty minutes after ablation, the wound area circumscribed by the border had started to reduce. **D)** Two hours after ablation, the wound area had substantially reduced in size. The wound border is still present, although less defined than before (white arrowheads). A cell can be seen projecting a process into the denuded area (white star). **E)** Three hours after ablation, the border was difficult to resolve (white arrowheads) as wound closure approached completion. Several support cells can be seen stretching toward the centre of the wound (asterisks). **F)** Four hours after laser ablation the epithelial wound is closed. Images are representative of the wound closure observed in seven independent experiments (n = 7). Times are expressed as minutes post laser ablation. All scale bars represent 20 μm.

laser ablation, the wound area transcribed by the border was decreased (Figure 3.2C). Two hours after laser ablation, the wound size was further reduced although the border was now less prominent (Figure 3.2D). In this example, a large cellular process was seen projecting into the wound area. Three hours after laser ablation, a faint border was the only indication that the wound was still partially open (Figure 3.2E). Support cells could be seen stretching towards the centre of the wound in this example. The wound was closed within four hours, with DIC microscopy being unable to discern a border or hole in the epithelium at this time (Figure 3.2F).

A quantification of wound areas from time-lapse experiments was performed as described in Section 2.8.3. Wound areas were calculated for seven independent time-lapse experiments. The starting wound size measured at 10 minutes post injury was 2072 ± 256 μm^2 (n = 7). Compared to this starting value, the relative wound area at 30 minutes was 93.2% ± 5.7% (p = 0.33), indicating that the wounds did not close significantly during this period. At all subsequent time points the wound size reduced significantly, with relative areas at 60, 120 and 180 minutes of 75.8% ± 6.6%, 37.6% ± 6.0% and 9.7% ± 4.1% respectively (all $p < 0.05$). All epithelial wounds were closed by 4 hours, although some achieved this within 3 hours (3 out of 7). The results of this analysis have been presented in Figure 3.3. The maximum rate of wound closure was observed between 60 and 120 minutes after laser ablation, equating to 791 $\mu m^2 h^{-1}$.

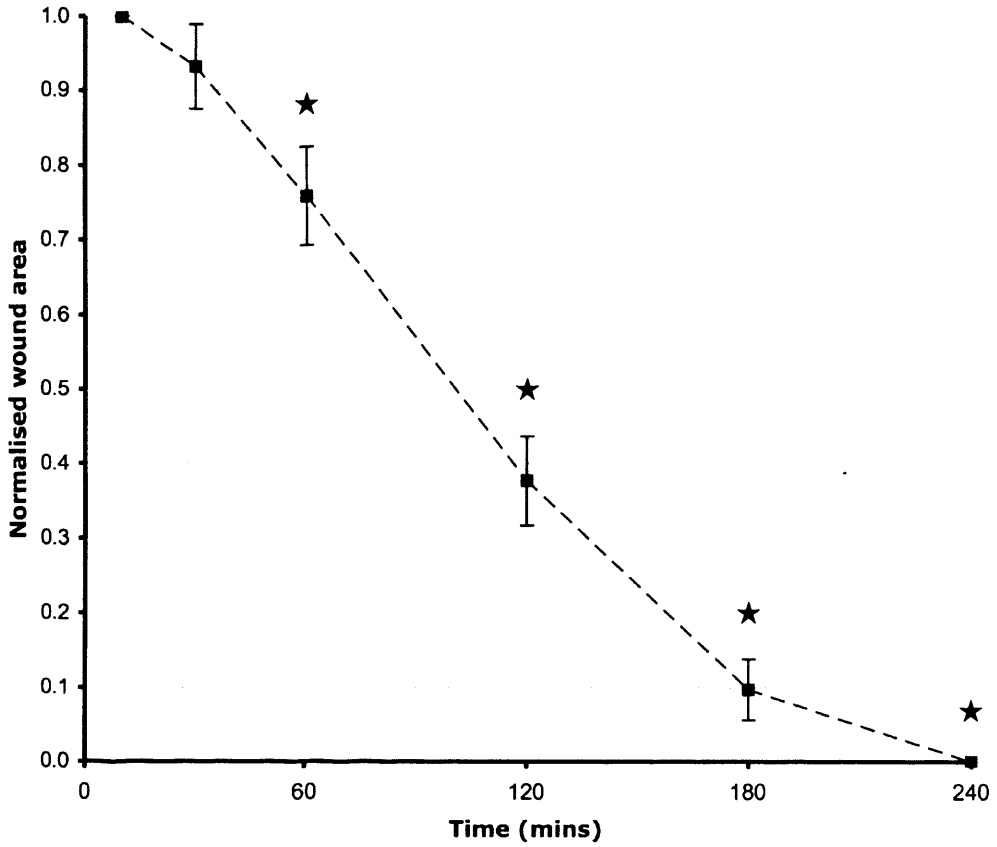

Figure 3.3 - Quantification of epithelial wound closure. The area covered by the epithelial wound was measured at discrete time-points during the closure process. Areas were normalised to the initial wound size measured at 10 minutes post-ablation. Data was collected from seven independent experiments. The wound area did not reduce significantly within the first 30 minutes, but did so thereafter. All wounds were closed by 4 hours. Data are expressed as means ± standard error.

★ denotes $p < 0.05$, using a two-tailed Student's *t*-test ($n = 7$).

3.2.4 An actin cable forms around epithelial wounds

The formation of a border circumscribing the wound was suggestive of an actin 'purse-string' mechanism, similar to that originally proposed in chick embryos (Martin and Lewis, 1992). To investigate whether an actin cable formed around epithelial wounds, a fluorescent phallotoxin was used to label filamentous actin (f-actin) in fixed cultures. Figure 3.4 is a representative set of confocal images captured from epithelia fixed at different stages during the wound closure process ($n \geq 3$ for each time point). Orthogonal projections of an undamaged section demonstrate the normal distribution of f-actin throughout the epithelium (Figure 3.4G). Hair cell bodies could be easily identified from their apical position in the pseudo-stratified epithelium, and by their lack of contact with the basal lamina. In particular, hair cell stereocilia and the apical junction complex (AJC) labelled intensely for f-actin.

Cultures fixed one minute after laser ablation revealed the full extent of the epithelial wound (Figure 3.4A). There was a complete absence of any cellular structure in the centre of the wound, the denuded zone. The exact location of the wound edge was difficult to discern as some cell bodies lacked definition and appeared diffuse. The AJC in some areas of the epithelium was discontinuous, suggesting that the associated somas were partially lysed. Within thirty minutes of laser ablation, the epithelium formed a defined border of f-actin around the perimeter of the wound; a presumptive actin cable (Figure 3.4B). Within sixty minutes of laser ablation, the actin cable appeared elliptical and continuous with the AJCs of the surrounding epithelium (Figure 3.4C). In the example shown, multiple lamellipodia are seen invading the denuded wound area in advance of the actin cable. Two hours after laser ablation, the wound shape was now distinctly oval and substantially reduced in area (Figure 3.4D). An orthogonal section at this time shows the redistribution of actin within the wounded epithelium (Figure 3.4H). As illustrated, the actin cable could be seen in two distinct configurations; with f-actin concentrated basally, or continuous from base to apex, where it joined with the AJC. The cable was not exclusively confined to the base or apex of the epithelium, and was not always associated with the AJC. Three hours after laser ablation, the wound was almost closed, with the actin cable describing a circle (Figure 3.4E). Four hours after laser ablation, the wound was closed (Figure 3.4F). An orthogonal projection of the closed wound demonstrated that the edges were pulled together such that the apical-basal polarity of the epithelium was maintained (Figure 3.4I). These experiments

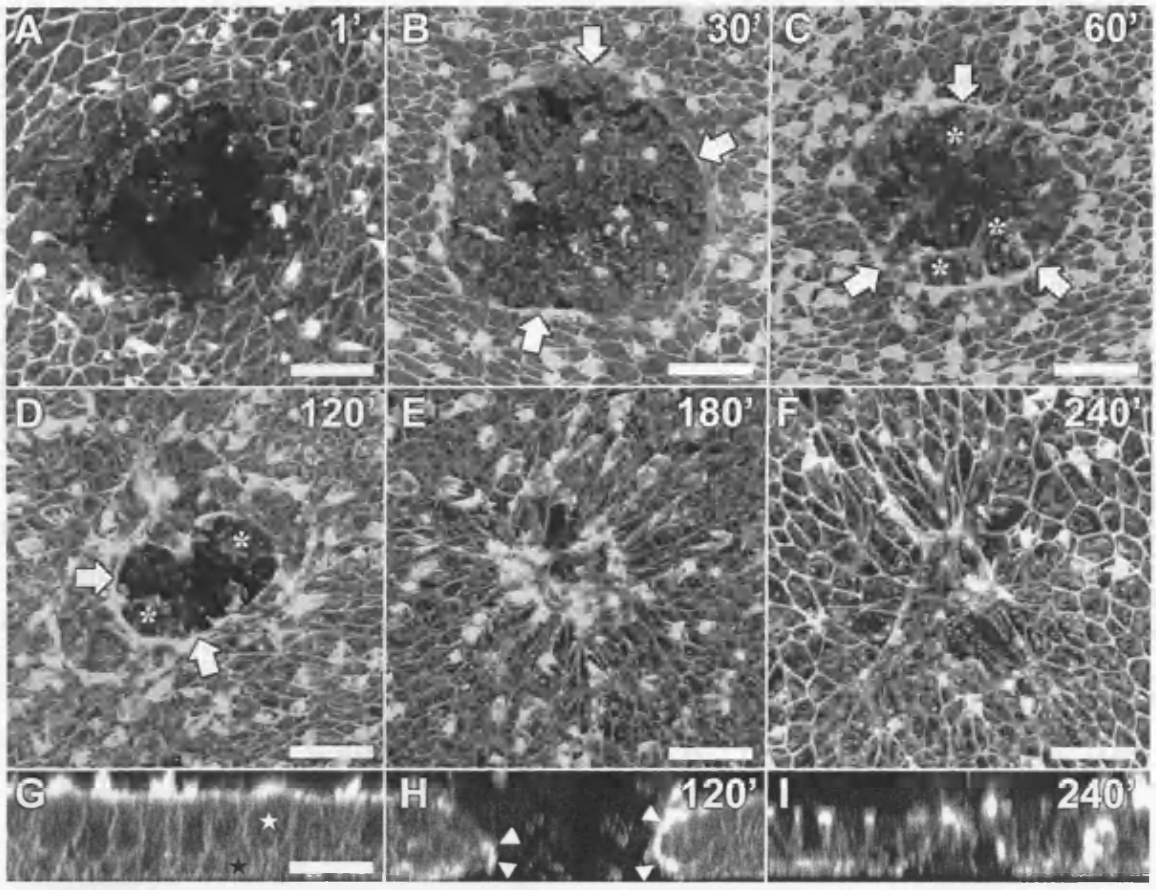

Figure 3.4 – An actin cable forms around epithelial wounds. Cultured sensory epithelia were laser ablated, and returned to the cell-culture incubator. Epithelia were fixed at specific intervals post ablation, and processed for phalloidin immunocytochemistry to reveal the filamentous actin cytoskeleton. Confocal microscopy was used to capture z-series of the sensory epithelium. **A-F)** Maximal projections of confocal volumes. In all images, f-actin is particularly concentrated in the apical junction complex (AJC) and sensory hair bundles. **A)** One minute after laser ablation, the edge of the wound is irregular. Discontinuous apical junctions suggest cells lining the wound edge have been lysed. **B)** Thirty minutes after laser ablation, the wound edge has become smooth in some regions, with the formation of a presumptive actin cable (white arrows). **C)** At 60 minutes, the wound has started to reduce in size. The actin cable is visible around the circumference of the wound (white arrows). The cable has an elliptical shape, indicative of significant epithelial tensions. Multiple lamellipodia are seen advancing into the denuded area (asterisk). **D)** After 120 minutes, the wound continues to close. Lamellipodia are still visible in the wound (asterisk). **E)** A faint actin cable is still visible at 180 minutes. The wound appears almost closed at this point. **F)** Epithelial wounds were healed within 4 hours. **G)** Orthogonal projection of an unwounded epithelium. F-actin is concentrated within the hair bundle and the AJC. Support cell (black star) and hair cell (white star) somas are visible. **H)** Orthogonal projection of an epithelium 120 minutes after laser ablation. The actin cable is seen as a band of increased f-actin at the wound edge (white arrowhead). **I)** Orthogonal projection of an epithelium 240 minutes after laser ablation. Both apical and basal components of the epithelium have been pulled together. Images are representative of wounds from at least 3 independent experiments ($n \geq 3$). All scale bars are 20 μm.

showed that in response to laser ablation f-actin reorganised to form a cable around the perimeter of the epithelial wound. Phalloidin labelling also revealed the presence of lamellipodia within the wound, which had proved difficult to resolve using phase contrasting techniques.

3.2.5 Live-cell imaging of β-actin during wound closure

The previous section described extensive remodelling of the actin cytoskeleton around epithelial wounds. These observations were made at discrete times, and in different epithelia; a necessity imposed by the requirement for tissue fixation. To examine the dynamic remodelling of the actin cytoskeleton in live preparations, sensory epithelia expressing a β-actin-EGFP fusion protein were imaged during wound closure. Epithelial cultures were derived from utricles infected with the RCASBP(B)-β-actin-EGFP viral construct. The resulting cultures displayed mosaic expression of β-actin-EGFP throughout the epithelium, in both support and hair cells (see Chapter 5 and Section 2.2.3 for a more detailed description of this system). Epithelia were laser ablated as before, and EGFP epi-fluorescence time-lapse captured using a Nipkow spinning-disk confocal microscope (n = 3). Figure 3.5 is a frame montage compiled from a time-lapse movie demonstrating some of the key events observed during the closure process. In this example, the ablation was made within a patch of β-actin-EGFP fluorescence, such that there was expression on nearly all sides of the wound. The formation of an actin cable and extensive lamellipodial activity were prominent in the experiment, and will be described separately. Although absolute patterns of transgene expression differed between epithelia, similar observations were made in the other two experiments.

The activity of lamellipodia during wound closure will be described initially. The first frame of the recording, taken five minutes after damage, showed the wound edge to be ragged and decorated with small regions of increased fluorescence (Figure 3.5A). Patches of increased fluorescence were representative of a local increase in β-actin-EGFP monomer concentration, suggestive of an active sequestration. Lamellipodia began to emerge from these patches and started to invade the denuded space within 12 minutes of wounding (Figure 3.5B,C). Lamellipodia were observed to repeatedly invade, and then retract from the denuded area throughout the remainder of

the time-lapse (Figure 3.5D-H). The largest lamellipodium observed during the time-lapse covered an area of 183 μm^2 (Figure 3.5E,F). Due to the complex behaviour of lamellipodia, no attempt was made to quantify their movement vectors. A qualitative observation was that lamellipodia did not engage in a random searching behaviour, instead tending to move normal to the wound border. Lamellipodia originated from support cells that were adherent to the substratum. Whilst the vast majority of lamellipodia can be seen to develop from support cells lining the wound edge, cryptic processes were also observed originating from cells behind the wound edge (Figure 3.5F,G).

Time-lapse recordings of β-actin-EGFP during wound closure also revealed new detail regarding the actin cable structure and its formation. Although the cable was not visible five minutes after laser wounding, there was already some evidence of its formation (Figure 3.5A). Amongst the puncta of increased EGFP fluorescence, two support cells had formed a border facing the wound edge. Increasing numbers of support cells adopted this phenotype as the experiment progressed, such that by 12 and 21 minutes after wounding, sections of a continuous border were apparent (Figure 3.5B,C). The cable was judged fully formed by 30 minutes, with its circumference describing an ellipse (Figure 3.5D). Due to the mosaic nature of expression, some cells lining the wound border were not expressing the β-actin-EGFP construct, however it was highly likely they too contributed to the cable formation using endogenous β-actin monomers. As the wound began to close, cells contributing to the actin cable underwent increasing deformations as they were stretched between the closing wound and their other anchors (Figure 3.5H). In parallel to this, the intensity of β-actin-EGFP fluorescence in the actin cable reduced as wound closure approached completion (Figure 3.5F-H). The full-length MPEG movie has been made available on a compact disc attached to this thesis (Appendix A, file://chapter3/EGFPwound.mpg). In conjunction with studies from this chapter, these data demonstrated the formation of an actin cable, in tandem with dynamic lamellipodial activity around epithelial laser wounds. The function of these structures will now be explored and discussed.

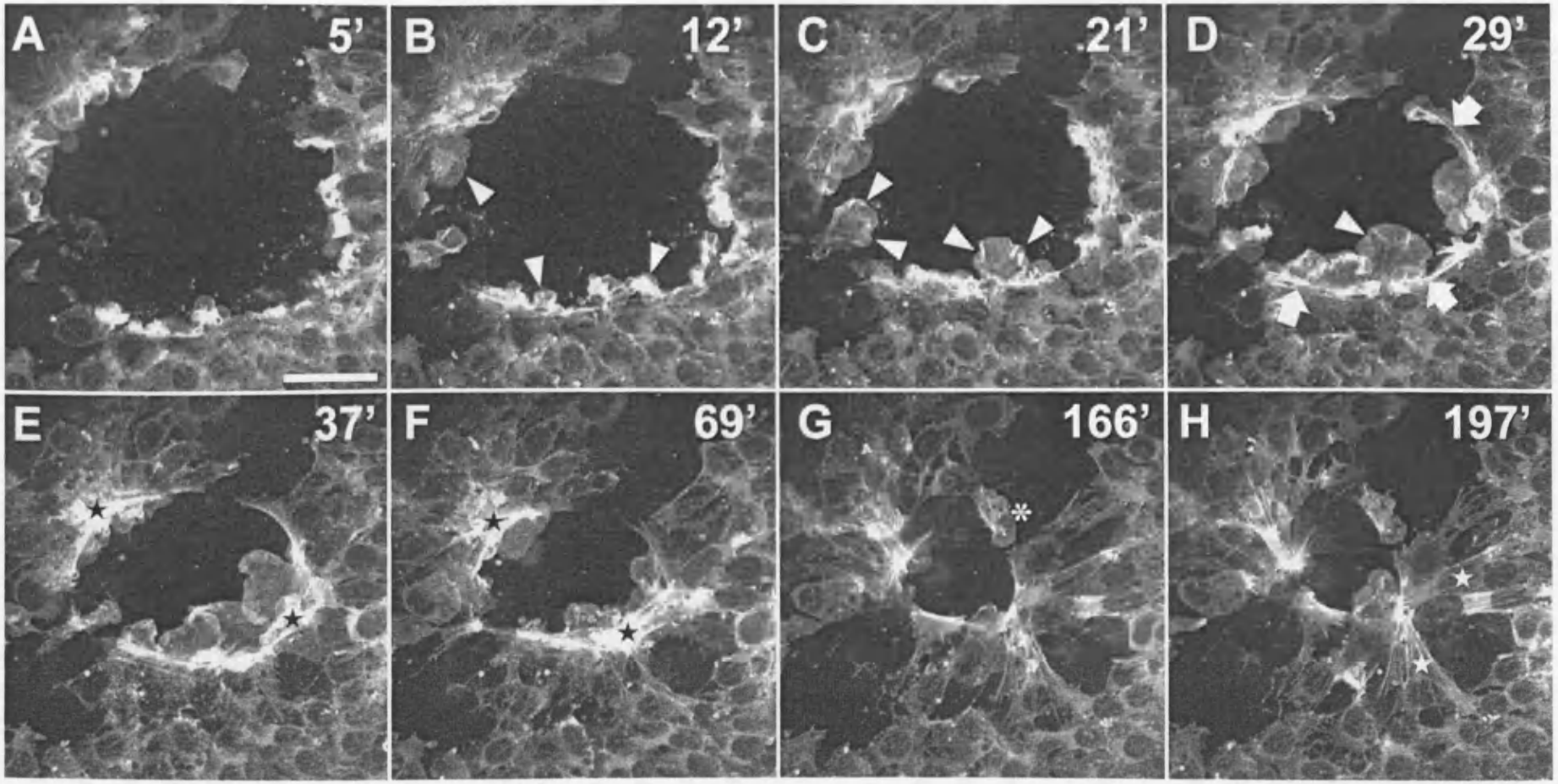

Figure 3.5 - Live-cell imaging of β-actin-EGFP during wound closure. Utricular epithelia expressing β-actin-EGFP were laser ablated and subsequently time-lapse imaged using a spinning-disk confocal microscope (n = 3). **A-H)** A series of frames taken from a single time-lapse movie. The focal plane was set at the base of the epithelium. **A)** Five minutes after ablation, areas of increased actin polymerisation are visible around the wound edge. Not all cells round the wound are expressing the β-actin-EGFP transgene. **B)** Multiple lamellipodia begin to invade the denuded area (white arrowheads). **C,D)** Lamellipodia enlarge and continue to invade the denuded area (white arrowheads). The actin cable becomes clearly visible, and describes an ellipse (white arrows). **E,F)** The wound begins to visibly contract. Focal nodes of increased β-actin-EGFP fluorescence are seen on opposite sides of the wound (black stars). **G,H)** The wound continues to contract, until it is almost closed. Support cells contributing to the actin cable undergo significant stretching as the wound approaches closure (white stars). A cryptic lamellipod can be seen originating from a cell behind the wound edge (white asterisk). All times are expressed in minutes post-ablation. Scale bar represents 20 μm.

3.2.6 Actin polymerisation & Rho kinase activity are required for cable formation

To investigate the mechanisms underlying actin cable formation, laser wounded epithelia were treated with cell permeant compounds that targeted the actin cytoskeleton. Treated epithelia were fixed sixty minutes after laser wounding, and the cytoskeleton imaged using a fluorescent phallotoxin. Treatment with 1 μM cytochalasin D, a fungal metabolite that inhibits actin polymerisation, was able to completely prevent formation of the actin cable around an epithelial wound (n = 3; Figure 3.6A,B). Sixty minutes after wounding, the AJCs at the epithelial surface appeared disorganised, and had not restructured into a characteristic ellipse (Figure 3.6A). At the base of the epithelium, a similar absence of cytoskeletal reorganisation was observed (Figure 3.6B). Support cells did not concentrate actin at the wound border, and failed to develop a cable. Cytochalasin D treatment also induced collapse of support cell stress fibres, manifest as a large number of bright puncta distributed throughout the base of the epithelium. Treatment with cytochalasin D did not appear to correlate with any effect upon the gross morphology of the AJC, or hair cell stereocilia at the epithelial surface.

This data demonstrated that cable formation was absolutely dependant upon *de novo* actin polymerisation. Proteins that initiate actin nucleation and promote polymerisation were thus of interest in the study of cable formation. Rho kinase ($p160^{ROCK}$) is a well characterised Rho effector that is essential for actin cable formation in other wound models (Russo et al., 2005). To examine whether this protein was also required for cable formation in wounded utricular epithelia, Y-27632 was used to inhibit ROCK activity. Y-27632 is cell permeant molecule that inhibits ROCK by competing for its ATP binding site (Uehata et al., 1997). Utricular epithelia were pre-treated with 30 μM Y-27632 and fixed 60 minutes after laser wounding (n = 3). Epithelia were subsequently processed for phalloidin immunocytochemistry as before. Y-27632 treatment prevented formation of a robust actin cable 60 minutes after laser wounding (Figure 3.6C). A circular border had formed around the wound, however it was faint and indistinct. In the presence of Y-27632, AJCs at the epithelial surface did not rearrange into the elliptical formation characteristic of a normal wounds. To investigate whether epithelial wounds could heal with the apparent lack of an actin cable, wounds were fixed 240 minutes after laser wounding in the continued presence of Y-27632 (n = 4). Epithelia treated in this manner were still able to achieve wound

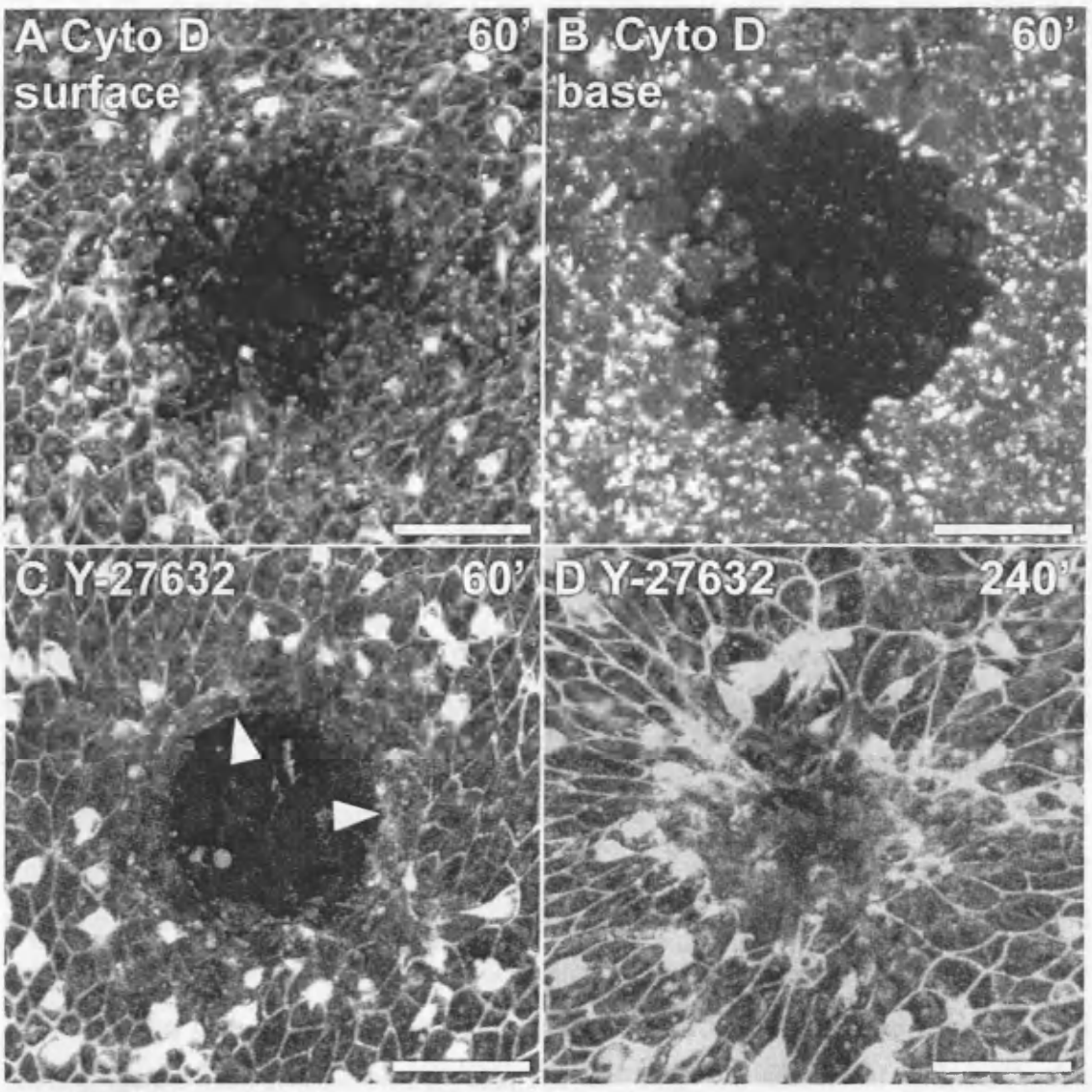

Figure 3.6 - Cytochalasin D & Y-27632 disrupt actin cable formation. Epithelia were pretreated with either 1 μM cytochalasin D or 30 μM Y-27632 to inhibit actin polymerisation or Rho kinase activity respectively. Laser ablated epithelia were and fixed and labelled with a fluorescent phalloidin. Confocal z-series were captured using a laser scanning confocal microscope. Images shown here are maximum projections of: the surface (A), the base (B), or the entire epithelium (C & D). **A,B)** Treatment with cytochalasin D prevented actin cable formation. Sixty minutes after ablation, support cells surrounding the wound failed to reorganise their cytoskeleton to form the cable. Cytochalasin D treatment did not affect the visual integrity of apical junction complexes elsewhere within the epithelium. Bright puncta throughout the base of the epithelium suggested that cytochalasin D triggered stress fibre collapse. The epithelium has been separated into an apical and basal half for visual clarity. **C)** Y-27632 treatment prevented formation of a robust actin cable sixty minutes after laser ablation. Some reorganisation of the wound edge was observed (white arrowheads), however the cytoskeleton failed to form a cable. **D)** Y-27632 treatment did not prevent wound closure four hours after laser ablation, but the epithelial surface were not united correctly. Times are expressed in minutes post-ablation. Images shown are represesentative of at least three independent experiments. All scale bars represent 20 μm.

closure (Figure 3.6D). Support cell processes from the base of the epithelium were able to enter the wound space and merge in the middle. A striking difference was observed at the epithelial surface, where the AJCs had not been drawn together to formed a continuous network. Y-27632 treatment did not appear to affect the gross morphology of the AJC or the sensory hair bundles. These data showed that whilst ROCK activity was essential for actin cable formation, it was not required for wound closure.

3.2.7 Non-muscle myosin II is required for cable formation & contraction

The molecular motor non-muscle (NM) myosin II has been shown to associate with actin cables in both wound and dorsal closure models (Bement et al., 1993; Young et al., 1993). To determine if this protein was associated with the actin cable described here, an antibody to NM-myosin IIB was used to probe wounded epithelia. Utricular epithelia were fixed sixty minutes after laser wounding, and were processed for NM-myosin IIB and phalloidin immunocytochemistry (n = 3). NM-myosin IIB was distributed throughout the base of the epithelium, and was concentrated within striate structures in particular (Figure 3.7A). When compared to the corresponding phalloidin image (Figure 3.7B), it was apparent that some NM-myosin IIB labelling associated with the actin cable, however this was limited to a small arc and did not extend around the entire wound. At the epithelial surface, NM-myosin IIB labelling was visible at hair cell – support cell apical junctions, and was additionally diffuse within the hair cell itself (Figure 3.7C). Intense NM-myosin IIB labelling was associated with AJCs that constituted the apical portion of the actin cable (Figure 3.7C,D). This association extended around the entire circumference of the wound. Orthogonal reconstructions of the confocal z-stack revealed an additional aggregate of NM-myosin IIB, continuous with the AJC, projecting away from the wound into the luminal space (Figure 3.7E). This mass of NM-myosin IIB co-localised with phalloidin labelling (Figure 3.7F), and possibly represented junctional debris from laser ablation induced cell lysis. Aside from the wound itself, intense NM-myosin IIB labelling was seen around the edge of the epithelium, where it associated with actin stress fibres (Figure 3.7G,H). It should be noted that not all myosin IIB labelling co-localised with actin structures. Intense NM-myosin IIB expression was also found in toroidal structures at the epithelial surface (Figure 3.7I). These structures colocalised with the convergence of apical junctions from multiple support cells (Figure 3.7J).

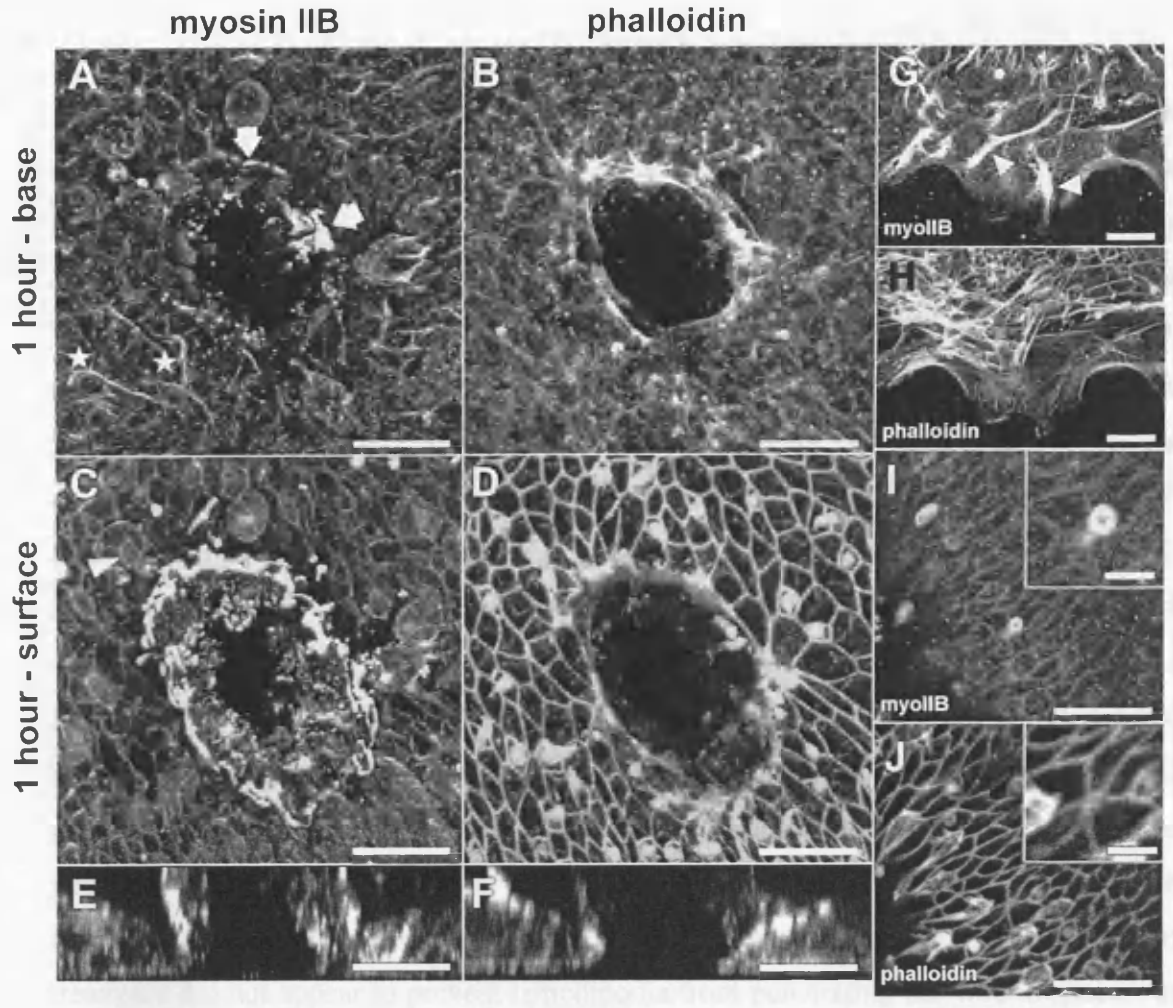

Figure 3.7 - Non-muscle (NM) myosin IIB expression in the wounded epithelium. Epithelia were laser ablated and allowed to heal for one hour. Fixed epithelia were processed for NM-myosin IIB and phalloidin immunocytochemistry. Z-stacks were captured using laser scanning confocal microscopy. The confocal stack has been presented as maximal projections of the basal and apical halves of the epithelium. **A,B)** NM-myosin IIB associated with sections of the actin cable at the base of the epithelium (white arrowheads), although it did not extend around the entire wound perimeter. NM-myosin IIB was also observed within striate structures (white stars). **C,D)** NM-myosin IIB also localised with the actin cable at the epithelial surface. NM-myosin IIB expression was more concentrated at support cell – hair cell apical junctions (white arrowhead). **E)** Orthogonal projection demonstrates the z-distribution of NM-myosin IIB within the epithelial wound. NM-myosin IIB was most concentrated at the epithelial surface. Large aggregates of NM-myosin IIB were observed projecting in the luminal space. This was not associated with any viable cell structure and likely represented debris from the original laser ablation. **F)** Corresponding orthogonal projection shows the distribution of f-actin in this example. **G,H)** NM-myosin IIB expression associated with f-actin around the border of the epithelial culture. Not all NM-myosin IIB labelling correlated with f-actin however (white arrowheads). **I,J)** NM-myosin IIB labelling was occasionally seen as torus at the epithelial surface (inset panels). This may represent an epithelial scar. All images are representative of three independent experiments. Scale bars represent 20 μm, except for inset panels, which are 5 μm.

These data demonstrated a clear association of NM-myosin IIB with the actin cable, particularly towards the epithelial surface. Experiments now focused on the functional significance of this association during wound closure. NM-myosin II has recently been shown to be necessary and sufficient for contraction of the supra-cellular actin cable that drives dorsal closure in *Drosophila* embryos (Franke et al., 2005). Blebbistatin, a cell-permeant inhibitor of NM-myosin II, was used to investigate whether this motor protein similarly provided the contractile force to effect wound closure in utricular sensory epithelia. Blebbistatin interferes with the release of ADP from the NM-myosin II ATPase, significantly reducing its activity (Kovacs et al., 2004). Epithelia were pretreated with 100 μM mixed isomers of blebbistatin for 2 hours prior to laser wounding. Wounded epithelia were then allowed to heal for various times in the continued presence of blebbistatin, before they were fixed and processed for phalloidin immunocytochemistry. Epithelia from these experiments exhibited a distinct phenotype when compared to 0.1% DMSO-treated controls from the equivalent time point (n = 4). One hour after laser ablation, a circular actin cable was observed at the base of the epithelium, although it was faint and ill defined (Figure 3.8A). Blebbistatin treatment did not appear to prevent lamellipodia from penetrating the wound space. An unexpected difference was seen at the epithelial surface, where the actin cable was not present. The AJCs appeared disorganised, and had failed to reorganise around the wound border (Figure 3.8B). These experiments suggested that blebbistatin was interfering with the correct formation of the actin cable at the epithelial surface. To exclude the possibility that the actin cable could still form, albeit more slowly, epithelia were treated with 100 μM blebbistatin and fixed three hours after laser ablation (n = 4). In these epithelia, a faint actin cable was present at the base of the epithelia (Figure 3.8C). At the epithelial surface, AJCs lining the wound edge were disorganised and did not form a coherent cable (Figure 3.8D). These data showed that NM-myosin II activity was required for effective formation of the actin cable.

Given that blebbistatin treatment interfered with actin cable formation, it was difficult to assess whether NM-myosin II activity was also generating contractile force to effect closure. In an attempt to address this question, epithelia were laser ablated in standard culture media, and were allowed 60 minutes for the actin cable to develop

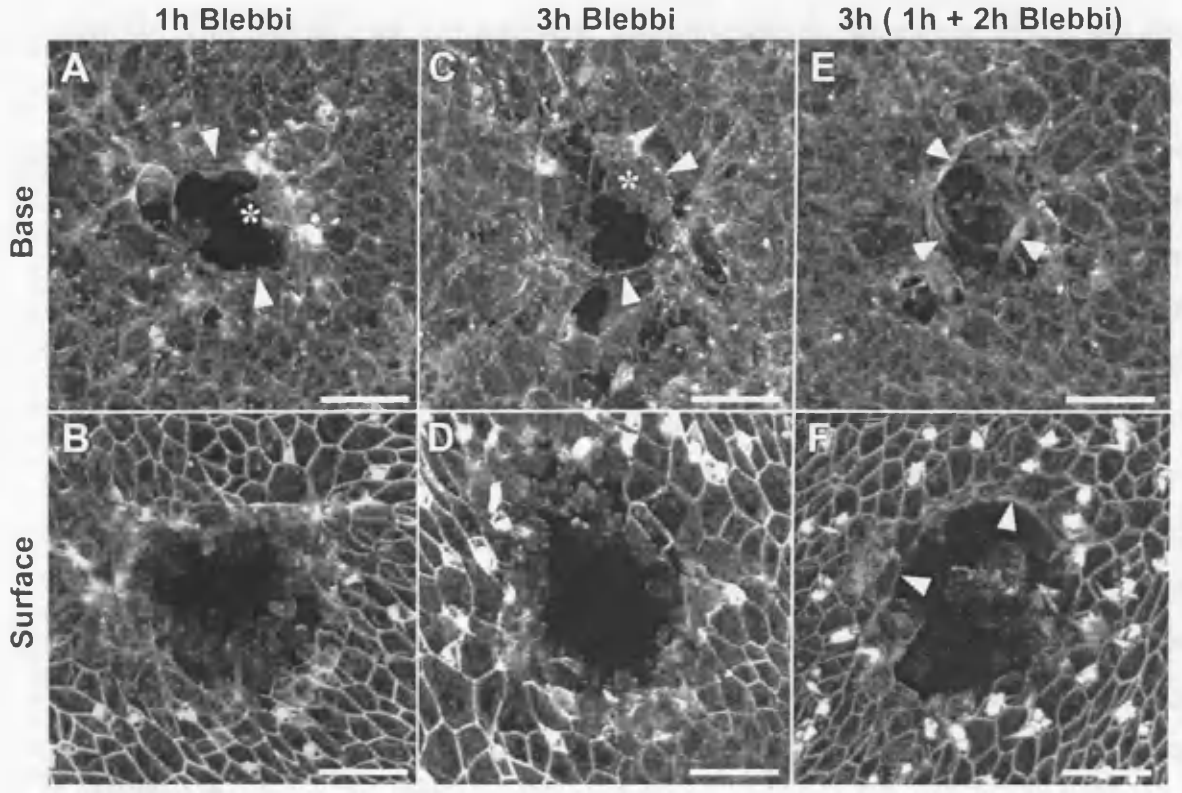

Figure 3.8 - NM-myosin II activity is required for cable formation & wound closure. Blebbistatin 100 μM was used to inhibit NM-myosin II activity in laser ablated epithelia. Fixed epithelia were processed for phalloidin immunocytochemistry and imaged using laser scanning confocal microscopy. Images are maximal projections of the basal (A,C,E) and surface (B,D,F) halves of the epithelium. **A,B)** Blebbistatin prevented actin cable formation assessed one hour after laser ablation. A faint border was observed toward the base of the epithelium (white arrowheads). Lamellipodia were present within the denuded area (asterisk). Apical junction complexes (AJC) at the surface appear disorganised around the wound. **C,D)** Blebbistatin treatment prevented wound closure assessed three hours after laser ablation. A faint border was present at the base of the epithelium (arrowheads). AJCs at the epithelial surface remain disorganised along the wound border. Lamellipodia were present within the denuded area (asterisk). **E,F)** Delayed blebbistatin addition prevented wound closure assessed three hours after laser ablation. Blebbistatin was now added to the culture media 1 hour after laser ablation (1h normal media + 2h with blebbistatin). The epithelial wound was still unable to close correctly, even though the actin cable formed initally. The actin cable was now indistinct, yet still visible at this time point (arrowheads). Although lamellipodia are present within the denuded space, the epithelial surfaces were not pulled together. Images are representative of at least three independent experiments. All scale bars represent 20 μm.

normally. Blebbistatin 100 μM was then supplemented to the culture media and the epithelia incubated for a further two hours before they were fixed (n = 4). Immunocytochemistry for phalloidin revealed a faint actin cable at the base of the epithelium, along with the presence of lamellipodia within the denuded area (Figure 3.8E). At the epithelial surface, edges of the wound had failed to be pulled together (Figure 3.8F). A robust actin cable was not observed at the epithelial surface. There was some indication that an actin cable had been present, as some sections of the wound edge appeared smooth and elliptical. This suggested that blebbistatin treatment had indeed eliminated the contractile ability of the actin cable. To quantify this effect, live-cell DIC images taken 60 and 180 minutes after laser ablation were used to measure wound sizes. Using these measurements, the average size of the wound at 60 minutes was 1854 ± 160 μm^2 (n = 4). The corresponding wound size at 180 minutes was 1500 ± 221 μm^2. This represented a non-significant reduction of 19.1% between these two points ($p = 0.13$). Over the equivalent period, control measurements from Section 3.2.3 displayed a significant 87.2% reduction in wound area ($p < 0.005$, n = 7). These data demonstrated that NM-myosin II activity was required for contraction of the actin cable.

3.2.8 ERK activation is an early wound signal

The experiments in this chapter have demonstrated that laser ablation of the sensory epithelia triggers an extensive remodelling of the actin cytoskeleton, including the formation of an acto-myosin cable and lamellipodial processes. Several groups have documented activation of the $p44/42^{ERK1/2}$ (ERK) MAPK within minutes of epithelial damage, which is required for both the induction of IEGs and wound edge migration (Dieckgraefe and Weems, 1999; Nobes and Hall, 1999; Matsubayashi et al., 2004). Experiments were now performed to establish whether this stress response mechanism was present in utricular epithelia, and if so, whether it was similarly required for wound closure.

To determine if ERK was activated in response to laser ablation, an antibody recognising the di-phosphorylated (active) isoforms of p44/p42 $ERK^{(T185,Y187)}$ was used to probe wounded epithelia. Figure 3.9 shows a representative set of maximal confocal projections from epithelia processed for phospho-ERK immunocytochemistry at 1, 5, 30 and 60 minutes after laser ablation (n ≥ 3 for each time-point). Epithelia fixed within

one minute of laser ablation displayed no activation around the wound site (Figure 3.9A). Five minutes after laser ablation, a symmetrical activation was observed around the wound site (Figure 3.9B). The extent of ERK activation was substantially reduced by 30 minutes (Figure 3.9C), and was only just visible above background by 60 minutes (Figure 3.9D). Additional information regarding the specificity of ERK activation was seen in single optical sections taken from the confocal z-series (Figure 3.9E,F). At the peak of activation, ERK phosphorylation was restricted exclusively to support cell cytoplasm. An orthogonal reconstruction of the confocal z-series illustrates the absence of phospho-ERK from hair cells (Figure 3.9G). Hair cells can be identified from the corresponding phalloidin reconstruction, by their characteristic cell shape and apical position within the epithelium (Figure 3.9H). These experiments demonstrated that laser ablation of the sensory epithelium elicited a transient activation of ERK within support cells only.

The function of ERK activation during epithelial wound closure was now explored using U0126, a cell-permeant inhibitor of the MEK1/2 kinase that phosphorylates ERK (Favata et al., 1998). Treatment with 20 μM U0126 (n = 4) was able to completely block the peak of ERK activation five minutes after laser ablation (Figure 3.9I). This experiments also provided an additional control for the specificity of phospho-ERK immunocytochemistry. To examine whether ERK activation was required for actin cable formation, epithelia were laser ablated and incubated for 60 minutes in the continued presence of 20 μM U0126 (n = 3). Phalloidin labelling of these epithelia revealed that the actin cable formed normally around the wound perimeter (Figure 3.7J). To examine whether ERK activation was required for wound closure, epithelia were laser ablated and incubated for 240 minutes in the continued presence of 20 μM U0126 (n = 3). In these experiments, wound closure was still achieved with no obvious phenotype (Figure 3.9K). These data demonstrated that ERK activation was not required for the normal closure of epithelial wounds.

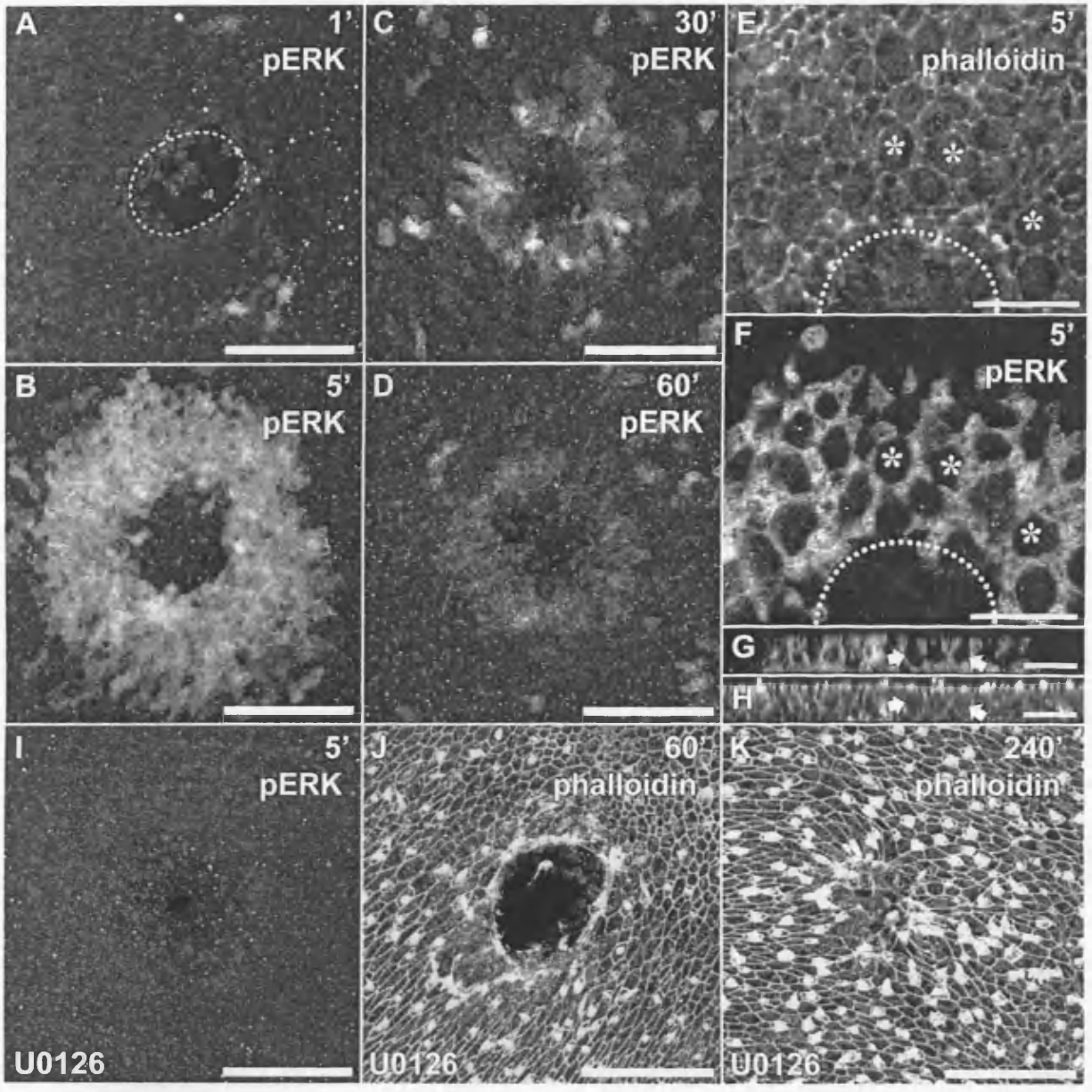

Figure 3.9 - Laser ablation triggers transient activation of the ERK MAPK. Epithelia were laser ablated and fixed after varying periods. Immunocytochemistry was used to detect the active, di-phosphorylated isoform of $p44/42^{ERK1/2}$ (ERK), and imaged with laser scanning confocal microscopy. **A - D)** Maximal projections of epithelia fixed at 1, 5, 30 & 60 minutes after ablation revealed the full extent of ERK activation. ERK activation was transient and peaked after five minutes. Some residual ERK activation was still present near the wound edge after 60 minutes. The border of the wound has been indicated (dotted line). **E,F)** A single optical section taken at the level of hair cell somas. At its peak five minutes after laser ablation, ERK activation was restricted to support cell somas only. Phalloidin labelling confirmed that activated ERK was not detected in sensory hair cells (asterisks). The wound edge has been marked on the image (dotted line). **G)** Orthogonal projection of the z-series five minutes after laser ablation. ERK activation was diffuse throughout support cells' nuclei and cytoplasm. Hair cell somas are seen as black spaces (white arrow). **H)** Corresponding phalloidin projection confirms that activated ERK was not found in sensory hair cells (white arrow). **I)** Incubation with 20 μM U0126, an inhibitor of MEK1/2, effectively blocked the ERK activation induced by laser ablation. **J)** Continuous inhibition with U0126 did not prevent actin cable formation 60 minutes after laser ablation. **K)** Continuous inhibition with U0126 did not prevent wound closure as assessed 4 hours after laser ablation. All images are representative of at least three independent experiments. Times are expressed in minutes post-ablation. All scale bars represent 50 μm, except for panels E,F,G & H which are 20 μm.

3.3 Discussion

This chapter describes a wound model of the avian utricular sensory epithelium. To simulate trauma, laser ablation was used to create puncture wounds within the sensory epithelium. It was found that epithelial wounds healed within 4 hours using an acto-myosin cable in combination with lamellipodial crawling. Formation of the actin cable required actin polymerisation and Rho kinase activity, and contraction was dependent upon NM-myosin II activity. Signalling through the p44/42 ERK MAP kinase was investigated, and found to be non-essential for wound closure.

3.3.1 Mechanism of laser ablation

Before discussing the relevance of any observations made in this chapter, it is important to consider the mechanisms of laser ablation. The laser employed here emitted in the visible spectrum, and possessed an extremely high power density with a pulse-width in the order of nanoseconds (see Section 2.5.1 for exact specifications). The incident pulse vaporised both water and organic matter at the focal point, due to absorption of the intense laser energy. The rapid expansion of material results in a local overpressure, termed a 'phase explosion', that is powerful enough to physically disrupt membranous structures in the immediate vicinity (Zhigilei et al., 2003). Wounding was thus photo-thermal, as opposed to photo-chemical. It is important to emphasise that vapourisation is restricted to the small volume where the laser energy is focused; the remaining damage being caused by overpressure induced cell lysis. Evidence of this mechanism could be observed immediately after wounding, with the presence of cell nuclei devoid of their plasma membranes. It follows that laser ablation of the sensory epithelium was multi-cellular in nature, destroying *both* support and hair cells without bias. Laser ablation is thus similar to mechanical injury, and can be considered qualitatively equivalent.

3.3.2 An acto-myosin 'purse-string' drives epithelial wound closure

Support cells that survived proximal to the site of laser irradiation constituted the wound margin by definition. Using time-lapse and fixed preparations, these cells were observed to remodel and form a circular border of f-actin around the wound. The actin cable was fully formed within thirty minutes of laser ablation, at which point it appeared smooth and fully continuous. Over the next three hours, the area circumscribed by the actin cable reduced as the wound edges were brought together.

These observations were strongly suggestive of an actin based 'purse-string' mechanism that has been proposed to affect wound closure in epithelial and epidermal systems (Martin and Lewis, 1992; Bement et al., 1993; Wood et al., 2002). The measured rate of closure was similar to that reported in wounded *Drosophila* embryos; 791 $\mu m^2 h^{-1}$ versus 540 $\mu m^2 h^{-1}$ respectively (Wood et al., 2002).

The three-dimensional nature of the actin cable, and its position within the sensory epithelium was investigated using immunocytochemistry. One hour after injury, the actin cable spanned from base to apex of the wound edge, and was continuous with the AJCs at the epithelial surface. It is proposed that AJCs constitute the apical-most component of the actin cable, formed from support cells lining the wound edge. Although association of the actin cable with specific junctional proteins was not investigated here, previous studies have demonstrated expression of N-cadherin, β-catenin and occludin in the AJCs of avian sensory epithelia (Kruger et al., 1999; Warchol, 2002). Since the actin cable was continuous with the AJC, it was highly likely that these proteins were also associated. If this were the case, it would suggest that the actin cable was a multi-cellular composite, with each support cell contributing a small 'arc' of apical junction towards the overall perimeter. In particular, the involvement of adherens junctions in the AJC would provide a strong physical connection between neighbouring cells, fusing the perimeter of actin 'arcs' into a functional load-bearing network. Unlike the apex, the basal component of the cable did not appear to correlate with any obvious cell structure, such as the AJC. Phalloidin immunocytochemistry suggested that the cable arose from actin filaments in support cells aligning parallel to the wound edge. It was unclear whether this was the basis of a composite cable system, or whether it represented the processes of a limited number of cells encircling the wound perimeter. The use of confocal time-lapse to visualise β-actin-EGFP during wound closure provided compelling evidence for the former hypothesis. The interpretation of β-actin-EGFP data was greatly facilitated by the mosaic nature of viral infection; allowing individual cell contributions to be assessed. This proved a significant advantage over phalloidin immunocytochemistry, where all cellular f-actin was labelled and discrimination was impossible. Using live-cell imaging, individual support cells were observed to form an arc that constituted a fraction of the wound border. This was strong evidence that the base of the cable was also a composite of

support cells lining the wound margin. How the individual components of the actin cable were interconnected was not specifically investigated in this thesis. Previous studies have demonstrated cadherin plaques interspersed between the sections of multi-cellular actin cables, consistent with the presence of zonulae adherens (Brock et al., 1996; Danjo and Gipson, 1998). Future experiments will document the distribution of cadherins and accessory proteins like β-catenin within the sensory epithelium, wounded or otherwise.

Experiments presented in this chapter also sought to uncover the function of the actin cable during wound closure. The purse-string model posits that the actin cable is able to generate contractile force that physically pulls the wound edges together (Martin and Lewis, 1992; Bement et al., 1993). Non-contractile actin cables have also been described, where wound closure is achieved through cell crawling and the extension of lamellipodia (Fenteany et al., 2000). In the latter example, the actin cable coordinates cell movement along the wound border, rather than generating any intrinsic forces. It was therefore important to decipher whether the actin cable described in this chapter was contractile, or whether it served as a structure to distribute forces originating elsewhere in the epithelium. In support of the actin cable as a contractile apparatus, was its close associated with the motor protein non-muscle (NM) myosin IIB. The association of NM-myosin II with actin cables during wound closure has been reported in previous studies (Bement et al., 1993; Brock et al., 1996; Danjo and Gipson, 1998). In agreement with these studies, NM-myosin IIB was recruited to sections of the actin cable that circumscribed the wound. NM-myosin IIB labelling was orientated tangential to the wound border, which was consistent with it generating a contractile force. Whilst there was strong NM-myosin IIB reactivity towards the apex of the cable, there was significantly less towards the base. This was unexpected as the elliptical shape of the actin cable betrayed that it was under significant tension. The antibody used in this study was a monoclonal raised again NM-myosin IIB; it was therefore impossible to exclude the possibility that the alternate NM-myosin IIA isoform was present. A future direction will be to probe wounded epithelia for both NM-myosin IIA & IIB, and investigate whether they possess varying distributions. Distinct sub-cellular domains have been described for the IIA and IIB isoforms in single cells (Kolega, 1998, 2003), however this has not been investigated in a wound model.

The most compelling evidence for a contractile actin cable came from experiments using an inhibitor of NM-myosin II. When blebbistatin was introduced to culture media *after* the actin cable had formed, the cable failed to contract significantly. This observation was in agreement with studies in *Drosophila*, where loss of function mutants have functionally identified NM-myosin II as the motor driving dorsal closure (Bement et al., 1993; Franke et al., 2005). Accordingly, blebbistatin treatment of the sensory epithelium resulted in severe defects of the wound closure process. The most striking effect was that the epithelial surface was not pulled together, and that the network of AJCs was not re-established in the wound space. It was noted that inhibition of NM-myosin II did not prevent lamellipodia from entering the wound space. Although lamellipodia attempted closure by covering the base of the wound space, they were unable to restore the apical-basolateral polarity of the epithelium. These experiments demonstrated that the actin cable was an acto-myosin structure, and that NM-myosin II activity was required to generate contractile force to drive closure and ultimately restore epithelial polarity in the wound space.

In addition to that seen surrounding laser wounds, other potential acto-myosin structures were identified in the sensory epithelium. Intense NM-myosin IIB labelling was found in toroidal structures corresponding to the apical junction of several support cells. It was possible that this represented a contractile acto-myosin cable that maintains epithelial integrity, similar to that reported in UV-treated MDCK monolayers (Rosenblatt et al., 2001). It was not clear from these experiments whether this was a support cell structure, or whether it was part of the hair cell cuticular plate (Hirokawa and Tilney, 1982). A more detailed examination of this acto-myosin structure is presented in Chapter 5.

3.3.3 Lamellipodial crawling as an independent mechanism of wound closure

Formation of an acto-myosin cable was not the only cytoskeletal event triggered by laser wounding. Another prominent response was the formation of lamellipodia. Initial investigations using DIC identified lamellipodia entering the wound space, however they proved difficult to resolve using this imaging modality. Studies using fluorescent phalloidin allowed lamellipodia to be easily identified, and revealed that these structures could enter the wound space in advance of the contracting acto-myosin cable. Unfortunately, the information gleaned from phalloidin labelled preparations

represented wound structure at the time of fixation only. Considering that lamellipodia are widely documented as motile structures, this technique was limited to providing a 'snapshot' of their activity. Time-lapse imaging of β-actin-EGFP circumvented this limitation and provided unparalleled insight into lamellipodia activity during wound closure. These recordings demonstrated that significant cytoskeletal activity was present within five minutes of epithelial wounding. At this time, there was already extensive membrane ruffling around the wound perimeter. Within twelve minutes of laser wounding, lamellipodia were already starting to invade the denuded space. Unfortunately, recordings were not able to capture the first five minutes of activity that occurred after laser ablation; a consequence of having to switch samples between microscopes and acquiring the appropriate focus. Despite this, these observations represented the earliest structural changes recorded in response to laser ablation. The signalling that initiated and controlled these events must have been active within the short period that elapsed between laser ablation and the start of the time-lapse.

Consideration will now be given to the function of lamellipodia during wound closure. Various reports have described epithelial wound closure driven by acto-myosin based cable contraction in association with lamellipodia (Bement et al., 1993; Wood et al., 2002), and also without (Martin and Lewis, 1992; Brock et al., 1996). The data presented in this thesis demonstrated that lamellipodia were present in the wound space throughout the majority of the closure process. Not only were lamellipodia observed forming at the leading edge, the use of β-actin-EGFP revealed cryptic processes that extended from several rows behind the wound border. Without additional experimentation, it was difficult to estimate how many support cells extended such cryptic processes towards the wound border. Nonetheless, these observations were suggestive of wound closure through cell-crawling (Farooqui and Fenteany, 2005). Experiments using the Rho kinase inhibitor Y-27632 provided functional evidence that cell crawling was important for wound healing in the utricular sensory epithelium. Blockade of Rho kinase function prevented formation of an actin cable around the epithelial wound, allowing the individual contribution of cell crawling to be assessed. It was found that without an actin cable, wounds were still able to close within four hours of laser ablation. Whilst support cell processes were able to effect closure at the base of the epithelium, the surface was not pulled together as in control wounds. It was

particularly evident that the AJC was not restored in the closed wound. These results were in agreement with experiments performed in *Drosophila* embryos, where inhibition of Rho GTPase activity abolishes actin cable formation, but does not prevent wound closure by lamellipodia (Wood et al., 2002). An important question left unanswered, was whether the wound would still close effectively without the contribution of lamellipodia. It has been shown here that the inhibition of actin cable formation or contraction did not prevent the epithelium from attempting to close using lamellipodial extension. An interesting experiment will be to assess the impact of wiskostatin, a N-WASP inhibitor, upon the wound closure process (Peterson et al., 2004).

Taken together, it has been shown that lamellipodial extension and cell crawling represent an additional mechanism of wound closure, independent of the contractile acto-myosin cable. It was evident that under normal conditions, these two processes could work in tandem to achieve epithelial wound closure. It is now proposed that the actin cable pulls the apical portion of the epithelium together, and that lamellipodial crawling act to restore the base. Thus, these two processes act in synergy to restore apical-basal polarity in the wounded epithelium.

3.3.4 Signals regulating actin cable formation

Experiments in this chapter identified several compounds that interfered with formation of the acto-myosin cable, providing some insight into the underlying mechanisms. In agreement with a previous study, treatment with cytochalasin D completely prevented reorganisation of the actin cytoskeleton around the wound edge (McCluskey and Martin, 1995). This indicated that actin cable formation was completely dependent upon *de novo* polymerisation of actin filaments. This finding confirmed that cable formation was an active process, and not simply manifest of intrinsic epithelial tensions released by laser wounding. A more subtle observation was made when epithelia were pretreated with blebbistatin, an inhibitor of NM-myosin II. In this experiment, actin cable formation was defective. Actin failed to reorganise into an elliptical cable at the surface, and was poorly defined towards the base of the epithelium. It is intriguing to consider how inhibition of NM-myosin II could elicit such a phenotype. A putative explanation can be constructed around a model of stress-induced microfilament alignment (Heath and Dunn, 1978; Kolega, 1986). This model is

based around observations that when a cell is placed under a longitudinal stress, the actin filaments rearrange along the axis that the force is acting. Sherratt *et al.* (1992), proposed that this forms the basis of actin cable formation, as wounding releases tensions normal to the wound edge, whilst tangential components remain intact. This redistribution of tensile stresses potentially provides the initial cue to rearrange or polymerise new actin filaments parallel to the wound border. It is speculated here that NM-myosin II can act within this system to drive contraction of these actin filaments, and further increase the tensile strain parallel to the wound border. This could potentially form the basis of a positive feedback system, where contractile force stimulates the formation of new filaments, allowing an even greater contractile force to be exerted *et cetera.* This wound model predicts that positive feedback would continue until the surrounding epithelial tissues become compliant and tensile stresses reduced in the cable. This feedback would allow the acto-myosin cable to regulate its own proportions, adapting according to the inertial resistances experienced. It follows that inhibition of NM-myosin II activity would eliminate the positive feedback, by preventing acto-myosin contractility, and the subsequent polymerisation or recruitment of additional filaments (Chrzanowska-Wodnicka and Burridge, 1996). The observed effects of blebbistatin upon actin cable formation were entirely consistent with this model. Additional support for this model was taken from observations in both phalloidin labelled and live-cell β-actin-EGFP time-lapse recordings. The actin cable frequently exhibited a non-uniform intensity around the wound perimeter. This might reflect asymmetries in both the mechanical stiffness and inertia of the surrounding epithelium. Areas of the wound that were less compliant would require more force to move, and would therefore display a correspondingly higher density of acto-myosin filaments in the cable. A similar observation has been reported during dorsal closure in *Drosophila* embryos (Franke et al., 2005).

If actin cable formation was dependent upon the redistribution of tensile stresses, a prediction can be made that this would be independent of the time that elapsed after laser ablation. This can be tested experimentally by wounding the epithelium in the presence of cytochalasin D, and then removing the inhibitor several hours later. If the actin cable still forms, this would be strong evidence for a signal intrinsic to the mechanical properties of the epithelium. Future experiments will

investigate whether this is the case, or if additional signals specific to the wounding event are required as co-factors.

In this chapter, the role of Rho kinase in actin cable formation was also examined. The Rho GTPase, and its effector Rho kinase are known to regulate actin cable formation in both wound and dorsal closure models (Brock et al., 1996; Fenteany et al., 2000; Jacinto et al., 2002; Russo et al., 2005). In agreement with these, it was demonstrated that Rho kinase was required for actin cable formation in wounded sensory epithelia. Several theories can explain why Rho kinase activity is essential for actin cable formation. Foremost is the possibility that Rho kinase elicits its effects through modulation of NM-myosin II. The regulatory myosin light chain (MLC), and myosin phosphatase (MYPT) are direct substrates for Rho kinase, with phosphorylation acting synergistically to increase NM-myosin II activity (Amano et al., 1996; Kimura et al., 1996). In the context of the stress-induced filament alignment model, inhibition of Rho kinase could reduce NM-myosin II activity, which has already been shown to be essential for successful formation and contraction of the actin cable (see above). It follows that if Rho kinase was controlling NM-myosin II activity, inhibition with Y-27632 could also prevent contraction of the actin cable. Evidence from another wound model suggests that this is not the case. Russo *et al.* (2005), have shown that whilst Rho kinase regulates actin cable formation, contraction is driven by the myosin light chain kinase (MLCK). Future experiments will be required to determine whether MLCK and Rho kinase play a functional role during cable contraction in the sensory epithelium. Finally, Rho kinase may influence actin cable formation through an interaction with the LIM kinase – cofilin pathway (Maekawa et al., 1999). Pharmacological blockade of Rho kinase can releases an inhibitory phosphorylation on cofilin, resulting in the de-stabilisation of existing actin filaments. In experiments presented here, Y-27632 treatment did not induce any noticeable collapse of stress fibre filaments, which were normally prevalent at the base of support cells. This was in contrast to cytochalasin D, which induced stress fibre collapse throughout the base of the epithelium.

3.3.5 ERK as an early wound signal

This chapter has demonstrated the activation of the extracellular signal-related kinases (ERK1/2) by epithelial wounding. ERK activation was assayed *in situ* using an antibody directed against the active di-phosphorylated isoform. When examined at

different time-points after laser ablation, these experiments yielded a complex profile of ERK activation, varying in both time and space around the epithelial wound. ERK activation reached a maximum five minutes after laser ablation, and returned to basal levels within sixty minutes. The observation that ERK was transiently activated in response to injury was entirely consistent with reports from other epithelial wound models (Dieckgraefe et al., 1997; Nobes and Hall, 1999; Matsubayashi et al., 2004; Nikolic et al., 2006). Experiments presented in this chapter also demonstrated a cell specific activation along the wound border, being restricted exclusively to support cells of the sensory epithelium. The absence of detectable ERK activation from hair cells was striking, and had clear implications for the nature of the signalling. Whether this indicated an absence of the actual ERK protein from hair cells, or a difference in the activation pathways was unknown. Nonetheless, these experiments identified a fundamental difference between how hair cells and support cells responded to epithelial wounding. Given the contribution of support cells to wound closure, this difference in signalling was of particular interest.

The potential function of ERK activation in the wounded sensory epithelium was investigated using the cell permeant MEK1/2 inhibitor, U0126. Actin cable formation and wound closure appeared normal whilst under U0126 blockade, suggesting that ERK activation was not essential for these processes. This was surprising, as ERK activity is required for the migration of wounded cell monolayers (Sharma et al., 2003; Matsubayashi et al., 2004). A possible explanation for this disparity is that ERK inhibition did reduce cell motility in utricular sensory epithelia, but that this was masked by the contribution of the acto-myosin cable. This suggests an element of redundancy in the wound closure process, where the acto-myosin cable can compensate and still achieve wound closure within a similar timescale. A future experiment to explore this redundancy will be to study wound closure under simultaneous Rho kinase and ERK blockade. In the absence of an acto-myosin cable, this may reveal whether ERK activation is required for cell crawling, as reported in other systems. It was also possible that ERK inhibition generated a subtler wound closure phenotype that evaded detection here. In particular, it has been shown that ERK can directly phosphorylate MLCK, resulting in a corresponding increase in MLC phosphorylation (Klemke et al., 1997). Given that ERK was active during the period of actin cable assembly and contraction, the potential interaction with MLCK was

intriguing. Although ERK inhibition did not alter the ultimate outcome of wound closure, it was possible that it altered the kinetics of actin cable contraction. This will be examined in future experiments using time-lapse studies.

Inhibition with U0126 elicited no evident phenotype, however this was not to suggest that ERK signal was redundant during wound closure. When considering other putative functions for ERK during wound closure, it is important to consider not only the temporal kinetics of activation, but also the cellular compartments within which ERK resides; the so called spatio-temporal profile (Marshall, 1995). At the peak of activation in the sensory epithelium, phosphorylated ERK was present within both cytosolic and nuclear compartments of the support cells. This profile indicated that ERK might be phosphorylating cytoplasmic in addition to nuclear targets. Potential cytosolic targets are focal adhesion kinase (FAK), paxillin and MLCK (reviewed by Huang et al., 2004). All these have important functions relating to the cytoskeleton and focal adhesion/integrin signalling. Nuclear substrates of ERK are diverse and include transcription factor such as Elk-1 and CREB (reviewed by Sharrocks, 2001). ERK signalling is also required for IEG induction around epithelial wounds (Martin and Nobes, 1992; Dieckgraefe et al., 1997; Dieckgraefe and Weems, 1999), and these have separately been shown to regulate wound migration (Tran et al., 1999). Future experiments will investigate some of these ERK substrates, and determine whether U0126 does in fact generate a more subtle wound closure phenotype. A function for ERK signalling in the induction of cell proliferation will be examined in the Chapter 4.

3.4 Conclusions

In conclusion, these experiments have detailed an epithelial wound repair mechanism in the avian utricular macula. A model of the sensory epithelium was established *in vitro* to facilitate the study of this phenomenon. Laser ablation was found to be an effective method to wound the sensory epithelium in a precise and repeatable manner. Epithelial support cell were able to close the wound within four hours using a contractile acto-myosin cable in conjunction with cell crawling. The combination of these two mechanisms ensured that apical-basal polarity was maintained once wound closure was complete. Wound closure was found to be absolutely dependant upon actin polymerisation. In addition, NM-myosin II activity was required for cable contraction. NM-myosin II and Rho kinase were also identified as important regulators of actin

cable formation. Finally, it was demonstrated although the ERK MAPK was transiently activated within five minutes of laser ablation, it was not essential for effective wound closure. It remains to be seen whether the repair mechanisms described here are active during specific pathologies of inner ear sensory epithelia.

4 Cell cycle activity in laser ablated sensory epithelia

4.1 Introduction

Support cell proliferation is an important component of the regenerative program in avian sensory epithelia (see Section 1.4). It is well established that in response to hair cell loss, support cells of the avian auditory and vestibular organs are able re-enter the cell cycle and proliferate. These newly generated mitotic progeny repopulate the sensory epithelium and subsequently differentiate into both support cells and hair cells. Although the relative timing of hair cell loss and the ensuing proliferation is well documented in the inner ear, the signals that couple epithelial trauma to cell cycle activity are not. This functional relationship is of particular interest, as hair cell loss does not always correlate with proliferation in other animal models, most notably the mammal.

The previous chapter described a wound closure mechanism that was activated in response to epithelial trauma. This work is now extended to investigate whether proliferation also occurs in response to trauma, in parallel to that reported in other wound models (see Section 1.5). A specific question was whether laser ablation could elicit a local increase in support cell proliferation, and thus be used as a system to study the avian regenerative process. Accordingly, the laser ablation model introduced in the previous chapter was now extended to allow measurements of cell proliferation using a 5-bromo-2'deoxyuridine (BrdU) incorporation assay. Circular wounds of the embryonic sensory epithelium did not generate a statistically significant increase in support cell proliferation. In contrast, larger wounds of the postnatal sensory epithelium elicited a significant increase within 48 hours of laser ablation. Using the latter model, experiments identified several intracellular signalling pathways that promoted support cell proliferation during wound closure in the avian sensory epithelium. These results will be discussed in relation to cell cycle control in other epithelial systems, and how these might compare to the avian inner ear.

4.2 Results

The experiments presented in this chapter use epithelial preparations of both embryonic (E21) and postnatal (P7-14) chick utricular maculae. Using laser ablation, epithelial cultures have been wounded using one of two paradigms; a puncture-wound as introduced in Chapter 3 or a linear stripe-wound. In these experiments, nuclear incorporation of the thymidine analog 5-bromo-2'deoxyuridine (BrdU) has been used to assay S-phase activity, and infer cell cycle progression.

4.2.1 Support cell proliferation in laser ablated embryonic epithelia

To determine quiescent levels of proliferation *in vitro*, BrdU incorporation was initially measured in unwounded cultures of the utricular sensory epithelium. Epithelial cultures of E21 chick utricles were prepared as described previously (see Section 2.4.1), and maintained for 47 hours in the continued presence of BrdU (n = 13 epithelia). Epithelia were then fixed and processed for HCS-1 and BrdU immunocytochemistry (see Section 2.7.3). HCS-1 recognises an unknown antigen that is specific to the cell membrane and cytoplasm of sensory hair cells. In unwounded samples, HCS-1 immunocytochemistry revealed that sensory hair cells were evenly distributed throughout the cultured epithelium (Figure 4.1A). The corresponding BrdU labelling was distributed throughout the epithelium, and restricted exclusively to cell nuclei (Figure 4.1B). A qualitative observation was that some BrdU nuclei appeared to be paired in close proximity, within approximately one nuclear diameter of each other. As BrdU is heritable to all cellular progeny, the presence of pairs was strongly suggestive of cell division within the assay period. BrdU labelling was almost exclusively found within support cells; BrdU positive hair cells were rarely observed.

Increased levels of support cell proliferation have been reported in acoustic, laser irradiation and ototoxic trauma models of the avian inner ear (Corwin and Cotanche, 1988; Ryals and Rubel, 1988; Weisleder and Rubel, 1993; Warchol and Corwin, 1996). Experiments were now performed to establish whether laser ablation of the utricular sensory epithelium *in vitro* was able to elicit a similar increase in support cell proliferation. Laser ablation was used to create puncture-wounds in the cultured epithelium, in an identical fashion to that described in Chapter 3. One hour after injury, BrdU was supplemented to the culture medium and epithelia maintained for a further 47 hours *in vitro* (n = 8 epithelia). HCS-1 immunocytochemistry demonstrated the location

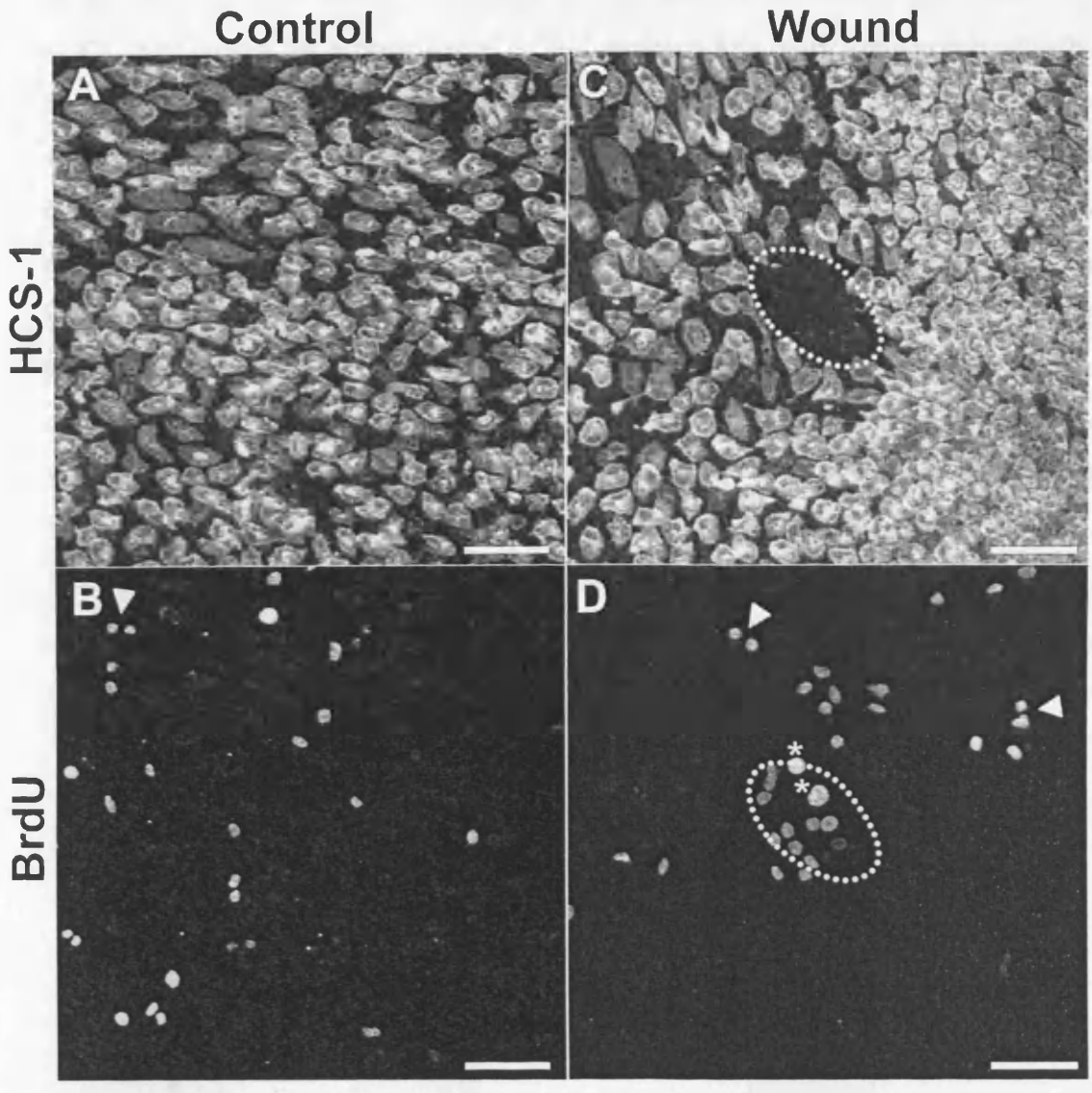

Figure 4.1 – Laser puncture-wounds of the utricular epithelium trigger proliferation. Embryonic (E21) utricles were prepared as epithelial cultures and puncture-wounded using laser ablation. Epithelia were cultured in the presence of BrdU for 47 hours following laser ablation, then fixed and processed for HCS-1 and BrdU immunocytochemistry. **A)** HCS-1 positive hair cells were distributed evenly throughout the unwounded epithelium. **B)** BrdU positive support cells were similarly distributed throughout the unwounded epithelium. A proportion of nuclei appear to be 'paired' (arrowheads). **C)** Laser ablation resulted in the loss of HCS-1 positive hair cells from the wound site (dotted line). **D)** BrdU positive cell were concentrated within the wound site (dotted line). BrdU positive cells were also present throughout the remainder of the epithelium. As before, some nuclei appear to be paired (arrowheads). Some nuclei appear to have different chromatin structure, possibly representing a difference in cell cycle at the time of fixation (asterisk). Scale bars represent 50 μm.

of the original laser wound, delineated by the absence of sensory hair cells (Figure 4.1C). Aside from the wound itself, HCS-1 positive hair cells were evenly distributed throughout the remainder of the epithelium. It must be stressed that although hair cells were absent from the wound environs, support cells were present within this region, having completed the closure process during the experiment (see Chapter 3). As in controls, BrdU positive nuclei were distributed throughout the epithelium, however they were now additionally clustered within the wound site (Figure 4.1D). The density of BrdU positive nuclei was quantified within a 100 μm locus in both control and wounded cultures (see Section 2.8.4). In unwounded control epithelia, the density of BrdU nuclei was estimated at 5.31 ± 0.99 nuclei per 10'000 μm^2 (n = 13 epithelia). Laser ablation increased the number of BrdU positive nuclei by 1.23 fold to 6.53 ± 1.11 nuclei per 10'000 μm^2 (n = 8 epithelia). Despite a visible increase of BrdU positive nuclei in some epithelial wounds, this was not statistically significant (p = 0.47, 2-tailed Student's *t*-test). This data is summarised in Figure 4.2.

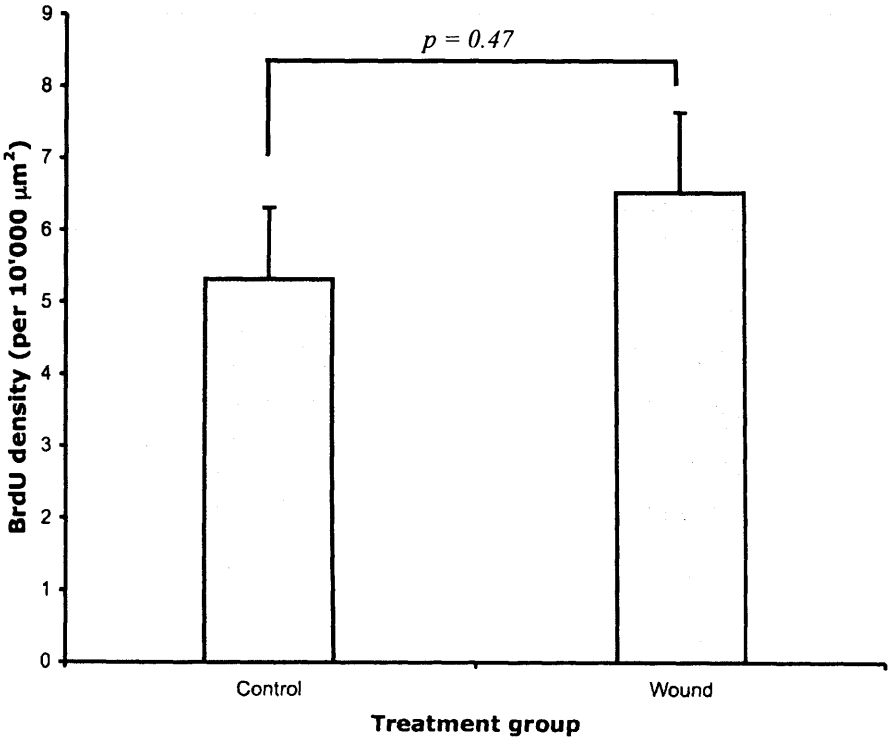

Figure 4.2 - Quantification of BrdU incorporation after laser puncture-wounding. BrdU positive nuclei were counted within a 100 μm radius circle of the wound site. Unwounded controls (n = 13 epithelia) were compared with laser wounds (n = 8 epithelia). The resulting count is expressed as nuclei per 10'000 μm^2. Laser puncture-wounding increased the number of BrdU positive nuclei by 1.23 fold, however this was not significant (p = 0.47, 2-tailed Student's *t*-test). Data are expressed as means ± SEM.

A possible explanation for the non-significance was that elevated levels of background proliferation inherent to both wound and control data sets were masking the increase. A previous report has demonstrated the inverse relationship between cell density and quiescent BrdU incorporation in the chick utricular epithelium (Warchol, 2002). Intriguingly, some control epithelia with lower cell densities were found to correlate with high levels of BrdU incorporation, despite not being wounded (Figure 4.3A). To examine whether variations in hair cell density were a complicating factor in experiments here, counts of HCS-1 positive somas were taken from control and wounded epithelia. In control epithelia, the average hair cell density was estimated to be 29.4 ± 2.1 HCS-1^{+ve} somas per 10'000 μm^2 (n = 13 epithelia). The hair cell density in wounded epithelia was similar, estimated to be 28.5 ± 2.0 HCS-1^{+ve} somas per 10'000 μm^2 (n = 8 epithelia). Hair cell densities were not significantly different between the two treatment groups (p = 0.87, 2-tailed Student's *t*-test). A scatter plot compiled from these data shows that there was a density threshold in control epithelia (~ 25 hair cells / 10'000μm^2), below which BrdU incorporation was markedly increased (Figure 4.3B). Therefore, epithelia with hair cell densities below this threshold were eliminated from both wounded and control data sets. The truncated data sets were then recomputed as before. In unwounded epithelia there were now 3.9 ± 0.9 BrdU positive nuclei (n = 8), compared to 4.1 ± 0.9 in wounded samples (n = 5). This represented a non-significant increase of over control levels (p = 0.88, 2-tailed Student's *t*-test).

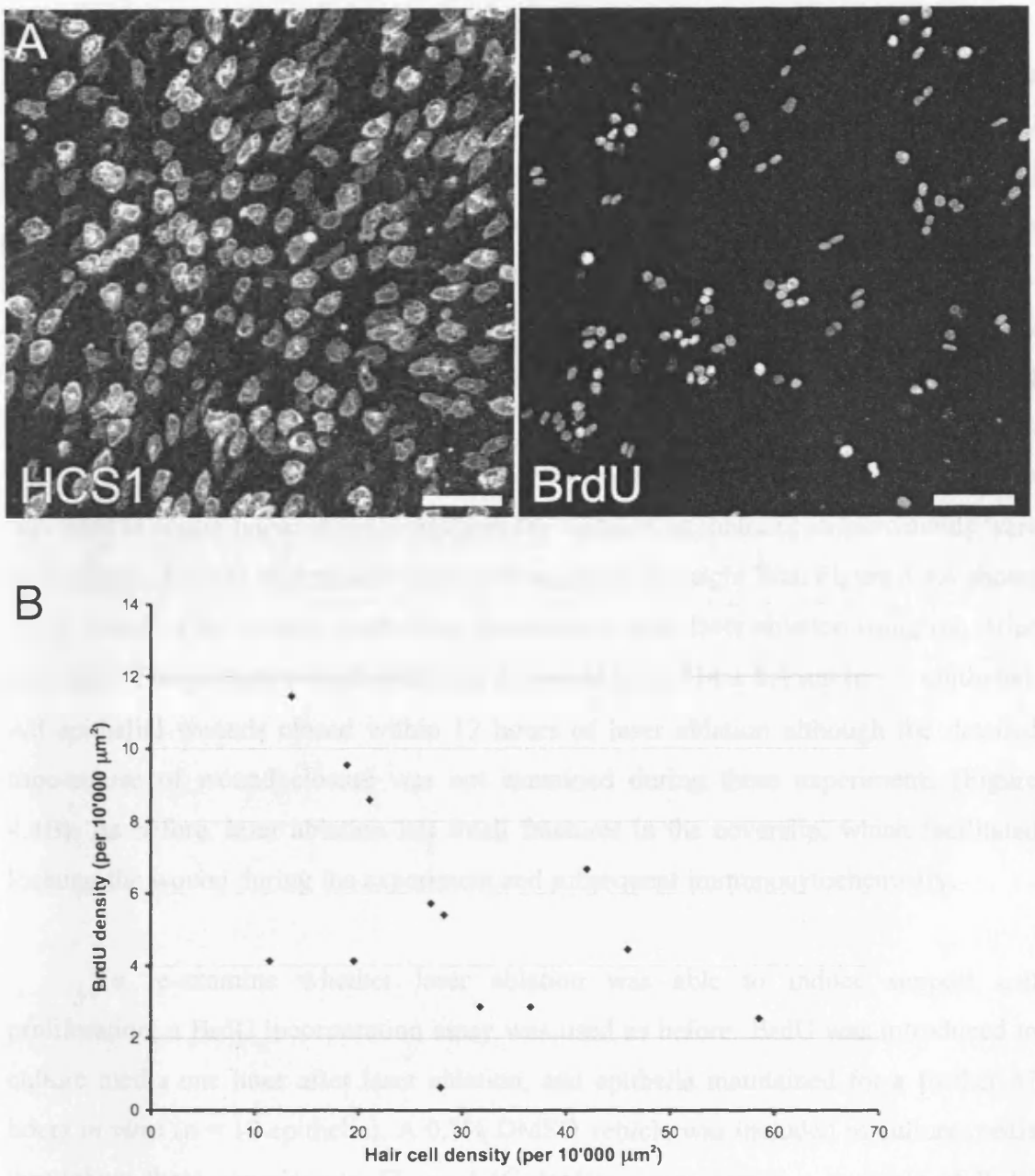

Figure 4.3 – Variable BrdU incorporation in unwounded epithelia. Some control epithelia displayed high levels of BrdU incorporatio even though they were not wounded. **A)** An unwounded epithelium showing a high quiescent level of BrdU incorporation. **B)** A scatter plot demonstrates the inverse relationship between HCS-1 hair cell density and BrdU incorporation (n = 13 epithelia). Scale bars represent 50 µm.

4.2.2 Support cell proliferation in laser ablated postnatal epithelia

The previous experiments demonstrated that in response to laser ablation, the embryonic model did not consistently display a significant increase in BrdU incorporation. An alternate culture and wounding paradigm was now adopted, based upon a previously published postnatal model (Warchol, 2002). Specific differences between this model and the embryonic culture paradigm are discussed in Section 2.4.1. Worthy of particular mention, this model was a culture of the entire utricular macula (cotillus & striola), as opposed to using just the cotillus as before. Epithelial cultures of the entire sensory macula were prepared from P7-14 chick utricles, as described in Section 2.4.1. In an attempt to elicit a more robust proliferative response, laser ablation was used to create linear stripe-wounds in the cultured epithelium; stripe-wounds were quite simply a series of puncture wounds arranged in a straight line. Figure 4.4A shows a live image of the sensory epithelium immediately after laser ablation using the stripe paradigm. The average wound width was measured to be 114 ± 8.4 μm (n = 9 epithelia). All epithelial wounds closed within 12 hours of laser ablation although the detailed time-course of wound closure was not examined during these experiments (Figure 4.4B). As before, laser ablation left small fractures in the coverslip, which facilitated locating the wound during the experiment and subsequent immunocytochemistry.

To re-examine whether laser ablation was able to induce support cell proliferation, a BrdU incorporation assay was used as before. BrdU was introduced to culture media one hour after laser ablation, and epithelia maintained for a further 47 hours *in vitro* (n = 12 epithelia). A 0.1% DMSO vehicle was included in culture media throughout these experiments. Figure 4.4C depicts a representative example of BrdU incorporation captured from a stripe-wounded epithelium. A large increase in the number of cells incorporating BrdU was observed clustered along the line of the original laser ablation. The increase in proliferation was symmetrical around the laser ablation. BrdU incorporation in areas > 100 μm away from the original laser ablation possessed visibly lower levels of BrdU incorporation. A large number of BrdU positive nuclei were present within 10 μm of each other. As before, this was suggestive of cell division occurring during the assay period. The density of BrdU nuclei was calculated in both wounded and unwounded regions of the sensory epithelium (see Section 2.8.4). In unwounded areas, BrdU incorporation was estimated to be 2.0 ± 0.4 nuclei per

10'000 μm^2 (n = 12 epithelia). In wounded areas, BrdU incorporation was estimated to be 15.0 ± 1.3 nuclei per 10'000 μm^2 (n = 12 epithelia), representing a significant 7.5 fold increase over unwounded areas ($p < 0.001$, 2-tailed Student's *t*-test). The robust increase induced by laser ablation made this model better suited for studying the regulation of cell-cycle progression in the wounded sensory epithelium.

4.2.3 Proliferative signalling through PI3K, ERK & JNK

Using the postnatal model, experiments were now performed to assess the impact of different signalling pathways upon cell cycle progression in the wounded sensory epithelium. A previous study in the avian utricular epithelium has demonstrated that phosphoinositide 3-OH kinase (PI3K) and ERK are both required for serum-induced support cell proliferation (Witte et al., 2001). Separately, experiments from Chapter 3 demonstrated that ERK was activated around the perimeter of epithelial wounds. Laser ablation was now used to assess whether these pathways were required for cell cycle progression induced by epithelial wounding. Signalling through another MAPK, c-Jun N-terminal kinase (JNK) was also investigated. To address these hypotheses, the epithelial wound assay was repeated whilst individual pathways were placed under pharmacological blockade. The cell permeant inhibitors U0126 10 μM, SP600125 15 μM and LY294002 30 μM were used to inhibit the ERK, JNK and PI3K signalling pathways respectively during these experiments. Cell cycle progression was assayed using BrdU incorporation as before. All the inhibitors tested were individually able to reduce the number of BrdU positive nuclei present within the epithelial wound, however none prevented wound closure as assessed 48 hours after laser ablation (Figure 4.4D-F). Based upon images taken shortly after laser ablation, the initial size of epithelial wounds did not vary significantly between the treatment groups ($p = 0.98$, one-way ANOVA). BrdU incorporation was quantified for epithelial wounds treated with U0126, SP600125 or LY294002. Treatment with 10 μM U0126 was used to inhibit MEK1/2 activity. In comparison to wounded epithelia that were treated with a 0.1% DMSO vehicle, U0126 significantly reduced the density of BrdU positive nuclei by 2.2 fold to 6.9 ± 1.2 nuclei per 10'000 μm^2 (n = 11 epithelia, $p < 0.001$). This reduced level was still significantly elevated compared to unwounded controls treated with a 0.1% DMSO vehicle ($p < 0.005$). Treatment with 15 μM SP600125 was used to inhibit JNK1/2/3 activity. Relative to wounded epithelia treated with a 0.1% DMSO vehicle, SP600125

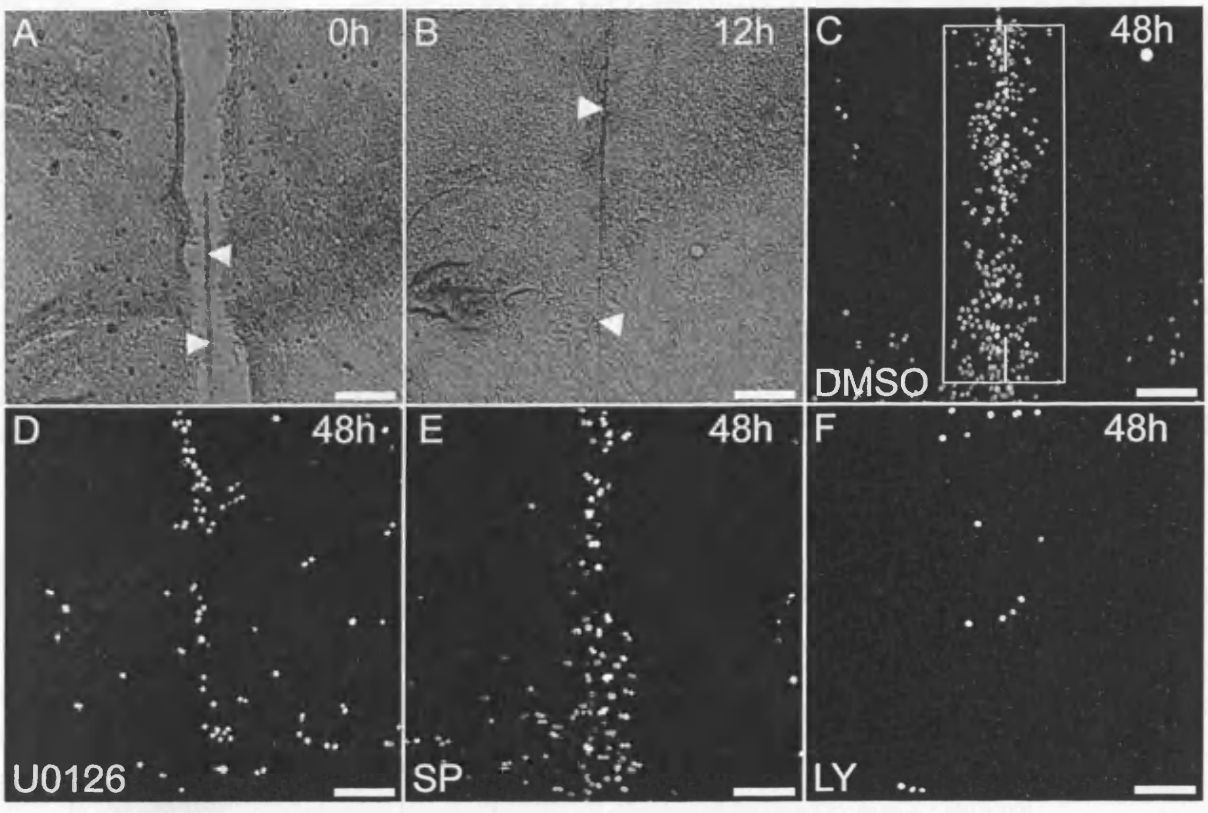

Figure 4.4 – Laser stripe-wounds of the utricular epithelium trigger proliferation. Postnatal (P7-14) chick utricles were prepared as epithelial cultures, and stripe-wounded using laser ablation. Epithelia were cultured in the presence of BrdU for 47 hours following ablation, then fixed and processed for HCS-1 and BrdU immunocytochemistry. **A)** Live-cell image of the sensory epithelium immediately after laser ablation. Laser ablation left small fractures within the underlying glass coverslip (white arrows). **B)** All epithelial stripe wounds closed within 12 hours. The laser ablation marks were still visible, allowing the wound site to be easily located (white arrows). **C)** In the presence of a 0.1% DMSO vehicle, wounding triggered local increase in the number of BrdU nuclei within 100 μm each side of the laser ablation site. The region used for BrdU analysis has been overlaid. Outside of this region, BrdU incorporation remained at a basal level. **D-F)** Treatment with U0126 10 μM, SP600125 15 μM or LY294002 30 μM visible reduced the number of BrdU positive nuclei within 100 μm of the laser ablation. BrdU images have been arranged such that the laser ablation runs vertically down the centre of each image. All images are representative of at least ten independent experiments ($n \geq 10$ epithelia for each group). All scale bars represent 100 μm.

significantly reduced BrdU positive nuclei by 1.5 fold to 9.8 ± 1.0 nuclei per 10'000 μm^2 (n = 14 epithelia, $p < 0.005$). This reduced level was still significantly elevated compared to unwounded controls treated with a 0.1% DMSO vehicle ($p < 0.001$). Finally, treatment with 30 μM LY294002 was used to inhibit PI3K activity. In comparison to wounded epithelia that were treated with a 0.1% DMSO vehicle, LY294002 significantly reduced the number of BrdU positive nuclei by 7.1 fold to 2.1 ± 0.6 nuclei per 10'000 μm^2 (n = 10 epithelia, $p < 0.001$). This reduced density was comparable with that observed in unwounded regions of an epithelia treated with a 0.1% DMSO vehicle ($p = 0.96$). These data have been summarised in Table 4.1 and as a graph (Figure 4.5).

Treatment group	N	BrdU nuclei (total)	BrdU nuclei (per 10'000 μm^2)
Unwounded 0.1% DMSO	12	24.4 ± 4.7	2.0 ± 0.4
Wounded 0.1% DMSO	12	180 ± 15.9	15.0 ± 1.3
Wounded 10μM U0126	11	82.4 ± 14.1	6.9 ± 1.2
Wounded 15μM SP600125	14	117 ± 12.2	9.8 ± 1.0
Wounded 30μM LY294002	10	24.8 ± 7.3	2.1 ± 0.6

Table 4.1 - Summary of BrdU data for stripe-wounded epithelia. N = number of epithelia in each treatment group. Data are expressed as means ± SEM.

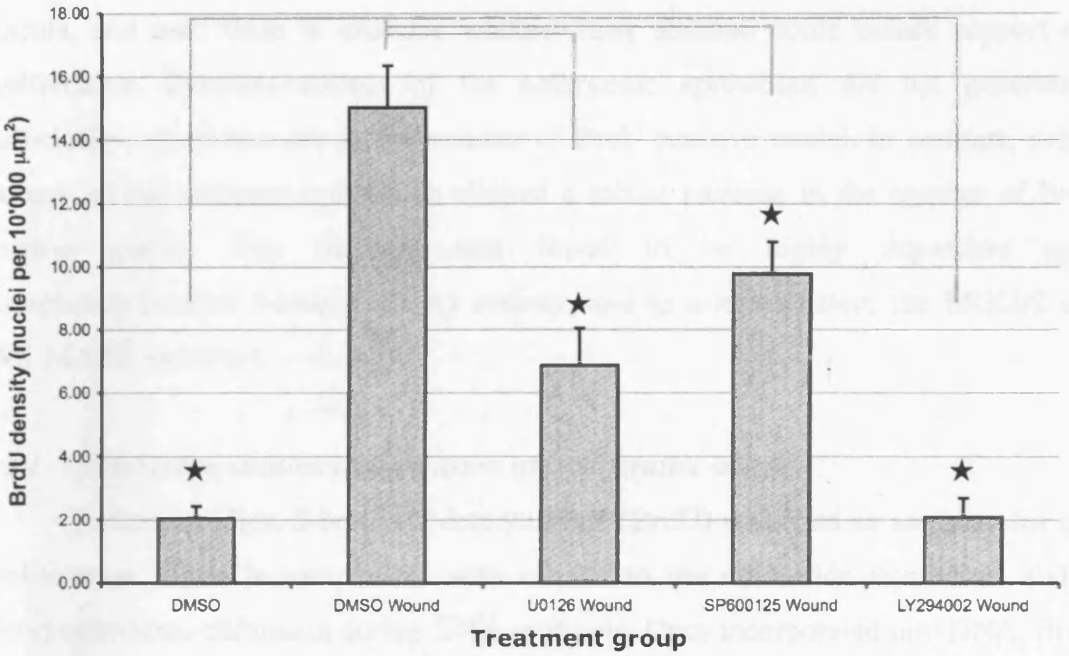

Figure 4.5 - Quantification of BrdU incorporation following laser stripe wounding. The number of BrdU positive nuclei was quantified within 100 μm of the laser ablation. Laser stripe-wounding was found to significantly increase the density of BrdU positive nuclei when compared to unwounded regions of the epithelium. Treatment with U0126 10 μM and SP600125 15 μM was able to significantly reduce BrdU incorporation with 100 μm of the laser ablation. Treatment with LY294002 30 μM was able to completely prevent the increase of proliferation within the epithelial wound. BrdU counts have been expressed as positive nuclei per 10'000 μm^2. Please refer to the text for a table of experimental values. Data are expressed as means ± SEM, and were obtained from at least ten independent epithelia per treatment group ($n \geq 10$). ★ denotes $p < 0.05$ compared to wounded DMSO group (Student's *t*-test, 2-tailed).

4.3 Discussion

This chapter has presented two *in vitro* epithelial models of the chick utricular macula, and used them to examine whether laser ablation could induce support cell proliferation. Puncture-wounds of the embryonic epithelium did not generate a statistically robust increase in the number of BrdU positive nuclei. In contrast, stripe-wounds of the postnatal epithelium elicited a robust increase in the number of BrdU positive nuclei. This increase was found to be highly dependent upon phosphatidylinositol 3-kinase (PI3K) activity, and to a lesser extent the ERK1/2 and JNK MAPK pathways.

4.3.1 BrdU incorporation as a measure of proliferative activity

In these studies, 5-bromo-2'deoxyuridine (BrdU) was used as an assay for cell proliferation. BrdU is competitive with respect to the nucleotide thymidine, and is incorporated into chromatin during DNA synthesis. Once incorporated into DNA, BrdU is heritable and persists in the chromatin of all subsequent cellular progeny. For these reasons, BrdU sees extensive usage as an indicator of S-phase activity, and for lineage tracing studies. To correctly interpret data presented in this chapter, it is important to consider the length of BrdU application used in these experiments. This study has used a long application (47 hours), providing ample time for any given cell to enter S-phase, and progress through G2 and mitosis. Due to the nature of inheritance, both daughter cells would contain BrdU in their chromatin, and both would be labelled using immunocytochemistry. Thus, a BrdU positive nucleus can signify either a cell in S-phase, or an interphase progeny from a previous mitosis. Due to the length of BrdU application, it was extremely difficult to differentiate between these two situations. It was certainly erroneous to infer that all BrdU positive nuclei observed in these experiments were in S-phase. Indeed, there was strong anecdotal evidence to suggest that mitosis was occurring during the assay period; manifest in the apparent pairing of some BrdU nuclei. Although this was a qualitative observation, it was likely that a cell incorporating BrdU during S-phase would subsequently divide, given the duration of the assay. A shorter BrdU assay period could have minimised the likelihood of cell divisions taking place, however this required prior knowledge of the S-phase kinetics. As this has yet to be established in this model, a longer application was used to capture all activity, at the expense of cell cycle timing information. In summary, BrdU

incorporation is presented as a general measure of cell cycle activity and not that of S-phase *per se*.

4.3.2 Epithelial wounds: embryonic vs. postnatal model

A major finding from experiments in this chapter was that support cells were able to proliferate in response to epithelial wounding. This was an important, given that support cell proliferation is an essential component of the avian regenerative process. Initially, laser ablation was used to create puncture-wounds in the embryonic sensory epithelium and BrdU incorporation used as a proliferation assay. Whilst this experiment yielded several clear examples of elevated BrdU incorporation within the original wound, the increase was not statistically significant. Subsequent experiments were performed in the postnatal sensory epithelium using the laser micro-beam to create stripe-wounds. In these experiments, a significant increase in BrdU labelling was observed within a 100 μm locus of the original ablation site. Although the mechanism of closure was not studied for stripe-wounds, it was highly likely to be based upon cell crawling, similar to that described for a wide variety of epithelia / monolayer culture systems (see Section 1.5.1). The average width of a stripe-wound was 114 μm, and it was interesting to observe that proliferation was restricted to within a similar locus. This suggested that a density dependent inhibition (DDI) might be in operation in this system. Possible mechanisms of DDI are discussed in the following section. A general question not investigated here, was whether support cell progeny in the wound had the capacity to differentiate into new sensory hair cells. This was unknown, and needs to be addressed in future experiments.

There were several explanations why the postnatal model displayed a significant increase in cell proliferation, whereas the embryonic model did not. Foremost, the scale of damage inflicted upon the sensory epithelium by laser wounding was substantially different. Laser stripe-wounds in the postnatal epithelium were clearly larger than those used in the embryonic model: stripe-wounds representing a continuous series of puncture-wounds. This allowed a larger wound area to be sampled, and under these circumstances, it was expected that the postnatal model would display a higher level of proliferation. Although stripe-wounds were not attempted in the embryonic epithelium, there is no evidence to suggest that they would respond any differently. Indeed, the

proliferation of cells as they migrate into a wound appears to be a common response of epithelia in general (see Section 1.5.3).

Another factor highlighted by these experiments was the difference in background proliferation between the embryonic and postnatal models. In the embryonic model, control levels of proliferation were elevated throughout the epithelium, acting to numerically mask any potential induction within the wound itself. In the postnatal epithelium, background levels of proliferation were approximately 2.5 fold lower than that observed in the embryonic model. Some level of quiescent proliferation was expected, considering the continual production and turnover of hair cells within the avian utricle (Jorgensen and Mathiesen, 1988; Kil et al., 1997). The chick utricle is not fully developed at E21 and hair cell numbers take several weeks to reach their full complement (Goodyear et al., 1999). Thus, the disparity in background proliferation between models may simply reflect the developmental stage at which the utricle was harvested. Another explanation for this variation is that all epithelia, regardless of developmental stage or treatment group, were subjected to the traumatic process of dissection and enzymatic digestion by thermolysin. In particular, mechanical injury resulting from the separation of the sensory epithelium from the mesenchymal stroma was likely to trigger proliferation in a similar manner to that of a laser wound. Although both embryonic and postnatal cultures were prepared in a similar fashion, the former was maintained *in vitro* for 24 hours before experimentation, whilst the latter was afforded 7 days to allow the entire macula to adhere to the substratum. It is likely that any dissection-induced proliferation would have subsided to a quiescent level during this extended culture period.

In summary, the induction of proliferation was not thought to be more efficacious in the postnatal epithelium compared to its embryonic counterpart. The differences were more appropriately formulated within a signal-to-noise ratio (SNR) argument. Due to the large wound size, the postnatal model possessed a high level of proliferation, coupled with negligible background activity; equating to a high SNR. Conversely, the smaller wounds of the embryonic model displayed a lower level of proliferation that was compounded with high background activity; resulting in a low SNR. The postnatal stripe-wound model was therefore the preferred system to study candidate signal pathways and examine their effect upon proliferative induction.

4.3.3 Timing & regulation of wound proliferation

As discussed in Section 4.3.1, S-phase kinetics could not be accurately extracted from the long BrdU application used in experiments here. No specific timing can be inferred, except that support cells entered S-phase within 48 hours of epithelial wounding. This broadly correlates with the reported S-phase latency of between 16-24 hours measured in models of acoustic trauma (Stone and Cotanche, 1994), aminoglycoside insult (Bhave et al., 1995) and laser irradiation of the basilar papilla (Warchol and Corwin, 1996). It is also in agreement with experiments using aminoglycoside treated utricles, which demonstrate maximum S-phase entry within 48 hours of drug administration (Matsui et al., 2000). Future experiments will require shorter BrdU assay periods in order to examine S-phase timing in detail.

This study has reported different dependencies for PI3K, ERK1/2 and JNK signalling in the induction of wound proliferation. In particular, inhibition of PI3K activity using LY294002 was able to completely block support cell proliferation in the epithelial wound. This striking effect was consistent with reports of growth-factor induced proliferation in both avian and mammalian utricular epithelia (Montcouquiol and Corwin, 2001b; Witte et al., 2001). It should be reiterated that the concentration of LY294002 used to inhibit PI3K activity in these experiments has also been shown to directly inhibit the mammalian target of rapamycin (mTOR; Brunn et al., 1996). The potent effects of LY294002 could therefore be attributed to interactions with mTOR in addition to PI3K itself. Support cell proliferation is sensitive to rapamycin, an inhibitor of mTOR (Montcouquiol and Corwin, 2001b; Witte et al., 2001). Nonetheless, the potency of LY294002 inhibition argued that PI3K and/or mTOR were essential to couple the events of epithelial wounding to the subsequent support cell proliferation. Phosphoinositide 3-kinases (PI3Ks) belong to a family of heterodimeric lipid kinases that catalyse phosphorylation of $PI(4,5)P_2$ at the 3' position to yield $PI(3,4,5)P_3$ (reviewed by Wymann and Marone, 2005). Production of $PI(3,4,5)P_3$ leads to recruitment and activation of Akt, a known regulator of cell growth and proliferation. When considering the potential functions of PI3K and Akt in wounded avian sensory epithelia, an enormous body of work exists in other systems. For example, Akt is known to phosphorylate a wide range of effectors, most notably the mammalian target of rapamycin (mTOR), glycogen synthase kinase 3β (GSK-3β) and the forkhead (FOXO) transcription factors. Of potential interest to the wound proliferation described here,

PI3K/Akt signalling is able to influence the G1/S-phase transition by controlling cytosolic levels of cyclin D1. In fibroblasts, cyclin D1 is normally targeted by GSK-3β for ubiquitination and subsequent degradation by the 26S proteasome. PI3K/Akt activity inhibits GSK-3β, allowing cyclin D1 levels to accumulate and promote S-phase entry (Diehl et al., 1998). The PI3K/Akt pathway is also able to reduce expression levels of $p27^{kip1}$, a cyclin dependent kinase inhibitor (CKI), through inhibition of the FOXO family of transcription factors in fibroblasts (Medema et al., 2000). Coincidentally, this CKI has attracted interest in sensory epithelia where it is restricted to the postmitotic support cell population, maintaining them in a state of cell-cycle arrest (Lowenheim et al., 1999; Torchinsky et al., 1999). Whether any of these mechanisms prove to be active within wounded sensory epithelia remains to be seen, however it is clear that PI3K/Akt signalling has the potential to synergistically promote S-phase.

In the postnatal model, support cell proliferation was concentrated within the approximately area of the original wound. This was suggestive of a density dependent inhibition (DDI) previously shown in other epithelial wound systems (see Section 1.5.3). Although a reduction in cell density was not investigated here, it was highly likely that this did occur within the wound. Warchol (2002) has described a DDI of proliferation around the edges of the avian utricular epithelium *in vitro* and documented the requirement for N-cadherin in this process. The localisation of β-catenin to cell junctions and the nucleus was also demonstrated in this study, although not explicitly linked to cell proliferation. Beta-catenin is an interesting molecule, as it functions both within the canonical Wnt pathway to promote proliferation, in addition to complexing with cadherins at the zonulae adherens. The ability of β-catenin to stimulate proliferation arises if it enters the nucleus, whereupon it interacts with the TCF/LEF family of transcription factors to induce expression of cyclin D1 (Shtutman et al., 1999). Cell-cell contact can thus regulate proliferation through the sequestration of β-catenin from the cytosol into the zonula adherens (reviewed by Nelson and Nusse, 2004). Given the suggested homology between the periphery of the epithelium and a wound edge within it, N-cadherin interactions and β-catenin might also regulate proliferation within the wound. Moreover, PI3K/Akt signalling can be integrated into this model. In fibroblasts, a complex of axin, APC and GSK-3β normally targets β-catenin for continual ubiquitination and degradation by the proteasome (Aberle et al., 1997).

Phosphorylation of GSK-3β by Akt halts this degradation, allowing cytosolic levels of β-catenin to accumulate in the cytosol and nucleus (Sharma et al., 2002). Future experiments will investigate whether this mechanism is also functional in the avian sensory epithelium.

Experiments in this chapter also addressed the contribution of the ERK and JNK MAPKs in the induction of wound proliferation. Inhibition of ERK or JNK activation was able to significantly reduce wound proliferation by approximately 55% and 36% respectively. Witte *et al.* (2001), reported a similar reduction in serum-induced proliferation when ERK was inhibited. The finding that ERK signalling was required for proliferation in epithelial wounds was intriguing, given the rapid activation kinetics demonstrated earlier (see Chapter 3). This effect was consistent with ERK's well characterised role inducing *cyclinD1* transcription (Lavoie et al., 1996), although this was not specifically demonstrated here. As U0126 was included in the culture media for the duration of the experiment, it cannot be said whether the initial ERK transient was sufficient to induce proliferation, as there may have been a subsequent wave of sustained activation as is the case in wounded MDCK monolayers (Matsubayashi et al., 2004). To clarify this, a future experiment will be to remove U0126 one hour after wounding and assay the resultant proliferation. This paradigm would inhibit the initial ERK transient but allow for any subsequent activation. Wound proliferation was also dependent upon JNK signalling. How JNK might interface with the cell-cycle machinery was unclear, although a recent study has shown that phosphorylated c-Jun can interact with β-catenin/TCF4 complexes and regulate proliferation in tumours (Nateri et al., 2005). In summary, inhibition of the ERK and JNK MAPK cascades elicited a partial reduction in BrdU labelling, suggesting that neither pathway was dominant in the induction of wound proliferation in the sensory epithelium.

It was intriguing to find that support cell proliferation in the wounded sensory epithelium was dependent upon the same pathways identified by Witte *et al.* (2001) using a serum-starvation protocol. The importance of this must be stressed, as although these two experimental paradigms are disparate, it suggests that they induce proliferation through similar mechanisms. One explanation was that growth factors could be released during epithelial wounding, thereby establishing a causal link between

the two stimuli. Another possibility is to consider the phenomena of contact inhibition and contend that the edge of an epithelial sheet is inherently similar to that of a wound. Consistent with this, support cells of the avian sensory epithelium continually proliferate around their edges *in vitro*. Serum can be used to augment this rate of proliferation (Witte et al., 2001), however it is not an essential factor (Warchol, 1995). Aside from any topological similarities, the reliance upon PI3K and ERK may simply reflect their ability to integrate a diverse range of cellular signals. Thus, although similar pharmacological sensitivities were observed, these did not necessarily reflect homologies in upstream activation. In the light of these results, it becomes clear that further investigation is require to determine the exact mechanisms of cell cycle regulation in wounded sensory epithelia. For example, although it was clear that PI3K activity was required for S-phase entry this could occur through several putative mechanisms. Was PI3K signalling removing a block on cell cycle progression, by alleviating the degradation of cyclin D1, and reducing expression of CKIs? Alternatively, was PI3K stimulating S-phase entry through interactions with β-catenin? Due to the large number of potential interactions with the cell cycle machinery, it will be important to answer these questions using inhibitors of PI3K effectors, such as Akt, GSK-3β and mTOR. It will also be interesting to study the sub-cellular distribution of β-catenin in the epithelial wound, and to examine whether PI3K inhibition can interfere with this. These experiments will shed light on how PI3K is able to regulate proliferation in the sensory epithelium.

Of equal importance will be the identification of signalling that is upstream of the PI3K and MAPK pathways. This holds especial relevance when comparisons are made between the avian and mammalian utricle. These two models display similar requirements for PI3K and ERK signalling when stimulated with growth factors *in vitro* (Montcouquiol and Corwin, 2001b; Witte et al., 2001), yet the mammalian utricle is not able to proliferate effectively when hair cell loss is induced experimentally (Warchol et al., 1993). As support cells of the mammalian utricular epithelium are capable of proliferation, this may represent a difference in the upstream signalling. The avian utricular epithelium thus presents an opportunity to study a functional system, where hair cell loss is coupled to a robust support cell proliferation. A candidate protein immediately upstream of both the PI3K and MAPK cascades is the Ras GTPase. Ras is

a proto-oncogene, and can regulate S-phase entry through parallel control of the PI3K and ERK MAPK pathways (Gille and Downward, 1999). Although this function in the inner ear would be entirely speculative, involvement of the Ras GTPase could integrate a potentially enormous diversity of inputs and couple them to support cell proliferation. The contribution of candidate proteins like Ras during the induction of epithelial wound proliferation will be an exciting area of further study.

4.4 Conclusions

In conclusion, these experiments have investigated whether laser ablation of the utricular epithelium was a suitable *in vitro* model to study the mechanisms of support cell proliferation. It was shown that the utricular epithelium could upregulate support cell proliferation within 48 hours of laser ablation. Experiments also identified several signalling cascades that were essential for support cell proliferation in the wounded epithelium. Inhibition of the PI3K pathway was able to completely block wound proliferation, emphasising its critical role during this process. Inhibitors of the ERK and JNK MAPK cascades were also able to elicit significant reductions in the level of wound proliferation. It will be important to verify that these pathways are able to regulate regenerative proliferation in noise and drug induced damage models of the avian inner ear.

5 Epithelial repair during aminoglycoside ototoxicity.

5.1 Introduction

In addition to their direct role in sensory transduction, hair cell epithelia also present an impermeant barrier that prevents K^+ rich endolymph from escaping into other fluid compartments. The importance of this barrier is highlighted in *claudin14* knockout mice, where defective tight junction formation is associated with progressive hair cell degeneration (Ben-Yosef et al., 2003). The epithelial barrier itself comprises a complex network of tight junctions that connect the apices of support cells and hair cells together (Jahnke, 1975). Hair cell loss due to normal turnover or ototoxic insult threatens to disrupt this barrier, jeopardising the ionic composition of both endolymph and perilymph. The formation of phalangeal scars at the epithelial surface has been proposed to limit any permeabilisations that may occur during hair cell loss (see Section 1.4.2). Despite the potential significance of epithelial repair, relatively little is known about these processes or their regulation.

This chapter is concerned with how the avian utricular macula responds to hair cell death, and investigates mechanisms that are employed to maintain transepithelial integrity. In particular, it examines whether any of the reparative phenomena described in Chapter 3 are observed during hair cell death. Attention was now focused upon an organotypic explant model treated with aminoglycosides to specifically induce apoptosis within the hair cell population. Immunocytochemistry was initially used to study the changes in epithelial structure that occurred during hair cell death. Further experiments using live-cell microscopy of β-actin-EGFP revealed extensive cytoskeletal remodelling of support cells adjacent to a dying hair cell. In particular, these experiments describe how support cells were able to form an actin cable around the neck of a hair cell; effectively decapitating it as the epithelial defect was closed. Moreover, support cells were found to sequester the dying hair cell soma within a calyx, a process that culminated in their phagocytosis and ultimate deletion from the sensory epithelium. The role of the support cell during hair cell death will be discussed, and mechanisms of epithelial repair compared with that observed in other systems.

5.2 Results

A transition was now made from the epithelial preparation to maintaining whole utricles as free-floating organ cultures (see Section 2.4.2). This method of culture allowed the sensory epithelium to be studied in a more organotypic state with the native basal lamina intact. Data presented in this chapter is taken exclusively from the utricular cotillus; the striola and rampa have been specifically avoided.

5.2.1 Epithelial structure of utricular explants in vitro

To detail the normal architecture of the sensory epithelium *in vitro*, utricular explants from E21 embryos were cultured for 48 hours, before being processed for phalloidin, HCS-1 and DAPI immunocytochemistry (n = 3 utricles; see Section 2.7.2). Figure 5.1 is a representative set of laser-scanning confocal micrographs captured from these explants, revealing the intricate cellular architecture of the utricle *in vitro*. The phallotoxin label for f-actin revealed the stratification of the undamaged sensory epithelium, and allowed the following layers to be delineated: surface, hair cell, support cell and stroma. At the epithelial surface, f-actin was especially concentrated within the hair bundle and the zonulae adherens/occludens that formed the apical junction complex. HCS-1 labelling was also present towards the epithelial surface, manifest as an annulus colocalised with the boundary between a hair cell and its support cell neighbours. A single hair bundle emerged from within each HCS-1 annulus, projecting into the luminal (endolymphatic) space. The otolithic membrane would normally populate this area, however it was removed prior to explant culture. A significant proportion of the epithelial surface area was constituted by support cell processes, which physically insulated neighbouring hair cells from one another.

The hair cell layer was immediately below the epithelial surface, and characterised by an ordered mosaic of relatively large hair cell somas. Aside from size, hair cell somas were distinguished by small protrusions of f-actin from their basolateral surface. The hair cell cortex also labelled with HCS-1, displaying a flask-like distribution of the antigen when viewed orthogonally. A single nucleus was present towards the base of each hair cell. With few exceptions, hair cell nuclei all displayed normal chromatin structure.

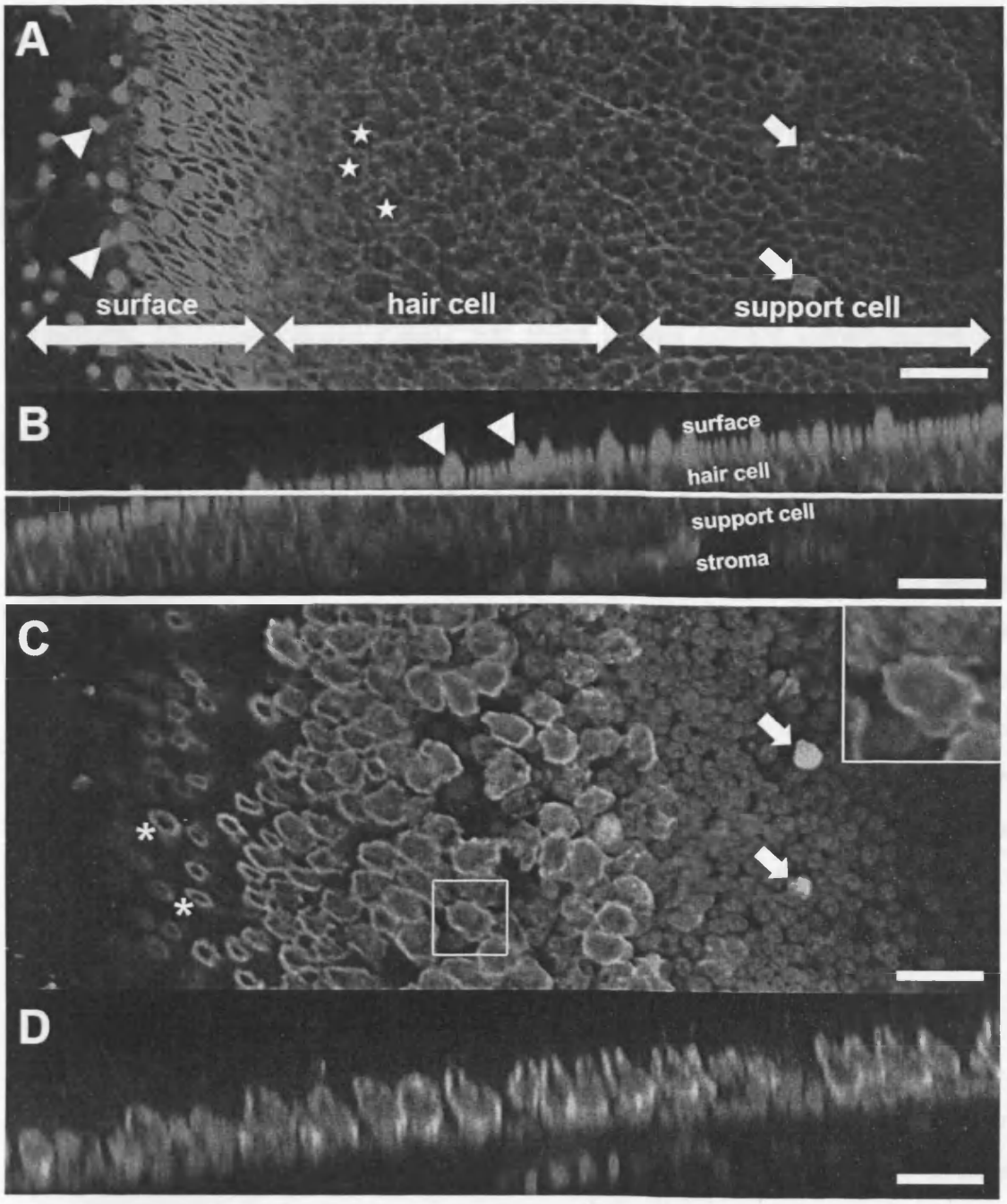

Figure 5.1 - Epithelial structure of the avian utricle *in vitro*. Utricles were harvested from E21 chick embryos and maintained as whole explant cultures. The otoconial matrix was removed in these preparations. After 48h *in vitro*, explants were fixed and processed for phalloidin (red), HCS-1 (green) and DAPI (blue) immunocytochemistry. Confocal microscopy was used to image the preparation with the epithelial surface positioned at an angle to the plane of sectioning (white line, panel B). **A)** Single confocal section of the phalloidin signal shows the distribution of f-actin within the different strata that comprise the sensory epithelium (surface, hair cell, support cell & stroma). Sensory hair bundles (arrowhead) and the AJC network at the apex label intensely with phalloidin. Hair cell somas are distinguished by their size and position within the epithelium (star). Support cells are packed tightly together at the base of the epithelium. Note the presence of inclusion bodies (arrows). **B)** Orthogonal projection of the phalloidin channel reiterates the stratified nature of the epithelium. **C)** Hair cell labelling with HCS-1 is predominantly cortical, and visible as an annulus at the epithelial surface (asterisk). Hair cells displayed normal chromatin structure (inset). Inclusion bodies colocalised with HCS-1 (arrows). **D)** Orthogonal projection demonstrates the stratification of hair cell and support cell nuclei. Images are representative of 3 utricles. Scale bars represent 20 μm.

Directly beneath the hair cells was the support cell layer. This homogenous layer was comprised entirely of densely packed support cell somas. Support cells intercalated between hair cells as they extended from the base to surface of the epithelium. The support cell nuclei were present in this layer and were found to display normal chromatin structure. Support cell and hair cell nuclei could be differentiated using both their size and location, the latter being larger and positioned more apically in the epithelium. The mesenchymal stroma was intact in this explant culture model, and contacted the basal surface of the support cell layer. Several anomalous objects were noted in the support cell layer. The first was the presence of thread-like processes that labelled for f-actin. These were thought to represent the remnants of nerves that are known to retract from the hair cells *in vitro* (Oesterle et al., 1993). The second anomaly documented were small dense aggregates of HCS-1 labelling encased within a shell of f-actin. These 'inclusion bodies' did not contain an intact nucleus, and were unlikely to represent a healthy cell type. The number of hair cells and inclusion bodies was quantified within the utricular cotillus (see Section 2.8.5). Density estimates of hair cell and inclusion bodies were estimated to be 106 ± 7.7 and 5.5 ± 0.2 per 10'000 μm^2 respectively. In summary, these data demonstrated that utricular explants maintained an organotypic structure for at least 48 hours *in vitro*. Of particular note was the survival of large numbers of hair cells without any evident pathology.

5.2.2 Epithelial structure during streptomycin ototoxicity

The previous section introduced an explant model of the utricle and demonstrated that it was viable *in vitro*. This model was now used to study the structure of the sensory epithelium during pharmacologically induced hair cell death. Utricular explants were treated with the aminoglycoside antibiotic streptomycin, which is known to induce extensive hair cells loss within the macula *in vitro* (Oesterle et al., 1993; Matsui et al., 2000). Utricular explants were prepared as before, and maintained for 24 hours *in vitro* to allow time to recover from any dissection trauma. Explants were then treated with 1 mM streptomycin sulphate for varying intervals (12, 18 or 24 hours), before they were fixed, and imaged as before (n = 3 utricles for each condition). A 48 hour treatment group was created from utricles that were treated for 24 hours with 1 mM streptomycin, and then maintained for a further 24 hours in normal medium (n = 3 utricles). The structure of the sensory epithelium during streptomycin ototoxicity will be described as a chronological progression. The epithelial structure at different time

points was compared to control explants maintained for 48 hours *in vitro* (see Section 5.2.1).

Compared to control explants, the cytoskeletal structure of the sensory epithelium appeared grossly normal following a 12 hours exposure to 1 mM streptomycin (Figure 5.2). Hair bundles were present at the epithelial surface, and coincided with an annulus of HCS-1 labelling around the apical extremity of the hair cell. Hair cell somas remained densely packed, and maintained their characteristic flask-like labelling of HCS-1. Indeed, the only discernable difference in the hair cell population was observed within their nuclei. Using DAPI to assess macroscopic nuclear structure, almost all hair cells within the sampled areas displayed chromatin condensation that was characteristic of pyknosis. Although streptomycin treatment induced nuclear degradation within hair cells, there was no visible effect upon the support cell population. Once again, the presence of inclusion bodies was noted in both the hair cell and support cell layers; characterised by their increased density of f-actin, and colocalisation with HCS-1 and fragments of DAPI labelling. At this time point, hair cell density in the utricular cotillus was estimated to be 117 ± 19.8 per 10'000 μm^2, and was not significantly different from controls ($p = 0.65$). Inclusion density was 7.4 ± 1.5 per 10'000 μm^2, a non-significant increase of 130% over controls ($p = 0.33$).

Utricular explants exhibited more severe manifestations of aminoglycoside ototoxicity after 18 hours of exposure to 1 mM streptomycin (Figure 5.3). Sensory hair bundles were visibly missing from the epithelial surface; mirrored by a loss of the corresponding hair cell soma. Of the remaining hair cells that were structurally intact within the epithelium, all possessed pyknotic nuclei. A sub-set of hair cells exhibited more severe disruption of chromatin structure, characteristic of karyorrhexis. HCS-1 positive inclusions were present in the hair cell and support cell layers, and were observed more frequently than in control explants. In addition, some inclusions appeared to contain objects that structurally resembled a hair cell soma, albeit with severe chromatin degradation. Support cell nuclei appeared normal after 18 hours of streptomycin treatment. Hair cell density within the utricular cotillus was estimated to be 58.3 ± 17.4 per 10'000 μm^2, representing a decrease to 55% of controls. Despite a visible reduction in hair cell density, this was not statistically significant ($p = 0.09$).

Inclusion density was 22.0 ± 7.3 per 10'000 μm^2, representing a non-significant increase of 400% over controls ($p = 0.15$).

Severe disruption of the sensory epithelium was observed after 24 hours incubation with 1 mM streptomycin (Figure 5.4). There was a large reduction in the number of hair bundles, mirrored by the loss of the corresponding hair cell soma and annular HCS-1 labelling at the epithelial surface. In parallel with hair cell loss, support cell processes appeared to expand to fill the resulting void, such that the epithelial surface was continuous. Disruption in the hair cell layer was associated with an increase in the number of inclusion bodies that present in both the hair cell and support cell layers. In addition to HCS-1, the majority of inclusions contained aggregates of karyorrhetic chromatin. No pathology was observed in the support cell population, although where present, inclusion bodies disrupted the uniform organisation normally observed in control explants. Hair cell density in the utricular cotillus was estimated at 38.8 ± 9.1 per 10'000 μm^2, representing a significant decrease to 37% of controls ($p < 0.05$). Inclusion density in the utricular cotillus was 28.8 ± 5.3 per 10'000 μm^2, representing a significant 524% increase over controls ($p < 0.05$).

The longest time point examined in this study was 48 hours, constituting a 24 hours exposure to 1 mM streptomycin followed by an additional 24 hours in normal culture medium (Figure 5.5). This protocol resulted in a near-total hair cell lesion. No hair bundles were observed at the epithelial surface, confirmed by a total absence of HCS-1 positive hair cell somas in the sample areas. Support cells continued to display normal chromatin structure, and these now constituted the sensory epithelium in its entirety. HCS-1 inclusion bodies were still present, although they were less numerous than that observed at 24 hours. Hair cell density in the utricular cotillus was 0.1 ± 0.1 per 10'000 μm^2, a significant reduction to 0.1% of the control values ($p < 0.05$). The density of inclusion bodies was 13.8 ± 4.7 objects per 10'000 μm^2, a non-significant increase of 251% over controls ($p = 0.22$). An intriguing observation made at this time point was the apparent expression of HCS-1 in a subset of 'intermediate' cells. These cells shared morphological characteristics common to both support cells and hair cells; namely, that they possessed an immature hair bundle, in addition to making contact with both the base and surface of the epithelium. HCS-1 expression within intermediate cells

was restricted to the basolateral cortex, similar to that seen in hair cells. Intermediate cells were easily distinguishable from inclusion bodies, the latter displaying cytosolic HCS-1 localisation in conjunction with severely degraded chromatin. Intermediate cells were not included within the hair cell count presented above. The density estimates described above have been tabulated (Table 5.1) and presented as a graph (Figure 5.6). To recapitulate, exposure to streptomycin for 12 or 18 hours did not result in any significant differences in hair cell or inclusion body densities. Significant changes were only observed after 24 hours of streptomycin exposure. In the period 12-24 hours only, hair cell and inclusion body densities appeared to be inversely proportional with respect to each other. Within this interval, two separate exponential functions were fitted to the hair cell and inclusion body estimates, and half-lives of 7.5 and 6.1 hours calculated respectively.

In summary, a 24 hours exposure to 1mM streptomycin was able to induce an extensive hair cell lesion throughout the utricular cotillus. Despite the massive loss of hair cells, the epithelial surface remained continuous. This suggested that support cells were able to remodel as hair cells were removed from the epithelium. These data also documented the presence of 'inclusion bodies' that appeared to contain the remnants of dying hair cells. These themes are now pursued in further detail.

Treatment group	N	Hair cell density (per 10'000 μm^2)	Inclusion density (per 10'000 μm^2)
Control 24h	3	106 ± 7.5	5.5 ± 0.2
12h 1mM Strep	3	117 ± 19.8	7.4 ± 1.5
18h 1mM Strep	3	58.3 ± 17.4	22.0 ± 7.3
24h 1mM Strep	3	38.8 ± 9.1	28.8 ± 5.3
24h 1mM Strep & 24h recovery	3	0.1 ± 0.1	13.8 ± 4.7

Table 5.1 Summary of density estimates during streptomycin ototoxicity. N = number of utricles per treatment group. Data are expressed as means ± SEM.

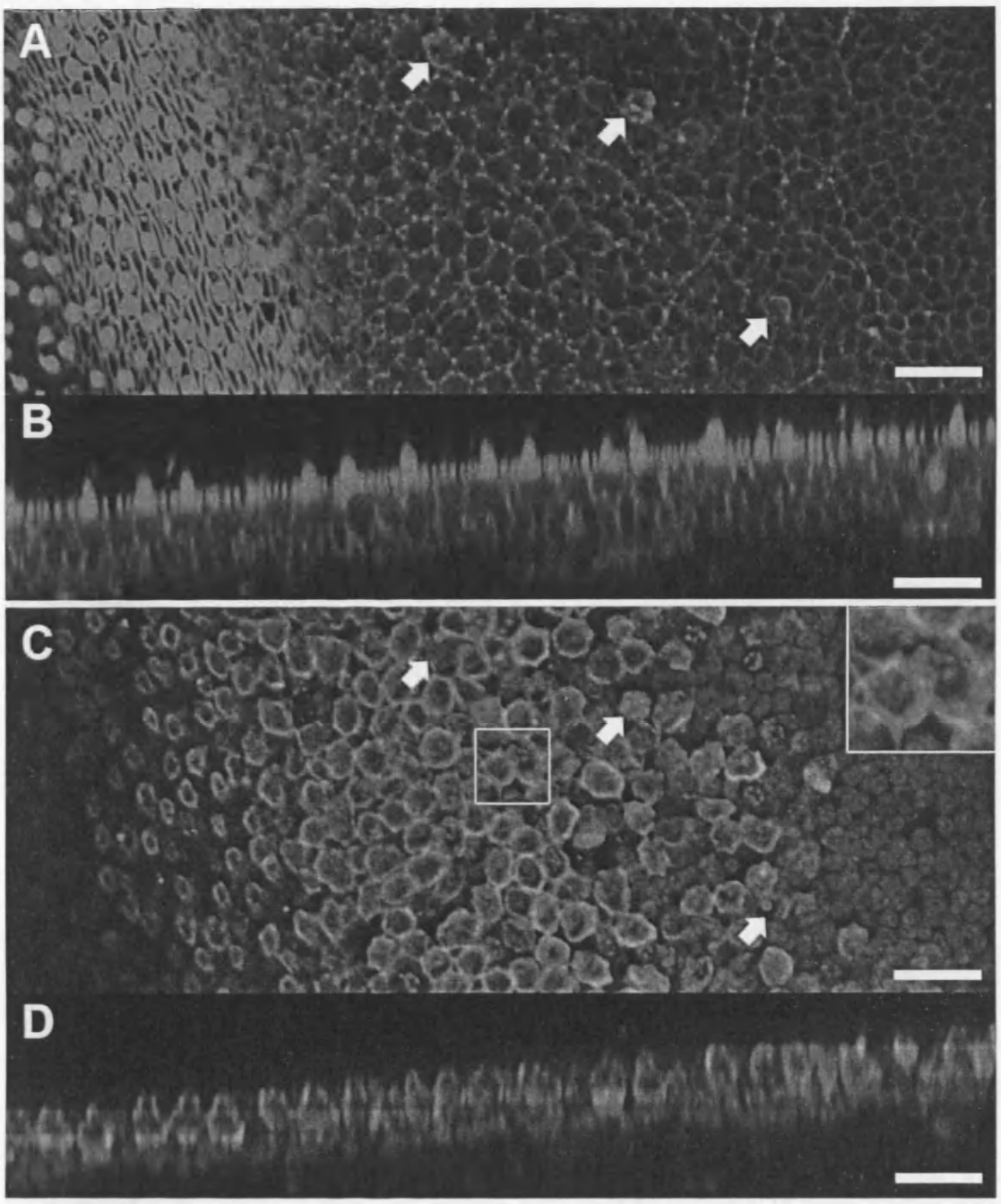

Figure 5.2 - Progression of streptomycin ototoxicity *in vitro* I (12 hours). Utricles were harvested and prepared as before. After an initial 24 hours in culture, 1 mM streptomycin sulphate was supplemented to the culture medium, and explants maintained for a further 12 hours. Organs were subsequently fixed and processed for phalloidin (red), HCS-1 (green) and DAPI (blue) immunocytochemistry. Imaging was performed as described before. **A,B)** The gross distribution of f-actin throughout the epithelium was unaffected by 12 hours of streptomycin treatment. Orthogonal projection confirmed the normal organisation of the epithelium in all strata. Phalloidin labelled inclusion bodies were present within the epithelium (arrows). **C,D)** Rings of HCS-1 labelling were still present at the epithelial surface (arrowheads). Orthogonal projection showed the normal cortical distribution of HCS-1. DAPI staining revealed that majority of hair cell nuclei were pyknotic (see inset), whilst support cell nuclei were unaffected by streptomycin treatment. Inclusions bodies contained HCS-1 and DAPI (arrows). Images are representative of 3 utricles. Scale bars represent 20 μm.

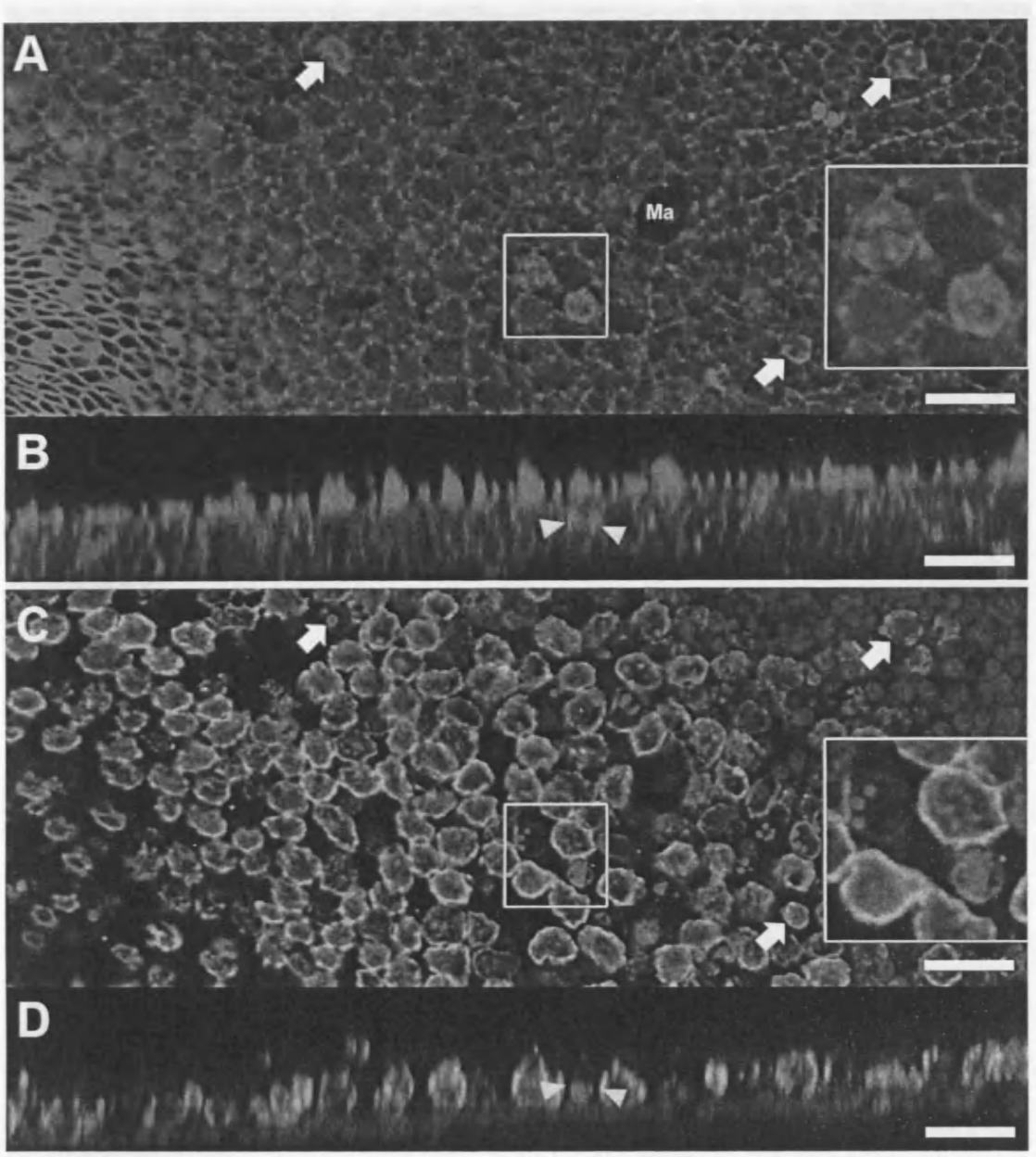

Figure 5.3 - Progression of streptomycin ototoxicity *in vitro* II (18 hours). Utricles were harvested and prepared as before. After an initial 24 hours *in vitro*, 1 mM streptomycin sulphate was supplemented to the culture medium, and explants maintained for a further 18 hours. Organs were fixed, and processed for phalloidin (red), HCS-1 (green) and DAPI (blue) immunocytochemistry. Imaging was performed as described before. **A,B)** Phalloidin labelling revealed a reduction in the number of hair bundles at the epithelial surface. The general structure of the hair cell layer was retained, although there were increased numbers of inclusion bodies within the epithelium (arrows). A presumptive macrophage was present at the base of the epithelium (Ma). Orthogonal projection showed the nature of one inclusion, which appeared as an increase in phalloidin labelling around the lateral edges of a sensory hair cell (arrowheads). **C,D)** Loss of hair cell bundles corresponded with a concomitant loss in HCS-1 labelling at the epithelial surface. Inclusion bodies colocalised with HCS-1 and DAPI (arrows). Hair cell nuclei displayed chromatin condensation characteristic of pyknotis and/or karyorrhexis. Images are representative of 3 utricles. Scale bars represent 20 μm.

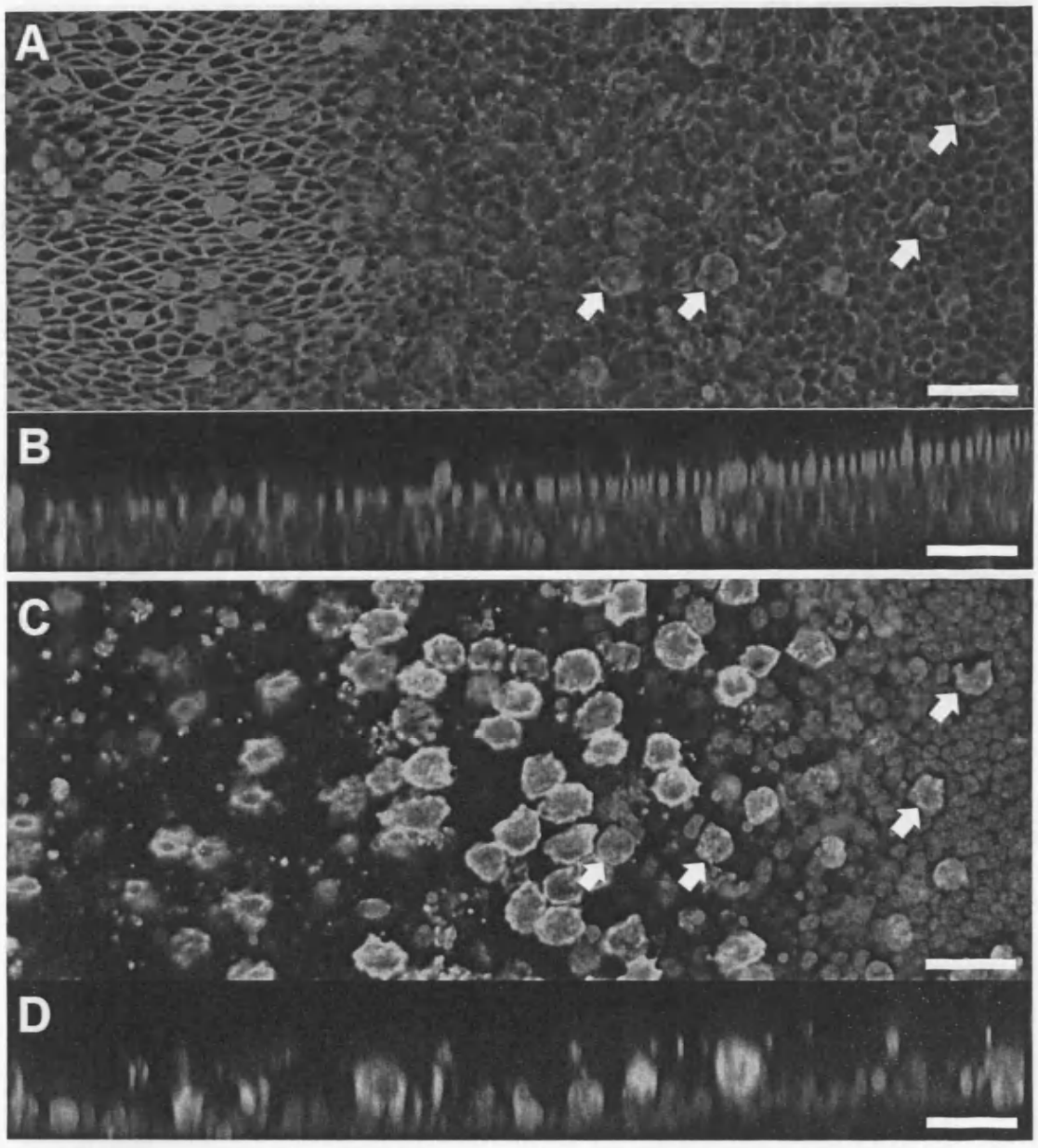

Figure 5.4 - Progression of streptomycin ototoxicity *in vitro* III (24 hours). Utricles were harvested and prepared as before. After an initial 24 hours *in vitro*, 1 mM streptomycin sulphate was supplemented to the culture medium, and explants maintained for a further 24 hours. Organs were fixed and processed for phalloidin (red), HCS-1 (green) and DAPI (blue) immunocytochemistry. Imaging was performed as before. **A,B)** There was a large reduction in the number of intact hair bundles at the epithelial surface, corresponding with fewer hair cell somas. In the absence of hair cells, support cells have expanded to replace them. Multiple inclusion bodies were visible within the sensory epithelium (arrows). Orthogonal projections showed the severe disruption occurring throughout the sensory epithelium. **C,D)** The loss of hair bundles was mirrored by reduction in HCS-1 labelling at the epithelial surface. Inclusion bodies colocalised with HCS-1 and DAPI (arrows). Inclusion bodies also displaced neighbouring support cell nuclei laterally. The orthogonal projection reiterated the severe disruption induced by a 24h exposure to streptomycin, with few hair cells remaining. Images are representative of 3 utricles. Scale bars represent 20 μm.

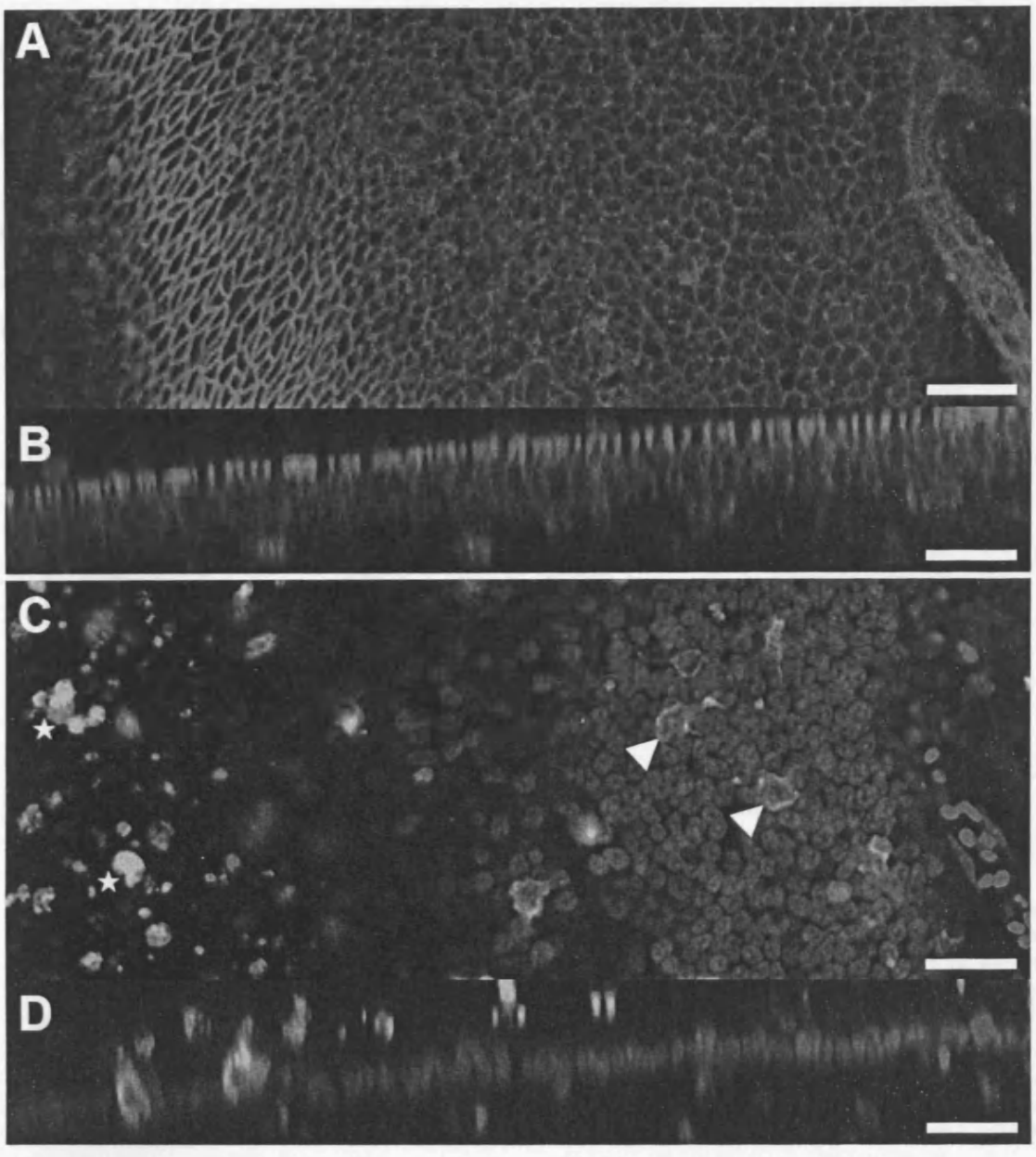

Figure 5.5 - Progression of streptomycin ototoxicity *in vitro* IV (48 hours). Utricles were harvested and prepared as before. After an initial 24 hours *in vitro*, 1 mM streptomycin sulphate was supplemented to the culture medium for 24 hours. Explants were maintained for a further 24 hours in normal culture medium. Explants were fixed and processed for phalloidin (red), HCS-1 (green) and DAPI (blue) immunocytochemistry. Imaging was performed as described before. **A,B)** Streptomycin treatment resulted in an almost total loss of hair cells from the sensory epithelium. Support cell processes enlarged to replace the absent hair cells, and orthogonal projection demonstrated these now comprised the epithelium in its entirety. **C,D)** HCS-1 labelling confirmed the total absence of hair cells from the sensory epithelium. HCS-1 positive cell debris was present in the lumen (stars). Some cells with intermediate morphology were present within the sensory epithelium. Intermediate cells extended from the base to the surface of the epithelium, and displayed cortical HCS-1 expression (arrows). Orthogonal projection showed that intermediate cells expressing HCS-1 had a nucleus originating at the support cell level. Images are representative of 3 utricles. Scale bars represent 20 μm.

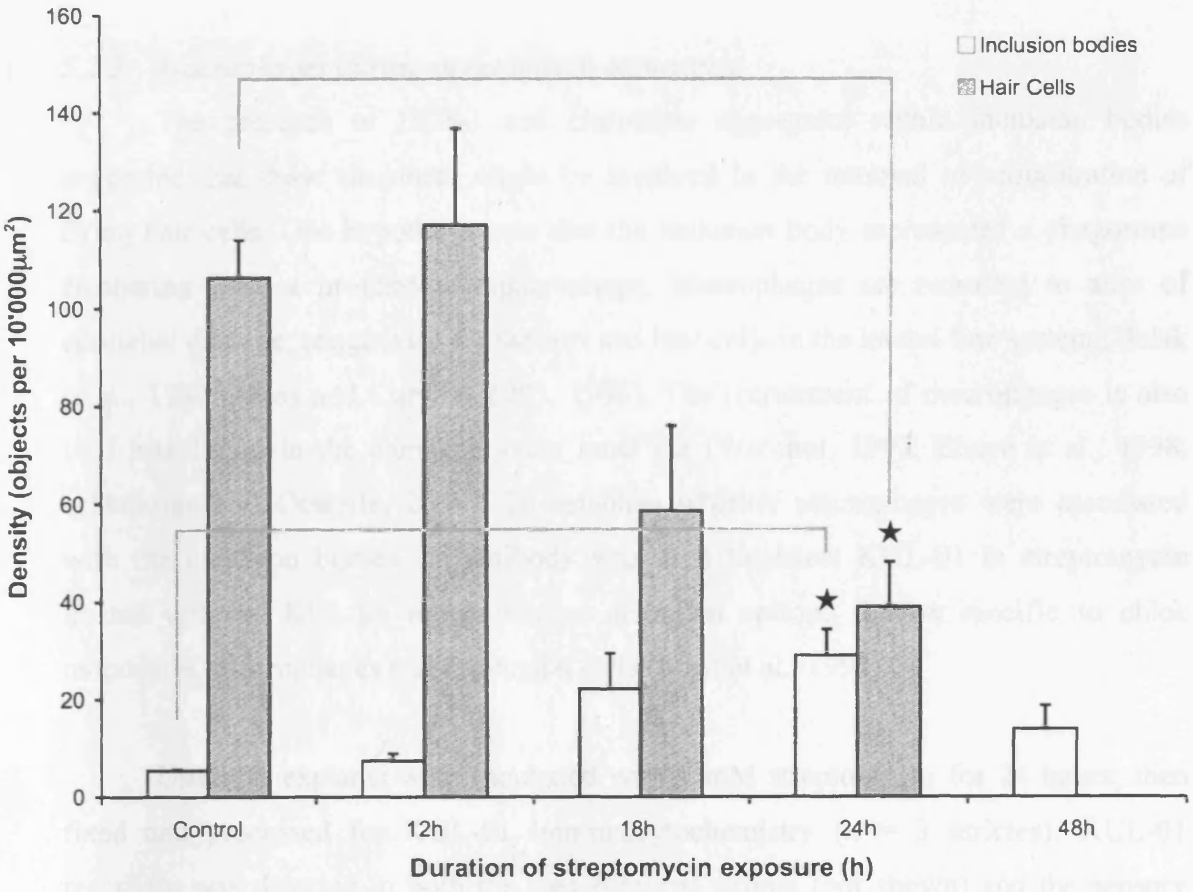

Figure 5.6 – Progression of streptomycin ototoxity *in vitro* (summary). The number of hair cells and inclusion bodies were quantified with a 200 x 200 µm region, selected blindly from the utricular cotillus. Two such regions were sampled and averaged together to yield an estimate of the total density within each utricle. Densities have been normalised to 10'000 μm^2. A significant reduction in hair cell density was observed after 24h incubation with 1 mM streptomycin. After 48h, there were no hair cells remaining in the sampled areas. The number of inclusion bodies was significantly increased after 24h of streptomycin. The criteria used to identify hair cells and inclusion bodies has been summarised in Section 2.8.5. Please refer to the text for a full commentary and table of values. Each treatment group consisted of 3 utricles (n = 3). Data are means ± SEM. (★) signifies $p < 0.05$ (Student's *t*-test, 2-tailed).

5.2.3 Macrophages during streptomycin ototoxicity

The presence of HCS-1 and chromatin aggregates within inclusion bodies suggested that these structures might be involved in the removal or sequestration of dying hair cells. One hypothesis was that the inclusion body represented a phagosome emanating from a professional macrophage. Macrophages are recruited to sites of epithelial damage, phagocytosing support and hair cells in the lateral line system (Balak et al., 1990; Jones and Corwin, 1993, 1996). The recruitment of macrophages is also well established in the damaged avian inner ear (Warchol, 1997; Bhave et al., 1998; O'Halloran and Oesterle, 2004). To establish whether macrophages were associated with the inclusion bodies, an antibody was used to detect KUL-01 in streptomycin treated utricles. KUL-01 recognises an unknown epitope that is specific to chick monocytes, macrophages and microglial cells (Mast et al., 1998).

Utricular explants were incubated with 1 mM streptomycin for 24 hours, then fixed and processed for KUL-01 immunocytochemistry (n = 3 utricles). KUL-01 reactivity was detected in both the mesenchymal stroma (not shown) and the sensory epithelium (Figure 5.7). KUL-01 colocalised within a subset of inclusion bodies, and closer inspection revealed that these contained aggregates of condensed chromatin. The vast majority of inclusions displayed no detectable levels of KUL-01. In addition to this subset of inclusion bodies, KUL-01 labelling was also localised within the cytoplasm of larger, ramified cells. Unlike KUL-01 positive inclusions, these structures possessed a structurally viable nucleus, and were of an order of magnitude larger. The density of ramified KUL-01 positive cells within the utricular cotillus was estimated to be 1.6 ± 0.4 per 10'000 μm^2. Immunocytochemical detection of CD45, a common leukocyte antigen, was also attempted to confirm their classification as macrophages. Repeated attempts to detect CD45 proved unsuccessful (data not shown). To determine whether these presumptive macrophages were engaged in the phagocytosis of hair cell debris, utricles reacted with HCS-1 were examined in more detail. As immunocytochemistry for HCS-1 was not combined with KUL-01 in the same tissue sample, presumptive macrophages were identified based upon their size and highly ramified morphology revealed with phalloidin. After 24 hours of streptomycin exposure, there were some instances where a HCS-1 positive inclusion was seen within a presumptive macrophage

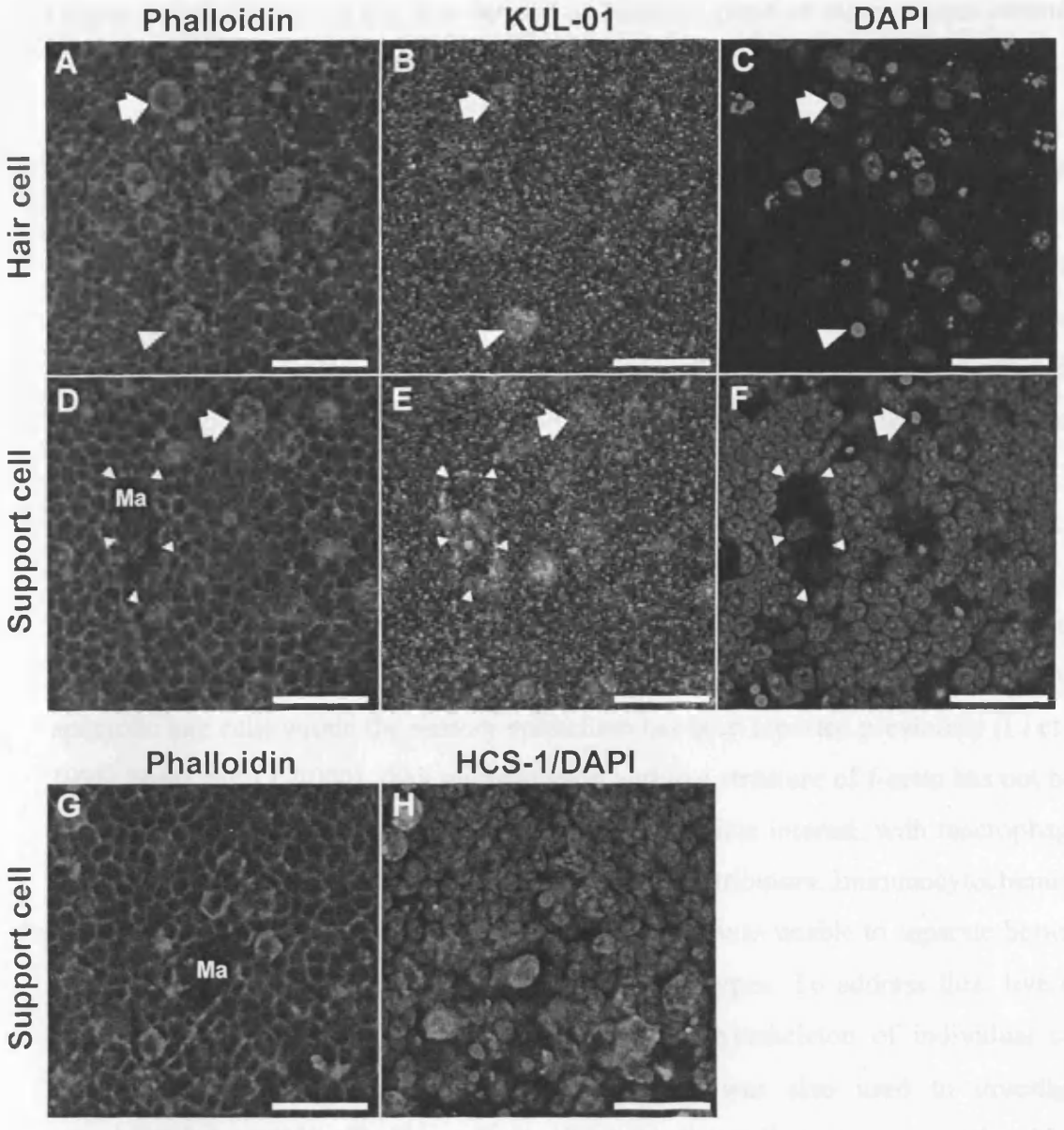

Figure 5.7 – Macrophages during streptomycin ototoxicity *in vitro*. Utricular explants were maintained for an initial 24h *in vitro*, followed by a 24h exposure to 1 mM streptomycin. Explants were fixed and processed for either HCS-1 (green) or KUL-01 (green), in addition to phalloidin (red) and DAPI (blue). **A-F)** Images from a single confocal stack have been split into corresponding support and hair cell layers. **A-C)** Inclusion bodies were present throughout the hair cell layer. Some inclusions labelled strongly with the macrophage marker KUL-01 (arrowheads), whilst others did not (arrows). KUL-01 positive inclusions did not associate with a healthy nucleus, suggesting that this was not a viable cell type. **D-F)** Inclusion bodies were also present in the support cell layer (arrows). A KUL-01 positive macrophage was identified by its large, ramified morphology (Ma). The macrophage displaced support cell nuclei laterally (small arrowheads). **G-H)** A presumptive macrophage colocalised with a degraded hair cell soma. It is not clear whether this represented phagocytic uptake or not. Images are representive of 3 utricles. Scale bars represent 20µm.

(Figure 5.7 G-H). Given the low density of KUL-01 positive macrophages estimated earlier (see above), these associations were correspondingly infrequent.

In summary, these data demonstrate that KUL-01 positive macrophages were present within the sensory epithelium during a period of hair cell loss. A limited number of inclusion bodies were also found to colocalise with KUL-01. Although this initially suggested that they might be macrophage processes, they did not associate with a viable cell soma or nucleus. Based upon this morphological evidence, it was unlikely that these structures were macrophages. The specificity of KUL-01 labelling will be considered later (see Section 5.3.3).

5.2.4 Remodelling of the support cells' cytoskeleton during hair cell death

The previous experiments suggested that dying hair cells were enclosed within epithelial inclusion bodies during streptomycin ototoxicity. Whilst the retention of apoptotic hair cells within the sensory epithelium has been reported previously (Li et al., 1995; Forge and Li, 2000), their encapsulation within a structure of f-actin has not been described. The origin of the f-actin was thus of immediate interest, with macrophages, support cells and hair cells themselves as potential contributors. Immunocytochemistry was of limited use when testing these hypotheses, as it was unable to separate between the cytoskeletal components of closely apposed cell types. To address this, live cell imaging of β-actin-EGFP was used to resolve the cytoskeleton of individual cells throughout the sensory epithelium. This approach was also used to investigate reorganisation at the epithelial surface where support cells were apparently able to remodel into a continuous sheet, despite the extensive loss of hair cells induced by streptomycin treatment.

Mosaic expression of β-actin-EGFP was induced using the RCAS system, a replication-competent avian retroviral vector derived from the Rous sarcoma virus (Hughes et al., 1987). Section 2.1.3 details the preparation of the RCASBP(B)-β-actin-EGFP proviral construct. Electroporation *in ovo* was used to transfect cells of the otic vesicle with proviral DNA (see Section 2.2.3). Introduction of proviral DNA at this primordial stage resulted in widespread expression of β-actin-EGFP in inner ear sensory epithelia when examined at embryonic days 17-19. The persistent nature of expression

suggested that either: proviral DNA had been stably integrated within cells of the otic vesicle and passed on to subsequent cellular progeny: or that the initial transfection resulted in the release of infectious viral particles. Sensory epithelia are referred to as infected, even though β-actin-EGFP expression could have been the result of either process.

Utricles infected with RCASBP(B)-β-actin-EGFP were harvested between embryonic days 17 and 19, and visualised acutely using a Nipkow spinning-disk confocal microscope (see Section 2.6.3). Infected utricles expressed the β-actin-EGFP transgene in both the sensory epithelium and the associated mesenchymal stroma. Figure 5.8 depicts a live confocal image taken from the utricular cotillus, demonstrating the different combinations of infected and non-infected cell types that gave rise to an expression mosaic. Three types of mosaics could be defined: with expression in support cells only: hair cells only: or a combination of both. Inspection of these different mosaics allowed the distribution of β-actin-EGFP to be resolved within individual cells types. In an infected hair cell, EGFP fluorescence was intensely concentrated within the hair bundle and to a lesser extent in a peri-cuticular ring circumscribing the apical junctions of the cell. Cytoplasmic fluorescence throughout the hair cell was comparatively low. Infected support cells exhibited elevated EGFP fluorescence within the apical junction complexes, in addition to a diffuse component distributed throughout their cytoplasm. Orthogonal reconstructions demonstrated that the pseudo-stratified structure was well preserved in infected sensory epithelia (Figure 5.8B,C). Due to the strong concentration of β-actin-EGFP within the hair bundle, this signal was deliberately saturated in order to detect cellular fluorescence elsewhere. These initial experiments confirmed that retrovirally induced expression of β-actin-EGFP did not adversely affect either epithelial morphology or hair cell differentiation within the utricle.

Utricular expression mosaics were now used to investigate how the sensory epithelium responded to hair cell death, and in particular to study the formation of inclusion bodies. Confocal time-lapse microscopy was used to capture β-actin–EGFP fluorescence in 4-dimensions (x,y,z vs. time) within the sensory epithelium (see Section 2.6.3). To induce hair cell death, infected utricles were time-lapse imaged in the

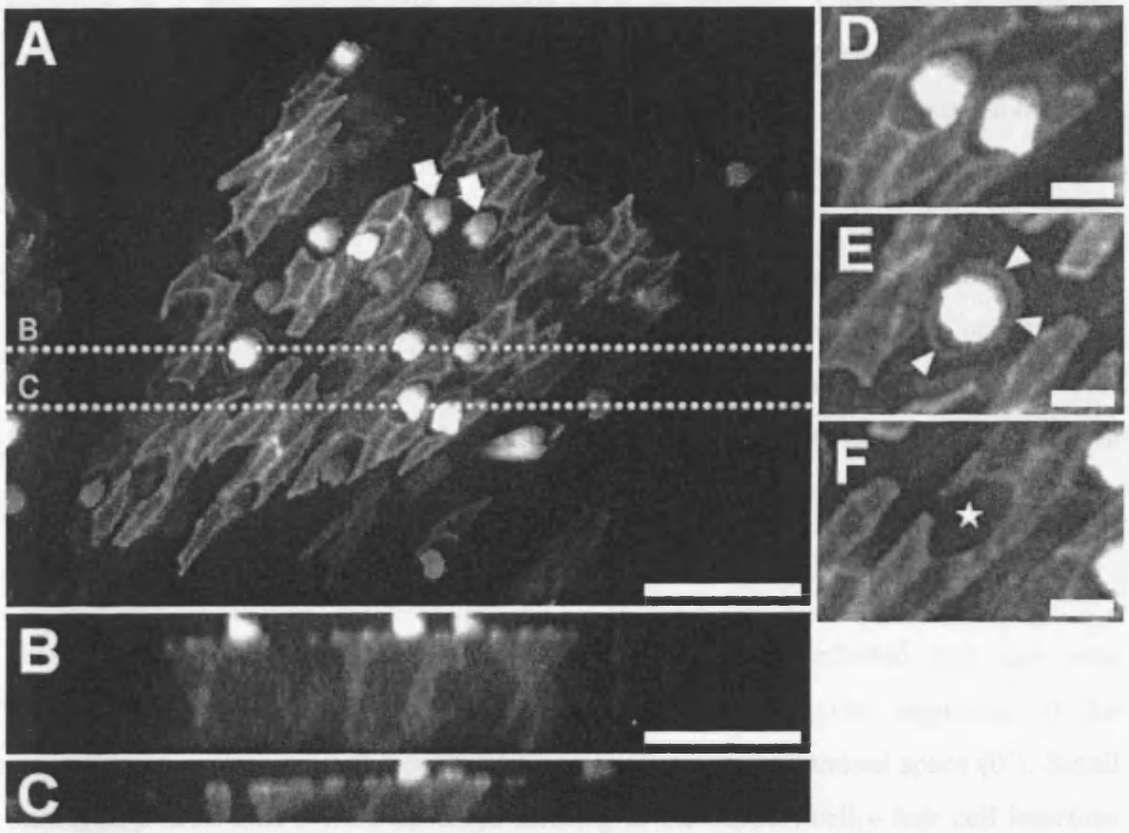

Figure 5.8 –Live cell imaging of β-actin-EGFP in the utricular sensory epithelium. Electroporation of the otic vesicle *in ovo* (E2.5) was used to induce expression of the retroviral RCASBP(B)-β-actin-EGFP construct throughout the developing inner ear. Utricles from infected embryos were harvested between E17-19, and imaged as whole explants using a Nipkow spinning disk confocal microscope. **A)** An example of β-actin-EGFP expression within the utricular cotillus. The stochastic nature of infection resulted in an expression mosaic. Non-expressing cells were still present and populated the 'dark' areas. Incorporation of β-actin-EGFP was particularly intense in the hair bundle (arrows). **B-C)** Orthogonal projection of epithelium reiterated the mosaic nature of expression with infected support cells intercalating around non-infected hair cells. The lines of orthogonal section have been indicated (dotted line, panel A). **D-F)** Examples of how different mosaics could be utilised to document cell specific activity. When both support cells and hair cells were infected, it was difficult to separate the individual populations of β-actin-EGFP (D). A solitary infected hair cell allowed a peri-cuticular ring (arrowheads) of hair cell β-actin-EGFP to be resolved (E). Conversely, a patch of support cell infection allowed their cytoskeleton to be documented without crosstalk from the hair cell (star; F). Explants were maintained at 37°C in a 5% CO_2 atmosphere during image caputure. Scale bars represent 50 μm (A-C) or 10 μm (D-F).

presence of 1 mM streptomycin sulphate (n = 4 utricles). Time-lapse experiments without streptomycin were also performed to control for the effects of imaging on cell survival (n = 3 utricles). Although the size and patterning of the mosaics varied between individual utricles, the observations that follow were consistent between experiments. In both streptomycin and control time-lapse experiments the distribution of β-actin-EGFP varied with respect to time. In particular, fluorescent microdomains at the apical junction complexes appeared to fluctuate, suggesting that these junctions underwent a continual replacement (Appendix A, file://chapter5/ApicalJunction.mpg). To address the specific question of inclusion bodies, attention was now focused upon hair cells in the streptomycin treated sensory epithelium, where a dramatic remodelling of β-actin-EGFP was observed (Figure 5.9).

In the first example, a mosaic consisting of an infected hair cell was neighbouring four infected support cells (Figure 5.9A). At the beginning of the sequence, a bundle projected from the hair cell soma into the luminal space (0'). Small puncta of β-actin-EGFP were observed forming at the support cell – hair cell interface below the epithelial surface. This activity continued for a further thirty minutes (+30'). An intense concentration of β-actin-EGFP then formed asymmetrically around the hair cell (+33'). This increase was only observed at the interface between the hair cell and infected support cells, indicating that the β-actin-EGFP did not originate from within the hair cell itself. By the next frame of the series, the structure started to contract and appeared to completely encapsulate the hair cell soma within a 'calyx' of β-actin-EGFP (+36'). Over the next four frames, multiple β-actin-EGFP processes penetrated the space occupied by the hair cell soma (+48'), and subsequently formed a number of vesicles (+54' to +84'). In parallel to this activity, a separate event was observed at the epithelial surface, where a ring of β-actin-EGFP formed around the apical junctions of the hair cell (+48'). The ring proceeded to contract over the following 36 minutes, pulling the neighbouring support cell surfaces together and constricting around the neck of the hair cell. The hair bundle was pinched off and ejected into the luminal space by this mechanism. This phenomenon was thought to be an actin cable, similar to that described during epithelial repair of MDCK monolayers (Rosenblatt et al., 2001). A MPEG movie of this entire sequence is available (Appendix A, file://chapter5/Calyx1.mpg).

In the second example, a non-infected hair cell was partially surrounded by infected support cells (Figure 5.9B). In contrast to the previous example, this type of mosaic allowed the support cells' cytoskeleton to be visualised without any contribution from the adjacent hair cell. At the start of the sequence, the position of the hair cell soma could be inferred from the morphology of the neighbouring support cells (0'). Three minutes later, support cells began to extend pseudopodia around the perimeter of the hair cell soma (+3'). This activity continued for a further 42 minutes (+45'), after which the volume of the hair cell soma reduced substantially (+51'). Support cells continued to extend β-actin-EGFP pseudopodia around the remains of the hair cell soma for an extended period (+51'-150'). The distribution of support cell β-actin-EGFP in this structure appeared identical to the inclusion bodies described earlier using phalloidin (see Section 5.2.2). Parallel to this activity, an actin cable was observed contracting around the hair cell neck (+51'). This process resulting in the support cells being pulled together as before (+150'). Although the hair bundle could not be visualised *ipso facto* in this type of mosaic, it was likely that this process also excised the bundle (see Figure 5.9A). A movie sequence is available (Appendix A, file://chapter5/Calyx2.mpg). For clarity, the encapsulation of a hair cell by the combined pseudopodia of multiple support cells will herein be referred to as the support cell calyx. Further examples of support cell calyx formation are described in the following section (see Section 5.2.5 & Figure 5.10).

Events similar to those described in streptomycin treated cultures were also observed in control experiments, albeit at a significantly lower frequency. In the presence of 1 mM streptomycin, 62.0 ± 14.0% of hair cells observed were removed by a support cell β-actin-EGFP calyx and actin cable within 24 hours of streptomycin addition (110 hair cells sampled, n = 4 utricles), compared to 3.0 ± 0.4% in sham-imaged controls (100 hair cells sampled, n = 3 utricles). This represented a significant 20.7 fold increase in the frequency of support calyx induction by streptomycin treatment ($p = 0.02$, 2-tailed Student's *t*-test).

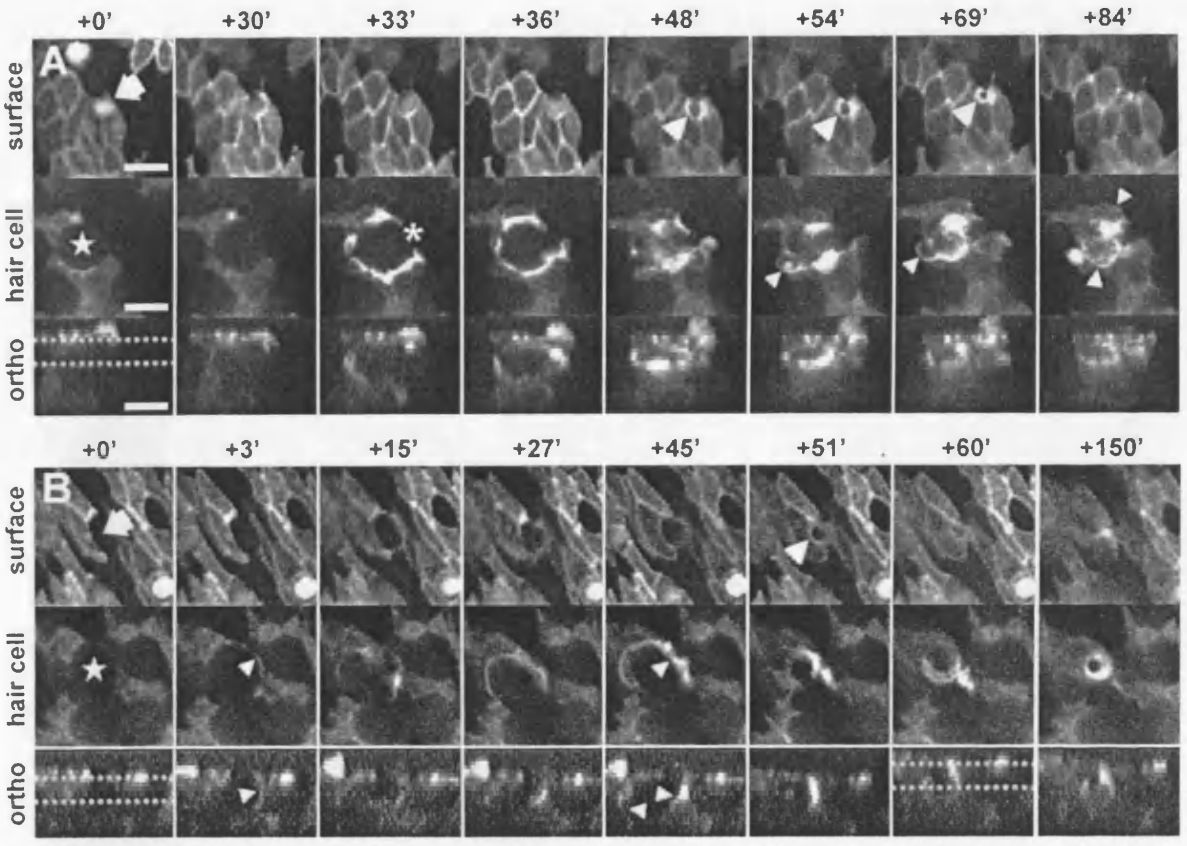

Figure 5.9 – Support cells form a 'calyx' of β-actin-EGFP during streptomycin ototoxicity. Utricles were harvested from E17-E19 chick embryos infected with the RCASBP(B)-β-actin-EGFP construct. Freshly isolated utricles were maintained as whole explants and time-lapse imaged using a Nipkow spinning disk confocal microscope. To selectively kill hair cells 1 mM streptomycin was supplemented to the imaging media. This figure depicts excerpts taken from two separate 24h time-lapse experiments.

A) An *infected* hair cell (star) was partially surrounded by infected support cells. The hair bundle was visible at the epithelial surface (arrow). The orthogonal reconstruction shows the planes of optical section. A rapid polymerisation of β-actin-EGFP occurred around the hair cell within 3 minutes (+33'). This increase was only observed at sites of contact with infected support cells, and was not symmetrical around the hair cell soma (asterisk). Orthogonal reconstructions showed that the hair cell soma was surrounded by a multicellular 'calyx' of support cell β-actin-EGFP (+36'). The calyx disintegrated into a series of smaller vesicles (small arrowheads), which persisted in the epithelium (+48'-84'). At the epithelial surface, a cable of β-actin-EGFP (arrowheads) formed around the hair cell neck (+48'). The actin cable contracted, pulling the neighbouring support cells together and severing the hair bundle from its soma (+54'-84').

B) In the second example, a *non-infected* hair cell was partially surrounded by infected support cells. The fewer number of infected cells allowed the individual calyx contributions to be better resolved. The position of the hair cell soma (star) and bundle (arrow) has been indicated. Support cells extended pseudopodia (small arrowheads) around the hair cell soma (+3'). Pseudopodia continue to extend around the hair cell soma (small arrowheads), forming the calyx with the other non-visible support cell contributions (+15'-45'). The calyx reduced in volume and persisted within the epithelium (+51'-150'). An actin cable was seen constricting at the epithelial surface (+51'). This likely resulted in decapitation of the hair bundle, although this was not visible in this particular mosaic (+150'). The hair cell was eliminated from the sensory epithelium at the conclusion of both series (A+B). Explants were maintained at 37°C in a 5% CO_2 atmosphere for the duration of imaging. Examples are representative of observations taken from four independent time-lapse experiments. Time stamps are relative to the first image (minutes). Scale bars represent 20 μm.

In summary, these data demonstrated that support cells actively remodelled their cytoskeleton during a period of streptomycin induced hair cell death. Support cells were found to extend pseudopodia and form a calyx of β-actin around the hair cell. This phenomenon was a compelling candidate for the inclusion bodies that were identified earlier in this chapter. In parallel to calyx formation, support cells also formed an actin cable that constricted around the neck of the hair cell. The cable decapitated the hair bundle and pulled the support cells together to seal over the underlying soma.

5.2.5 Support cells sequester and phagocytose the hair cell corpse

The previous section demonstrated that the hair cell soma was engulfed within a support cell calyx during streptomycin ototoxicity. The fate of an engulfed hair cell soma was now investigated in more detail. Two possibilities were considered; that the hair cell soma was phagocytosed by the surrounding support cells (Li et al., 1995; Forge and Li, 2000), or that the calyx was an intermediate stage awaiting phagocytosis by a professional macrophage. To address these hypotheses, a cell-impermeant DNA intercalating dye was used to visualise the chromatin of dying hair cells. The carbocyanine dye TOTO-3 was chosen for its emission in the far-red spectrum, allowing it to be easily discriminated from EGFP. This combination of fluorochromes allowed simultaneous dual-wavelength recordings of EGFP and TOTO-3 to be captured during streptomycin-induced hair cell death.

To induce calyx formation, β-actin-EGFP transgenic utricles were acutely isolated as before, and time-lapsed imaged with 1 mM streptomycin and 0.1 μM TOTO-3 supplemented to the culture media (n = 2 utricles). Figure 5.10 presents two representative examples of calyx formation taken from these experiments. In the first example, a non-infected hair cell was surrounded by four infected support cells (Figure 5.10A). The position of the hair cell at the beginning of this sequence was inferred from the distribution of β-actin-EGFP in adjacent support cells (+0'). In this example, support cells constructed an actin cable that constricted before the calyx was induced (+100'); this has been omitted from the series for clarity. A coordinate increase in support cell β-actin-EGFP fluorescence was observed around the hair cell, characteristic of calyx formation described earlier (+105'). At this time, there was negligible TOTO-3 signal present within the hair cell soma. TOTO-3 fluorescence was detected as the

support cell calyx developed (+110'), and continued to increase in intensity as the calyx reduced in volume (+115'). This provided excellent evidence that the support cell calyx actually contained a hair cell nucleus. In addition, punctate TOTO-3 labelling was resolved within the cytoplasm of a support cell (+305'). Since TOTO-3 is cell impermeant and support cell nuclei labelling was not observed, this was definitive evidence for the phagocytic uptake of hair cell chromatin from within the calyx. In this example, the TOTO-3 labelled support cell calyx persisted within the sensory epithelium beyond the end of the time-lapse experiment (+305'). A movie of this sequence is available (Appendix A, file://chapter5/TotoCalyx1.mpg).

In the second example, a patch of infected support cells can be seen contacting one side of a non-infected hair cell (Figure 5.10B). The position of the sensory hair cell can be inferred from the surrounding support cell morphology (+0'). TOTO-3 fluorescence was not detected within the hair cell at the beginning of this sequence. Calyx induction was observed as a simultaneous increase in β-actin-EGFP fluorescence restricted to the interface between infected support cells and the hair cell (+5'). A faint TOTO-3 signal was now visible within the calyx, reiterating the presence of a hair cell nucleus. As the time-lapse progressed, β-actin-EGFP pseudopodia were observed to extend approximately half way around the nucleus (+10'), subsequently retracting to form a visible TOTO-3 positive phagosome within a support cell's cytoplasm (+15'). At this time there were no β-actin-EGFP processes enveloping the hair cell nucleus, although it was likely that non-infected support cells were also extending pseudopodia. Within 25 minutes, another β-actin-EGFP pseudopod extended (+40') and proceeded to engulf the entire hair cell nucleus (+65'). The hair cell nucleus was now visible as a large phagosome within the support cell soma. Remains of the hair cell were visible as small puncta of TOTO-3 fluorescence in the extracellular space. A movie of this sequence is available (Appendix A, file://chapter5/TotoCalyx2.mpg).

These data also suggested that TOTO-3 could be used to monitor hair cell integrity during streptomycin ototoxicity. A more detailed analysis was now performed to determine the relative timings of calyx induction compared to onset of TOTO-3 fluorescence in the hair cell nucleus (see Section 2.8.5). A frequency histogram was constructed to illustrate these timings in a random sample of 21 hair cells from the

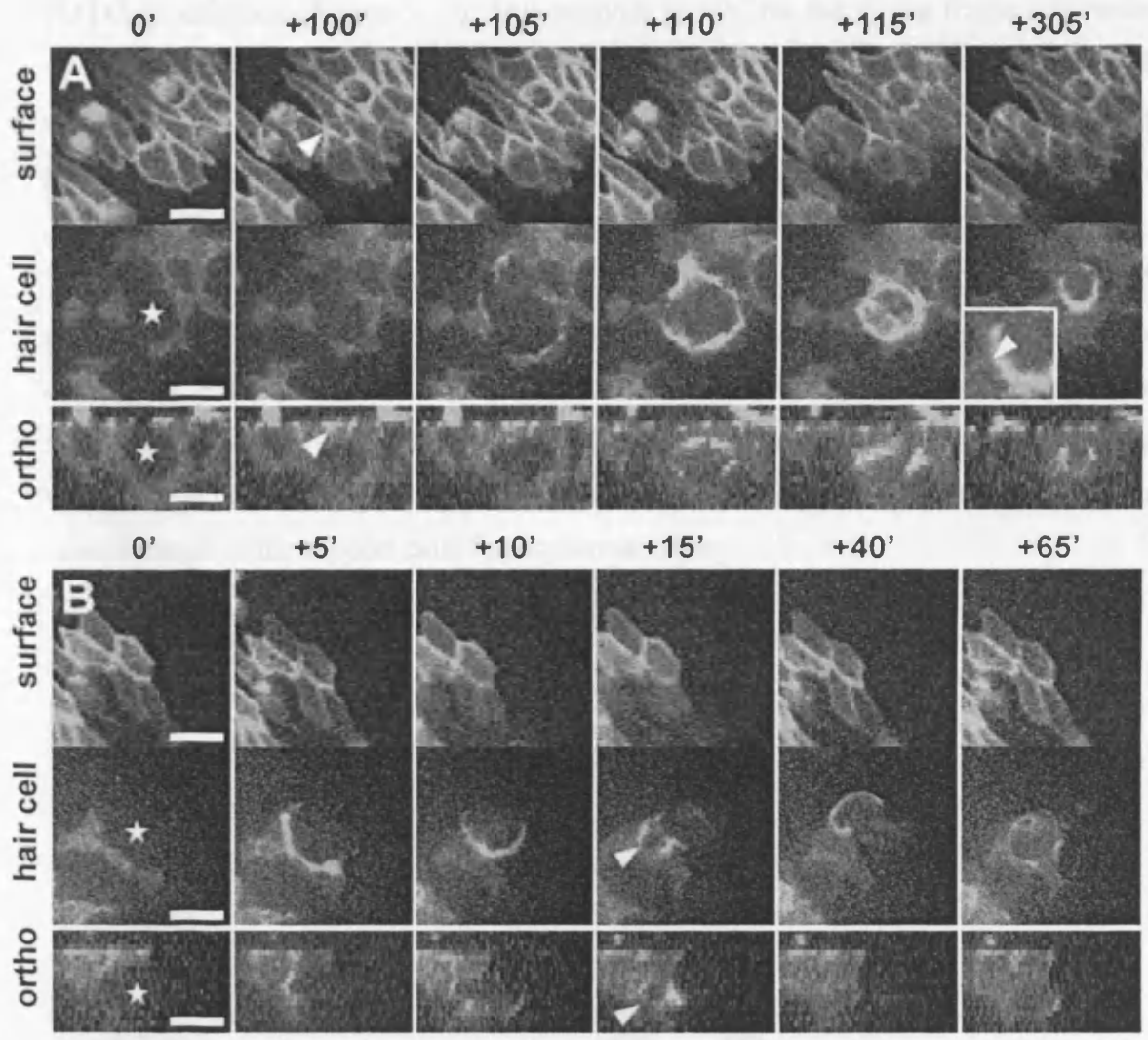

Figure 5.10 – Support cells phagocytose a dying hair cell during streptomycin ototoxicty. Utricles were harvested from E17-E19 chick embryos infected with the RCASBP(B)-β-actin-EGFP construct as before. Freshly isolated utricles were imaged in the presence of 1 mM streptomycin for 24 hours. In addition, a DNA intercalating dye TOTO-3 0.1 μM was supplemented to the imaging media. Dual-channel time-lapse was performed for EGFP (green) and TOTO-3 (blue).

A) In this example, infected support cells surround a non-infected hair cell (star). Support cell processes at the epithelial surface were pulled together by an actin cable excising the hair bundle (arrow, +100'); these frames are omitted from this series (see Figure 5.9 for detailed examples). A rapid polymerisation of β-actin-EGFP occurred within 5 mins, and was only present at sites where the hair cell interfaced with an infected support cell (+105'). As the calyx developed, TOTO-3 began to fluoresce within the hair cell as it bound DNA (+110'). The TOTO-3 signal intensified as the calyx reduced in volume (+115'). The calyx and TOTO-3 signal persisted within the epithelium (+305'). Puncta of TOTO-3 could be resolved within a support cell, indicating uptake of hair cell DNA (inset arrow).

B) In this example, a non-infected hair cell (star) was flanked by 3 infected support cells. The calyx formed within 5 minutes, and was only visible along the border with infected support cells (+5'). Support cell pseudopodia extended around the TOTO-3 labelled hair cell nucleus (+10'). A TOTO-3 phagosome (arrowhead) was seen within the support cell (+15'). The hair cell nucleus was engulfed and internalised by a support cell (+65'). Some TOTO-3 debris remained. Explants were maintained at 37°C in a 5% CO_2 atmosphere for the duration of imaging. Time stamps are relative to the first frame of the series (minutes). Scale bars are 20 μm. Examples are representative of observations from 2 independent experiments.

TOTO experiments (Figure 5.11). This analysis shows that the modal frame difference was zero; both the increase in TOTO-3 fluorescence and calyx induction occurred within the same frame. In only one example was the increase in TOTO-3 found to precede calyx induction.

In summary, dual-channel recordings of β-actin-EGFP and TOTO-3 allowed support cell phagocytosis of hair cell material to be documented during streptomycin ototoxicity. Whilst these observations did not exclude the possibility that macrophages were also active within the sensory epithelium, it demonstrated that the support cells were competent as phagocytes. Thus, the calyxeal structure described here was a manifestation of the support cell phagocytic machinery.

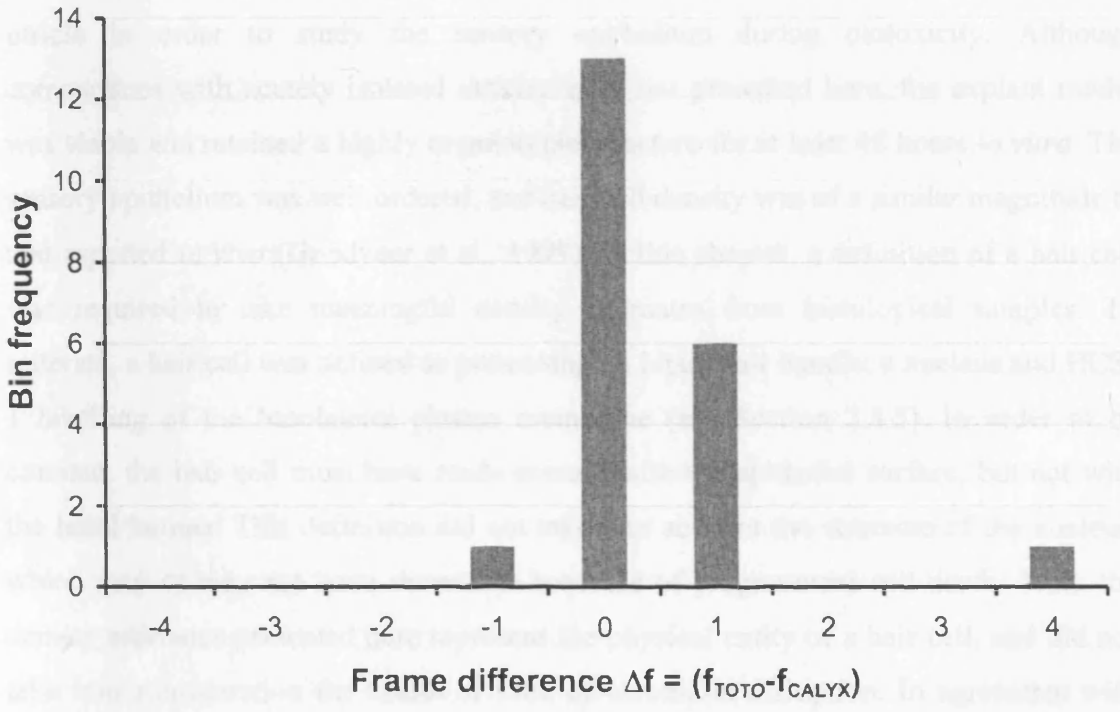

Figure 5.11 – Relative timings of TOTO-3 & calyx induction during hair cell death. A frequency histogram showing the timing of support cell calyx induction relative to the initial increase in TOTO-3 fluorescence. $\Delta f = (f_{TOTO}) - (f_{CALYX})$. Positive values of Δf indicate an increase in TOTO-3 after calyx induction. The modal difference was 0 frames, demonstrating that calyx formation occurred with, or in advance of an increase in TOTO-3 fluorescence. The frame duration was 5 minutes for these time-lapse recordings. N = 21 hair cells sampled from 2 independent experiments.

5.3 Discussion

This chapter has used immunocytochemistry and live-cell β-actin-EGFP recordings to describe structural changes to the utricular sensory epithelium during streptomycin ototoxicity. These studies demonstrate that a dying hair cell soma was retained within a support calyx formed of pseudopodia. Experiments using TOTO-3 to label hair cell chromatin further demonstrated that support cells actively phagocytosed the hair cell soma from the sensory epithelium. Support cells also constructed an actin cable that constricted to repair the epithelial defect, severing and ejecting the hair bundle in the process. These findings are now discussed in more detail.

5.3.1 Streptomycin ototoxicity in an explant model of the utricle

Experiments in the first half of this chapter utilised an explant preparation of the utricle in order to study the sensory epithelium during ototoxicity. Although comparisons with acutely isolated utricles were not presented here, the explant model was viable and retained a highly organotypic structure for at least 48 hours *in vitro*. The sensory epithelium was well ordered, and hair cell density was of a similar magnitude to that reported *in vivo* (Goodyear et al., 1999). In this chapter, a definition of a hair cell was required to take meaningful density estimates from histological samples. To reiterate, a hair cell was defined as possessing an intact hair bundle, a nucleus and HCS-1 labelling of the basolateral plasma membrane (see Section 2.8.5). In order to be counted, the hair cell must have made contact with the epithelial surface, but not with the basal lamina. This definition did not take into account the structure of the nucleus, which may or may not have shown the sequelae of programmed cell death. Thus, the density estimates presented here represent the physical entity of a hair cell, and did not take into consideration the health or state of chromatin disruption. In agreement with previous reports, treatment with streptomycin was able to trigger extensive hair cell loss throughout the utricular macula (Oesterle et al., 1993; Weisleder and Rubel, 1993; Matsui et al., 2000). The severity of streptomycin ototoxicity was found to progress in a chronological fashion. The first effects were observed 12 hours after streptomycin addition, when hair cells started to exhibit pyknotic chromatin structure. This was consistent with aminoglycosides inducing hair cell death through apoptosis (Forge, 1985; Li et al., 1995; Kil et al., 1997; Forge and Li, 2000; Matsui et al., 2002). The structural correlates of ototoxicity became more pronounced as the duration of streptomycin treatment was extended beyond 12 hours, resulting in significant loss of

hair cells from the epithelium. Of the hair cells that remained integrated within the epithelium after 24 hours, all exhibited severe chromatin degradation. These cells were committed to die, as a further 24 hours incubation in normal culture media yielded a total loss of hair cells from within the utricular cotillus (48 hour protocol). It should be noted that there were a small number of cells expressing HCS-1 present 48 hours after streptomycin treatment; the nature of these cells will be discussed elsewhere (see Section 6.4). Thus, a distinction was made between hair cells that were healthy and those that were structurally intact yet in the throws of programmed cell death. It is largely a philosophical argument as to when a cell ceases to 'live'. To be consistent in the following discussion, nuclei with visible signs of chromatin degradation will be referred to as dying, *i.e.,* in the process of programmed cell death. Once engulfed within a support cell calyx the hair cell soma will be referred to a corpse.

5.3.2 A dying hair cell is sequestered within a support cell calyx

In the avian inner ear, the general process of hair cell corpse removal appears to involve their ejection from the sensory epithelium. Whilst there is a report of hair cell internalisation (Raphael, 1993), the majority appear to be ejected from the basilar papilla (Cotanche, 1987; Marean et al., 1993; Mangiardi et al., 2004), as is also reported to be the case in the utricle (Weisleder and Rubel, 1993; Matsui et al., 2000). In contrast to previous reports from the utricle, the experiments presented here did not find any evidence for corpse ejection during streptomycin ototoxicity. Indeed, as hair cells were lost, the presence of inclusion bodies was noted within the sensory epithelium. These objects contained aggregates of HCS-1 and DAPI, suggesting that they were the remnants of a hair cell. The significance of the f-actin shell encapsulating the inclusion proved more elusive, with immunocytochemistry unable to discern whether it originated from a hair cell, support cell or macrophage. Time-lapse microscopy of β-actin-EGFP allowed these questions to be answered, in addition to revealing how these structures were formed. By observing different expression mosaics, support cells were found to contribute the f-actin that formed the inclusion body. The inclusion body will henceforth be referred to as a 'support cell calyx', to better reflect the origin of this structure. It must be stressed that the support cell calyx described here was not to be confused with the synaptic calyx found innervating type I hair cells in the striola. All the data in this chapter was collected exclusively from the utricular cotillus, where only bouton-innervated type II hair cells were present.

Live-cell time-lapse studies allowed an unparalleled insight into the activity of support cells during hair cell death. The first indication of calyx formation proper was the increased polymerisation of β-actin-EGFP at the hair cell – support cell interface. This initial event was symmetrical in all the support cells surrounding the hair cell and was rapidly induced, occurring within three minutes. Expression mosaics were particularly informative here, demonstrating that individual support cells were able to extend β-actin-EGFP pseudopodia around the hair cell soma (see Figure 5.10). The combined pseudopodial contributions of the neighbouring support cells formed the calyx. In parallel with calyx formation, support cells formed an actin cable at the epithelial surface, which constricted around the neck of the hair cell (see Section 5.3.4). This resulted in the support cell apices being pulled together, severing the hair cell soma and ejecting the cuticular plate, bundle and a volume of cytoplasm into the luminal space. This mechanism trapped the remainder of the hair cell corpse beneath the epithelium within a support cell calyx. Once formed, the calyx persisted within the epithelium, during which vesicles of β-actin-EGFP separated from the calyx and entered the surrounding support cells. Live-cell experiments using TOTO-3 confirmed that these phagocytic vesicles contained hair cell chromatin (see Section 5.3.3). A schematic model summarising these processes is presented in Figure 5.12.

Whilst the internalisation of hair cell corpses has been described in the sensory epithelia of mammals (Forge, 1985; Raphael and Altschuler, 1991b; Li et al., 1995; Forge and Li, 2000; Abrashkin et al., 2006), and of poikilotherms (Baird et al., 1996; Baird et al., 2000; Gale et al., 2002), this phenomenon has not previously been documented in the chick utricle. Previous reports from the chick utricle have suggested that hair cell corpses are ejected from the sensory epithelium (Weisleder and Rubel, 1993; Matsui et al., 2000). Closer examination of these published data reveals that ejection likely refers to that of the hair bundle and a volume of cytoplasm. This was entirely consistent with data from this chapter, where the cuticular plate and hair bundles were excised and ejected by the constricting support cell actin cable. Separate from the demonstration of internalisation, this chapter has also shown that rather simply being a vacuole beneath the epithelial surface, hair cell corpses were actively sequestered within a support cell calyx. Although many groups have shown the

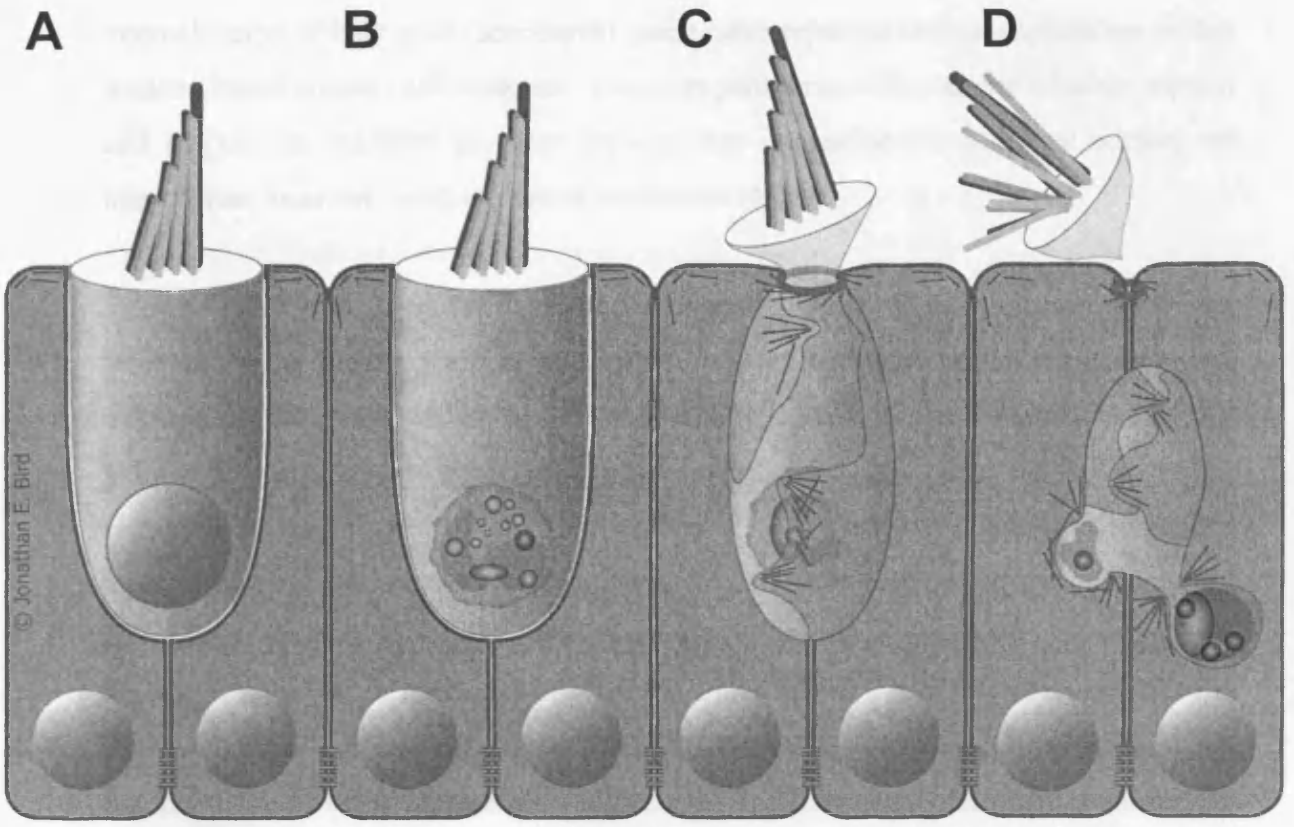

Figure 5.12 – A model of support cell activity during streptomycin ototoxicity. A representation of how support cells actively remodel to eliminate a dying hair cell from the utricular sensory epithelium. The process has been presented as a chronological progression (from left to right). Hair cell and support cell cytoplasm have been rendered as blue and green respectively. Aside from the nucleus, other organelles have been excluded for clarity. **A)** A healthy hair cell is surrounded basolaterally by support cells. Gap junctions connect the base of neighbouring support cells together. At the surface, a combination of adherens and tight junctions confer mechanical strength and impermeability to the epithelium. **B)** Aminoglycoside antibiotics induce programmed cell death throughout the hair cell population. Pyknotic chromatin condensation is visible within the hair cell nucleus. Support cell nuclei are not affected by exposure to aminoglycosides. A professional macrophage may intervene at this stage to phagocytose the hair cell from within the sensory epithelium. **C)** After an extended period, an unknown signal(s) triggers extensive remodelling of the support cells' cytoskeleton. Basolaterally, multiple support cell pseudopodia envelop the hair cell corpse within a calyx. At the epithelial surface, support cells form an actin cable that constricts around the apex of the hair cell. Newly polymerised filaments of β-actin are shown in red. **D)** Pseudopodia contributing to the calyx disrupt and internalise the hair cell corpse within phagosomes. The actin cable excises the hair bundle and unites support cells to effect repair of the epithelial defect. The hair cell has now been eliminated from the sensory epithelium. Please refer to the text for a more thorough discussion of these processes.

internalisation of hair cells (see above), none have reported their encapsulation within an actin based support cell structure. Future experiments will examine whether support cell calyxes are manifest in other systems that internalise the hair cell corpse, the mammalian inner ear being an area of particular interest.

Are support cell calyxes the predominant mode of corpse removal in the utricular epithelium? In explant cultures, a 24 hours treatment with streptomycin was sufficient to remove approximately 68 hair cells (per 10'000 μm^2) from the epithelium, yet only 29 calyxes were observed. Considering a single calyx was responsible for the removal of a single hair cell, there was a clear disparity in these quantities. It could be argued that ejection was occurring in parallel to internalisation, as proposed in the mammalian utricle (Li et al., 1995) and that this might account for the remainder. However, no evidence for the ejection of the entire hair cell corpse was encountered in fixed explants or live-cell experiments. The most likely explanation for this inconsistency was that hair cell loss was absolute, whereas calyxes could form around hair cells and phagocytose the corpses before the tissue was fixed and visualised.

5.3.3 Support cells as epithelial phagocytes

Dual channel recordings of β-actin-EGFP and TOTO-3 provided compelling evidence for the support cell phagocytosis of the hair cells. As TOTO-3 only labelled the DNA of permeabilised cell types, it proved an effective method with which to selectively visualise the chromatin of hair cell corpses. Using this technique, TOTO-3 positive phagosomes emerged from the calyx and entered into the surrounding support cells. In a more overt demonstration of phagocytosis, a single support cell engulfed and internalised an entire TOTO-3 positive hair cell nucleus (Figure 5.10B). Although uptake of hair cell DNA was shown here, it was also highly likely that other cytoplasmic material was present within support cell phagosomes. These experiments supplement the previous reports of support cell phagocytosis by detailing the actual mechanism of engulfment and internalisation for the first time (Forge, 1985; Li et al., 1995; Forge and Li, 2000; Taylor and Forge, 2005; Abrashkin et al., 2006).

In addition to providing definitive evidence for support cells phagocytosis, dual-wavelength recordings of β-actin-EGFP and TOTO-3 gave further insight into the

support cell calyx and its behaviour. Support cells were seen to engaged in an apparent melee, retracting and re-extending pseudopodia to engulf portions of the corpse. This was reflected in the varying size of hair cell material that was internalised in any given phagosome; ranging from small puncta of TOTO-3 to almost the entire nucleus in some instances (see Figure 5.10). This suggested that support cells could actively compete against each other for the hair cell corpse, similar to macrophages fighting over a solitary erythrocyte (Swanson et al., 1999). There was no evidence that a given support cell was more efficacious at engulfing a corpse than any of its neighbours, although it cannot be excluded that there was a subset of support cells preferentially able to internalise such a large object. It was more likely that engulfment was a stochastic process and that in some instances the whole nucleus was internalised, whilst in others it was divided into several smaller particles.

In addition to the non-professional phagocytic activity of support cells, there is a population of professional macrophages that also reside within the avian sensory epithelium (Warchol, 1997; Bhave et al., 1998; Warchol, 1999; O'Halloran and Oesterle, 2004). Macrophages have been shown to phagocytose hair cells and debris from various sensory epithelia (Balak et al., 1990; Jones and Corwin, 1993, 1996; Warchol, 1997), and there was some limited evidence to suggest that this was also the case here (Figure 5.7G-H). It was intriguing to consider why two populations of phagocytes might be active within the avian utricular epithelium. Did they function in parallel to achieve corpse removal, or was there a more complex relationship between them? Observations made in other systems are helpful when examining these possibilities. Support cells of the utricular sensory epithelium are not unique in their ability to engulf cell corpses and debris; many other cell types demonstrate 'non-professional phagocytic behaviour (reviewed by Rabinovitch, 1995). Phagocytosis by epithelial cells has been identified in the retinal pigment epithelium (Young and Bok, 1969; Steinberg, 1974), the lens epithelium (Ishizaki et al., 1993), the mammary epithelium (Walker et al., 1989; Monks et al., 2005) and the small airway epithelium (Walsh et al., 1999; Sexton et al., 2001). Moreover, a study by Parnaik *et al.* (2000) has shown that whilst *professional* phagocytes are able to engulf cells early within the apoptotic programme, *non-professional* phagocytes require the programme to be significantly advanced before engulfment is possible. This is proposed to introduce redundancy into the corpse removal process, favouring engulfment by a professional

phagocyte before reverting to a non-professional backup. This principle has been demonstrated *in vivo* using a PU.1 null mouse mutant that lacks macrophages and neutrophils (Wood et al., 2000). In the absence of professional phagocytes, the large numbers of apoptotic cells normally produced during development are engulfed by ancillary cell types.

It is proposed here that a similar redundancy operates within the avian utricular epithelium. In this model, the resident population of macrophages would be sufficient to phagocytose apoptotic bodies produced through normal hair cell turnover (Jorgensen, 1991; Kil et al., 1997). Support cell phagocytosis would not be the predominant mechanism of corpse removal in this situation. In contrast, during periods of severe pathophysiology the scale of hair cell death would massively exceed the capacity for macrophage corpse removal. In this situation, dying hair cells would be left unattended in the epithelium for extended periods allowing them to further degenerate. At this point, support cells would intervene and phagocytose the remaining corpses. To add some dimensions to this argument, in control utricular explants there were in excess of 100 hair cells per 10'000 μm^2 within the sensory epithelium. After 24 hours of streptomycin treatment, 1.5 macrophages were estimated within an equivalent area (see Section 5.2.3). Clearly, the total loss of hair cells induced by streptomycin treatment would represent an inordinate challenge for the limited numbers of macrophages shown here. Aside from this argument of scale, there was good evidence for the delayed intervention of support cells as proposed here. Twelve hours of streptomycin was sufficient to induce widespread pyknosis throughout the hair cell population, however support cell calyxes were not observed at this time. Only after 24 hours of streptomycin treatment were the numbers of support cell calyxes significantly elevated within the sensory epithelium (see Figure 5.6). This suggests that there was 12 hours latency between the onset of pyknosis within hair cells and their ultimate engulfment within a support cell calyx. This latency was consistent with the data of Parnaik *et al.* (2000).

Brief comment should be made regarding the KUL-01 antibody used in this study. KUL-01 was originally reported as a marker for avian monocytes, macrophages and activated microglial cells (Mast et al., 1998). As well as labelling ramified cells within the sensory epithelium, KUL-01 was found to label a subset of support cell calyxes. Typically, KUL-01 was restricted within the calyx and did not associate with a

viable cell soma of any description; it was thus highly unlikely that this represented a macrophage. As the epitope for KUL-01 is currently unknown, a plausible explanation was that the antibody recognised a protein that was required for some aspect of phagocytosis. This is comparable to identifying both leukocytes and neoplastic fibroblasts with L-plastin (Goldstein et al., 1985). Thus, KUL-01 might bind to a protein that confers a phagocytic phenotype, rather than identifying a particular cell lineage.

5.3.4 Scar formation at the epithelial surface

Scar formation describes the process whereby support cells reorganise to eliminate a hair cell from the epithelial surface (see Section 1.4.2). In the experiments presented here, extensive surface remodelling was observed during streptomycin ototoxicity. Using the phallotoxin label for f-actin, support cells were found to compensate for hair cell loss by adjusting their shape, such that the surface continuum of apical junction complexes was maintained. The full extent of support cell reorganisation was emphasised when total hair cell loss was induced using the 48 hours streptomycin protocol (see Section 5.2.2). No surface discontinuities were present in these examples. Instead, support cells reorganised to form a simple columnar epithelium that was largely devoid of hair cells. These observations of support cell reorganisation were comparable to that reported in aminoglycoside-treated mammalian and bullfrog vestibular organs (Meiteles and Raphael, 1994; Baird et al., 2000; Gale et al., 2002).

Although fixed preparations were suitable for study of the initial and concluding stages of scar formation, due to the unpredictable onset of aminoglycoside action, it was difficult to capture any intermediate events using this technique. Live-cell imaging of β-actin-EGFP allowed the complete process of scar formation to be visualised. These studies revealed a cable of f-actin accumulating around the neck of the hair cell, which subsequently constricted to pull the surrounding support cells together. At the end of this sequence, the cuticular plate and hair bundle were effectively excised by the invading support cells processes. As a result, the hair bundle was ejected into the luminal space and the hair cell corpse was trapped beneath the epithelial surface. Crucially, the actin cable was identified as a support cell structure using β-actin-EGFP expression mosaics. This was an important finding, as a cable of filamentous actin also circumscribes the peri-cuticular region of the hair cell (Hirokawa and Tilney, 1982).

Whilst it cannot be discounted that the hair cell was also generating contractile force to assist in scar formation, several lines of thought argued against this. Foremost, the peri-cuticular cable would likely be disrupted as the cuticular plate itself was ejected during scar formation. Secondly, experiments in MDCK cells have shown that an apoptotic body does not generate contractile force to drive its own extrusion from the epithelium (Rosenblatt et al., 2001). It is likely that a similar situation exists in the sensory epithelium.

Data from this chapter has shown that a support cell based actin cable underlies scar formation in the chick utricular macula. Support cells have been documented projecting microfilaments beneath the hair cell cuticular plate in both auditory (Forge, 1985; Raphael and Altschuler, 1991a, b; Leonova and Raphael, 1997) and vestibular sensory epithelia (Li et al., 1995; Forge and Li, 2000; Gale et al., 2002), however this is the first description of such a multicellular contractile structure. The involvement of an actin cable is not without precedence. Actin cables underlie diverse repair processes ranging from multicellular wounds (Martin and Lewis, 1992; Bement et al., 1993) to the restitution of single cell epithelial defects (Rosenblatt et al., 2001). The latter study in particular shares significant homology with the data from this chapter. Using β-actin-EGFP expressing MDCK monolayers, Rosenblatt *et al.* demonstrated ejection of an apoptotic cells by a contractile actin cable. The cable was formed by the neighbouring cells, and its contraction was essential for the restoration of transepithelial resistance. It seems likely that a similar mechanism is employed to maintain integrity in the utricular sensory epithelium, although electrophysiological evidence is not presented to support this unequivocally (see Section 6.4). It is intriguing to note that the cable described by Rosenblatt *et al.* initially formed basolaterally to affect cell ejection, whilst that in the utricle formed apically to excise the hair bundle and internalise the cell corpse.

Future experiments will focus around describing the actin cable in higher spatial and temporal detail. An important question to address will be whether a myosin motor associates with the actin cable, and if so, whether its function can be altered using the appropriate pharmacological tools. It will also be important to confirm whether an actin cable underlies scar formation in other hair cell epithelia: those of the mammalian inner ear being worthy of particular attention.

5.3.5 Support cell signalling during calyx and scar formation

The potential signal(s) that trigger support cell calyx and scar formation are of great interest. Although no attempts were made to pharmacologically dissect their identity here, some general statements could be made. The following arguments are directed at calyx formation, however they are equally applicable to the contractile actin cable. As shown earlier, calyx induction around a hair cell was both symmetrical and rapid, with all the neighbouring support cells responding within a three-minute window (the time-lapse frame duration). This suggested that at least one of the signal(s) was of such fidelity that neighbouring support cells were able to respond in a highly coordinate fashion. It also suggested that the signal(s) were omni directional, with all neighbouring support cells being able to receive it equally. These requirements were characteristic of either a mechanical or a diffusible factor, as opposed to a biochemical signal presented on the hair cell surface.

Comment could also be made regarding the timing of these putative signals. In explant cultures of the utricle, 12 hours of streptomycin treatment was sufficient to induce pyknotic changes in hair cell nuclei, yet few calyxes were observed at this time point. This suggested that the signals for support cell calyx formation were active after the cell had initiated the apoptotic program. Future experiments will test this hypothesis by examining whether the caspase inhibitors z-Val-Ala-Asp(Ome)-fluoromethyl ketone (zVAD-FMK), and Boc-Asp(Ome)-fluoromethyl ketone (BAF) are able to prevent calyx formation during streptomycin ototoxicity. These pan-caspase inhibitors have been shown to prevent hair cell death during aminoglycoside and cisplatin induced ototoxicity (Liu et al., 1998; Forge and Li, 2000; Cunningham et al., 2002; Matsui et al., 2002; Matsui et al., 2003), however it remains to be determined whether support cell calyxes still form under these conditions. If engulfment occurred after initiation of the apoptotic program, as suggested by data in this chapter, then the presence of phosphatidyl-D-serine on the outer leaflet of the hair cell plasma membrane may be a potential signal for calyx induction. Phosphatidyl-D-serine (PS) is exposed on the surface of apoptotic cells, and can be sufficient to trigger phagocytosis by a professional macrophage (Fadok et al., 1992). Given the requirements for symmetrical and rapid calyx induction outlined earlier, PS would likely operate in conjunction with other signals.

When considering other mechanisms that may be involved during calyx formation, inspiration can be drawn from the studies of apoptotic corpse removal in *C.elegans*. Seminal studies have identified a group of conserved genes that regulate corpse engulfment; *ced-1, ced-2, ced-5, ced-6, ced-7, ced-8* and *ced-10* (Hedgecock et al., 1983; Ellis et al., 1991). These genes encode a variety of components involved in the engulfment process, ranging from cell surface receptors to cytoskeletal associated proteins (reviewed by Reddien and Horvitz, 2004). Of the two signalling cascades that have been delineated, both converge upon the Rac GTPase (CED-10), which coordinates the extension of pseudopodia around the apoptotic corpse (Reddien and Horvitz, 2000; Kinchen et al., 2005). Due to the general intractability of gene transfer within hair cell epithelia, it is not feasible to introduce the dominant negative constructs commonly used to modulate Rac function. RNA interference may present an alternative route with which to study the physiological correlates of Rac GTPase function during periods of hair cell pathophysiology.

5.4 Conclusions

These experiments have documented how the utricular macula responds to aminoglycoside ototoxicity *in vitro*. It was shown that a 24 hours treatment with 1 mM streptomycin was sufficient to induce hair cell death throughout the utricular cotillus. Studies using immunofluorescence and live-cell imaging showed that a hair cell corpse was engulfed within the support cell calyx; a structure formed from the pseudopodia of neighbouring support cells. Further experiments revealed the phagocytic uptake of the hair cell corpse by support cells contributing to the calyx. In parallel with calyx formation, support cells formed an actin cable around the neck of the hair cell, which constricted to sever the hair bundle and repair the epithelial defect. These data demonstrate that actin cables underlie scar formation and epithelial repair in the avian utricular macula.

6 General discussion

Experiments throughout this thesis have addressed a range of phenomena that are involved in the repair and regeneration of the avian inner ear. This final discussion will attempt to assimilate these themes together, and place them within a broader context of inner ear biology.

6.1 The chick and RCAS as a model system for inner ear research

This thesis has utilised the chick embryo as an experimental model of the avian inner ear. The chick is a well-established model for inner ear research, finding applications in regenerative as well as behavioural, developmental and physiological studies. The main benefits of the chick model are easy harvest of the inner ear from both embryonic and postnatal animals, and access to a variety of organ culture paradigms that facilitate microscopic visualisation and intervention *in vitro*. A further advantage conferred by use of the chick model is the ability to manipulate the developing embryo *in ovo*. Using this property, electroporation was used to transduce the otic primordium with a recombinant RCAS provirus, allowing inner ear transgenesis to be performed. In this thesis, the RCAS retroviral vector was used to drive expression of a β-actin-EGFP fusion protein throughout the sensory patches of the inner ear. Two properties conferred by the RCAS retroviral system proved of particular experimental value. Alternating patterns of support cell and hair cell infection resulted in fluorescent expression mosaics throughout the sensory epithelium. The application of expression mosaics was demonstrated in this thesis, where they were used to separate complex cytoskeletal interactions on a single cell basis. The second property conferred by the RCAS system was the remarkable preservation of morphology within infected cell types. Integration of the proviral DNA and the associated β-actin-EGFP transgene did not correlate with any evident cellular toxicity or deleterious effects. This was in stark contrast to the author's exhaustive efforts to induce plasmid DNA expression in the sensory epithelium using electrophoretic, lipid or biolistic techniques. These resulted in either unacceptable levels of cell death or extremely low transfection efficiencies, if indeed they induced expression at all. The elegance of *in ovo* electroporation was to induce the transgene within the otic vesicle well before the formation of the actual sensory patches. The otic primordium was highly plastic at this stage, and able to accommodate the trauma of electroporation. Following transfection, the RCAS vector ensured stable integration of

the transgene, and its inheritance to cellular progeny through clonal expansion and/or subsequent cycles of infection.

Hornburger & Fekete (1996) were the first researchers to demonstrate that RCAS could be used to effectively induce ectopic gene expression throughout the developing chick central nervous system. The RCAS system has since been used as an important tool to study cell fate specifications within the developing inner ear. To the best of the author's knowledge, this thesis contains the first report of viable RCAS-driven expression in the inner ear of an E19 embryo. This is an interesting period for audition, as although the onset of sensory transduction occurs around E12 in the avian embryo (Saunders et al., 1973), it has been shown that this response matures significantly between E17-19 (Rebillard and Rubel, 1981). This suggests that RCAS expression vectors may now find general usage in the study of avian sensory physiology and pathology, in addition to that of developmental biology. An immediate possibility would be the study of the hair bundle, which exhibited robust expression of β-actin-EGFP within its component stereocilia. This would allow live-cell imaging of the hair bundle to be performed after that pioneered by Schneider *et al.* (2002). Although the RCAS system does place limitations upon the size of transgene that can be successfully delivered (~ 2000 bp), the ability to study avian sensory physiology whilst expressing recombinant proteins and/or gene reporter constructs is an exciting area of future research.

Experiments in this thesis have used chick inner ears harvested from different developmental stages, ranging from E17 to P14. A general criticism of studying any embryonic tissue, avian or otherwise, is that the reported activity may be a result of developmental plasticity rather than representative of a real process in adults. An example of this has been documented in the mammalian inner ear, where embryonic cochleae are able to replace lost hair cells, whilst those from neonates do not (Kelley et al., 1995). In contrast, a demarcation between the embryonic and postnatal responses has not been described in the avian inner ear: regenerative responses are present in both embryonic and postnatal organs. Nonetheless, there is now a precedent to repeat the key experiments from this thesis in postnatal animals, to confirm whether the mechanisms identified are still functional.

6.2 A conserved mechanism of epithelial repair

This thesis has investigated how the avian sensory epithelium responded to both laser ablation and aminoglycoside insult. Although the former was mechanical and the latter pharmacological by nature, there were striking similarities between the ensuing repair processes. In response to laser ablation, support cells were found to construct a contractile actin cable around the perimeter of the epithelial wound, in addition to invading the denuded space with multiple lamellipodia (see Chapter 3). A similar response was observed during aminoglycoside ototoxicity. Support cells constructed an actin cable at the epithelial surface, in addition to projecting pseudopodia around the dying hair cell itself (see Chapter 5). To re-emphasise, both forms of epithelial insult triggered a polarised multi-support cell response that comprised formation of an actin cable and lamellipodia. In particular, the close correlation between actin cables suggested that these were instantiations of the same phenomenon, simply manifest on a different physical scale. This statement found resonance with other wound models, where actin cables drive epithelial repair in both single (Rosenblatt et al., 2001; Florian et al., 2002) and multi-cellular defects alike (Martin and Lewis, 1992; Bement et al., 1993).

From a comparative perspective, this homology highlights the potential utility of laser ablation to understand how the sensory epithelium responds to aminoglycoside insult. Accordingly, future experiments will test the involvement of NM-myosin II and Rho kinase in the formation of epithelial scars as described in Chapter 5. There was already some evidence to support the involvement of NM-myosin II during this process. In the experiments of Chapter 3, small annuli of NM-myosin IIB immuno-labelling were localised to the intersection of several support cells at the epithelial surface (see Figure 3.7I). These support cells intersections were identical to the epithelial scars observed during streptomycin treatment, and likely correlated with a dying hair cell *in vitro*. Although the putative association of NM-myosin IIB to sites of epithelial scarring requires further characterisation, it can be predicted that the inhibition of NM-myosin II would abolish cable formation and/or contraction during streptomycin treatment. It is not envisaged that NM-myosin II inhibition would interfere with calyx formation, given that lamellipodia were shown to form normally elsewhere (see Figure 3.8). Similar results were expected if a Rho kinase inhibitor were introduced during streptomycin treatment. It will be intriguing to test these hypotheses, and by doing so evaluate

whether laser ablation really was useful for making functional predictions. There is certainly strong evidence in other systems for the role of both NM-myosin II and Rho-kinase in the repair of epithelial defects (Rosenblatt et al., 2001; Florian et al., 2002).

Given the parallels between laser ablation and streptomycin ototoxicity, further hypotheses can be constructed. Laser ablation of the sensory epithelium was shown to trigger a transient phosphorylation of ERK1/2 in support cells surrounding the wound (see Figure 3.9). Might ERK also be activated in support cells surrounding a dying hair cell? The activation of ERK by trauma is by no means unique to sensory epithelia of the inner ear; it can be considered a conserved response that is elicited in many wound models (Dieckgraefe et al., 1997; Nobes and Hall, 1999; Matsubayashi et al., 2004; Nikolic et al., 2006). Given this ubiquity, future experiments will use immuno-cytochemistry to examine ERK activation in the sensory epithelium during streptomycin treatment. A parallel approach will be to use pharmacological inhibitors of MEK1+2 to assess whether these can interfere with epithelial scar formation. Other experiments will document the putative activation of the JNK and p38 MAPK pathways during epithelial trauma. These will likely yield valuable information concerning the support cell signals that coordinate epithelial repair.

The ability of both laser ablation and streptomycin to activate a homologous epithelial repair programme was unexpected. Laser ablation was a mechanical wounding technique that destroyed hair cells and support cells without preference. In contrast, streptomycin triggered programmed hair cell death without affecting support cell survival. Did the sensory epithelium engage in an identical repair program irrespective of the trauma inflicted, or could there be some common element between the two wounding techniques? Although the former hypothesis was certainly possible, there were also some clear similarities between the two wounding techniques. Laser ablation was able to liberate extensive amounts of hair cell and support cell cytoplasm directly into the extracellular space. Streptomycin treatment was also likely to result in release of hair cell cytoplasm, as permeability experiments with TOTO-3 demonstrated (see Section 5.2.5). A number of biologically active molecules are present within the cytoplasm, some of which have the potential to directly influence support cells activity. Of special interest is adenosine 5'-triphosphate (ATP). ATP is stored in high concentrations (~mM) within the cell's cytoplasm, and has been shown to elicit Ca^{2+}

transients when applied extracellularly to support cells of the mammalian cochlea (Gale et al., 2004). Future experiments will investigate the involvement of purinergic signalling during repair of the sensory epithelium.

6.3 Is laser ablation a useful model for repair and regeneration?

One of the aims of this thesis was to investigate whether laser ablation was an appropriate model for the study of repair and regeneration in the avian inner ear. Several studies have used laser ablation to destroy individual hair cells within sensory epithelia (Balak et al., 1990; Kelley et al., 1995; Jones and Corwin, 1996; Warchol and Corwin, 1996; Gale et al., 2004), however none have created multi-cellular wounds on the scale such as that described here. There was no immediate association between multi-cellular wounds of the sensory epithelium and documented pathologies of the inner ear. Whilst it can be argued that laser ablation of the auditory sensory epithelium was similar to the disruption induced by impulse noise trauma (see Section 1.4.1), no such correlate exists within the vestibular system. Despite this, laser ablation was found to elicit several responses that were characteristic of hair cell loss *in vivo*. For example, support cells are known to form epithelial scars at the sites of hair cell loss. The utility of laser ablation as a model for this process has already been commented upon, reproducing some aspects of scar formation to a remarkable degree (see Section 6.2).

Another characteristic of hair cell loss in the avian inner ear is an increase in support cell proliferation (see Section 1.4.3). As demonstrated in Chapter 4, laser ablation was also able to model some aspects of this process. Support cells were found to re-enter the cell cycle within 48 hours of laser ablation, which was in broad agreement with the latency described both *in vivo* and *in vitro* (Stone and Cotanche, 1994; Bhave et al., 1995; Warchol and Corwin, 1996; Matsui et al., 2000). Crucially, experiments in this thesis did not investigate whether support cell progeny were able to differentiate into new sensory hair cells or not, a clear limitation of the model in its current form. Other studies have demonstrated the presence of BrdU positive hair cells in cultured avian utricles, suggesting that there was no barrier to differentiation occurring *in vitro* (Warchol and Corwin, 1993). Future experiments will investigate whether new hair cells are produced in response to laser ablation, as this will substantially augment the potential value of this model.

The parallels between the events following laser ablation and those of hair cell loss *in vivo* raise an intriguing question. Could the support cell response in both paradigms be indicative of a more generalised wound repair programme? This type of comparison is insightful when considering how support cell proliferation might be regulated during epithelial trauma. Wounding of cell monolayers is known to induce cell proliferation in a qualitatively similar manner to that observed using laser ablation (Vasiliev et al., 1969; Farooqui and Fenteany, 2005). In these systems, there is good evidence that a density dependent inhibition (DDI) regulates proliferation within the denuded area (Stoker and Rubin, 1967; Rosen and Misfeldt, 1980). A mechanism of DDI involving N-cadherin has already been described within the avian utricle (Warchol, 2002), and there was some evidence for its involvement following laser ablation (see Chapter 4). An analogous situation can now be envisaged during hair cell loss *in vivo*. As support cells expand to replace a missing hair cell, they would also experience a *de facto* reduction in local cell density. Thus, the process of scar formation itself might provide density cues that induce support cell proliferation.

Future experiments will address this hypothesis, and further investigate potential mechanisms of DDI within the sensory epithelium. Data from this thesis have already yielded some intriguing clues. In epithelial laser wounds that were incubated with the PI3K inhibitor LY294002, wound closure was able to proceed in the absence of support cell proliferation (see Section 4.2.3). Although the target of PI3K activity was to be determined, the effect was to uncouple wound repair from support cell proliferation. This promises to be an exciting area of research; especially when the potential for PI3K to interact with contact-mediated signalling is considered (see Section 4.3.3). Coincidentally, there are other situations where wound closure can proceed without support cell proliferation. In the mammalian utricle, epithelial scars form around dying hair cells (Meiteles and Raphael, 1994), yet only a limited increase in support cell proliferation is reported (Warchol et al., 1993). Can the poor induction of support cell proliferation be explained by a defect in sensing or communicating changes in cell density within the mammalian sensory epithelium? This is a good example of where general wound biology can help identify differences between repair that occurs with, and without proliferation.

6.4 The importance of support cells in hearing and deafness

Support cells fulfil a variety of functions within inner ear sensory epithelia; these include the provision of basic mechanical and metabolic support, in addition to maintaining the epithelial barrier during periods of hair cell pathology. In systems that regenerate, support cells can also undergo cell division and/or phenotypic conversion to repopulate the sensory epithelium with new hair cells. Experiments from this thesis have detailed a range of these support cell phenomena, in addition to uncovering some new ones.

This thesis has documented evidence for two mechanisms involved in avian hair cell regeneration: support cell proliferation and phenotypic conversion. Chapter 4 demonstrated that laser ablation *in vitro* was able to upregulate support cell proliferation within the sensory epithelium, indicative of the dominant mechanism of regeneration first described in Aves (Corwin and Cotanche, 1988; Ryals and Rubel, 1988). There was also some evidence to suggest that support cell phenotypic conversion was occurring *in vitro*. Chapter 5 noted the appearance of an intermediate cell type 48 hours after the addition of streptomycin. This intermediate type had the general morphology of a support cell, however it also expressed HCS-1 and displayed a small hair bundle in some cases. It was tempting to state that this intermediate morphology was evidence for phenotypic conversion, the non-mitotic process of a support cell transforming into a hair cell. Further studies are required to strengthen this assertion, as this morphology has also been reported during normal hair cell differentiation (Stone and Rubel, 2000a). Given that these experiments were performed in E21 chick embryos, it was also possible that the intermediate morphology was associated with the ongoing production of hair cells (Goodyear et al., 1999).

Experiments in this thesis have also documented how support cells undertook repair of the avian utricular epithelium. Whilst the 'phalangeal scar' associated with epithelial repair has been documented by many authors (Bohne, 1976; Hawkins, 1976; Forge, 1985; Raphael and Altschuler, 1991a), this thesis contains the first description of a complete mechanism that potentially underlies its formation. The ability of support cells to form an actin cable around sites of epithelial trauma was documented for both mechanical and pharmacological insults. A remaining functional question was whether the actin cable was required for restoration of transepithelial resistance, the quantitative

measure of barrier integrity. These types of experiment were not attempted due to the practical limitations of providing a high resistance seal around the edge of the epithelium. In the absence of conclusive electrical measurements, a simple logic argued that wound repair should result in the restoration of transepithelial resistance. Consider that either a laser wound or a dying hair cell can be approximated by a hollow cylinder transecting the epithelium, through which ions can flow with low impedance. From basic physics, the resistance of this cylinder is directly proportional to its length, and inversely so to its cross-sectional area. Thus, by virtue of the reduced cross-sectional area realised through wound closure, the resistance would increase correspondingly. In agreement with this simple approximation, there is excellent evidence that actin cables restore the transepithelial resistance in wounded MDCK and gut epithelial cell monolayers (Rosenblatt et al., 2001; Florian et al., 2002), and it is reasonable to assume that similar function was affected in the utricular sensory epithelium. It remains to be seen whether actin cables are responsible for scar formation in mammalian sensory epithelia, and this will prove an important area of further study.

An unexpected finding of this thesis was that support cells in the avian utricular epithelium were also acting as non-professional phagocytes; engulfing hair cell corpses as they underwent programmed cell death. There was already some evidence that support cells might be acting as epithelial phagocytes during aminoglycoside ototoxicity (Forge, 1985; Li et al., 1995; Forge and Li, 2000; Taylor and Forge, 2005; Abrashkin et al., 2006). Whilst these studies demonstrated the presence of degraded chromatin and hair cell associated proteins within support cells' cytoplasm, none have documented the actual uptake mechanism itself. The data in this thesis constitutes the first definitive report of the actual process of engulfment and phagocytosis of a dying hair cell by its support cell neighbours. This study is also the first to give an indication of how prevalent this phenomenon was. Within the chick utricle, it was estimated that 62% of hair cells were engulfed within 24 hours of streptomycin treatment (see Section 5.2.4). Considering that no evidence of ejection was observed, this suggested that support cell phagocytosis was the dominant mechanism of hair cell removal within the chick utricle.

The results from this thesis have highlighted several avenues for future research. One line of enquiry will centre upon a more detailed characterisation of the epithelial repair process during hair cell pathophysiology. These studies will benefit from a

natural dichotomy present within the avian inner ear. Unlike the utricle that has been shown to retain apoptotic hair cells within the epithelium, the basilar papilla ejects the entire corpse into the luminal space (Cotanche, 1987; Mangiardi et al., 2004). Support cells of the basilar papilla also form epithelial 'scars' upon hair cell ejection (Cotanche and Dopyera, 1990; Raphael, 1993), and likely maintain barrier integrity whilst doing so. Do support cells in the basilar papilla utilise calyxes and/or actin cables during epithelial repair? It will be intriguing to examine how these mechanisms might be differentially employed to generate the distinct endpoints of hair cell ejection versus internalisation.

Another line of enquiry will examine whether abnormalities in the support cell repair programme might be manifest as pathologies *in vivo*. For example, could genetic mutations abrogate the ability of support cells to undertake the epithelial repair programme? If scar formation proved defective, any compromise of the epithelial barrier would be persistent. The resulting ingress of K^+-rich endolymph would likely result in further degeneration of the remaining hair cell population, as has been reported in the inner ears of *claudin14*$^{-/-}$ mutant mice (Ben-Yosef et al., 2003). Instead of a disabling mutation, abnormal support cell signalling might conversely sensitise the repair process, rendering it unstable and vulnerable to spontaneous activation. As support cell actin cables and calyxes have not been described until now, the sequelae of their aberrant activity have not been considered. A clear precedent is now established by this thesis; could abnormal support cell signalling lead to the repair process being activated around a healthy hair cell? It was evident that the support cells' actin cable could effectively excise the cuticular plate and bundle from the soma. Could this process also culminate in the decapitation of a healthy hair cell? Alternatively, might support cells form a calyx and mistakenly phagocytose a healthy hair cell soma from within the epithelium? If either of these phenomena were to materialise on a large scale, there were obvious consequences for continued sensory transduction within the epithelium. Future experiments will investigate whether hair cell 'execution' is a real support cell phenomenon, and if so, whether this represents a novel mechanism of inner ear pathology. Given these potential new functions, a greater emphasis is now placed upon understanding the support cell and its potential regulation during pathophysiology.

6.5 Conclusions

The studies presented in this thesis have investigated the mechanisms of epithelial repair employed within the chick utricle. In response to laser ablation of the sensory epithelium, support cells formed a contractile actin cable that drove re-epithelialisation of the wound. Correct wound closure was dependent upon Rho-kinase and NM-myosin II activity within support cells. Support cells were equally important during periods of aminoglycoside-induced hair cell death, forming a multi-cellular actin cable that maintained epithelial integrity around a dying hair cell. In addition, support cells were able to phagocytose the hair cell corpse from within the epithelium. In other experiments, the signals that regulate support cell proliferation were investigated. Support cell proliferation was increased following laser ablation, and this was found to be entirely dependent upon signalling through PI3K.

7 Bibliography

Abercrombie M, Heaysman JE (1954) Observations on the social behaviour of cells in tissue culture. II. Monolayering of fibroblasts. Exp Cell Res 6:293-306.

Aberle H, Bauer A, Stappert J, Kispert A, Kemler R (1997) beta-catenin is a target for the ubiquitin-proteasome pathway. Embo J 16:3797-3804.

Abrashkin KA, Izumikawa M, Miyazawa T, Wang CH, Crumling MA, Swiderski DL, Beyer LA, Gong TW, Raphael Y (2006) The fate of outer hair cells after acoustic or ototoxic insults. Hear Res.

Adler HJ, Raphael Y (1996) New hair cells arise from supporting cell conversion in the acoustically damaged chick inner ear. Neurosci Lett 205:17-20.

Adler HJ, Komeda M, Raphael Y (1997) Further evidence for supporting cell conversion in the damaged avian basilar papilla. Int J Dev Neurosci 15:375-385.

Ahmad M, Bohne BA, Harding GW (2003) An in vivo tracer study of noise-induced damage to the reticular lamina. Hear Res 175:82-100.

Ahmed ZM, Goodyear R, Riazuddin S, Lagziel A, Legan PK, Behra M, Burgess SM, Lilley KS, Wilcox ER, Riazuddin S, Griffith AJ, Frolenkov GI, Belyantseva IA, Richardson GP, Friedman TB (2006) The tip-link antigen, a protein associated with the transduction complex of sensory hair cells, is protocadherin-15. J Neurosci 26:7022-7034.

Alagramam KN, Murcia CL, Kwon HY, Pawlowski KS, Wright CG, Woychik RP (2001) The mouse Ames waltzer hearing-loss mutant is caused by mutation of Pcdh15, a novel protocadherin gene. Nat Genet 27:99-102.

Amano M, Ito M, Kimura K, Fukata Y, Chihara K, Nakano T, Matsuura Y, Kaibuchi K (1996) Phosphorylation and activation of myosin by Rho-associated kinase (Rho-kinase). J Biol Chem 271:20246-20249.

Baird RA, Steyger PS, Schuff NR (1996) Mitotic and nonmitotic hair cell regeneration in the bullfrog vestibular otolith organs. Ann N Y Acad Sci 781:59-70.

Baird RA, Burton MD, Fashena DS, Naeger RA (2000) Hair cell recovery in mitotically blocked cultures of the bullfrog saccule. Proc Natl Acad Sci U S A 97:11722-11729.

Balak KJ, Corwin JT, Jones JE (1990) Regenerated hair cells can originate from supporting cell progeny: evidence from phototoxicity and laser ablation experiments in the lateral line system. J Neurosci 10:2502-2512.

Bartolami S, Goodyear R, Richardson G (1991) Appearance and distribution of the 275 kD hair-cell antigen during development of the avian inner ear. J Comp Neurol 314:777-788.

Bement WM, Forscher P, Mooseker MS (1993) A novel cytoskeletal structure involved in purse string wound closure and cell polarity maintenance. J Cell Biol 121:565-578.

Bement WM, Mandato CA, Kirsch MN (1999) Wound-induced assembly and closure of an actomyosin purse string in Xenopus oocytes. Curr Biol 9:579-587.

Ben-Yosef T, Belyantseva IA, Saunders TL, Hughes ED, Kawamoto K, Van Itallie CM, Beyer LA, Halsey K, Gardner DJ, Wilcox ER, Rasmussen J, Anderson JM, Dolan DF, Forge A, Raphael Y, Camper SA, Friedman TB (2003) Claudin 14 knockout mice, a model for autosomal recessive deafness DFNB29, are deaf due to cochlear hair cell degeneration. Hum Mol Genet 12:2049-2061.

Bermingham NA, Hassan BA, Price SD, Vollrath MA, Ben-Arie N, Eatock RA, Bellen HJ, Lysakowski A, Zoghbi HY (1999) Math1: an essential gene for the generation of inner ear hair cells. Science 284:1837-1841.

Bermingham-McDonogh O, Rubel EW (2003) Hair cell regeneration: winging our way towards a sound future. Curr Opin Neurobiol 13:119-126.

Berridge MJ, Bootman MD, Roderick HL (2003) Calcium signalling: dynamics, homeostasis and remodelling. Nat Rev Mol Cell Biol 4:517-529.

Bhave SA, Oesterle EC, Coltrera MD (1998) Macrophage and microglia-like cells in the avian inner ear. J Comp Neurol 398:241-256.

Bhave SA, Stone JS, Rubel EW, Coltrera MD (1995) Cell cycle progression in gentamicin-damaged avian cochleas. J Neurosci 15:4618-4628.

Bloor JW, Kiehart DP (2002) Drosophila RhoA regulates the cytoskeleton and cell-cell adhesion in the developing epidermis. Development 129:3173-3183.

Boettger T, Hubner CA, Maier H, Rust MB, Beck FX, Jentsch TJ (2002) Deafness and renal tubular acidosis in mice lacking the K-Cl co-transporter Kcc4. Nature 416:874-878.

Bohne BA (1976) Healing of the Noise Damaged Inner Ear. Saint Louis, MO.: Washington University Press.

Bohne BA, Rabbitt KD (1983) Holes in the reticular lamina after noise exposure: implication for continuing damage in the organ of Corti. Hear Res 11:41-53.

Bohne BA, Harding GW (2000) Degeneration in the cochlea after noise damage: primary versus secondary events. Am J Otol 21:505-509.

Brock J, Midwinter K, Lewis J, Martin P (1996) Healing of incisional wounds in the embryonic chick wing bud: characterization of the actin purse-string and demonstration of a requirement for Rho activation. J Cell Biol 135:1097-1107.

Brunn GJ, Williams J, Sabers C, Wiederrecht G, Lawrence JC, Jr., Abraham RT (1996) Direct inhibition of the signaling functions of the mammalian target of rapamycin by the phosphoinositide 3-kinase inhibitors, wortmannin and LY294002. Embo J 15:5256-5267.

Burnstock G (2006) Purinergic signalling--an overview. Novartis Found Symp 276:26-48; discussion 48-57, 275-281.

Carnicero E, Zelarayan LC, Ruttiger L, Knipper M, Alvarez Y, Alonso MT, Schimmang T (2004) Differential roles of fibroblast growth factor-2 during development and maintenance of auditory sensory epithelia. J Neurosci Res 77:787-797.

Chen L, Sun W, Salvi RJ (2001) Electrically evoked otoacoustic emissions from the chicken ear. Hear Res 161:54-64.

Chen P, Segil N (1999) p27(Kip1) links cell proliferation to morphogenesis in the developing organ of Corti. Development 126:1581-1590.

Chen P, Zindy F, Abdala C, Liu F, Li X, Roussel MF, Segil N (2003) Progressive hearing loss in mice lacking the cyclin-dependent kinase inhibitor Ink4d. Nat Cell Biol 5:422-426.

Chrzanowska-Wodnicka M, Burridge K (1996) Rho-stimulated contractility drives the formation of stress fibers and focal adhesions. J Cell Biol 133:1403-1415.

Clark JA, Pickles JO (1996) The effects of moderate and low levels of acoustic overstimulation on stereocilia and their tip links in the guinea pig. Hear Res 99:119-128.

Cody AR, Robertson D, Bredberg G, Johnston BM (1980) Electrophysiological and morphological changes in the guinea pig cochlea following mechanical trauma to the organ of Corti. Acta Otolaryngol 89:440-452.

Conrad PA, Giuliano KA, Fisher G, Collins K, Matsudaira PT, Taylor DL (1993) Relative distribution of actin, myosin I, and myosin II during the wound healing response of fibroblasts. J Cell Biol 120:1381-1391.

Corey DP, Garcia-Anoveros J, Holt JR, Kwan KY, Lin SY, Vollrath MA, Amalfitano A, Cheung EL, Derfler BH, Duggan A, Geleoc GS, Gray PA, Hoffman MP, Rehm HL, Tamasauskas D, Zhang DS (2004) TRPA1 is a candidate for the mechanosensitive transduction channel of vertebrate hair cells. Nature 432:723-730.

Corwin JT (1981) Postembryonic production and aging in inner ear hair cells in sharks. J Comp Neurol 201:541-553.

Corwin JT (1985) Perpetual production of hair cells and maturational changes in hair cell ultrastructure accompany postembryonic growth in an amphibian ear. Proc Natl Acad Sci U S A 82:3911-3915.

Corwin JT, Cotanche DA (1988) Regeneration of sensory hair cells after acoustic trauma. Science 240:1772-1774.

Corwin JT, Oberholtzer JC (1997) Fish n' chicks: model recipes for hair-cell regeneration? Neuron 19:951-954.

Cotanche DA (1987) Regeneration of hair cell stereociliary bundles in the chick cochlea following severe acoustic trauma. Hear Res 30:181-195.

Cotanche DA, Dopyera CE (1990) Hair cell and supporting cell response to acoustic trauma in the chick cochlea. Hear Res 46:29-40.

Cotanche DA, Henson MM, Henson OW, Jr. (1992) Contractile proteins in the hyaline cells of the chicken cochlea. J Comp Neurol 324:353-364.

Cruz RM, Lambert PR, Rubel EW (1987) Light microscopic evidence of hair cell regeneration after gentamicin toxicity in chick cochlea. Arch Otolaryngol Head Neck Surg 113:1058-1062.

Cunningham LL, Cheng AG, Rubel EW (2002) Caspase activation in hair cells of the mouse utricle exposed to neomycin. J Neurosci 22:8532-8540.

Danjo Y, Gipson IK (1998) Actin 'purse string' filaments are anchored by E-cadherin-mediated adherens junctions at the leading edge of the epithelial wound, providing coordinated cell movement. J Cell Sci 111 (Pt 22):3323-3332.

Daudet N, Vago P, Ripoll C, Humbert G, Pujol R, Lenoir M (1998) Characterization of atypical cells in the juvenile rat organ of corti after aminoglycoside ototoxicity. J Comp Neurol 401:145-162.

DeRosier DJ, Tilney LG, Egelman E (1980) Actin in the inner ear: the remarkable structure of the stereocilium. Nature 287:291-296.

Di Palma F, Holme RH, Bryda EC, Belyantseva IA, Pellegrino R, Kachar B, Steel KP, Noben-Trauth K (2001) Mutations in Cdh23, encoding a new type of cadherin, cause stereocilia disorganization in waltzer, the mouse model for Usher syndrome type 1D. Nat Genet 27:103-107.

Dieckgraefe BK, Weems DM (1999) Epithelial injury induces egr-1 and fos expression by a pathway involving protein kinase C and ERK. Am J Physiol 276:G322-330.

Dieckgraefe BK, Weems DM, Santoro SA, Alpers DH (1997) ERK and p38 MAP kinase pathways are mediators of intestinal epithelial wound-induced signal transduction. Biochem Biophys Res Commun 233:389-394.

Diehl JA, Cheng M, Roussel MF, Sherr CJ (1998) Glycogen synthase kinase-3beta regulates cyclin D1 proteolysis and subcellular localization. Genes Dev 12:3499-3511.

Dulbecco R, Stoker MG (1970) Conditions determining initiation of DNA synthesis in 3T3 cells. Proc Natl Acad Sci U S A 66:204-210.

Ellis RE, Jacobson DM, Horvitz HR (1991) Genes required for the engulfment of cell corpses during programmed cell death in Caenorhabditis elegans. Genetics 129:79-94.

Fadok VA, Voelker DR, Campbell PA, Cohen JJ, Bratton DL, Henson PM (1992) Exposure of phosphatidylserine on the surface of apoptotic lymphocytes triggers specific recognition and removal by macrophages. J Immunol 148:2207-2216.

Farooqui R, Fenteany G (2005) Multiple rows of cells behind an epithelial wound edge extend cryptic lamellipodia to collectively drive cell-sheet movement. J Cell Sci 118:51-63.

Favata MF, Horiuchi KY, Manos EJ, Daulerio AJ, Stradley DA, Feeser WS, Van Dyk DE, Pitts WJ, Earl RA, Hobbs F, Copeland RA, Magolda RL, Scherle PA, Trzaskos JM

(1998) Identification of a novel inhibitor of mitogen-activated protein kinase kinase. J Biol Chem 273:18623-18632.

Fechner FP, Nadol JJ, Burgess BJ, Brown MC (2001) Innervation of supporting cells in the apical turns of the guinea pig cochlea is from type II afferent fibers. J Comp Neurol 429:289-298.

Fenteany G, Janmey PA, Stossel TP (2000) Signaling pathways and cell mechanics involved in wound closure by epithelial cell sheets. Curr Biol 10:831-838.

Fettiplace R, Hackney CM (2006) The sensory and motor roles of auditory hair cells. Nat Rev Neurosci 7:19-29.

Field C, Li R, Oegema K (1999) Cytokinesis in eukaryotes: a mechanistic comparison. Curr Opin Cell Biol 11:68-80.

Flock A, Cheung HC (1977) Actin filaments in sensory hairs of inner ear receptor cells. J Cell Biol 75:339-343.

Flock A, Flock B, Murray E (1977) Studies on the sensory hairs of receptor cells in the inner ear. Acta Otolaryngol 83:85-91.

Florian P, Schoneberg T, Schulzke JD, Fromm M, Gitter AH (2002) Single-cell epithelial defects close rapidly by an actinomyosin purse string mechanism with functional tight junctions. J Physiol 545:485-499.

Folkman J, Moscona A (1978) Role of cell shape in growth control. Nature 273:345-349.

Forge A (1985) Outer hair cell loss and supporting cell expansion following chronic gentamicin treatment. Hear Res 19:171-182.

Forge A, Li L (2000) Apoptotic death of hair cells in mammalian vestibular sensory epithelia. Hear Res 139:97-115.

Forge A, Li L, Nevill G (1998) Hair cell recovery in the vestibular sensory epithelia of mature guinea pigs. J Comp Neurol 397:69-88.

Forge A, Li L, Corwin JT, Nevill G (1993) Ultrastructural evidence for hair cell regeneration in the mammalian inner ear. Science 259:1616-1619.

Franke JD, Montague RA, Kiehart DP (2005) Nonmuscle Myosin II Generates Forces that Transmit Tension and Drive Contraction in Multiple Tissues during Dorsal Closure. Curr Biol 15:2208-2221.

Furness DN, Hackney CM (1985) Cross-links between stereocilia in the guinea pig cochlea. Hear Res 18:177-188.

Gale JE, Meyers JR, Periasamy A, Corwin JT (2002) Survival of bundleless hair cells and subsequent bundle replacement in the bullfrog's saccule. J Neurobiol 50:81-92.

Gale JE, Piazza V, Ciubotaru CD, Mammano F (2004) A mechanism for sensing noise damage in the inner ear. Curr Biol 14:526-529.

Garetz SL, Rhee DJ, Schacht J (1994) Sulfhydryl compounds and antioxidants inhibit cytotoxicity to outer hair cells of a gentamicin metabolite in vitro. Hear Res 77:75-80.

Gille H, Downward J (1999) Multiple ras effector pathways contribute to G(1) cell cycle progression. J Biol Chem 274:22033-22040.

Girod DA, Duckert LG, Rubel EW (1989) Possible precursors of regenerated hair cells in the avian cochlea following acoustic trauma. Hear Res 42:175-194.

Goldstein D, Djeu J, Latter G, Burbeck S, Leavitt J (1985) Abundant synthesis of the transformation-induced protein of neoplastic human fibroblasts, plastin, in normal lymphocytes. Cancer Res 45:5643-5647.

Gong TW, Hegeman AD, Shin JJ, Adler HJ, Raphael Y, Lomax MI (1996) Identification of genes expressed after noise exposure in the chick basilar papilla. Hear Res 96:20-32.

Goodyear R, Richardson G (1992) Distribution of the 275 kD hair cell antigen and cell surface specialisations on auditory and vestibular hair bundles in the chicken inner ear. J Comp Neurol 325:243-256.

Goodyear RJ, Gates R, Lukashkin AN, Richardson GP (1999) Hair-cell numbers continue to increase in the utricular macula of the early posthatch chick. J Neurocytol 28:851-861.

Goodyear RJ, Legan PK, Wright MB, Marcotti W, Oganesian A, Coats SA, Booth CJ, Kros CJ, Seifert RA, Bowen-Pope DF, Richardson GP (2003) A receptor-like inositol lipid phosphatase is required for the maturation of developing cochlear hair bundles. J Neurosci 23:9208-9219.

Gordon SR (1983) The localization of actin in dividing corneal endothelial cells demonstrated with nitrobenzoxadiazole phallacidin. Cell Tissue Res 229:533-539.

Gordon SR, Staley CA (1990) Role of the cytoskeleton during injury-induced cell migration in corneal endothelium. Cell Motil Cytoskeleton 16:47-57.

Gordon SR, Essner E, Rothstein H (1982) In situ demonstration of actin in normal and injured ocular tissues using 7-nitrobenz-2-oxa-1,3-diazole phallacidin. Cell Motil 2:343-354.

Gotlieb AI, May LM, Subrahmanyan L, Kalnins VI (1981) Distribution of microtubule organizing centers in migrating sheets of endothelial cells. J Cell Biol 91:589-594.

Grose R, Harris BS, Cooper L, Topilko P, Martin P (2002) Immediate early genes krox-24 and krox-20 are rapidly up-regulated after wounding in the embryonic and adult mouse. Dev Dyn 223:371-378.

Gulley RL, Reese TS (1976) Intercellular junctions in the reticular lamina of the organ of Corti. J Neurocytol 5:479-507.

Hamburger V, Hamilton HL (1992) A series of normal stages in the development of the chick embryo. 1951. Dev Dyn 195:231-272.

Hamernik RP, Turrentine G, Roberto M, Salvi R, Henderson D (1984) Anatomical correlates of impulse noise-induced mechanical damage in the cochlea. Hear Res 13:229-247.

Hansen M, Boitano S, Dirksen ER, Sanderson MJ (1993) Intercellular calcium signaling induced by extracellular adenosine 5'-triphosphate and mechanical stimulation in airway epithelial cells. J Cell Sci 106 (Pt 4):995-1004.

Harada Y, Taniguchi M, Namatame H, Iida A (2001) Magnetic materials in otoliths of bird and fish lagena and their function. Acta Otolaryngol 121:590-595.

Harden N (2002) Signaling pathways directing the movement and fusion of epithelial sheets: lessons from dorsal closure in Drosophila. Differentiation 70:181-203.

Harris GG, Frishkopf LS, Flock A (1970) Receptor potentials from hair cells of the lateral line. Science 167:76-79.

Hashino E, Salvi RJ (1993) Changing spatial patterns of DNA replication in the noise-damaged chick cochlea. J Cell Sci 105 (Pt 1):23-31.

Hashino E, Tanaka Y, Sokabe M (1991) Hair cell damage and recovery following chronic application of kanamycin in the chick cochlea. Hear Res 52:356-368.

Hawkins JE (1976) Drug Ototoxicity. In: Handbook of Sensory Physiology, V, Auditory System (Keidel WD, Neff WD, eds), pp 707-748. Berlin, Heidelberg, New York: Springer-Verlag.

Hawkins JE, Jr. (1950) Cochlear signs of streptomycin intoxication. J Pharmacol Exp Ther 100:38-44.

Hawkins JE, Jr. (1973) Comparative otopathology: aging, noise, and ototoxic drugs. Adv Otorhinolaryngol 20:125-141.

Heath JP, Dunn GA (1978) Cell to substratum contacts of chick fibroblasts and their relation to the microfilament system. A correlated interference-reflexion and high-voltage electron-microscope study. J Cell Sci 29:197-212.

Hedgecock EM, Sulston JE, Thomson JN (1983) Mutations affecting programmed cell deaths in the nematode Caenorhabditis elegans. Science 220:1277-1279.

Henderson D, Bielefeld EC, Harris KC, Hu BH (2006) The role of oxidative stress in noise-induced hearing loss. Ear Hear 27:1-19.

Hergott GJ, Sandig M, Kalnins VI (1989) Cytoskeletal organization of migrating retinal pigment epithelial cells during wound healing in organ culture. Cell Motil Cytoskeleton 13:83-93.

Hirokawa N, Tilney LG (1982) Interactions between actin filaments and between actin filaments and membranes in quick-frozen and deeply etched hair cells of the chick ear. J Cell Biol 95:249-261.

Hirose K, Hockenbery DM, Rubel EW (1997) Reactive oxygen species in chick hair cells after gentamicin exposure in vitro. Hear Res 104:1-14.

Hirose K, Discolo CM, Keasler JR, Ransohoff R (2005) Mononuclear phagocytes migrate into the murine cochlea after acoustic trauma. J Comp Neurol 489:180-194.

Holt JR, Gillespie SK, Provance DW, Shah K, Shokat KM, Corey DP, Mercer JA, Gillespie PG (2002) A chemical-genetic strategy implicates myosin-1c in adaptation by hair cells. Cell 108:371-381.

Homburger SA, Fekete DM (1996) High efficiency gene transfer into the embryonic chicken CNS using B-subgroup retroviruses. Dev Dyn 206:112-120.

Hormia M, Badley RA, Lehto VP, Virtanen I (1985) Actomyosin organization in stationary and migrating sheets of cultured human endothelial cells. Exp Cell Res 157:116-126.

Huang C, Jacobson K, Schaller MD (2004) MAP kinases and cell migration. J Cell Sci 117:4619-4628.

Huang C, Rajfur Z, Borchers C, Schaller MD, Jacobson K (2003) JNK phosphorylates paxillin and regulates cell migration. Nature 424:219-223.

Huang S, Ingber DE (1999) The structural and mechanical complexity of cell-growth control. Nat Cell Biol 1:E131-138.

Huang S, Ingber DE (2002) A discrete cell cycle checkpoint in late G(1) that is cytoskeleton-dependent and MAP kinase (Erk)-independent. Exp Cell Res 275:255-264.

Hudspeth AJ (1975) Establishment of tight junctions between epithelial cells. Proc Natl Acad Sci U S A 72:2711-2713.

Hudspeth AJ, Corey DP (1977) Sensitivity, polarity, and conductance change in the response of vertebrate hair cells to controlled mechanical stimuli. Proc Natl Acad Sci U S A 74:2407-2411.

Hudspeth AJ, Jacobs R (1979) Stereocilia mediate transduction in vertebrate hair cells (auditory system/cilium/vestibular system). Proc Natl Acad Sci U S A 76:1506-1509.

Hughes SH, Greenhouse JJ, Petropoulos CJ, Sutrave P (1987) Adaptor plasmids simplify the insertion of foreign DNA into helper-independent retroviral vectors. J Virol 61:3004-3012.

Hutson MS, Tokutake Y, Chang MS, Bloor JW, Venakides S, Kiehart DP, Edwards GS (2003) Forces for morphogenesis investigated with laser microsurgery and quantitative modeling. Science 300:145-149.

Ingber DE (2006) Cellular mechanotransduction: putting all the pieces together again. Faseb J 20:811-827.

Ishizaki Y, Voyvodic JT, Burne JF, Raff MC (1993) Control of lens epithelial cell survival. J Cell Biol 121:899-908.

Izumikawa M, Minoda R, Kawamoto K, Abrashkin KA, Swiderski DL, Dolan DF, Brough DE, Raphael Y (2005) Auditory hair cell replacement and hearing improvement by Atoh1 gene therapy in deaf mammals. Nat Med 11:271-276.

Jacinto A, Martinez-Arias A, Martin P (2001) Mechanisms of epithelial fusion and repair. Nat Cell Biol 3:E117-123.

Jacinto A, Wood W, Balayo T, Turmaine M, Martinez-Arias A, Martin P (2000) Dynamic actin-based epithelial adhesion and cell matching during Drosophila dorsal closure. Curr Biol 10:1420-1426.

Jacinto A, Wood W, Woolner S, Hiley C, Turner L, Wilson C, Martinez-Arias A, Martin P (2002) Dynamic analysis of actin cable function during Drosophila dorsal closure. Curr Biol 12:1245-1250.

Jahnke K (1975) The fine structure of freeze-fractured intercellular junctions in the guinea pig inner ear. Acta Otolaryngol Suppl 336:1-40.

Jiang H, Sha SH, Schacht J (2006) Rac/Rho pathway regulates actin depolymerization induced by aminoglycoside antibiotics. J Neurosci Res 83:1544-1551.

Jiang H, Sha SH, Forge A, Schacht J (2005) Caspase-independent pathways of hair cell death induced by kanamycin in vivo. Cell Death Differ.

Jones JE, Corwin JT (1993) Replacement of lateral line sensory organs during tail regeneration in salamanders: identification of progenitor cells and analysis of leukocyte activity. J Neurosci 13:1022-1034.

Jones JE, Corwin JT (1996) Regeneration of sensory cells after laser ablation in the lateral line system: hair cell lineage and macrophage behavior revealed by time-lapse video microscopy. J Neurosci 16:649-662.

Jorgensen JM (1988) The number and distribution of calyceal hair cells in the inner ear utricular macula or some reptiles. Acta Zool 69:169-175.

Jorgensen JM (1989) Number and distribution of hair cells in the utricular macula of some avian species. J Morphol 201:187-204.

Jorgensen JM (1991) Regeneration of lateral line and inner ear vestibular cells. Ciba Found Symp 160:151-163; discussion 163-170.

Jorgensen JM, Mathiesen C (1988) The avian inner ear. Continuous production of hair cells in vestibular sensory organs, but not in the auditory papilla. Naturwissenschaften 75:319-320.

Kanzaki S, Beyer LA, Swiderski DL, Izumikawa M, Stover T, Kawamoto K, Raphael Y (2006) p27(Kip1) deficiency causes organ of Corti pathology and hearing loss. Hear Res 214:28-36.

Katayama A, Corwin JT (1989) Cell production in the chicken cochlea. J Comp Neurol 281:129-135.

Katayama A, Corwin JT (1993) Cochlear cytogenesis visualized through pulse labeling of chick embryos in culture. J Comp Neurol 333:28-40.

Kawamoto K, Ishimoto S, Minoda R, Brough DE, Raphael Y (2003) Math1 gene transfer generates new cochlear hair cells in mature guinea pigs in vivo. J Neurosci 23:4395-4400.

Kelley MW, Talreja DR, Corwin JT (1995) Replacement of hair cells after laser microbeam irradiation in cultured organs of corti from embryonic and neonatal mice. J Neurosci 15:3013-3026.

Kelsell DP, Dunlop J, Stevens HP, Lench NJ, Liang JN, Parry G, Mueller RF, Leigh IM (1997) Connexin 26 mutations in hereditary non-syndromic sensorineural deafness. Nature 387:80-83.

Kiehart DP (1999) Wound healing: The power of the purse string. Curr Biol 9:R602-605.

Kiehart DP, Galbraith CG, Edwards KA, Rickoll WL, Montague RA (2000) Multiple forces contribute to cell sheet morphogenesis for dorsal closure in Drosophila. J Cell Biol 149:471-490.

Kil J, Warchol ME, Corwin JT (1997) Cell death, cell proliferation, and estimates of hair cell life spans in the vestibular organs of chicks. Hear Res 114:117-126.

Kimura K, Ito M, Amano M, Chihara K, Fukata Y, Nakafuku M, Yamamori B, Feng J, Nakano T, Okawa K, Iwamatsu A, Kaibuchi K (1996) Regulation of myosin phosphatase by Rho and Rho-associated kinase (Rho-kinase). Science 273:245-248.

Kinchen JM, Cabello J, Klingele D, Wong K, Feichtinger R, Schnabel H, Schnabel R, Hengartner MO (2005) Two pathways converge at CED-10 to mediate actin rearrangement and corpse removal in C. elegans. Nature 434:93-99.

Klemke RL, Cai S, Giannini AL, Gallagher PJ, de Lanerolle P, Cheresh DA (1997) Regulation of cell motility by mitogen-activated protein kinase. J Cell Biol 137:481-492.

Klepeis VE, Cornell-Bell A, Trinkaus-Randall V (2001) Growth factors but not gap junctions play a role in injury-induced Ca2+ waves in epithelial cells. J Cell Sci 114:4185-4195.

Kolega J (1986) Effects of mechanical tension on protrusive activity and microfilament and intermediate filament organization in an epidermal epithelium moving in culture. J Cell Biol 102:1400-1411.

Kolega J (1998) Cytoplasmic dynamics of myosin IIA and IIB: spatial 'sorting' of isoforms in locomoting cells. J Cell Sci 111 (Pt 15):2085-2095.

Kolega J (2003) Asymmetric distribution of myosin IIB in migrating endothelial cells is regulated by a rho-dependent kinase and contributes to tail retraction. Mol Biol Cell 14:4745-4757.

Kotecha B, Richardson GP (1994) Ototoxicity in vitro: effects of neomycin, gentamicin, dihydrostreptomycin, amikacin, spectinomycin, neamine, spermine and poly-L-lysine. Hear Res 73:173-184.

Kovacs M, Toth J, Hetenyi C, Malnasi-Csizmadia A, Sellers JR (2004) Mechanism of blebbistatin inhibition of myosin II. J Biol Chem 279:35557-35563.

Kruger RP, Goodyear RJ, Legan PK, Warchol ME, Raphael Y, Cotanche DA, Richardson GP (1999) The supporting-cell antigen: a receptor-like protein tyrosine phosphatase expressed in the sensory epithelia of the avian inner ear. J Neurosci 19:4815-4827.

Kwan KY, Allchorne AJ, Vollrath MA, Christensen AP, Zhang DS, Woolf CJ, Corey DP (2006) TRPA1 contributes to cold, mechanical, and chemical nociception but is not essential for hair-cell transduction. Neuron 50:277-289.

Lambert PR (1994) Inner ear hair cell regeneration in a mammal: identification of a triggering factor. Laryngoscope 104:701-718.

Lang H, Liu C (1997) Apoptosis and hair cell degeneration in the vestibular sensory epithelia of the guinea pig following a gentamicin insult. Hear Res 111:177-184.

Lavoie JN, L'Allemain G, Brunet A, Muller R, Pouyssegur J (1996) Cyclin D1 expression is regulated positively by the p42/p44MAPK and negatively by the p38/HOGMAPK pathway. J Biol Chem 271:20608-20616.

Lee YS, Liu F, Segil N (2006) A morphogenetic wave of p27Kip1 transcription directs cell cycle exit during organ of Corti development. Development 133:2817-2826.

Leonova EV, Raphael Y (1997) Organization of cell junctions and cytoskeleton in the reticular lamina in normal and ototoxically damaged organ of Corti. Hear Res 113:14-28.

Levenberg S, Yarden A, Kam Z, Geiger B (1999) p27 is involved in N-cadherin-mediated contact inhibition of cell growth and S-phase entry. Oncogene 18:869-876.

Lewis J (1998) Notch signalling and the control of cell fate choices in vertebrates. Semin Cell Dev Biol 9:583-589.

Li G, Gustafson-Brown C, Hanks SK, Nason K, Arbeit JM, Pogliano K, Wisdom RM, Johnson RS (2003) c-Jun is essential for organization of the epidermal leading edge. Dev Cell 4:865-877.

Li L, Forge A (1997) Morphological evidence for supporting cell to hair cell conversion in the mammalian utricular macula. Int J Dev Neurosci 15:433-446.

Li L, Nevill G, Forge A (1995) Two modes of hair cell loss from the vestibular sensory epithelia of the guinea pig inner ear. J Comp Neurol 355:405-417.

Liberman MC, Dodds LW (1987) Acute ultrastructural changes in acoustic trauma: serial-section reconstruction of stereocilia and cuticular plates. Hear Res 26:45-64.

Lindeman HH (1969) Regional differences in sensitivity of the vestibular sensory epithelia to ototoxic antibiotics. Acta Otolaryngol 67:177-189.

Lipton A, Klinger I, Paul D, Holley RW (1971) Migration of mouse 3T3 fibroblasts in response to a serum factor. Proc Natl Acad Sci U S A 68:2799-2801.

Liu W, Staecker H, Stupak H, Malgrange B, Lefebvre P, Van De Water TR (1998) Caspase inhibitors prevent cisplatin-induced apoptosis of auditory sensory cells. Neuroreport 9:2609-2614.

Lowenheim H, Furness DN, Kil J, Zinn C, Gultig K, Fero ML, Frost D, Gummer AW, Roberts JM, Rubel EW, Hackney CM, Zenner HP (1999) Gene disruption of p27(Kip1) allows cell proliferation in the postnatal and adult organ of corti. Proc Natl Acad Sci U S A 96:4084-4088.

Lynch ED, Gu R, Pierce C, Kil J (2004) Ebselen-mediated protection from single and repeated noise exposure in rat. Laryngoscope 114:333-337.

Maekawa M, Ishizaki T, Boku S, Watanabe N, Fujita A, Iwamatsu A, Obinata T, Ohashi K, Mizuno K, Narumiya S (1999) Signaling from Rho to the actin cytoskeleton through protein kinases ROCK and LIM-kinase. Science 285:895-898.

Magie CR, Meyer MR, Gorsuch MS, Parkhurst SM (1999) Mutations in the Rho1 small GTPase disrupt morphogenesis and segmentation during early Drosophila development. Development 126:5353-5364.

Mangiardi DA, McLaughlin-Williamson K, May KE, Messana EP, Mountain DC, Cotanche DA (2004) Progression of hair cell ejection and molecular markers of apoptosis in the avian cochlea following gentamicin treatment. J Comp Neurol 475:1-18.

Manley GA, Brix J, Kaiser A (1987) Developmental stability of the tonotopic organization of the chick's basilar papilla. Science 237:655-656.

Mantela J, Jiang Z, Ylikoski J, Fritzsch B, Zacksenhaus E, Pirvola U (2005) The retinoblastoma gene pathway regulates the postmitotic state of hair cells of the mouse inner ear. Development 132:2377-2388.

Marcotti W, van Netten SM, Kros CJ (2005) The aminoglycoside antibiotic dihydrostreptomycin rapidly enters mouse outer hair cells through the mechano-electrical transducer channels. J Physiol 567:505-521.

Marean GC, Burt JM, Beecher MD, Rubel EW (1993) Hair cell regeneration in the European starling (Sturnus vulgaris): recovery of pure-tone detection thresholds. Hear Res 71:125-136.

Marshall CJ (1995) Specificity of receptor tyrosine kinase signaling: transient versus sustained extracellular signal-regulated kinase activation. Cell 80:179-185.

Martin P (1997) Wound healing--aiming for perfect skin regeneration. Science 276:75-81.

Martin P, Lewis J (1992) Actin cables and epidermal movement in embryonic wound healing. Nature 360:179-183.

Martin P, Nobes CD (1992) An early molecular component of the wound healing response in rat embryos--induction of c-fos protein in cells at the epidermal wound margin. Mech Dev 38:209-215.

Mast J, Goddeeris BM, Peeters K, Vandesande F, Berghman LR (1998) Characterisation of chicken monocytes, macrophages and interdigitating cells by the monoclonal antibody KUL01. Vet Immunol Immunopathol 61:343-357.

Matsubayashi Y, Ebisuya M, Honjoh S, Nishida E (2004) ERK activation propagates in epithelial cell sheets and regulates their migration during wound healing. Curr Biol 14:731-735.

Matsui JI, Ogilvie JM, Warchol ME (2002) Inhibition of caspases prevents ototoxic and ongoing hair cell death. J Neurosci 22:1218-1227.

Matsui JI, Gale JE, Warchol ME (2004) Critical signaling events during the aminoglycoside-induced death of sensory hair cells in vitro. J Neurobiol 61:250-266.

Matsui JI, Oesterle EC, Stone JS, Rubel EW (2000) Characterization of damage and regeneration in cultured avian utricles. J Assoc Res Otolaryngol 1:46-63.

Matsui JI, Haque A, Huss D, Messana EP, Alosi JA, Roberson DW, Cotanche DA, Dickman JD, Warchol ME (2003) Caspase inhibitors promote vestibular hair cell survival and function after aminoglycoside treatment in vivo. J Neurosci 23:6111-6122.

McCluskey J, Martin P (1995) Analysis of the tissue movements of embryonic wound healing--DiI studies in the limb bud stage mouse embryo. Dev Biol 170:102-114.

McDowell B, Davies S, Forge A (1989) The effect of gentamicin-induced hair cell loss on the tight junctions of the reticular lamina. Hear Res 40:221-232.

McFadden EA, Saunders JC (1989) Recovery of auditory function following intense sound exposure in the neonatal chick. Hear Res 41:205-215.

McNeil PL, Murphy RF, Lanni F, Taylor DL (1984) A method for incorporating macromolecules into adherent cells. J Cell Biol 98:1556-1564.

Medema RH, Kops GJ, Bos JL, Burgering BM (2000) AFX-like Forkhead transcription factors mediate cell-cycle regulation by Ras and PKB through p27kip1. Nature 404:782-787.

Meiteles LZ, Raphael Y (1994) Scar formation in the vestibular sensory epithelium after aminoglycoside toxicity. Hear Res 79:26-38.

Monks J, Rosner D, Geske FJ, Lehman L, Hanson L, Neville MC, Fadok VA (2005) Epithelial cells as phagocytes: apoptotic epithelial cells are engulfed by mammary alveolar epithelial cells and repress inflammatory mediator release. Cell Death Differ 12:107-114.

Montcouquiol M, Corwin JT (2001a) Brief treatments with forskolin enhance s-phase entry in balance epithelia from the ears of rats. J Neurosci 21:974-982.

Montcouquiol M, Corwin JT (2001b) Intracellular signals that control cell proliferation in mammalian balance epithelia: key roles for phosphatidylinositol-3 kinase, mammalian target of rapamycin, and S6 kinases in preference to calcium, protein kinase C, and mitogen-activated protein kinase. J Neurosci 21:570-580.

Morgan BA, Fekete DM (1996) Manipulating gene expression with replication-competent retroviruses. Methods Cell Biol 51:185-218.

Nadol JB, Jr. (1978) Intercellular junctions in the organ of Corti. Ann Otol Rhinol Laryngol 87:70-80.

Nateri AS, Spencer-Dene B, Behrens A (2005) Interaction of phosphorylated c-Jun with TCF4 regulates intestinal cancer development. Nature 437:281-285.

Navaratnam DS, Su HS, Scott SP, Oberholtzer JC (1996) Proliferation in the auditory receptor epithelium mediated by a cyclic AMP-dependent signaling pathway. Nat Med 2:1136-1139.

Nelson WJ, Nusse R (2004) Convergence of Wnt, beta-catenin, and cadherin pathways. Science 303:1483-1487.

Nicotera TM, Hu BH, Henderson D (2003) The caspase pathway in noise-induced apoptosis of the chinchilla cochlea. J Assoc Res Otolaryngol 4:466-477.

Nikolic DL, Boettiger AN, Bar-Sagi D, Carbeck JD, Shvartsman SY (2006) The role of boundary conditions in the experimental model of wound healing. Am J Physiol Cell Physiol (*in press*).

Nobes CD, Hall A (1995) Rho, rac, and cdc42 GTPases regulate the assembly of multimolecular focal complexes associated with actin stress fibers, lamellipodia, and filopodia. Cell 81:53-62.

Nobes CD, Hall A (1999) Rho GTPases control polarity, protrusion, and adhesion during cell movement. J Cell Biol 144:1235-1244.

Nusrat A, Delp C, Madara JL (1992) Intestinal epithelial restitution. Characterization of a cell culture model and mapping of cytoskeletal elements in migrating cells. J Clin Invest 89:1501-1511.

O'Halloran EK, Oesterle EC (2004) Characterization of leukocyte subtypes in chicken inner ear sensory epithelia. J Comp Neurol 475:340-360.

Oesterle EC, Rubel EW (1993) Postnatal production of supporting cells in the chick cochlea. Hear Res 66:213-224.

Oesterle EC, Hume CR (1999) Growth factor regulation of the cell cycle in developing and mature inner ear sensory epithelia. J Neurocytol 28:877-887.

Oesterle EC, Tsue TT, Rubel EW (1997) Induction of cell proliferation in avian inner ear sensory epithelia by insulin-like growth factor-I and insulin. J Comp Neurol 380:262-274.

Oesterle EC, Bhave SA, Coltrera MD (2000) Basic fibroblast growth factor inhibits cell proliferation in cultured avian inner ear sensory epithelia. J Comp Neurol 424:307-326.

Oesterle EC, Tsue TT, Reh TA, Rubel EW (1993) Hair-cell regeneration in organ cultures of the postnatal chicken inner ear. Hear Res 70:85-108.

Ohinata Y, Yamasoba T, Schacht J, Miller JM (2000) Glutathione limits noise-induced hearing loss. Hear Res 146:28-34.

Ohlemiller KK, Wright JS, Dugan LL (1999) Early elevation of cochlear reactive oxygen species following noise exposure. Audiol Neurootol 4:229-236.

Parnaik R, Raff MC, Scholes J (2000) Differences between the clearance of apoptotic cells by professional and non-professional phagocytes. Curr Biol 10:857-860.

Peterson JR, Bickford LC, Morgan D, Kim AS, Ouerfelli O, Kirschner MW, Rosen MK (2004) Chemical inhibition of N-WASP by stabilization of a native autoinhibited conformation. Nat Struct Mol Biol 11:747-755.

Piazza V, Ciubotaru CD, Gale JE, Mammano F (2006) Purinergic signalling and intercellular Ca(2+) wave propagation in the organ of Corti. Cell Calcium.

Pickles JO, Comis SD, Osborne MP (1984) Cross-links between stereocilia in the guinea pig organ of Corti, and their possible relation to sensory transduction. Hear Res 15:103-112.

Pirvola U, Xing-Qun L, Virkkala J, Saarma M, Murakata C, Camoratto AM, Walton KM, Ylikoski J (2000) Rescue of hearing, auditory hair cells, and neurons by CEP-1347/KT7515, an inhibitor of c-Jun N-terminal kinase activation. J Neurosci 20:43-50.

Poje CP, Sewell DA, Saunders JC (1995) The effects of exposure to intense sound on the DC endocochlear potential in the chick. Hear Res 82:197-204.

Pujol R, Puel JL (1999) Excitotoxicity, synaptic repair, and functional recovery in the mammalian cochlea: a review of recent findings. Ann N Y Acad Sci 884:249-254.

Rabinovitch M (1995) Professional and non-professional phagocytes: an introduction. Trends Cell Biol 5:85-87.

Radice GP (1980) The spreading of epithelial cells during wound closure in Xenopus larvae. Dev Biol 76:26-46.

Rand HW (1915) Wound closure in actinian tentacles with reference to the problem of organisation. Rouxz Arch Entwicklungsmech Organismen 41:159-214.

Raphael Y (1992) Evidence for supporting cell mitosis in response to acoustic trauma in the avian inner ear. J Neurocytol 21:663-671.

Raphael Y (1993) Reorganization of the chick basilar papilla after acoustic trauma. J Comp Neurol 330:521-532.

Raphael Y, Altschuler RA (1991a) Scar formation after drug-induced cochlear insult. Hear Res 51:173-183.

Raphael Y, Altschuler RA (1991b) Reorganization of cytoskeletal and junctional proteins during cochlear hair cell degeneration. Cell Motil Cytoskeleton 18:215-227.

Raphael Y, Altschuler RA (2003) Structure and innervation of the cochlea. Brain Res Bull 60:397-422.

Rebillard G, Rubel EW (1981) Electrophysiological study of the maturation of auditory responses from the inner ear of the chick. Brain Res 229:15-23.

Reddien PW, Horvitz HR (2000) CED-2/CrkII and CED-10/Rac control phagocytosis and cell migration in Caenorhabditis elegans. Nat Cell Biol 2:131-136.

Reddien PW, Horvitz HR (2004) The engulfment process of programmed cell death in caenorhabditis elegans. Annu Rev Cell Dev Biol 20:193-221.

Retzius G (1881) Das Gehororgan der Wirbelthiere.

Ridley AJ, Schwartz MA, Burridge K, Firtel RA, Ginsberg MH, Borisy G, Parsons JT, Horwitz AR (2003) Cell migration: integrating signals from front to back. Science 302:1704-1709.

Roberson DF, Weisleder P, Bohrer PS, Rubel EW (1992) Ongoing production of sensory cells in the vestibular epithelium of the chick. Hear Res 57:166-174.

Roberson DW, Rubel EW (1994) Cell division in the gerbil cochlea after acoustic trauma. Am J Otol 15:28-34.

Roberson DW, Kreig CS, Rubel EW (1996) Light microscopic evidence that pre-mitotic transdifferentiation may give rise to new hair cells in the regenerating auditory epithelium. Auditory Neuroscience 2:195-205.

Roberson DW, Alosi JA, Cotanche DA (2004) Direct transdifferentiation gives rise to the earliest new hair cells in regenerating avian auditory epithelium. J Neurosci Res 78:461-471.

Robertson D, Johnstone BM, McGill TJ (1980) Effects of loud tones on the inner ear: a combined electrophysiological and ultrastructural study. Hear Res 2:39-43.

Rosen P, Misfeldt DS (1980) Cell density determines epithelial migration in culture. Proc Natl Acad Sci U S A 77:4760-4763.

Rosenblatt J, Raff MC, Cramer LP (2001) An epithelial cell destined for apoptosis signals its neighbors to extrude it by an actin- and myosin-dependent mechanism. Curr Biol 11:1847-1857.

Rossman KL, Der CJ, Sondek J (2005) GEF means go: turning on RHO GTPases with guanine nucleotide-exchange factors. Nat Rev Mol Cell Biol 6:167-180.

Ruben RJ (1967) Development of the inner ear of the mouse: a radioautographic study of terminal mitoses. Acta Otolaryngol:Suppl 220:221-244.

Runhaar G, Schedler J, Manley GA (1991) The potassium concentration in the cochlear fluids of the embryonic and post-hatching chick. Hear Res 56:227-238.

Russo JM, Florian P, Shen L, Graham WV, Tretiakova MS, Gitter AH, Mrsny RJ, Turner JR (2005) Distinct temporal-spatial roles for rho kinase and myosin light chain kinase in epithelial purse-string wound closure. Gastroenterology 128:987-1001.

Ryals BM, Rubel EW (1988) Hair cell regeneration after acoustic trauma in adult Coturnix quail. Science 240:1774-1776.

Rybak LP, Whitworth CA (2005) Ototoxicity: therapeutic opportunities. Drug Discov Today 10:1313-1321.

Sage C, Huang M, Vollrath MA, Brown MC, Hinds PW, Corey DP, Vetter DE, Chen ZY (2006) Essential role of retinoblastoma protein in mammalian hair cell development and hearing. Proc Natl Acad Sci U S A 103:7345-7350.

Sage C, Huang M, Karimi K, Gutierrez G, Vollrath MA, Zhang DS, Garcia-Anoveros J, Hinds PW, Corwin JT, Corey DP, Chen ZY (2005) Proliferation of functional hair cells in vivo in the absence of the retinoblastoma protein. Science 307:1114-1118.

Sammak PJ, Hinman LE, Tran PO, Sjaastad MD, Machen TE (1997) How do injured cells communicate with the surviving cell monolayer? J Cell Sci 110 (Pt 4):465-475.

Sans A, Chat M (1982) Analysis of temporal and spatial patterns of rat vestibular hair cell differentiation by tritiated thymidine radioautography. J Comp Neurol 206:1-8.

Santos-Sacchi J, Dallos P (1983) Intercellular communication in the supporting cells of the organ of Corti. Hear Res 9:317-326.

Saunders JC, Coles RB, Gates GR (1973) The development of auditory evoked responses in the cochlea and cochlear nuclei of the chick. Brain Res 63:59-74.

Schneider ME, Belyantseva IA, Azevedo RB, Kachar B (2002) Rapid renewal of auditory hair bundles. Nature 418:837-838.

Sefton BM, Rubin H (1970) Release from density dependent growth inhibition by proteolytic enzymes. Nature 227:843-845.

Seidman M, Babu S, Tang W, Naem E, Quirk WS (2003) Effects of resveratrol on acoustic trauma. Otolaryngol Head Neck Surg 129:463-470.

Selden SC, 3rd, Schwartz SM (1979) Cytochalasin B inhibition of endothelial proliferation at wound edges in vitro. J Cell Biol 81:348-354.

Selden SC, 3rd, Rabinovitch PS, Schwartz SM (1981) Effects of cytoskeletal disrupting agents on replication of bovine endothelium. J Cell Physiol 108:195-211.

Sexton DW, Blaylock MG, Walsh GM (2001) Human alveolar epithelial cells engulf apoptotic eosinophils by means of integrin- and phosphatidylserine receptor-dependent mechanisms: a process upregulated by dexamethasone. J Allergy Clin Immunol 108:962-969.

Sha SH, Schacht J (1999) Salicylate attenuates gentamicin-induced ototoxicity. Lab Invest 79:807-813.

Sha SH, Schacht J (2000) Antioxidants attenuate gentamicin-induced free radical formation in vitro and ototoxicity in vivo: D-methionine is a potential protectant. Hear Res 142:34-40.

Sharma GD, He J, Bazan HE (2003) p38 and ERK1/2 coordinate cellular migration and proliferation in epithelial wound healing: evidence of cross-talk activation between MAP kinase cascades. J Biol Chem 278:21989-21997.

Sharma M, Chuang WW, Sun Z (2002) Phosphatidylinositol 3-kinase/Akt stimulates androgen pathway through GSK3beta inhibition and nuclear beta-catenin accumulation. J Biol Chem 277:30935-30941.

Sharrocks AD (2001) The ETS-domain transcription factor family. Nat Rev Mol Cell Biol 2:827-837.

Sherratt JA, Martin P, Murray JD, Lewis J (1992) Mathematical models of wound healing in embryonic and adult epidermis. IMA J Math Appl Med Biol 9:177-196.

Shtutman M, Zhurinsky J, Simcha I, Albanese C, D'Amico M, Pestell R, Ben-Ze'ev A (1999) The cyclin D1 gene is a target of the beta-catenin/LEF-1 pathway. Proc Natl Acad Sci U S A 96:5522-5527.

Siemens J, Lillo C, Dumont RA, Reynolds A, Williams DS, Gillespie PG, Muller U (2004) Cadherin 23 is a component of the tip link in hair-cell stereocilia. Nature 428:950-955.

Sobkowicz HM, August BK, Slapnick SM (1996) Post-traumatic survival and recovery of the auditory sensory cells in culture. Acta Otolaryngol 116:257-262.

Sobkowicz HM, August BK, Slapnick SM (1997) Cellular interactions as a response to injury in the organ of Corti in culture. Int J Dev Neurosci 15:463-485.

Sponsel HT, Breckon R, Hammond W, Anderson RJ (1994) Mechanisms of recovery from mechanical injury of renal tubular epithelial cells. Am J Physiol 267:F257-264.

St Croix B, Sheehan C, Rak JW, Florenes VA, Slingerland JM, Kerbel RS (1998) E-Cadherin-dependent growth suppression is mediated by the cyclin-dependent kinase inhibitor p27(KIP1). J Cell Biol 142:557-571.

Steinberg RH (1974) Phagocytosis by pigment epithelium of human retinal cones. Nature 252:305-307.

Stoker MG, Rubin H (1967) Density dependent inhibition of cell growth in culture. Nature 215:171-172.

Stone JS, Cotanche DA (1994) Identification of the timing of S phase and the patterns of cell proliferation during hair cell regeneration in the chick cochlea. J Comp Neurol 341:50-67.

Stone JS, Rubel EW (1999) Delta1 expression during avian hair cell regeneration. Development 126:961-973.

Stone JS, Rubel EW (2000a) Temporal, spatial, and morphologic features of hair cell regeneration in the avian basilar papilla. J Comp Neurol 417:1-16.

Stone JS, Rubel EW (2000b) Cellular studies of auditory hair cell regeneration in birds. Proc Natl Acad Sci U S A 97:11714-11721.

Stone JS, Choi YS, Woolley SM, Yamashita H, Rubel EW (1999) Progenitor cell cycling during hair cell regeneration in the vestibular and auditory epithelia of the chick. J Neurocytol 28:863-876.

Swanson JA, Johnson MT, Beningo K, Post P, Mooseker M, Araki N (1999) A contractile activity that closes phagosomes in macrophages. J Cell Sci 112 (Pt 3):307-316.

Takasaka T, Smith CA (1971) The structure and innervation of the pigeon's basilar papilla. J Ultrastruct Res 35:20-65.

Takeuchi S (1979) Wound healing in the cornea of the chick embryo. IV. Promotion of the migratory activity of isolated corneal epithelium in culture by the application of tension. Dev Biol 70:232-240.

Takeuchi S (1983) Wound healing in the cornea of the chick embryo. V. An observation and quantitative assessment of the cell shapes in the isolated corneal epithelium during spreading in vitro. Cell Tissue Res 229:109-127.

Tanaka K, Smith CA (1978) Structure of the chicken's inner ear: SEM and TEM study. Am J Anat 153:251-271.

Taylor RR, Forge A (2005) Hair cell regeneration in sensory epithelia from the inner ear of a urodele amphibian. J Comp Neurol 484:105-120.

Theopold HM (1977) Comparative surface studies of ototoxic effects of various aminoglycoside antibiotics on the organ of Corti in the guinea pig. A scanning electron microscopic study. Acta Otolaryngol 84:57-64.

Tilney LG, Tilney MS (1984) Observations on how actin filaments become organized in cells. J Cell Biol 99:76s-82s.

Tilney LG, Derosier DJ, Mulroy MJ (1980) The organization of actin filaments in the stereocilia of cochlear hair cells. J Cell Biol 86:244-259.

Todaro GJ, Lazar GK, Green H (1965) The initiation of cell division in a contact-inhibited mammalian cell line. J Cell Physiol 66:325-333.

Torchinsky C, Messana EP, Arsura M, Cotanche DA (1999) Regulation of p27Kip1 during gentamicin mediated hair cell death. J Neurocytol 28:913-924.

Tran PO, Hinman LE, Unger GM, Sammak PJ (1999) A wound-induced [Ca2+]i increase and its transcriptional activation of immediate early genes is important in the regulation of motility. Exp Cell Res 246:319-326.

Trinkhaus JP (1984) Cells into Organs: The Forces that Shape the Embryo: Prentice-Hall.

Trussell LO (2002) Transmission at the hair cell synapse. Nat Neurosci 5:85-86.

Tsue TT, Oesterle EC, Rubel EW (1994) Diffusible factors regulate hair cell regeneration in the avian inner ear. Proc Natl Acad Sci U S A 91:1584-1588.

Uehata M, Ishizaki T, Satoh H, Ono T, Kawahara T, Morishita T, Tamakawa H, Yamagami K, Inui J, Maekawa M, Narumiya S (1997) Calcium sensitization of smooth muscle mediated by a Rho-associated protein kinase in hypertension. Nature 389:990-994.

Vasiliev JM, Gelfand IM, Domnina LV, Rappoport RI (1969) Wound healing processes in cell cultures. Exp Cell Res 54:83-93.

Vaughan RB, Trinkaus JP (1966) Movements of epithelial cell sheets in vitro. J Cell Sci 1:407-413.

Verrier B, Muller D, Bravo R, Muller R (1986) Wounding a fibroblast monolayer results in the rapid induction of the c-fos proto-oncogene. Embo J 5:913-917.

Walker NI, Bennett RE, Kerr JF (1989) Cell death by apoptosis during involution of the lactating breast in mice and rats. Am J Anat 185:19-32.

Walsh GM, Sexton DW, Blaylock MG, Convery CM (1999) Resting and cytokine-stimulated human small airway epithelial cells recognize and engulf apoptotic eosinophils. Blood 94:2827-2835.

Wang J, Van De Water TR, Bonny C, de Ribaupierre F, Puel JL, Zine A (2003) A peptide inhibitor of c-Jun N-terminal kinase protects against both aminoglycoside and acoustic trauma-induced auditory hair cell death and hearing loss. J Neurosci 23:8596-8607.

Wang Y, Hirose K, Liberman MC (2002) Dynamics of noise-induced cellular injury and repair in the mouse cochlea. J Assoc Res Otolaryngol 3:248-268.

Wangemann P (2002) K+ cycling and the endocochlear potential. Hear Res 165:1-9.

Wangemann P (2006) Supporting sensory transduction: Cochlear fluid homeostasis and the endocochlear potential. J Physiol.

Warchol ME (1995) Supporting cells in isolated sensory epithelia of avian utricles proliferate in serum-free culture. Neuroreport 6:981-984.

Warchol ME (1997) Macrophage activity in organ cultures of the avian cochlea: demonstration of a resident population and recruitment to sites of hair cell lesions. J Neurobiol 33:724-734.

Warchol ME (1999) Immune cytokines and dexamethasone influence sensory regeneration in the avian vestibular periphery. J Neurocytol 28:889-900.

Warchol ME (2002) Cell density and N-cadherin interactions regulate cell proliferation in the sensory epithelia of the inner ear. J Neurosci 22:2607-2616.

Warchol ME, Corwin JT (1993) Supporting cells in avian vestibular organs proliferate in serum-free culture. Hear Res 71:28-36.

Warchol ME, Corwin JT (1996) Regenerative proliferation in organ cultures of the avian cochlea: identification of the initial progenitors and determination of the latency of the proliferative response. J Neurosci 16:5466-5477.

Warchol ME, Lambert PR, Goldstein BJ, Forge A, Corwin JT (1993) Regenerative proliferation in inner ear sensory epithelia from adult guinea pigs and humans. Science 259:1619-1622.

Weisleder P, Rubel EW (1993) Hair cell regeneration after streptomycin toxicity in the avian vestibular epithelium. J Comp Neurol 331:97-110.

Weisleder P, Tsue TT, Rubel EW (1995) Hair cell replacement in avian vestibular epithelium: supporting cell to type I hair cell. Hear Res 82:125-133.

Wersall J (1956) Studies on the structure and innervation of the sensory epithelium of the cristae ampulares in the guinea pig; a light and electron microscopic investigation. Acta Otolaryngol Suppl 126:1-85.

Wersall J, Hawkins JE, Jr. (1962) The vestibular sensory epithelia in the cat labyrinth and their reactions in chronic streptomycin intoxication. Acta Otolaryngol 54:1-23.

Wilcox ER, Burton QL, Naz S, Riazuddin S, Smith TN, Ploplis B, Belyantseva I, Ben-Yosef T, Liburd NA, Morell RJ, Kachar B, Wu DK, Griffith AJ, Riazuddin S, Friedman TB (2001) Mutations in the gene encoding tight junction claudin-14 cause autosomal recessive deafness DFNB29. Cell 104:165-172.

Witte MC, Montcouquiol M, Corwin JT (2001) Regeneration in avian hair cell epithelia: identification of intracellular signals required for S-phase entry. Eur J Neurosci 14:829-838.

Wood W, Turmaine M, Weber R, Camp V, Maki RA, McKercher SR, Martin P (2000) Mesenchymal cells engulf and clear apoptotic footplate cells in macrophageless PU.1 null mouse embryos. Development 127:5245-5252.

Wood W, Jacinto A, Grose R, Woolner S, Gale J, Wilson C, Martin P (2002) Wound healing recapitulates morphogenesis in Drosophila embryos. Nat Cell Biol 4:907-912.

Woods C, Montcouquiol M, Kelley MW (2004) Math1 regulates development of the sensory epithelium in the mammalian cochlea. Nat Neurosci 7:1310-1318.

Woolley K, Martin P (2000) Conserved mechanisms of repair: from damaged single cells to wounds in multicellular tissues. Bioessays 22:911-919.

Wymann MP, Marone R (2005) Phosphoinositide 3-kinase in disease: timing, location, and scaffolding. Curr Opin Cell Biol 17:141-149.

Yamane H, Nakai Y, Takayama M, Iguchi H, Nakagawa T, Kojima A (1995) Appearance of free radicals in the guinea pig inner ear after noise-induced acoustic trauma. Eur Arch Otorhinolaryngol 252:504-508.

Yamashita H, Oesterle EC (1995) Induction of cell proliferation in mammalian inner-ear sensory epithelia by transforming growth factor alpha and epidermal growth factor. Proc Natl Acad Sci U S A 92:3152-3155.

Yang WP, Henderson D, Hu BH, Nicotera TM (2004) Quantitative analysis of apoptotic and necrotic outer hair cells after exposure to different levels of continuous noise. Hear Res 196:69-76.

Yarnell MM, Schnebli HP (1974) Release from density-dependent inhibition of growth in the absence of cell locomotion. J Cell Sci 16:181-188.

Ylikoski J, Xing-Qun L, Virkkala J, Pirvola U (2002) Blockade of c-Jun N-terminal kinase pathway attenuates gentamicin-induced cochlear and vestibular hair cell death. Hear Res 163:71-81.

Young PE, Richman AM, Ketchum AS, Kiehart DP (1993) Morphogenesis in Drosophila requires nonmuscle myosin heavy chain function. Genes Dev 7:29-41.

Young RW, Bok D (1969) Participation of the retinal pigment epithelium in the rod outer segment renewal process. J Cell Biol 42:392-403.

Zegers MM, Forget MA, Chernoff J, Mostov KE, ter Beest MB, Hansen SH (2003) Pak1 and PIX regulate contact inhibition during epithelial wound healing. Embo J 22:4155-4165.

Zhao Y, Yamoah EN, Gillespie PG (1996) Regeneration of broken tip links and restoration of mechanical transduction in hair cells. Proc Natl Acad Sci U S A 93:15469-15474.

Zheng JL, Gao WQ (2000) Overexpression of Math1 induces robust production of extra hair cells in postnatal rat inner ears. Nat Neurosci 3:580-586.

Zheng JL, Helbig C, Gao WQ (1997) Induction of cell proliferation by fibroblast and insulin-like growth factors in pure rat inner ear epithelial cell cultures. J Neurosci 17:216-226.

Zheng JL, Keller G, Gao WQ (1999) Immunocytochemical and morphological evidence for intracellular self-repair as an important contributor to mammalian hair cell recovery. J Neurosci 19:2161-2170.

Zhigilei LV, Leveugle E, Garrison BJ, Yingling YG, Zeifman MI (2003) Computer simulations of laser ablation of molecular substrates. Chem Rev 103:321-348.

Zigler JS, Jr., Lepe-Zuniga JL, Vistica B, Gery I (1985) Analysis of the cytotoxic effects of light-exposed HEPES-containing culture medium. In Vitro Cell Dev Biol 21:282-287.

Appendix A

This CD-R contains several movies that are referenced from the text. The movies are presented as uncompressed MPEGs, and are compatible with standard distributions of Windows XP, OS X and Linux.